Insights into the glucose photometabolism by

Rubrivivax benzoatilyticus JA2

A Thesis Submitted to the

UNIVERSITY OF HYDERABAD
Hyderabad, India

For the Degree of
DOCTOR OF PHILOSOPHY

By

Deepshikha
(Reg. No. 16LPPH03)
Department of Plant Sciences
School of Life Sciences
University of Hyderabad
Hyderabad-500 046
Telangana, India

January 2021

UNIVERSITY OF HYDERABAD

(A Central University established in 1974 by an Act of the Parliament)

HYDERABAD 500046

प्रतिष्ठित संस्थान
INSTITUTION OF EMINENCE

CERTIFICATE

This is to certify that **Ms. Deepshikha** has carried out the research work embodied in the present thesis under the supervision and guidance of Prof. Ch. Venkata Ramana for a full period prescribed under the Ph.D. ordinances of this University. We recommend her thesis entitled **"Insights into the glucose photometabolism by *Rubrivivax benzoatilyticus* JA2"** for submission for the degree of Doctor of Philosophy of the University.

29/01/2021

HEAD
Dept. Plant Sciences

अध्यक्ष / HEAD
वनस्पति विज्ञान विभाग / Dept. of Plant Sciences
जीवन विज्ञान संकाय / School of Life Sciences
हैदराबाद विश्वविद्यालय / University of Hyderabad
हैदराबाद / Hyderabad-500 046, भारत / INDIA

DEAN
School of Life Sciences

DEAN
School of Life Sciences
University of Hyderabad
Hyderabad - 500 046.

29/1/2021

SUPERVISOR
Prof. Ch. V. Ramana

Prof. Ch. Venkata Ramana Ph.D
Department of Plant Sciences School of Life Sciences
University of Hyderabad, P.O. Central University,
Hyderabad - 500 046, India

UNIVERSITY OF HYDERABAD

(A Central University established in 1974 by an Act of the Parliament)

HYDERABAD 500046

प्रतिष्ठित संस्थान
INSTITUTION OF EMINENCE

DECLARATION

I, **Deepshikha,** hereby declare that this thesis entitled **"Insights into the glucose photometabolism by *Rubrivivax benzoatilyticus* JA2"** submitted by me under the guidance and supervision of **Prof. Ch. Venkata Ramana** is an original and independent research work. I also declare that this work is original and has not been submitted previously in part or in full to this University or any other University or Institution for the award of any degree or diploma.

Deepshikha

Deepshikha
(Ph.D. student)

23/1/2021

Supervisor
Prof. Ch. V. Ramana

Prof. Ch. Venkata Ramana Ph.D.
Department of Plant Sciences School of Life Sciences
University of Hyderabad, P.O. Central University,
Hyderabad - 500 046, India

UNIVERSITY OF HYDERABAD
(A Central University established in 1974 by an Act of the Parliament)
HYDERABAD 500046

प्रतिष्ठित संस्थान
INSTITUTION OF EMINENCE

CERTIFICATE

This is to certify that this thesis entitled **"Insights into the glucose photometabolism by *Rubrivivax benzoatilyticus* JA2"** is a record of bonafide work carried out by **Ms. Deepshikha**, research scholar bearing registration number 16LPPH03, for the award of Doctor of Philosophy in the Department of Plant Sciences, School of Life Sciences, University of Hyderabad, under my guidance and supervision. This thesis is free from plagiarism and has not been submitted in any part or to full to this or any other University or Institute for the award of any degree or diploma.

Parts of the thesis has been:

A. Published in following publication:

Deepshikha Gupta, Mujahid Mohammed, Lakshmi Prasuna Mekala, Sasikala Chintalapati and Venkata Ramana Chintalapati (2019). iTRAQ-Based quantitative proteomics revealed insights into metabolic and molecular responses of glucose-grown cells of *Rubrivivax benzoatilyticus* JA2. J. Proteomics 194, 49-59.

B. Presented in the following conferences:

- Poster presentation Title **"Diabetic bacteria?". Deepshikha G.,** Ch. Sasikala., Ch. V. Ramana. 59th Annual Conference of Association of Microbiologists of India (AMI) December 09-12, 2018.
- Oral presentation Title **"Glucose induces photosynthetic damage leading to viable but non-culturable (VBNC) state in *Rubrivivax benzoatilyticus* JA2". Deepshikha G.** and Ch. V. Ramana. 8th International Conference Photosynthesis and Hydrogen Energy Research for Sustainability. October 30 – November 4, 2017.

Further, the student has passed the following courses towards the fulfillment of the coursework requirement for Ph.D. degree.

S.no	Course	Name	Credits	Pass/Fail
1.	PL-801	Analytical Techniques	4	Pass
2.	PL-802	Research Ethics, Data Analysis and Biostatistics	3	Pass
3.	PL-803	Lab work and Seminar	5	Pass

HEAD 29/01/2021
Dept. Plant Sciences
अध्यक्ष / HEAD
पादपी विज्ञान विभाग / Dept. of Plant Sciences
जीवन विज्ञान संकाय / School of Life Sciences
हैदराबाद विश्वविद्यालय / University of Hyderabad
हैदराबाद / Hyderabad-500 046, भारत / INDIA

DEAN
School of Life Sciences
DEAN
School of Life Sciences
University of Hyderabad
Hyderabad - 500 046.

29/1/2021
SUPERVISOR
Prof. Ch. V. Ramana
Prof. Ch. Venkata Ramana Ph.D
Department of Plant Sciences School of Life Sciences
University of Hyderabad, P.O. Central University,
Hyderabad - 500 046, India

ACKNOWLEDGEMENTS

As the no work on the mother earth is a solo effort and this work is also not the exception! I take this opportunity to thank everyone who helped me in the journey of PhD.

I would like to take this opportunity to extend my gratitude to my supervisor ***Prof. Ch. Venkata Ramana*** *for his unrelenting encouragement and constant support, without whom, this endeavor would not have been possible. Working under him gave me a true sense of freedom, broadened my scientific outlook, and inculcated a spirit of positive attitude in me. I am deeply indebted of his unfailing support in every scientific aspect like writing, communication, presentation skills, which enabled me towards the successful completion of this Ph.D. program. Above all, I can't forget his care and help showed towards me at difficult times during the entire tenure of my doctoral research.*

I thank my doctoral committee members ***Prof. S. Rajagopal*** *and* ***Dr. K. Gopinath*** *for their valuable suggestions during my work.*

I thank the former Deans, ***Prof. P. Reddanna, Prof. M.N.V. Prasad, Prof. Ramaiah*** *and the present Dean,* ***Prof. S. Dayananda****, School of Life Sciences and former Head,* ***Prof. Ch. Venkata Ramana****, and present Head,* ***Prof. G. Padmaja****, Dept. of Plant Sciences, for their support in all possible ways.*

I am grateful to ***Prof. Ch. Sasikala****, CEN, IST, JNTU for her fruitful discussions and extending her lab. I extend my sincere gratitude for her immense support and guidance in every scientific aspect and her help in nurturing my writing skills which helped in successful completion of this Ph.D. program.*

I am extremely grateful to my teachers, who taught me just not science, also ethics and morals in life.

I thank DST- WOS-A for providing me with the platform to make a comeback. Infrastructural support provided by UGC-SAP, DBT-CREBB and DST-FIST to the Dept. of Plant Sciences are highly acknowledged.

I would like to thank my present and former labmates from UoH and JNTU for their help and cooperation throughout my research.

The help and cooperation of the non-teaching staff in the school, Centre for Nanotechnology and at CIL, UoH is deeply acknowledged.

Words fail to express my heartfelt gratitude for my parents, and all my family members especially my daughters to whom I'm forever indebted for their unconditional love, support,inspiration and endless patience, without their cooperation I would not have come so far.

All that I cherish today is the grace of God. I thank the Almighty God for answering my prayers, for granting me the strength, wisdom, knowledge and showering his blessings upon me during research work.

I am thankful to one and all, who helped me directly or indirectly at every stage of my research work.

I dedicate this work to my father and father-in-law.

Deepshikha*….*

Table of contents

List of Figures

List of Tables

Abstract

Anoxygenic phototrophic bacteria (APB) display phenomenal metabolic plasticity leading to distinct phenotypes. They bloom under varying habitat using an array of organic/inorganic compounds as carbon sources/electron donors, yet their metabolic adaptation to fluctuating carbon regime is largely unexplored and thus remains elusive. Further, hyperglycemic effect on macro-organisms (mostly animals, including humans) is widely investigated but the same on microorganisms is in its infancy and not elucidated clearly hence, remains an open question. Thus, there is a requirement of robust investigation to enhance our current knowledge of hyperglycemic effect on microorganisms. Present study is an attempt to glean biological insights of adaptive strategies employed by an APB member, *Rubrivivax benzoatilyticus*, in response to the hyperglycemic effect. The study aimed at deciphering the bacterial adjustments at physiological, biochemical, metabolomic, proteomic and genomic level in response to hyperglycemia. Our investigation highlights that carbon source, determining the metabolic fate of the cells, can reshape the energy dynamics.

Rbx. benzoatilyticus displayed altered growth rates, reduction in cellular size and photobleaching along with hampered photosynthetic gadgetry under photoheterotrophic growth on glucose, as compared with malate. The organism grows chemotrophically when glucose is provided as an electron donor but a change in its life style *i.e* when forced to grow photoheterotrophically, it switched to a non-cultivable state. Fatty acid metabolism was significantly influenced with a ten-fold increase in the ratio of saturated fatty acid: unsaturated fatty acid content of the non-cultivable cells as compared with exponential phase of glucose grown *Rbx. benzoatilyticus* cells, signifying membrane rigidity.

GC-MS based metabolic profiling followed by multivariate statistical analyses of footprint (exometabolome) revealed the marked variation in the metabolism of malate and glucose grown cells. Metabolomes from different samples separated from each other forming distinct clusters, as observed in hierarchical clustering analysis, wherein the metabolomes from malate grown cells clustered together and those from glucose grown cells grouped together. Five component principal component analyses explained the variance amongst the samples suggesting different metabolic states. Partial least square- discriminat analysis identified the key metabolic features responsible for the differences in the metabolic state of the samples. Carbohydrates, fatty acids, organic acids, amino acid and their derivatives were largely responsible for metabolic dissimilarity and group segregation in the model. Amino acids and amines were specifically observed in the exometabolome of malate grown samples

while discrepancy in alkanes and fatty acids was more in the exometabolome of glucose grown samples as compared with the respective malate grown samples. We postulated that non cultivability of glucose grown cells is due to the metabolic reprogramming of *Rbx. benzoatilyticus* cells.

Genomic DNA, isolated from malate or glucose grown cells, unravelled nucleotide variations at 128 positions in comparison with *Rbx. benzoatilyticus* genome that was sequenced ten years back. Out of which, 57 variants, identified in both the genomes, were speculated to be a consequence of several passages that *Rbx. benzoatilyticus* cells underwent during the past ten years. Remaining 69 variations were unique to glc-genome which is perhaps the result of substrate (glucose) effect. Apart from this, two genes from the photosynthetic gene cluster 'spheroidene monooxygenase (EC 1.14.15.9)' and 'chlorophyll *a* synthase (ChlG; EC 2.5.1.62)' were truncated at N-terminal end in the glc-genome.

Exogenous glucose has effected *Rbx. benzoatilyticus* at different levels of cellular organization. Proteomic profiling revealed extensive metabolic remodelling in the glucose grown cells wherein signal-transduction, selective-transcription, DNA-repair, transport and protein quality control processes were up-regulated to cope with the changing milieu. Proteins involved in DNA replication, translation, electron-transport, photosynthetic machinery were down-regulated possibly to conserve the energy. Glycolysis/gluconeogenesis, tricarboxylic acid pathway and pigment biosynthesis were also down-regulated. The cell has activated alternative energy deriving routes *viz*., fatty acid β-oxidation, glyoxylate cycle, acetate-switch and Entner-Doudoroff pathway. Protein dynamic datum suggested that proteins related to primary metabolism down-regulated prior to those of secondary metabolism.

Here, the study illuminates the plausible cellular events and adaptive metabolic tactics employed by *Rbx. benzoatilyticus* in response to less-preferred carbon source (glucose). It also uncovered novel insights into the metabolic plasticity of APB to the fluctuating milieu. Overall, the omics analyses explicated the molecular/metabolic adjustment associated with glucose grown *Rbx. benzoatilyticus* cells. Present investigation intended to understand how glucose has globally influenced the metabolic networks of *Rbx. benzoatilyticus* modulating the metabolic phenotype. The study brought out a novel concept of "diabetic bacteria" which made us realize that many bacteria are intolerant to glucose. The research unlocks the gateway, enhancing our outlook to perceive microorganisms with new perspective in relation to their physiological life styles.

List of abbreviations

Acronym	Expanded form
malate/glucose	Either malate or glucose
µg	Microgram
µl	Microliter
µs	Microsecond
2D-LC/MS	Two dimensional liquid chromatography
ACN	Acetonitrile
AGE	Agarose gel electrophoresis
Aldh	Aldehyde dehydrogenase
APB	Anoxygenic photosynthetic bacteria
APS	Ammonium persulfate
ATP	Adenosine triphosphate
BLAST	Basic Local Alignment Search Tool
bp	Base pair
BSTFA	N,O-bis(trimethylsilyl)trifluoroacetamide
CLSM	Confocal laser scanning microscopy
CoA	Coenzyme-A
DEP	Differentially expressed proteins
DIC	Differential interference contrast
DNA	Deoxyribonucleic acid
ED pathway	Entner Doudoroff pathway
EMP pathway	Embden-Meyerhof-Parnas pathway
ETC	Electron transport chain
eV	Electron volt
FACS	Fluorescence-activated cell sorting
FAME	Fatty acid methyl esters
FC	Fold change
FDA	Fluorescein diacetate
FTIR	Fourier transformation infra-red
g	Force of gravity
$g.l^{-1}$	Gram per liter
GC-MS	Gas chromatography- mass spectrophotometry
gDNA	Genomic DNA
glc	Glucose
GO	Gene ontology
GRAVY	Grand average hydropathy index
h	Hour
HEPES	4-(2-hydroxyethyl)-1-piperazineethanesulfonic acid
HPLC	High performance liquid chromatography
iTRAQ	Isobaric tag for relative and absolute quantitation
KEGG	Kyoto encyclopedia of genes and genomes
LC-MS/MS	Liquid chromatography-tandem mass spectrometry
LHC	Light harvesting complex
LCB	Local collinear block
m/z	Mass-to-charge ratio
mal	Malate

min	Minutes
MK-8	Menaquinone-8
ml	Millilitre
mM	Millimolar
NCBI	National Center for Biotechnology information
NIST	National institute of standards and technology
nm	Nanometer
$^{\circ}$C	Degree Celsius
$^{\circ}$C.min^{-1}	Degree Celsius per minute
OD	Optical density
ox PPP	oxidative part of pentose phosphate pathway
PAGE	Polyacrylamide gel electrophoresis
PATRIC	Pathosystems Resource Integration Center
PCA	Principal component analysis
PHAs	Poly-β-hydroxyalkanoates
PI	Propidium iodide
PMF	Proton motive force
PPP	Pentose phosphate pathway
Q8	Ubiquinone-8
RAST	Rapid Annotation using Subsystem Technology
Rbx. benzoatilyticus	*Rubrivivax benzoatilyticus* JA2 (=ATCC BAA-35 =JCM 13220=MTCC 7087)
Rbx. gelatinosus	*Rubrivivax gelatinosus* IL144
RC	Reaction centre
RNA	Ribonucleic acid
rRNA	Ribosomal ribonucleic acid
SD	Standard deviation
SDS	Sodium dodecyl sulfate
SEM	Scanning electron microscopy
TCA cycle	Tricarboxylic acid cycle
TCEP	Tris (2-Carboxyethyl) phosphine
TEM	Transmission electron microscopy
TEMED	N,N,N′,N′-Tetramethylethane-1,2-diamine
TLC	Thin layer chromatography
Tris-HCl	Tris (hydroxymethyl) aminomethane hydrochloride
VIP	Variable importance in projection
w/v	Weight per volume

Chapter 1: Introduction

1. Introduction and literature survey

1.1. Omics: a multidisciplinary approach

As the life flourished from single-celled prokaryote to multi-celled eukaryote, so have the technologies to study and understand their complex regulatory mechanism, behaviour and adaptations. With the advent of highly sophisticated molecular biology techniques and state-of-art instruments, understanding the underlying regulatory mechanisms has become feasible. The multi-omics approach is not an exception to this, which removes the hurdles in understanding the entire spectrum of the organism's phenotype. This growing field comprises genomics that tells what can happen, transcriptomics that tells what appears to happen, proteomics that tells what makes it happen, metabolomics that tells what has happened and phenomics that tells what is observed to have happened (Fig. 1.1). Thus, the power of each one is bolstered by the other "omic" technology (De Maayer et al., 2014). Present study also made use of phenomics, metabolomics, proteomics and genomics to render dialectic thinking and to uncover the metabolic adaptations adjusted by *Rubrivivax benzoatilyticus* in response to the changing carbon regime.

1.1.1. Comparative genomics

Comparative genomics is the study where genomic features like: DNA sequence, genes, gene order, regulatory sequences and gene landmarks are compared between different organisms. The principle behind is that the evolutionarily conserved DNA often encodes the common features of different organisms (Harridson, 2003). Thus, the approach starts with aligning the genome sequences and looking for the orthologous sequences in the alignment which aids in inferring genome and molecular evolution that can be placed in context of population genetics or phenotypic evolution (Buddhi et al., 2020).

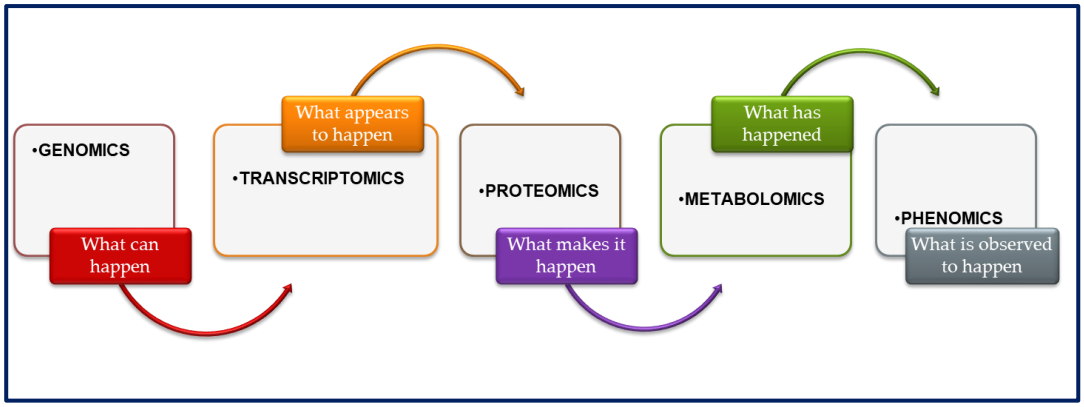

Fig. 1. 1: Cascade of events in omics.

Omics study comprises of genomics that tells about what can happen, transcriptomics that tells about what appears to happen, proteomics that tells about what makes it happen, metabolomics that tells about what has happened and phenomics that tells about what is observed to have happened.

Genomics has its root in the early 1980s with the comparison of viral genomes wherein picornaviruses (small RNA viruses that infect animals) and cowpea mosaic virus (infecting plants) were reported to share substantial sequence similarity and the gene order (Argos et al., 1984). The first large scale comparative genomic study compared the genomes from varicella-zoster virus and Epstein-Barr virus containing more than 100 genes each (Mcgeoch and Davison, 1986).

The first report of the genome sequence from free living cellular organism, *Haemophilus influenzae* Rd appeared in 1995 (Fleischmann et al., 1995). The next one published in the same year, being smallest free living parasitic bacterium, *Mycoplasma genitalium*, compared the genome of the two and it was the first comparative study of the genomes (Fraser et al., 1995). With this, new information on genomes were comparative-genomic studies, inevitably. For instance, with the availability of genome from *Saccharomyces cerevisiae*, the baker's yeast and the first eukaryote to have its complete genome sequenced (Goffeau et al., 1996), *Caenorhabditis elegans*, a roundworm (Consortium, 1998), and *Drosophila melanogaster*, a fruit fly (Adams et al., 2000), investigators compared the genomes of the three along with the prokaryote, *H. influenza*

(Rubin et al., 2000). Another research article on comparative analysis of human and mouse gene structure appeared in the same year (Batzoglou et al., 2000) and this was followed by an endless list of articles based on comparative genomics.

Next generation sequencing (NGS) have demonstrated the capacity to sequence DNA at unprecedented speed, thereby enabling previously unimaginable scientific achievements and novel biological applications (Zhang et al., 2010). NGS, introduced in 2007, have produced a massive genomic data allowing researchers to generate manifold genomic information at once. Mapping unassembled reads against a well annotated reference genome, it quickly uncovers single-nucleotide polymorphisms (SNP) or insertions and deletions providing a list of possible gene differences that could be the basis for (any) functional variation amongst species or strains (Hu et al., 2011).

The impact of NGS technologies on genomics will be far reaching and likely to change the field for years to come. *De novo* sequencing also called parallel sequencing as they are carried out by fragmenting the entire genome into small pieces and then ligating the latter to the designated adapters for random read along DNA synthesis (sequencing by synthesis). Since, sequences are assembled without comparing directly against the reference sequence; these technologies are appropriate for new genetic material or those that differs significantly from a previous sequenced strain (Bhattacharyya et al., 2002; Goo et al., 2004). Sequencing technologies have been applied in a wide range of contexts like whole-genome sequencing (WGS), detecting transcription factor binding sites and expression profiling of non-coding RNA.

Microbial metabolomics, proteomics and transcriptomics are variable and dynamic based on the environmental conditions, but genome is quite stable and thus plays a vital role in understanding the physiology of the organism. The expansion of NGS and its subsequently reduced cost have resulted in WGS a routine analysis for many studies including those of

coronavirus, the causative agent of recent pandemic Covid-19. To investigate the viral quasi-species, enormous strains and variants of coronavirus have been sequenced world-wide. The sequence of these strains has been compared to spot mutations the virus underwent and many more are in pipeline.

1.1.2. Proteomics

Proteomics is the large scale analysis of all the proteins in a cell at a particular instant or situation. Initially, proteomics was performed using 2D-gel electrophoresis wherein proteins with their estimated isoelectric point and molecular weights were compared to the database. Later, quantitative approaches utilizing the state-of-art instruments with mass spectrometry (MS) or tandem mass spectrometry (MS/MS) and stable isotope labelling offered gradual departure of 2D gel electrophoresis. The basic idea is that equal amount of one sample is derivatized with “light” isotope while the other incorporates “heavy” version of same chemical tag. Both the samples, after mixing together, are analyzed in the single experiment. Identical moieties of the different samples co-elute and the peaks are distinguishable by their mass difference due to the heavy and light isotope labels. The MS data quantitates the pairs of peaks and the MS/MS fragment data identifies them. As, the data from both the samples are collected in the same experiment, this technique eliminates the possibility of biasness that could have been introduced during peaks comparison from different experiments. Stable Isotope Labelling by Amino Acids in Cell Culture (SILAC) and Isotope coded affinity tags (ICAT) make use of this principle.

Tandem Mass Tags (TMT) reagents are a type of isobaric multiplexing tag, first reported in 2003. In the isobaric multiplexing tagging strategy, the overall molecular mass of each tag is same but the positions of light and heavy isotopes are adjusted so as to affect the mass of “reporter ion” and “balancer” regions within the compound (Fig. 1.2A). iTRAQ reagents also make use of heavy isotopes of carbon, nitrogen, and oxygen which are

incorporated into the structure in order to shift the reporter and balancer masses. Eight reporter ions are available to attain multiplexing of the order of eight samples thus, iTRAQ can minimize the overall time and variation.

The principle and workflow of iTRAQ

iTRAQ, introduced by Applied Biosystems Incorporation (2004), stands for Isobaric tag for relative and absolute quantitation. The isobaric tagging reagents comprise of a peculiar charged reporter group, a neutral balancer group, and a peptide reactive group. The latter labells all the peptides of a sample digest, by covalently linking an iTRAQ reagent's isobaric tag, to the amino group at the N-terminus along with that of lysine side chain. The neutral balancer group warrants the iTRAQ labelled-peptides, from different samples, exhibits the identical masses to retain an overall mass of 145 Da for 4-plex and 305 Da for 8-plex experiment (Fig. 1.2A).

The protein sample is hydrolyzed to yield a mixture of peptides. Generally, each protein sample is reduced, cysteine blocked, and digested with trypsin for an iTRAQ experiment. All peptides from single sample are labelled with one of the iTRAQ tag and those from different samples with different iTRAQ reagent tags. The labelled protein samples are mixed together to acquire the mass spectrum by subjecting the peptides to liquid chromatography-tandem mass spectrometry (LC-MS/MS) analysis. The same peptide from different samples, being identical in molecular weight irrespective of which iTRAQ reagent it is tagged, appears as the single peak in the MS (Fig. 1.2B). Each such peptide peak is collected separately to perform MS/MS where the balancer group detaches from the peptide reactive group and is lost. The same peptide, now with different isotopic labells, produces reporter ions with different masses, and thus exhibit different peaks (Fig. 1.2C). Analyzing the related data with software and databases provide the quantitative information.

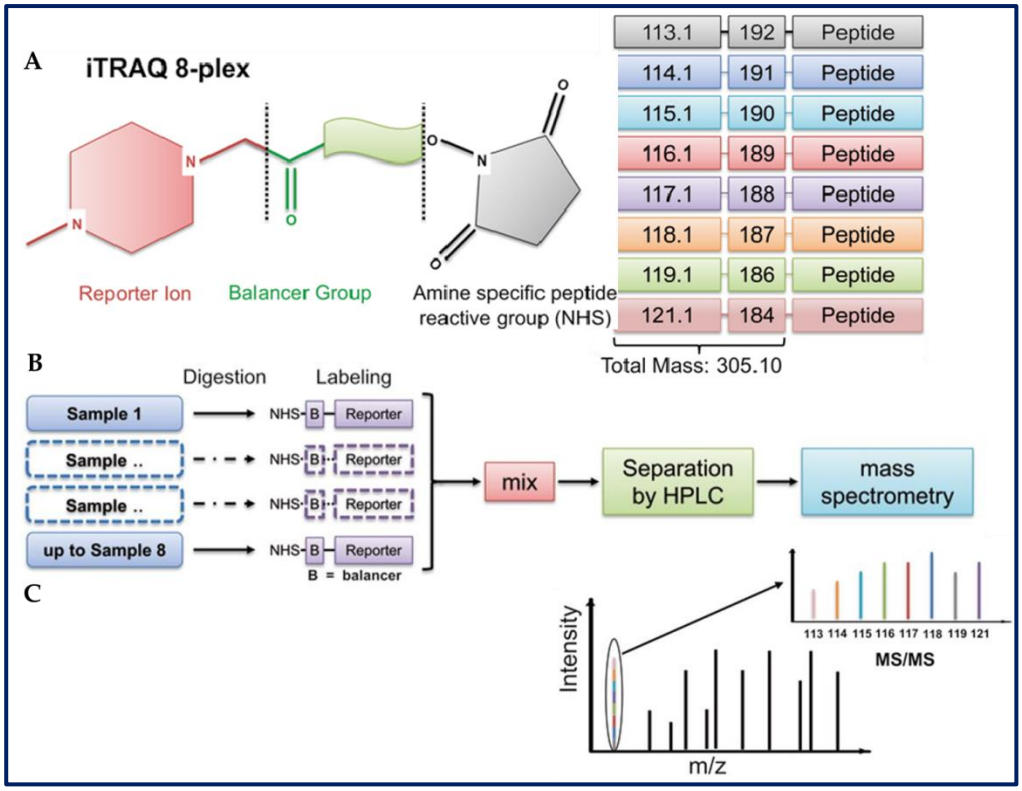

Fig. 1. 2: The workflow of iTRAQ proteome analysis.

Composition of the iTRAQ reagent (A), multiplexing up to 8 samples (B) and analysis by mass spectrometry (C).

iTRAQ reagent comprises of reporter ions with different mass, a balancer group for balancing the reporter ion isobaric with each other and a amine specific reactive group that links the reagent to peptide. Up to 8 samples are tagged with different iTRAQ reagents which are then mixed in a single tube to be separated by HPLC and analysed by mass spectrometry. iTRAQ, isobaric tag for relative and absolute quantitation; HPLC, high performance liquid chromatography; m/z, mass to charge ratio; MS/MS, tandem mass spectrometry.

1.1.3. Metabolomics

Metabolomics or metabolic profiling is the large scale scientific study of biochemical processes involving metabolites that can be substrates, intermediates or end products of the metabolism. Metabolites are end products of gene expression and metabolic profiling offers unique snapshot of physiological status of cell (Tremaroli et al., 2009; Tang, 2011) providing the glimpses of cellular metabolism in response to the perturbations. The first paper using the word ‘metabolomics’ dates back to 1998 (Oliver et al, 1998).

The study of extracellular metabolites has been prevalent in scientific literature (Badenoch-Jones et al., 1982; Vavilova et al., 1988; Tambiev et al., 1989). But, global exo-metabolite profiling was only realized during mid-2000 with recent advancement and improved chromatographic separation along with the detection of hundreds to thousands of compounds (Kell et al., 2005). Both LC-MS and GC-MS involve an initial chromatographic separation stage followed by separation according to their mass to charge ratio. Recent advances in mass spectrometry imaging have allowed for spatial localization of released metabolites (Louie et al., 2013). The first work to demonstrate the biological relevance of comparative profiling of exo-metabolite pools was not until 2003, when the term "metabolite foot-printing" was coined by Jess Allen and co-workers (Allen et al., 2003). This work attracted a great deal of interest in the community, particularly for characterization of microbial metabolism (Mapelli et al., 2008).

Exometabolomics, also known as metabolic foot-printing, makes use of changes in the culture medium as a result of cell growth, which can be achieved by comparing fresh or uninoculated media versus spent media (Silva et al., 2015). Often, fluctuations in the exometabolome mirror the changes happening inside the cell reflecting its metabolic state (Fu et al., 2014; Pinu et al., 2018).

1.2. Microorganisms are ubiquitously present

Microorganisms are continuously exposed to the ever-changing environmental conditions and they perceive a myriad of stimuli. Their successful colonization of niche and survival depends on sensing and orchestrating the gene expression which is under the control of the sophisticated complex regulatory system. Diverse environmental factors *viz.* pH, temperature, salinity, light, nutrients or oxygen modulates microbial cellular phenotype and bacteria remodels its metabolic/molecular machinery to adapt to the changing conditions. As a result, either they have adapted/tuned to these altering cues or they have adopted a strategy

to escape these fluctuations. Endo-sporulation (Errington, 2003; Wang et al., 2013), biofilm formation under unfavourable conditions (Stanley and Lazazzera, 2004), catabolic repression (Görke and Stülke, 2008), phenotype switching (Carja et al., 2014) and stringent response (Bergkessel et al., 2016; Carneiro et al., 2016) are some examples of the fine-tuned regulatory responses to the diverse cues. Highly sophisticated regulatory mechanisms and metabolic versatility allows the bacteria to colonize diverse habitats by extending the nutrient utilization range as well as molecular adaptations (Bobrovskyy and Vanderpool, 2013; Carbonero et al., 2014).

Bacteria have vast array of regulatory mechanisms allowing it to dwell in immensely diverse niches and acclimatize inhospitable surroundings (Boutte and Crosson, 2013). The stringent response allows bacteria to reprogram its regulatory mechanisms in response to the variable environment. The paucity of favourable environment leads the organism to switch to a prolonged non-growing state with very little to no metabolic activity. These non-growing states are much less investigated than growing states thus, rendering several basic bacterial physiology related questions unanswered (Bergkessel et al., 2016).

1.3. Bacteria and their viability

Bacteria spend majority of their life in non-growing states as a result, their viability is a silent question of controversy. The most commonly accepted definition for microbial viability is appearance of observable colony forming unit (CFU) when a sample is plated on a suitable solid medium or increase in turbidity in an appropriate liquid medium. But this definition lacks the status of cell wall/ membrane integrity status or metabolic activity. Nocker and Camper (2009) described different approach taking together culturability, membrane integrity and metabolic activity. Based on this approach, four different states of bacterial viability are possible. Firstly, the ‘living’ bacteria regarded as culturable with intact cell wall/ membrane and metabolically active. Second category is the ‘viable but non-

culturable' (VBNC) bacteria. Bacteria in this category are metabolically active with intact cell wall/ membrane but are not culturable. Next are the 'ghost' bacteria that have intact cell wall/ membrane but metabolically inactive and non-culturable. Finally, 'membrane compromised' cells that have compromised cell wall/ membrane without any metabolic activity and are non-culturable.

1.4. Photometabolism by anoxygenic phototrophic bacteria (APB)

Anoxygenic phototrophic bacteria (APB) are a physiological group of phototrophic bacteria which perform anoxygenic photosynthesis. The members of the phototrophic Proteobacteria are metabolically versatile as they are capable of metabolizing an array of carbon sources under different growth modes. Also they can grow under different growth modes *viz*. photolithoautotrophic, photolithoheterotrophic, photoorganoheterotrophic, chemoorganoheterotrophic (aerobic respiration [aerobic dark] and fermentation [anaerobic dark]) modes using an extended range of inorganic/organic compounds (Sasikala et al., 1993; Larimer et al., 2004; Adnan et al., 2015). They grow best as anaerobic photoorganotrophs and also have the capability to grow facultatively as aerobic or microaerophilic chemoorganoheterotrophs. They can photometabolize variety of inorganic/organic compounds wherein light and light reactions provides the energy and reducing equivalents respectively and the substrates catabolized serves as the by-products for growth of the organisms.

1.4.1. Their uniqueness

APB are unique as they lack photosystem II and thus carry out anoxygenic photosynthesis with more reduced electron donor than water. For photosynthetic electron donor, they depend on substances with a lower redox potential than water, such as reduced sulfur compounds, sulfur, molecular hydrogen or simple organic compounds (Pfennig, 1977). The acquisition of phototrophic ability in these bacteria occurred by lateral gene transfer as

advocated by the evidence of similar pigments and photocomplexes amongst different species (Nagashima et al., 1997).

1.4.2. Their occurrence

APB are pigmented bacteria, attracting attention because of their coloration and ability to perform photosynthesis in the absence of oxygen (Nagashima et al., 1997). They are present in fresh waters, brackish waters, marine habitats, wastewaters, hot spring waters, moist soils and paddy fields, sewage waters and are also found in the extreme conditions of Antarctica. Extremophilic phototrophs have provided new insights into the evolution of photosynthesis and play ecological roles as primary producers in their unusual habitats (Madigan, 2003). Anoxygenic phototrophic extremophiles includes *Thermochromatium tepidum, Chlorobium tepidum, Choloflexus aurantiacus, Rhodovulum sulfidophilum, Rhodovulum strictum, Rhodovulum iodosum, Rhodovibrio salinarum, Rhodovibrio sodomensis, Rhodothalassium salexigens, Rhodobium orientis, Roseospira mediosalina* (Imhoff, 2001), *Rhodopseudomonas acidophila* (Pfennig, 1969 now called as *Rhodoblastus acidophilus*) and *Rhodopseudomonas globiformis* (Pfennig, 1974; now called as *Rhodopila globiformis*).

1.4.3. Their application

Anoxygenic phototrotic bacteria grow in the polluted environments and have been potentially used in the waste remediation and treatment along with power generation (Gest and Kamen, 1949; Siefert et al., 1978; Hiraishi et al., 1989; Kobayashi and Kobayashi, 1995; Sasikala and Ramana, 1995a; Madukasi et al., 2010; Hülsen et al., 2016; Mahidhara et al., 2020). These bacteria are also known for the production of hydrogen, polyhyroxyalkanoic acids, carotenoids and metabolites useful in numerous applications (Sasikala et al., 1993; Sasikala et al., 1994; Sasikala and Ramana, 1995; Sunayana et al., 2005; Zeng et al., 2007; Kumavath et al., 2011; Ramaprasad et al., 2013; Mujahid et al., 2015; Mekala et al., 2019).

(Zeng et al., 2007)Also, they serve as an excellent model systems for the study of photosynthesis under diverse environmental cues (Roh et al., 2004; Steunou et al., 2004).

1.5. Different growth modes for different substrates

APB are capable of catabolising an array of carbon sources including CO_2, HCO_3^-, aromatics, alcohols, sugars, amino acids and organic acids under different growth modes like photoautotrophy, chemoautotrophy, photoheterotrophy, chemoheterotrophy, mixotrophy or fermentation. For instance, study on *Rbx. benzoatilyticus* revealed growth mode dependent differential metabolism of phenylalanine and activation of condition-specific pathways, suggesting growth-mode driven metabolic adaptations (Mekala et al., 2018).

1.6. Different pathways for different substrates

APB catabolises different substrates using different pathways. Some of the organic acids are catabolised *via* reverse TCA cycle; aromatic hydrocarbons *via* reductive hydrolytic cleavage and sugars *via* Emden-Meyerhof-Parnas (EMP) pathway, Entner-Doudoroff (ED) pathway or pentose phosphate pathway (PPP). They make use of different pathways which depends on the organism, substrate metabolized and the growth mode (K. Sasikala et al., 1993). For instance, *Rhodobacter sphaeroides* (renamed as *Luteovulum sphaeroides*; Suresh et al., 2019) and *Rhodobacter capsulatus* photometabolises glucose *via* ED pathway under phototrophic as well as chemotrophic growth but, fructose *via* EMP pathway under phototrophy and ED pathway under chemotrophy (Sasikala et al., 1993).

1.7. APB as excellent model systems for the study of photosynthetic regulations

The anoxygenic photosynthesis is a simpler form of photosynthesis than the oxygenic process and APB have emerged as an ideal model system for dissecting the physiology, biochemistry and molecular biology of photosynthesis (Raymond et al., 2003; Swingley et al., 2009). Species of *Rhodobacter* and *Rhodopseudomonas* have been the workhorses for the laboratory studies of anoxygenic photosynthesis. The studies with anoxygenic phototrophs

have contributed for understanding the evolution of photosynthesis in major ways (Raymond et al., 2003; Swingley et al., 2009)., They rely on substances with lower redox potential than water for photosynthetic electron donor, *viz.* reduced sulfur compounds, sulfur, molecular hydrogen or simple organic compounds (Pfennig, 1977). Phototrophic bacteria have simplified photosynthetic apparatus with fewer subunits and unique photosystem, albeit their carbon metabolism pathways are rather complex (Gennis, 1993; Blankenship, 2002).

The photosynthetic apparatus is encoded by numerous genes organized in a so-called photosynthetic gene cluster (PGC). PGC, a cluster of gene organization in several photosynthetic bacteria, is crucial for environmental adaptation (Liotenberg et al., 2008). PGC contain five main sets of genes: *bch*, *puf*, *puh* (for RC assembly), *crt* and various regulatory genes. The length of *L. sphaeroides* PGC is 40.7 kb comprising 38 open reading frames encoding the reaction center H, L and M subunits, the alpha and beta polypeptides of the light- harvesting I (B875) complex, and the enzymes of bacteriochlorophyll and carotenoid biosynthesis (Naylor, 1999). The LH II polypeptides are encoded by a region of DNA lying outside the PGC known as the puc operon (Youvan & Ismail, 1985).

Anoxygenic photosynthesis is tightly regulated. APB have been an excellent model systems to understand the photosynthetic regulation and their adaptive responses to different growth modes (Kiley and Kaplan, 1988; Tadros et al., 2000; Braatsch et al., 2002; Maness et al., 2002; Steunou et al., 2004; Hassani et al., 2010; Lu et al., 2018;). Previous studies uncovered how environmental cues such as light and oxygen modulate growth and photosynthetic machinery in APB (Roh et al., 2004; Steunou et al., 2004). Though APB thrive under diverse habitats, studies related to their adaptive strategies to changing conditions are largely restricted to few environmental cues (Roh et al., 2004; Glaeser and Klug, 2005; Volpicella et al., 2014; Mujahid et al., 2015; Zhao et al., 2015; Wasai et al., 2018).

1.8. Rubrivivax benzoatilyticus, a betaproteobacterium and a member of APB

Rubrivivax benzoatilyticus is an anoxygenic phototrophic bacterium and the type strain was isolated from a flooded paddy soil near Eluru, Andhra Pradesh, India and culture is also available at different culture collections (=ATCC BAA-35^T = JCM 13220^T = MTCC 7087^T) (Ramana et al., 2006). *Rbx. benzoatilyticus* has capability to utilize a range of aliphatic and aromatic hydrocarbons as growth substrates under different growth modes (Ramana et al., 2006). But, longer phototrophic incubations on glucose eventually resulted in photobleaching and inoperative photosynthetic gadgetry of the organism (Gupta et al., 2019).

Menaquinone-8 (MK-8) and ubiquinone-8 (Q8) are the two major quinones of *Rbx. benzoatilyticus* (Gupta et al., 2019). *Rbx. benzoatilyticus* contains sphaeroidene, spirilloxanthin and bacteriochlorophyll *a* as pigment system (Ramana et al., 2006). It has a unique chimeric pathway for carotenoid biosynthesis that is both spirilloxanthin as well as spheroidene biosynthetic pathway (Ramana et al., 2006). On the other hand, this is not the case with other APB which have either of the two pathways. Also, genomic information of *Rbx. benzoatilyticus* is available in NCBI database (Mohammed et al., 2011).

1.9. Bacterial adaptations to combat inhospitable environment or stress

Bacteria are ubiquitously present in the nature and they are constantly exposed to the dynamic environmental changes perceiving a myriad of stimuli for instance, nutrition, pressure, temperature, light, pH, salinity, chemicals and many others. As a result, either they have adapted/tuned to these altering cues or they have adopted a strategy to escape these fluctuations. These environmental stimuli choreograph the preferences of metabolic pathways leading to a transformed phenotype. The phenotypic switch is reflected as alterations in the morphology or membrane profiling of the organism. Bacteria adopt several survival tactics to overcome which are as mentioned below:

1.9.1. Membrane modifications are the frontline adaptation for bacteria

Cell membrane or envelope is the protective barrier at the frontline of interaction with the surroundings. Bacteria, being poikilotherms, cannot insulate themselves from the environment, nor can they move away from environmental disturbances this leaves them vulnerable to physical and chemical perturbations (Russel, 1997). Indeed, bacteria repair and modify their envelope in response to environmental assaults. Different bacterial taxa have evolved strategies for maintaining membrane fluidity in response to environmental perturbations. Bacteria adjust their phospholipid composition in response to temperature stress as observed in *Bacillus caldotenax* and *Bacillus megaterium* (Denich et al., 2003). But, changes in phospholipid composition are less commonly documented than changes in fatty acyl chain composition.

Cyclopropane fatty acyl chains, commonly found in Gram-negative bacteria, confer fluidity of cell membrane assisting in tolerance towards the disturbance (Russel, 1984). In response to perturbations, bacteria amend their phospholipid's acyl chain organization by altering the proportion of (1) saturation to unsaturation, (2) cis to trans unsaturation, (3) branched to unbranched structures and type of branching, and (4) acyl chain length (Denich et al., 2003). Altering the proportion of saturated-unsaturated fatty acid is the most commonly observed mechanism to modulate membrane fluidity as long term response (Russel, 1984). The probable reason for this could be the kink in the hydrocarbon chains introduced by the cis-double bond of unsaturated fatty acids that causes them to spread apart (Gruner et al., 1985). Cis-unsaturated fatty acids, owing to their bent steric structures, do not pack efficiently (Heipieper et al., 1994). Trans-unsaturated fatty acids, due to their long linear structures that behave more like saturated fatty acids lying in a linear manner, take up lesser volume creating a more ordered membrane (Diefenbach et al., 1992). When cells are not

actively growing, conversion of the cis to trans ratio is an energy efficient alternate way to regulate membrane fluidity as short term response (Die-fenbach et. al., 1992).

1.9.2. Chaperones induce stress tolerance

Molecular chaperones are well-known for contributing to cellular homeostasis of the cells under both optimal as well as adverse growth conditions. They are responsible for protein folding, assembly, translocation and degradation across an array of cellular processes. During stress episodes, proteins tend to aggregate, these denatured or aggregated proteins hamper the growth of the cell. Heat shock proteins, that are mainly chaperones, co-chaperones and proteases, prevent aggregation, refold the misfolded proteins or degrade denatured proteins thereby helping in the quality control of proteins (Dunlop, 2011). Thus, the different classes of chaperones, in synchrony, play complementary and often overlapping roles contributing to the protection of the cell (Wang et al., 2003).

1.9.3. PHA granule formation

Many bacteria produce poly-β-hydroxyalkanoates (PHAs) as intracellular storage compounds for carbon and energy (Quillaguaman et al., 2010; Sasikala and Ramana, 1996). PHA granules are endobiopolymers, chemically polyesters of β-hydroxyalkanoic acids, forming water insoluble inclusion bodies in the cytoplasm (Gorenflo et al., 1999). These inclusion bodies are composed of hydroxyalkanoic acid polymer and catalytic or non-catalytic proteins on its surface, predominant ones being 3-hydroxybutyrate (3HB) homopolymers or copolymer of 3HB and 3-hydroxyvelarates (Sudesh et al., 2000). PHA synthase are catalytic proteins involved in the synthesis and degradation of PHAs. Phasins are non-catalytic proteins that are involved in the formation and regulation of PHA granules (York et al., 2001; Galan et al., 2012). Based on the degree of polymerization, PHAs are categorized as short chain, medium chain or long chain PHAs. In bacteria, fatty acid biosynthesis/degradation and many other pathways provide monomers for PHAs biosynthesis

(Sudesh et al., 2000). PHAs enhance the survival of bacteria under environmental stress (Castro et al., 2010). Numerous environmental and endogenous signals *viz.* nutrient limitations, desiccation, nitrogen/carbon ratio, toxic chemical stress and sporulation induce PHA biosynthesis in bacteria (Gorenflo et al., 1999). Biosynthesis and accumulation of PHA during temperature stress was implicated by *Pseudomonas aeruginosa* PAO1 (Pham et al., 2004) while, disruption of PHA biosynthesis reduced the survival ability of *Aeromonas hydrophila* 4AK4 under stress conditions (Zhao et al., 2007). PHA content positively correlated with increased survival rates of *Pseudomonas* sp. exposed to adverse conditions like UV irradiation, desiccation, thermal, oxidative stress, salinity and osmotic pressure (Castro et al., 2010).

1.9.4. ROS generation

Reactive oxygen species (ROS) seems to play a role in mediating cellular homeostasis or signals to combat stress either in a constructive or destructive way. The ROS accumulation and scavenging mechanisms seem to balance the pathways influenced by stress. How these operate in combating the stress is still elusive. Various studies have shown that the reactive oxygen species are potentially strong enough not only to cause oxidative damage to cells during stress but also play a crucial role as signal molecule during environmental stress (Torres et al., 2006). The rapid ROS accumulation is essentially a prerequisite for the cell and studies revealed that during stress, accumulated ROS primarily depends on the balance between ROS produced and ROS scavenged (Kwak et al., 2006). This balance critically depends on various factors like alterations in growth conditions, the stress duration, severity and also the ability of system's molecular machinery to rapidly acclimatize with the energy imbalance (Yatsunami et al., 2014).

1.9.5. Metabolic adaptations

The key goal of the organism is to 1) preserve the energy supply and biosynthetic precursors for maintaining the vital macromolecular constituents of the cell; 2) sustain active regulatory mechanism for sensing and responding to the surroundings and 3) preserve the electrochemical gradient of the membrane (Koch, 1997; Nyström and Gustavsson, 1998). The continual supply of energy and building blocks is greatly interdependent on the maintenance of the PMF (Bergkessel et al., 2016). Most bacteria redirect their metabolism with impressive metabolic flexibility, switch to alternate routes for energy and building blocks at the same time balancing flux through central metabolic pathways as a response to specific nutrient supply limitations.

1.9.5.1. Alternate substrates as sources for energy and re-routing the metabolic pathways for biosynthesis

Cells adopt a strategy and catabolise cellular components serving two purposes: providing nutrients and removing the extra burden of upholding cellular machinery that became dispensable. As a result, there is a shrinkage in cellular size and volume which improves the surface area to volume ratio of the cell, theoretically, increase in efficiency of substrate transport (Bergkessel et al., 2016). A microarray analysis of carbon starved *Vibrio harveyi* cells showed up-regulation of genes involved in fatty acid β-oxidation concomitant with reduced cell size. Genes involved in metabolic reactions requiring acetyl-CoA, major product generated from fatty acid degradation, also up-regulated. Several of these genes are involved in the glyoxylate shunt, an anaplerotic pathway that bypasses steps of tricarboxylic acid (TCA, substantially down-regulated during starvation) cycle that produces reducing equivalents (Kaberdin et al., 2015). Thus, another strategy that cell adopts is to re-route metabolic flux.

1.9.5.2. Tuning the capacity and degree of gene expression to compensate the limited substrate

The common features of the non-growing states are the limitations for energy, nucleotides and amino acids that perhaps impose constraints to gene expression. The sigma factor RpoS and the stringent response alarmone guanosine pentaphosphate, together, leads to the decline in total rates of gene expression. They also lead to redirection of biosynthetic capacity away from ribosome biogenesis to prevention or repair of DNA damage, osmoprotection, refolding damaged proteins or increasing the synthesis of missing biosynthetic intermediates (Bergkessel et al., 2016).

Strategy for tolerating shortage of nucleotides and amino acids is to limit the count of active polymerases and ribosomes. As a result, fewer of these complexes compete for the limited supply of substrates. Ribosome degradation has vital role in regulating the number of ribosomes with dual benefits of limiting the active ribosomes and converting unused ribosomes to nutrients (Deutscher, 2003; Zundel et al., 2009).

1.10. Glucose, key determinant of cell fate

Carbon source is a vital factor (essential nutrient) that shapes the microbial physiology and metabolism (Ruiz et al., 2010; Bester et al., 2011; Bren et al., 2016; Waschina et al., 2016; Westfall and Levin, 2018). Sensing and adapting to the fluctuating carbon sources in the environment is crucial for survival (Kotte et al., 2010; Chantranupong et al., 2015). A number of recent studies demonstrated that carbon source has profound effect on cellular phenotype and microbial behaviour (Bester et al., 2011; Njoroge et al., 2012; Kotte et al., 2014; Wang and Tang, 2017; Westfall and Levin, 2018). Carbon sources are known to alter the cellular physiology and photosynthetic machinery in phototrophic organisms like plant, algae (Koch, 1996; Graverholt and Eriksen, 2007; Oesterhelt et al., 2007) and cyanobacteria (Lebedeva et al., 2005). APB are capable of using an extended

range of carbon source for their growth under different growth modes; yet, how they respond and adapt to the changing carbon regimes is largely unexplored.

Glucose was well reported to limit photosynthetic apparatus in plants, algae (Koch, 1996; Graverholt and Eriksen, 2007; Oesterhelt et al., 2007) and cyanobacteria (Lebedeva et al., 2005). Apart from micro-organisms and photosynthetic organisms, external glucose causes dysfunctioning of mitochondria as observed in endothelial cells (Koziel and Woyda-ploszczyca, 2012) and is a key determinant of cell fate (Poulsen et al., 2014). Also, glucose is well documented for causing diabetes which effects different organs causing disorders like retinopathy. Furthermore, at the molecular level also, reports suggest glucose affects functioning of mitochondria, inducing ROS (Fakhruddin et al., 2017), generation of SNPs or instability of DNA leading to the transformed phenotype.

Currently, there are knowledge gaps on molecular/ metabolic adaptations of APB in response to external perturbations caused by carbon source (glucose). Glucose evidently altered cellular morphology and modulated metabolism of *Rbx. benzoatilyticus* at the same time boosting alternate energy driving routes (Gupta et al., 2019). The present study is an attempt to glean novel biological insights using omics approach.

1.11. Rationale behind this study

The biochemistry of glucose photometabolism by APB was comprehensively investigated for a decade (1970 – 1980). But, these studies were confined to the metabolism of *L. sphaeroides* and *R. capsulatus*. Though, *L. sphaeroides* or *R. capsulatus* grew on glucose photoheterotrophically as well as chemoheterotrophically without photobleaching. However, cells of another APB, *Rbx benzoatilyticus*, when grown on glucose photoheterotrophically were photobleached on longer phototrophic (anaerobic light) incubations, which is not the case with *L. sphaeroides* or *R. capsulatus*. Lethal effect of glucose was also observed on chemotrophic bacteria (*Salmonella),* yeast (*Saccharomyces*)

and other organisms. Thus, today we realised that many bacteria are intolerant to glucose. Thereby, we propose that this subject of 'microbial glucose metabolism' also need due attention that will open the "black box" of the arena, "diabetic bacteria", in relation to their physiological life styles.

Despite being so versatile in growth modes and carbon source utilization, a paradigm shift from glucose as electron donor to its lethality on *Rbx. benzoatilyticus* was observed and this caught our attention. The subject anaerobic 'photometabolism of glucose', albeit, extensively studied during 1970's and 1980's, remained largely untouched thereafter. These studies were mainly restricted to either *R. capsulatus* or *L. spheroides* as model organisms which cannot be generalized to the entire APB group. Thus, how other members of APB respond to the glucose photometabolism is a long standing mystery.

Further, hyperglycemic effect on eukaryotic cells of macro-organisms is well documented but the same on micro-organisms is not investigated so far. Thus, the extent to which it is lethal for the microorganism is still an open question. A robust study at cellular level is required to better understand the influence of glucose to the metabolic pathways at physiological level. This provoked us to probe into the insights of the glucose photometabolism with altogether a different organism (other than *L. sphaeroides* or *R. capsulatus*), *Rubrivivax benzoatilyticus* with the following aim.

1.12. Key goal of this study

To comprehend the toxic effect of glucose photometabolism by *Rubrivivax benzoatilyticus*.

1.12.1. Objectives of this study

To achieve the key goal, study was commenced with two broad objectives -

- To decipher the adaptive response of *Rbx. benzoatilyticus* in the presence of glucose over malate.
- To elucidate the dynamic events leading to lethality caused by glucose on *Rbx. benzoatilyticus*.

Chapter 2: Materials and methods

2. Materials and Methods

2.1. Glassware, chemicals and devices

2.1.1. Glassware and cleaning

The glassware used for this study including the test tubes, measuring cylinders, pipettes, culturing flasks, petri dishes, reagent bottles, screw cap test tubes were either of Borosil or Duran brand. The glassware were soaked in the diluted chromic acid solution (potassium dichromate and sulphuric acid) for overnight and washed with tap water and teepol detergent and finally rinsed with deionized water and dried.

2.1.2. Deionized water

Deionized water was acquired from deionizer plant (ion exchange India Ltd. Model-CA20/U). Distilled and double distilled water were obtained from the distillation plant (Millipore) and used for the preparation of media, stock solutions and reagents.

2.1.3. Chemicals

The analytical grade chemicals from HiMedia, Sigma-Aldrich, Fluka, Merck solvents, Fermentas and Thermofisher Scientific were used for this study.

2.1.4. Determination of pH

pH of the culture media and stock solutions were determined using a digital pH meter (Digisun electronics, India model DI-707). The pH meter was often calibrated using standard buffer solutions (pH 4.2, 7 and 9.2).

2.1.5. Buffers and standard solutions

Buffer solutions were prepared in deionised or sterile (Milli Q) water . Buffers were prepared using standard protocols and the pH was adjusted at room temperature.

2.1.5.1. General buffers

Phosphate buffer: 50 mM potassium phosphate, pH range 5.5, 6.5, 7.5.

Phosphate buffered saline (PBS): 137 mM NaCl, 2.7 mM KCl, 10 mM Na_2HPO_4 and 1.8 mM KH_2PO_4; pH 7.4

Borate buffer: 50 mM borate, pH 10.

Tris buffer: 50 mM Tris/HCl, pH 7.5

2.1.5.2. Buffers used for proteome analysis

Proteome extraction buffer: 50 mM HEPES-KOH, pH 7.5; 0.1% SDS (w/v), 0.1% Triton-X-100 (w/v).

Re-suspension buffer: 50 mM Tris, pH 8.0; 100 mM NaCl, 1 mM EDTA.

2D Nano LC-ESI-MS/MS: Buffer A (98% H_2O, 2% acetonitrile (ACN), 0.1% formic acid, and 0.005% trifluoroacetic acid (TFA; v/v),

Buffer B (100% ACN, 0.1% formic acid, and 0.005% TFA (v/v).

2.1.5.3. SDS-PAGE buffers and solutions

Stacking gel: 5% polyacrylamide (30/0.8 acrylamide/bisacrylamide (w/w)); 125 mM Tris/HCl, pH 6.8; 0.1% (w/v) SDS; 0.015% (v/v) TEMED; 0.05% (w/v) APS.

Separating gel: 12.5% polyacrylamide (30/0.8 acrylamide/bisacrylamide (w/w)); 375 mM Tris/HCl, pH 8.8; 0.1% (w/v) SDS; 0.015% (v/v) TEMED; 0.05% (w/v) APS.

Running buffer: 25 mM Tris/HCl, pH 8.3; 0.192 M glycine; 0.1% (w/v) SDS.

Sample/loading buffer (5x concentrated): 50 mM Tris/HCl, pH 6.8; 100 mM DTT;

2% (w/v) SDS; 0.1% bromophenol blue; 10% glycerol.

Fixation/staining solution: 0.1% (w/v) Coomassie brilliant blue R-250 dissolved in 45/45/10 Methanol/H_2O /acetic acid (v/v/v).

Destaining solution: 12.5/77.5/10 isopropanol/H_2O dest /acetic acid (v/v/v).

2.1.6. Reagents for sugar estimation

Alkaline copper tartarate: 96 ml reagent A + 4 ml reagent B

Reagent A−2.5 g Na_2CO_3, 2.0 g $NaHCO_3$, 2.5 g potassium sodium tartarate and 20 g Na_2SO_4 dissolved in 100 ml water.

Reagent B−15 g $CuSO_4$ dissolved in 100 ml water. A drop of H_2SO_4 was dispensed.

Arsenomolybdate reagent: 2.5 g $(NH_4)_6Mo_7O_{24}$, 2.5 ml H_2SO_4 dissolved in 45 ml water was mixed well with 0.3 g Na_2HAsO_4 dissolved in 25 ml water and incubated at 37 °C for 24 to 48 h.

2.1.7. Dyes for confocal microscopy

Nile red and fluorescein diacetate (FDA) stock solutions (1 $mg.ml^{-1}$, w/v) were prepared in DMSO (dimethyl sufoxide) and 1 $mg.ml^{-1}$ (w/v) calcofluor white, resazurin and propidium iodide (PI) stock solutions were prepared in sterile Mill-Q water. All the dyes were stored at -20°C in dark.

2.2. Media preparation and sterilization

2.2.1. Malate mineral medium (ingredients $g.l^{-1}$)

KH_2PO_4 -0.5, $MgSO_4.7H_2O$ -0.2, NaCl-0.4, NH_4Cl -0.37, $CaCl_2.2H_2O$-0.05, Malate-3.0, yeast extract-0.2, ferric citrate (0.1% w/v) 5 $ml.l^{-1}$, Trace elements SL7 1 ml. (SL7 ($mg.ml^{-1}$): HCl (25% v/v) 1 ml; $ZnCl_2$-7; $MnCl_2.4H_2O$-100; H_3BO_3-60; $CoCl_2.6H_2O$-200; $CuCl_2.H_2O$-20; $NiCl_2.6H_20$-20; $NaMoO_4.6H_2O$-40). Media components were dissolved in distilled water and the pH of 6.8 was adjusted with 5N NaOH. Malate was substituted with other carbon sources (22 mM), except glucose, whenever required.

2.2.2. Glucose mineral medium

Glucose-medium was prepared by adding sterile glucose (dextrose) stock (2 M) to separately autoclaved mineral medium (without carbon source) to give a final concentration of 22 mM.

2.2.3. Nutrient agar (ingredients $g.l^{-1}$)

NaCl - 5, Peptone -10, yeast -3.5 and agar-20; pH 7.0

2.2.4. Sterilization

Culture media, glassware, microcentrifuge tubes and microtips were sterilized by autoclaving at 15 lbs, 120°C for 20 min. Thermolabile stock solutions were filter sterilised through 0.22 µm membrane filter (Millipore).

2.3. Organism and growth conditions

2.3.1. Organism

Rubrivivax benzoatilyticus $JA2^T$ (=ATCC $BAA\text{-}35^T$=JCM 13220^T= MTCC 7087^T) was taken as the model organism for all the experiments.

2.3.2. Photoheterotrophic (Anaerobic) and aerobic growth

Rbx. benzoatilyticus was grown photoheterotrophically (anaerobic, 30 ± 2°C; light 2,400 lux) in fully filled screw cap test tubes (15 ml capacity) on mineral medium supplemented with ammonium chloride (7 mM) as nitrogen source and either malate (as control) or glucose (22 mM) as carbon source/electron donor at pH 6.8. Exponential phase malate grown cells (OD_{660nm} ~0.25) were used as inoculum (10%). For aerobic experiments, culture was grown in 250 ml Erlenmeyer flasks (⅓ volume) with shaking at 150 rpm and 30°C.

2.3.3. Maintenance of stock culture

Rbx. benzoatilyticus stock culture was preserved as agar stabs. Stabs were prepared in malate mineral medium containing agar (2 % w/v), filled to the ¾ volume of screw cap test tubes (5 ml capacity). Pure culture of *Rbx. benzoatilyticus* was stabbed into the solidified mineral medium, illuminated (2,400 lux) and incubated at 30 ± 2°C. After 2-3 days of growth, the stab cultures were preserved under refrigeration (4°C) for further use.

2.3.4. Purity of the cultures

Purity of the culture was regularly monitored before and after the experiment. Culture was routinely streaked on nutrient agar plates and incubated at 30 ± 2°C for examining its purity.

2.3.5. Growth and biomass

Growth was monitored turbidometrically ($OD_{660\ nm}$) using colorimeter (Systronics Model-112) against un-inoculated media as blank. Biomass was calculated as dry weight using the formula 0.1 ($OD_{660\ nm}$) = 0.15 mg.dry wt.ml^{-1} generated from the plot of OD at 660 nm against dry weight.

2.3.6. Bacterial viability

Viability was determined by streaking the cells on nutrient agar petri plates under aseptic conditions and observing colonies after 48 h incubation. Otherwise, passaging the cells on malate mineral medium and observing for turbidity under photoheterotrophic growth.

2.3.7. Preparation of resting cells

Rbx. benzoatilyticus cells were grown on malate minimal medium for 48 h under photoheterotrophic conditions. After exponential growth phase, cells were collected by centrifugation (10,000 x g; 4°C; 10 min) in sterile Okridge tubes (Tarson) under aseptic conditions. Spent media was discarded; cell bio mass, after washing with mineral medium devoid of carbon source, was re-suspended in malate or glucose medium for further experimentation.

2.4. Microscopic analysis

2.4.1. Differential interference contrast (DIC) microscopy

Malate/glucose grown logarithmic and stationary phase live cultures were mounted on glass slides and directly visualized under 100 X objective of DV-ELITE microscope (GE Healthcare Life Sciences). Atleast five random loci were visualized for each sample.

2.4.2. Confocal laser scanning microscopy (CLSM)

Glucose grown stationary phase cells were harvested by centrifugation (10,000 x g, 4°C, 8 min) and stained with FDA, nile red and calcofluor white by dispensing 5 µl of each dye (1 $mg.ml^{-1}$) to the cells. After 20 min incubation in dark, leftover dye was removed and the cells were washed with sterile Mill-Q water. Similarly, cells were also stained with resazurin and PI. Stained samples, after mounting on glass slide, were seen under confocal microscope. Probes were examined at their corresponding excitation and emission wavelengths- FDA ($Ex_{490}/Em_{514\ nm}$), nile red ($Ex_{552}/Em_{636\ nm}$), calcofluor white ($Ex_{400}/Em_{480\ nm}$).

2.4.3. Flow cytometric analysis

The flow cytometric assay (FCA) was performed on a BD FACSAria cell sorter (Becton Dickinson Biosciences) using FACSDiva Version 6.1.3 software. Stationary phase malate or glucose grown cells stained with FDA ($_{Ex}$ 490/$_{Em}$ 514 nm) were used for the assay. Cells were harvested (10,000 x g, 4°C, 8 min), immediately stained and incubated in dark for 20-25 min at room temperature before analysis. Stationary phase malate grown cells and the same killed artificially (by keeping it in boiling water bath for 15-20 min) were used as positive and negative control respectively for FDA staining of glucose suppressed cells. The experiment was repeated thrice and the pattern was reproducible.

2.4.4. Scanning electron microscopy (SEM)

Cells of stationary phase malate or glucose grown cultures were harvested by centrifugation (10,000 x g, 4°C, 8 min) and samples were prepared for scanning electron microscopy (SEM) as reported by Mujahid et al. (2015) with slight amendments. Cell pellet was washed with 0.1M PBS, pH 7.2. Washed cells were prefixed in mixture of glutaraldehyde (2.4% final concentration) and ruthenium red (0.01%) for 30 min at 4°C; centrifuged and suspended in the same for overnight fixation at 4°C. Fixed cells were

removed by centrifugation (10,000 x g, 4°C, 8 min), washed thrice with PBS and post-fixed for 2 h at 4°C in 1% osmium tetroxide solution. Post-fixed cells were collected by centrifugation (10,000 x g, 4°C, 8 min), washed thrice with PBS followed by series of ethanolic washes (20%, 30%, 50%, 70%, 90% & 100% ($^{v}/_{v}$)) for dehydration. Finally, cells were incubated in 100% ethanol for 20 min. Dehydrated cells, after mounting on glass pieces (0.5 x 0.5 cm) and drying in a critical point dryer, were fixed to SEM stubs; sputtered with gold and examined under SEM (ZEISS, FEG, Ultra 55- using 5 keV).

2.4.5. Transmission electron microscopy (TEM)

Malate or glucose grown cells of stationary phase culture were centrifuged (10,000 x g, 4°C, 8 min); suspended in PBS (0.1 M, pH 7.4) and outsourced to Ruska labs, Rajendranagar, Hyderabad, India for fixing and TEM sectioning. The protocol adopted in brief; the cells were prefixed in 2.5% glutaraldehyde in 0.1 M phosphate buffer (pH 7.2) at 4°C for 24 h. Later, cells were washed with PBS and post-fixed in 1% osmium tetroxide for 2 h, then washed with deionized water. Samples were dehydrated by series of ethanolic washes; infiltrated and embedded in araldite 6005 resin or spur resin for 48-72 h at 60-80°C for complete polymerization. Ultrathin (50-70 nm) sections were made with a glass knife on ultra-microtome (Leica Ultra cut UCT-GA-D/E-1/100); mounted on copper grids; stained with saturated uranyl acetate, counter stained with Reynolds lead citrate and observed under TEM (Tecani).

2.5. Extraction and isolation

2.5.1. Extraction of pigments

Sample from the culture (5 ml) was centrifuged; supernatant was discarded and the packed cells were resuspended in a small volume of water. Pigments (carotenoids and bacteriochlorophyll *a*) were extracted with methanol: acetone (2:7 v/v) for qualitative and quantitative analysis of pigments. The absorbance was read at 456, 510 and 775 nm

spectrophotometrically (for quantitative analysis) and expressed as "per mg dry weight" (Cohen-Bazire et al., 1957).

2.5.2. Isolation of photosystems

Cells of stationary phase malate or glucose grown cultures were centrifuged. The supernatant was discarded and the cell biomass was dissolved in 50 mM Tris-HCl buffer (pH 7.5 and containing 0.1% triton X-100), for sonication followed by overnight incubation at 4 $^{\circ}$C. The sonicated samples were centrifuged at 18,000 X g, 4 $^{\circ}$C for 30 min to remove cell debris. Clear supernatant was layered onto a sucrose step gradient (0.8 M to 0.2 M). The gradients were centrifuged at 180,000 X g for 16 h at 4 $^{\circ}$C to separate the reaction centre and light harvesting complexes. The bands thus obtained were collected and the absorption spectra were recorded from 300 to 900 nm.

2.5.3. Extraction of quinones

Quinones were extracted in chloroform methanol (2:1 v/v) from equal biomass (dry weight) of culture; evaporated to dryness; again extracted in acetone; purified by preparative TLC with petroleum ether: diethyl ether = 8:2 (v/v) as solvent system. Extracted quinones were detected by HPLC using methanol: diisopropyl ether=3:1 (v/v) as solvent system.

2.5.4. Extraction of extracellular metabolites (exometabolome)

Glucose (22 mM) and malate (22 mM) grown cultures were harvested by centrifugation. Cell biomass was used for proteome analysis (refer to section 2.7.1) and spent media for metabolome analysis (Fig. 2.1). Culture supernatant was evaporated to dryness in the rotary flash evaporator and metabolites were extracted by adding 1 ml methanol. Methanol extract was used for GC-MS analysis (section 2.6.4) followed by multivariate statistical analysis (Fig. 2.1).

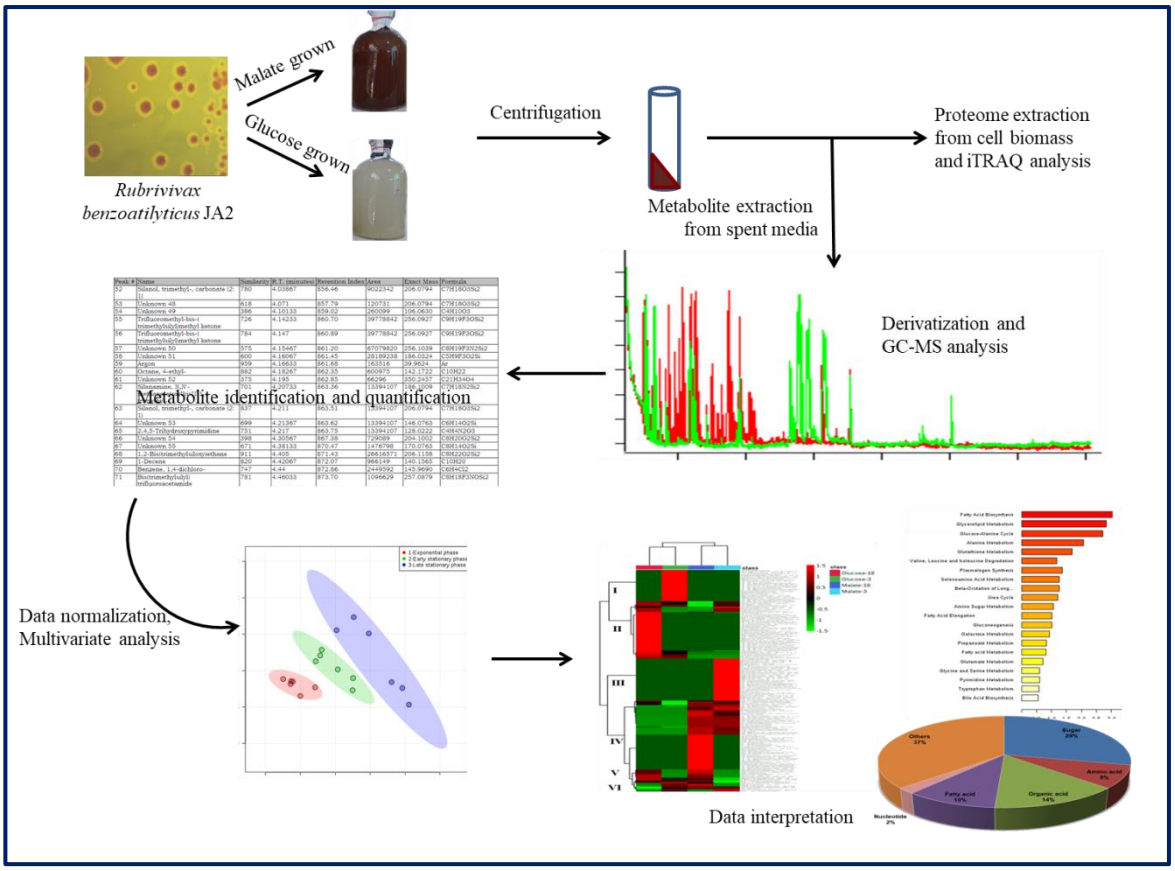

Fig. 2. 1: Schematic representation of GC-MS based metabolic profiling of malate/glucose grown *Rbx. benzoatilyticus* cells.

2.6. Analytical methods

2.6.1. Estimation of reducing sugar

Reducing sugars in the culture spent media were estimated by Somogyi-Nelson method using glucose as standard (Norton, 1944). 50 µl of the sample was mixed with 2 ml water followed by 1 ml alkaline copper tartarate reagent and incubated for 10 min in boiling water bath and cooled to room temperature. Arsenomolybdate reagent (1 ml) was dispensed to it and the absorbance was read at 620 nm. Glucose was used as standard.

2.6.2. Fatty acid analysis

Logarithmic and late stationary phase malate or glucose grown cells were harvested by centrifugation (10,000 x g for 10 min) and lyophilized for 4-6 h. Lyophilized samples

were outsourced to Royal Life Sciences Pvt Ltd , Secundrabad, India to assess the fatty acid profile and they adopted the following protocol. Fatty acids were saponified, methylated and extracted from lyophilized sample by using the protocol of Sherlock microbial identification system (MIDI Inc.). Fatty acid methyl esters (FAME) were analysed by gas chromatography equipped with Sherlock MIS software [Microbial ID; MIDI 6.0 version; Agilent: 6850; peak identification was done based on the RTSBA6 database] (Cally et al, 2009).

2.6.3. High Performance Liquid Chromatography (HPLC)

Pigments and quinones were analysed by HPLC (Prominence LC-20AT Shimadzu, Japan) using Phenomenex C-18 column (Luna, 5µm, 250 x 4.6 mm) equipped with photodiode array detector. Carotenoids and chlorophylls were separated using acetonitrile: methanol: tetrahydrofuran (58:35:7 v/v/v) as mobile phase under isocratic mode at 1 $ml.min^{-1}$ flow rate. Quinones were analysed using methanol: diisopropyl ether (3:1 v/v) as mobile phase at 1 $ml.min^{-1}$ flow rate under isocratic mode. Quinones were detected using photodiode array detector at 270 nm and carotenoids/chlorophyll at 300-800 nm.

2.6.4. Gas chromatography mass spectrometry (GC-MS) of exometabolome

The extracted exometabolome samples (as described in section 2.5.4) were derivatized, to protect their functional groups, with 40 µl BSTFA (N,O-bis(trimethylsilyl)trifluoroacetamide) and TMCS (trimethylchlorosilane) (99:1 Sigma Aldrich); incubated at 70 $^{\circ}C$ for 4 h and immediately analysed by GC-MS (Agilent 7890). Derivatized sample (1 µl) was analysed using HP-5 column (30 m, internal diameter 0.32 mm, thickness 0.25 µm) in splitless mode with helium as carrier gas at a constant flow of 1.5 $ml.min^{-1}$. Oven temperature was initially held at 70$^{\circ}C$ for 2 min: ramped to 250 $^{\circ}C$ by 10$^{\circ}C$ min^{-1}; held for 1 min finally ramped to 280 $^{\circ}C$ by 5$^{\circ}C$ min^{-1} and isocratic hold for 15 min (280 $^{\circ}C$). System was operated with the following parameters: transfer line temperature-225$^{\circ}C$, source temperature- 230$^{\circ}C$, ionization energy -70 eV and acquisition delay for 120 s.

Mass spectra were recorded at 35-1000 m/z in full scan mode.The data obtained from GC-MS analysis was processed, log transformed (log_2) and subjected to multivariate statistical analysis using MetaboAnalyst (www.metaboanalyst.ca/MetaboAnalyst).

2.7. Proteomic response of strain JA2

2.7.1. Extraction of proteome

Glucose grown cells (biological triplicate) were harvested at three time points (exponential (G3), early stationary (G9) and late stationary phases (G18)) and malate grown cells (biological triplicate) were harvested at single time point (exponential phase, M3) by centrifugation (4 °C, 10000 g, 10 min). The experimental design contains two independent experiments comprising M3, G3, G9 and G18 (each with three biological replicates that were pooled to create single sample in order to minimise biological variation; Fig. 2.2).

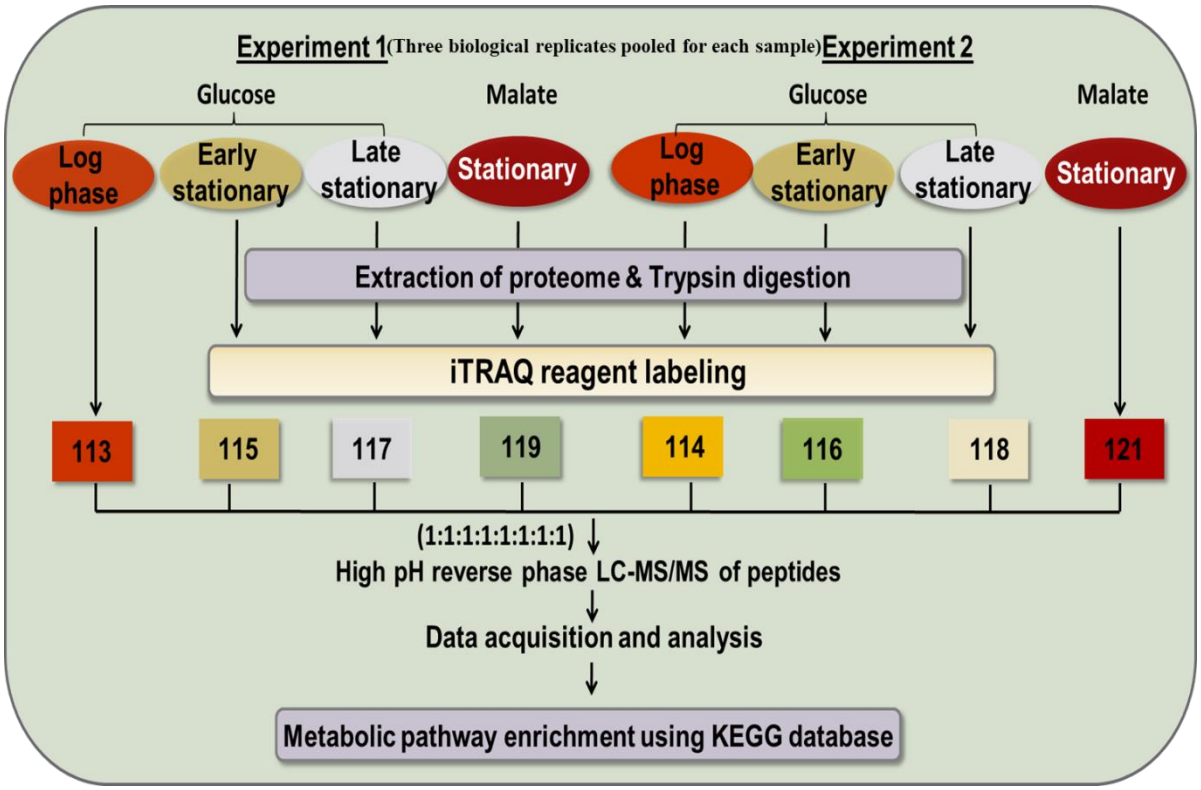

Fig. 2. 2: Schematic representation of isobaric tags for relative and absolute quantitation (iTRAQ) based proteome analysis of *Rbx. benzoatilyticus* (adopted from Gupta et al. 2019).

Cells were washed twice with 50 mM HEPES-KOH buffer (pH 7.5); suspended in HEPES-KOH buffer containing 0.1% SDS (w/v) and 0.1% triton-X-100 (v/v) and sonicated (MS 72 probe, 50% power, 7 cycles, 4 $^{\circ}$C) to lyse the cells. The lysate was incubated for 30 min at 4 $^{\circ}$C and centrifuged (20,000 x g, 4°C, 30 min). Total proteins were precipitated overnight from clear supernatant by 6 volumes of pre-chilled acetone (1:6) at -20 $^{\circ}$C . The precipitated proteins were washed twice with chilled acetone. Acetone was decanted and proteins were lyophilized and stored at -20 $^{\circ}$C until further use.

2.7.2. Isobaric tag for relative and absolute quantitation (iTRAQ) labelling of proteome

Isobaric tag for relative and absolute quantitation (iTRAQ) labelling and analysis was outsourced to University of California, San Diego USA, and they adopted the following protocol. Protein samples (100 µg) were resuspended in TNE buffer (50 mM Tris pH 8.0, 100 mM NaCl, 1 mM EDTA). The samples were processed for labelling according to Povero *et al.* and the trypsinized samples (8 samples) were labelled with isobaric tags (iTRAQ8, ABSCIEX, Ross *et al.*2004), where each sample was labelled with a specific tag (113,114 for G3; 115, 116 for G9; 117, 118 for G18 and 119, 121 for M3 ones) according to the manufacturer's instruction. All labelled peptides from each set were then pooled in the ratio of 1:1:1:1 and fractionated using high pH reverse phase chromatography (HPRP-Xterra C18 reverse phase, 4.6 mm x 10 mm 5µ particle (Waters)). The chromatography conditions were as follows: the column was heated to 37°C and a linear gradient from 5-35% Buffer B (Buffer B-20 mM ammonium formate pH 10 in 80% ACN-water, Buffer A- 20 mM ammonium formate pH 10 aqueous) was applied for 80 min at 0.5 mL.min^{-1} flow rate. A total of 42 fractions of 0.5 ml volume were collected. For LC-MS/MS analysis some fractions were pooled to create a final 16 pooled samples. Each of the pooled fractions were analyzed

by HPLC coupled with tandem mass spectroscopy (LC-MS/MS) using nano-spray ionization. Figure 2.2 depicts the schematic outline of iTRAQ based proteome analysis.

2.7.3. Mass spectral data analysis, protein identification and quantification

The LC-MS/MS was performed as per Povero *et al.* with slight modifications. In brief, the nano-spray ionization experiments were performed using a Triple TOF 5600 hybrid mass spectrometer (ABSCIEX) interfaced with nano-scale reversed-phase UPLC (Waters corporation nanoACQUITY) using a 20 cm-75 micron ID glass capillary packed with 2.5-µm C18 (130) CSHTM beads (Waters Corporation). Peptides were eluted from the C18 column into the mass spectrometer using a linear gradient (5–80%) of ACN at a flow rate of 250 µl.min^{-1} for 1h. The buffers used to create the ACN gradient were: Buffer A and Buffer B (Section 2.1.5.2). MS/MS data were acquired in a data-dependent manner in which the MS1 data was acquired for 250 ms at m/z of 400 to 1250 Da and the MS/MS data were acquired from m/z of 50 to 2,000 Da. The Independent data acquisition (IDA) parameters were as follows; MS1-TOF acquisition time of 250 milliseconds, followed by 50 MS2 events of 48 milliseconds acquisition time for each event. The threshold to trigger MS2 event was set to 150 counts when the ion had the charge state +2, +3 and +4. The ion exclusion time was set to 4 seconds. The collision energy was set to iTRAQ experiment setting. Finally, the collected data were analyzed using Protein Pilot 5.0 (ABSCIEX) for peptide identifications.

2.7.4. MS/MS database search and iTRAQ quantitation

ProteinPilot 5.0 (ABSCIEX) paragon algorithm was used for peptide identifications. There are no settings for data extraction to create a peak list from the ".wiff" instrument files for this software. The search and quantitation parameters were set: (i) Sample Type "iTRAQ 8-plex quantification"; (ii) Cysteine alkylation "iodoacetamide"; (iii) Enzyme digestion, "Trypsin"; (iv) Special factors "none"; (v) Species "none"; (vi) Sequence Database, search was performed against genome project *Rubrivivax benzoatilyticus* JA2 database (version

AEWG00000000.1); (vii) Search effort "Thorough ID"; (viii) Search using False Discovery Rates. Keratin and trypsin were included as common contaminant. The results were normalized using the bias correction in the Pro Group™ Algorithm Results. After bias correction, the data was sorted based on *p*-values. For each protein ratio reported, the program calculates a *p*-value.

Detected proteins were filtered using the criteria: unused protscore >2 (99% confidence level) with minimum two unique peptides (95% confidence level), false discovery rate < 1% and considered for fold change (FC) analysis. Each of the protein was attributed to four FC expression ratios calculated in double duplex style at each time point. Proteins with iTRAQ FC ratios <0.8 (log_2FC <−0.26) were considered as down-regulated and >1.2 (log_2FC >0.26) as up-regulated (with $p \leq 0.05$ in at least two out of four expression ratios). Differentially expressed proteins (DEP) were categorized based on their function according to KEGG (Kyoto Encyclopedia of Genes and Genomes, www.genome.jp/kegg/) database. *In silico* molecular weight, isoelectric focusing and grand average hydropathy (GRAVY) of proteins were predicted using ExPASy tools (www.expasy.org).

2.8. Genomic DNA analysis

2.8.1. Isolation of genomic DNA

DNA was isolated from late stationary phase malate and glucose grown cells of *Rbx. benzoatilyticus* using the Genetix's genome isolation kit (Nucleo-pore gDNA Fungal/Bacterial Mini Kit) according to the manufacture's protocol. Genome's authenticity was confirmed by sequencing 16S rRNA gene.

2.8.2. Genome sequencing and annotations

The two samples of genomic DNA were outsourced to Agrigenome Pvt. Ltd., Cochin, India for genome sequencing. They adopted the following criteria: library preparation- NEBNext Ultra DNA library preparation kit; sequencing platform- Illumina Hiseq x10 with

100X genome coverage; pre-processing the sequenced data- Adaptor Removal (ver. 2.3.0); assembly of the sequencers- Unicycler (ver. 0.4.8) with default parameters. Annotations were performed with the RAST (Rapid Annotation using Subsystem Technology) server. *In silico* DNA–DNA hybridization was calculated online using GGDC website server.

2.9. Softwares and databases used for this study

- http://cgview.ca/
- iPath 3: interactive Pathways Explorer (embl.de)
- RAST Server - RAST Annotation Server (nmpdr.org)
- www.expasy.org
- www.genome.jp/kegg
- www.metaboanalyst.ca/MetaboAnalyst
- www.ncbi.nlm.nih.gov
- www.patricbrc.org

Chapter 3: Results

3. Results

In all the experiments, glucose grown cells of *Rubrivivax benzoatilyticus* strain JA2 were compared with those of malate grown cells (of same physiological age) under phototrophic growth mode unless otherwise mentioned. Exponential phase (24 h) malate grown cells under phototrophic conditions were used as inoculum (10 %) for all the experiments.

3.1. Physiological and morphological implications

3.1.1. Glucose photometabolism by APB.

The photometabolism of glucose by different species of APB was studied (Table 3.1). As seen in the table, many APB species are able to grow and photo metabolise glucose, as they do with other carbon sources, without effecting pigmentation. Whereas, some are able to grow on glucose but lose their pigmentation on longer incubations. Still other APB neither grew on (or metabolised) glucose nor lost their pigmentation. It is inferred that, though majority of APB members can photometabolise glucose, yet it is not a preferred carbon source for all APB rather it has some lethal or harmful effect on certain spp. observed as the loss of pigmentation (Table 3.1).

3.1.2. Effect of different carbon sources on Rbx. benzoatilyticus.

The photometabolism of different organic carbon sources on *Rbx. benzoatilyticus* was studied. *Rbx benzoatilyticus* was grown on Biebl and Pfennig's phototrophic media supplemented with 7 mM ammonium chloride (NH_4Cl) as nitrogen source and different organic compounds (22 mM) as carbon source as listed in table 3.2 and incubated for 18 days. It was observed that non-sugar carbon sources well supported the growth of cells. Monosaccharides supported the growth but resulted in loss of pigmentation and cultivability

(examined as growth on sub-culturing) upon 18 d and longer phototrophic incubations (Table 3.2). Disaccharides and sugar substrates more reduced than glucose did not support the growth of *Rbx. benzoatilyticus* but retained the pigmentation and ability to grow (after 18 d incubation) when sub-cultured subsequently on favoured substrates (Table 3.2). This directed us to examine the effect of glucose (common sugar) against malate (as control), a favoured substrate for *Rbx. benzoatilyticus*.

3.1.3. Effect of glucose on growth and pigmentation of Rbx. benzoatilyticus.

Rubrivivax benzoatilyticus was grown phototrophically on either malate or glucose as sole carbon source to study the growth curve. The growth was measured as turbidity periodically. The organism displayed altered growth characteristics on the two carbon sources (Fig. 3.1). Glucose grown culture of *Rbx. benzoatilyticus* exhibited a lag phase of nearly 24 h whereas no lag phase was observed when grown on malate (Fig. 3.1). Malate grown culture attained stationary phase in four days, while glucose grown culture took 8-9 days of phototrophic incubation to attain stationary phase (Fig. 3.1A,B). Nevertheless, the final optical density (OD_{660nm}) of stationary phase culture grown on malate or on glucose displayed similar value of ~0.4. This implies that *Rbx. benzoatilyticus* exhibited an increased doubling time (13.5 ± 2.7 h) on glucose compared with malate (9.6 ± 2.2 h). Also, malate grown cultures sustained the pigment (carotenoids/chlorophylls) production (Fig. 3.1A), while in glucose grown culture loss of pigmentation was observed (Fig. 3.1B). The trend for loss in total carotenoid content was similar to the trend for loss in bacteriochlorophyll *a*.

Table 3. 1: Photoheterotrophic growth of a few anoxygenic phototrophic bacteria with glucose as sole carbon source/e- donor.

Organism	Growth on glucose	Loss in pigmentation	Inference	Reference
Rhodobacter capsulatus	+	N	Organism grows well on glucose phototrophically.	Sasikala et. al., 1993
Rhodobacter sphaeroides 2.4.1	+	N		Sasikala et. al., 1993
Rhodobacter johrii JA192	+	N		Girija et. al., 2010
Afifella aestuarii JA968	+	N		Buddhi et al., 2020
Rhodobacter alkalitolerans JA916	+	Y	Organism grows on glucose but loses its pigmentation on longer incubations.	This study
Rubrivivax benzoatilyticus JA2	+	Y		This study
Rubrivivax benzoatilyticus JA1026	+	Y		This study
Rhodobacter sediminicola JA983	-	N	Glucose does not support the growth of the organism as sole carbon source.	This study
Rhodomicrobium lacus JA643	-	N		This study
Rhodomicrobium udaipurense JA980	-	N		This study

+, observed; -, absent; Y; loss in pigmentation was observed on longer incubation (18 d); N, No pigment loss was observed.

Different bacterial species of APB group were grown on mineral medium photoheterotrophically with NH_4Cl (7 mM) as nitrogen source and glucose (22 mM) as carbon source for 18 days.

Table 3. 2: Effect of carbon sources on growth and cultivability of *Rbx. benzoatilyticus*

Carbon source (22 mM)	Growth	Pigmentation	Cultivability on sub-culturing	Inference
Malate	+	+	+	Well supports the growth of *Rbx. benzoatilyticus*.
Fumarate	+	+	+	
Lactate	+	+	+	
Pyruvate	+	+	+	
Glucose	+	-	-	*Rbx. benzoatilyticus* transited to a non-cultivable state.
Fructose	+	-	-	
Sucrose	-	+	+	Substrates do not support the growth of *Rbx. benzoatilyticus* but cells are viable.
Lactose	-	+	+	
Gluconate	-	+	+	
Glucuronate	-	+	+	

+, observed; -, absent;

Malate grown mid exponential phase culture ($OD_{660\ nm}$ 0.25) of *Rbx. benzoatilyticus* was used as inoculum (10%) for the experiment. Culture was grown photoheterotrophically on mineral medium with NH_4Cl (7 mM) as nitrogen source and different organic compounds (22 mM) as sole carbon source for 18 days. Growth was monitored as turbidity. Cultivability was assessed by sub-culturing on malate medium after 18 days of photoheterotrophic incubations.

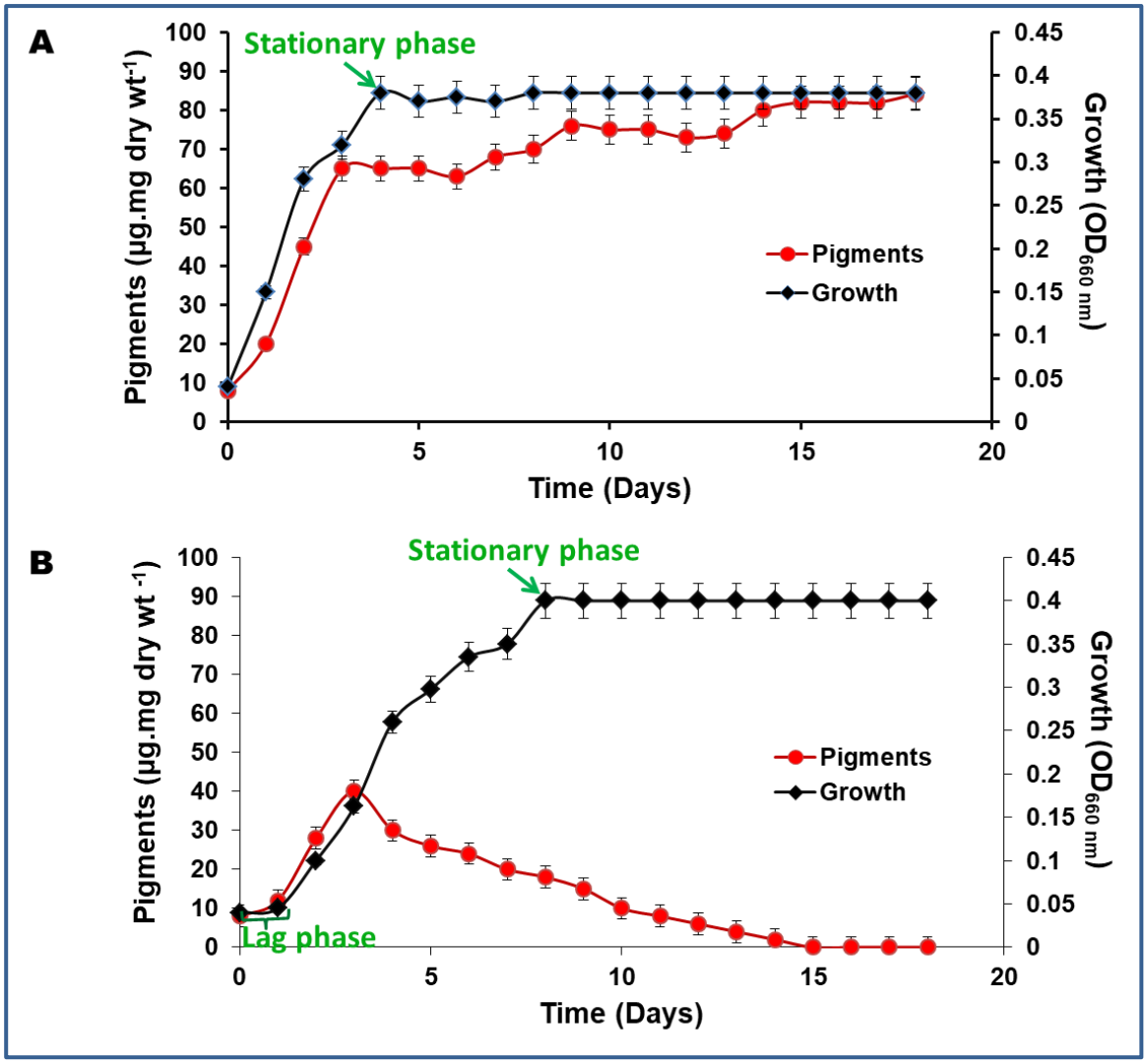

Fig. 3. 1: Growth curve and pigment kinetics of *Rbx. benzoatilyticus*.

*Growth curve and pigment kinetics of malate grown (**A**) and glucose grown (**B**) cells*

Cells of Rbx. benzoatilyticus were grown on Biebl and Pfennig's mineral medium with 7mM NH_4Cl as nitrogen source and 22 mM malate/glucose as carbon source for 18 days of photoheterotrophic incubations. Malate grown mid exponential phase culture ($OD_{660\ nm}$ 0.25) of Rbx. benzoatilyticus was used as inoculum (10%). The growth was monitored as turbidity at 660 nm every 24 h against uninoculated media blank. Pigments were extracted in methanol: acetone (2:7 v/v) and quantitated spectrophotometrically.

Datum is the representation of mean ± standard deviation from three independent experiments performed in duplicates.

3.1.4. pH of Rbx. benzoatilyticus spent media under the influence of glucose.

The pH of the spent media from glucose grown cultures (stationary phase) of *Rbx. benzoatilyticus* decreased from 6.8 at the time of inoculation to 4.4 at late stationary phase, while that of malate grown cultures increased from 6.8 at the time of inoculation to 8.6 at late stationary phase. This indicates different metabolic states of *Rbx. benzoatilyticus* JA2 under the influence of the two carbon sources.

3.1.5. Effect of glucose on morphology of Rbx. benzoatilyticus.

Average size of 6-7 µm was maintained by malate grown *Rbx. benzoatilyticus* cells irrespective of growth phase as seen in DIC images (Fig. 3.2 A,C). On the contrary, ~50 % reduction in the cell size (3-4 µm) at stationary phase as compared to logarithmic phase glucose-grown cells (6-7 µm) of *Rbx. benzoatilyticus* was seen (Fig. 3.2 B,D). Further, the reduction in cell size of glucose-grown stationary phase cells compared to malate was also supported by SEM analysis (Fig. 3.2 E,F). Additionally, cell aggregate formation and accumulation of plenty of polyhydroxyalkanoate (PHA) granules were observed at stationary phase glucose-grown cells (Fig. 3.2 D,H) while no aggregates were seen in malate-grown cells (Fig. 3.2 B).

3.1.6. Cultivability analysis of glucose grown *Rbx. benzoatilyticus* cells.

The loss of pigmentation by *Rbx. benzoatilyticus* on glucose prompted us to inspect the cultivability of the cells by sub-culturing the glucose grown cells periodically (after 3, 6, 12, 18 and 21 days of incubation on glucose) onto fresh malate media (malate being a preferred carbon source over glucose to *Rbx. benzoatilyticus*; see section 3.1.3 and 4.1). The growth $OD_{660\ nm}$, against uninoculated media as blank, was recorded 96 h after transferring and plotted as bar-chart (Fig. 3.3). Gradual loss in the cultivability was observed in glucose grown cultures upon transfer to fresh malate media, wherein longer the cells exposed to glucose, more the time taken for the restoration of growth finally attaining a state of no

resuscitation (Fig. 3.3). Three days old glucose fed culture of *Rbx. benzoatilyticus* (when transferred to malate media) attained stationary phase along with pigmentation within 96 h. Six and twelve days glucose grown cultures also restored the growth along with regaining the pigmentation but with a longer lag phase and longer duration to reach stationary phase growth ($OD_{660\ nm}$ ~0.4). In contrast, eighteen days old culture neither exhibited growth nor regained pigmentation even after a month of incubation, upon transferring to malate medium (Fig. 3.3) suggesting that *Rbx. benzoatilyticus* when grown on glucose entered into a non-cultivable state over time.

3.1.7. Longer incubations rather than glucose *per se* is responsible.

Complete loss of pigmentation (Fig. 3.1 B) along with non-cultivability at eighteen days and longer incubated cells of *Rbx. benzoatilyticus* (Fig. 3.3) provoked a question whether glucose itself or its longer incubations is the trigger to the state of non-cultivability. Though, figure 3.3 clearly demonstrates that 18 days and longer incubated cells undergo a state of non-cultivability. However, when exponential phase ($OD_{660\ nm}$ ~0.2) glucose grown *Rbx. benzoatilyticus* cells were repeatedly transferred to glucose medium (up to five repeated transferrings also), cells were able to grow (but without regaining pigmentation). In contrast, when glucose grown exponential phase cells of each such transferring were transferred to malate medium, growth along with pigmentation was observed. This led us to examine metabolomic and proteomic changes during longer incubations (selecting 3 time points - exponential phase or actively growing state (G3); complete pigment loss (G9) and non-cultivable/growth arrested state (G18)) to elucidate the metabolic adaptations leading to a transition in the physiology of the organism (refer to sections 3.3.2 and 3.4.3).

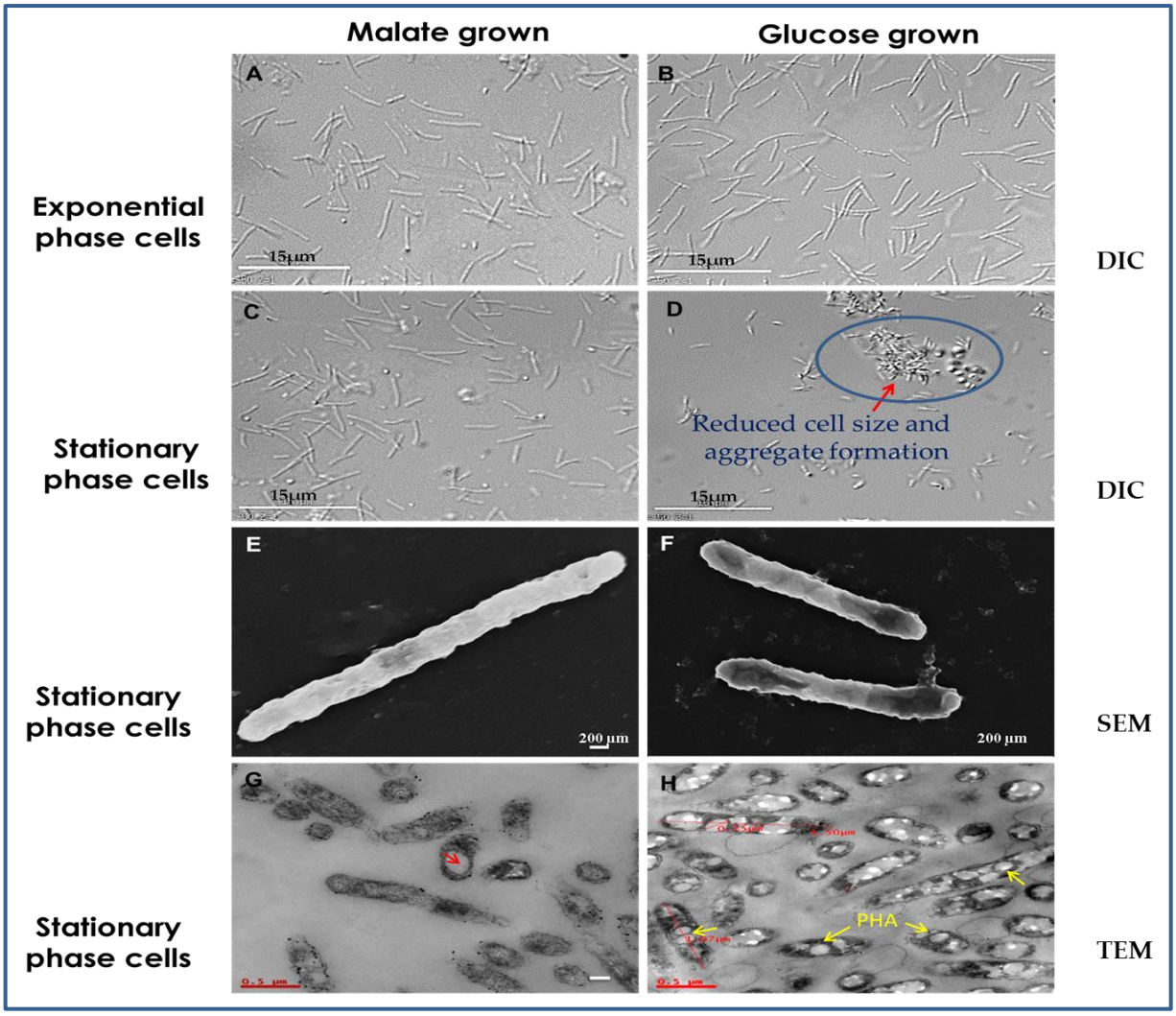

Fig. 3. 2: Morphological variation between malate/glucose grown *Rbx. benzoatilyticus* cells.

*Differential interference contrast (DIC) images of exponential phase (**A, B**) and stationary phase (**C, D**) malate, glucose grown cells respectively. Scanning electron micrograph (SEM) of stationary phase malate/glucose grown cells (**E, F**). Transmission electron micrograph (TEM) of stationary phase malate/glucose grown cells (**G, H**).*

Experimental conditions for growth were same as described under Fig. 3.1, except for DIC images were taken at 3 (growing exponential phase) and 18 (late stationary phase) days after inoculation. Cells were also harvested 18 days after inoculation, fixed for SEM and fixed, sectioned on grid for TEM. Blue circle highlights cell aggregate formation and size reduced to half. Yellow arrow indicates PHA granules. PHA, polyhydroxy alkanoate.

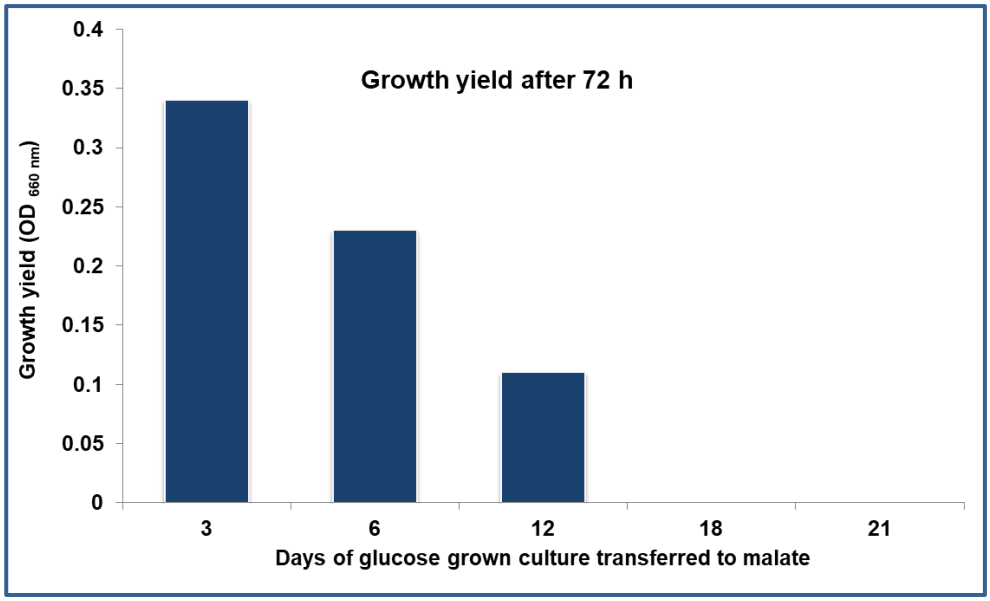

Fig. 3. 3: Cultivability analysis of glucose grown *Rbx. benzoatilyticus* cells.

Glucose grown cells of Rbx. benzoatilyticus were periodically transferred to malate medium and the growth yield, measured turbidometrically as $OD_{660\ nm}$ 72 h after sub-culturing, was plotted as bar chart.

3.1.8. Confocal laser scanning microscope (CLSM) analysis of non-cultivable glucose grown *Rbx. benzoatilyticus* cells.

Late stationary phase glucose grown *Rbx. benzoatilyticus* cells (G18) were stained with DAPI but no fluorescence was observed in the microscope. Alternately, cells from G18 were stained with FDA (a cellular esterase monitoring dye), nile red (staining PHAs) and CFW (binds to polysaccharide polymer) and analysed under microscope. Positive signal of green, red and blue fluorescence for FDA (Fig. 3.4 A), nile red (Fig. 3.4 B) and CFW (Fig. 3.4 C) respectively indicates G18 cells to be viable with PHA granules and presence of polysaccharides (Fig. 3.4 D).

3.1.9. Enumeration of FDA positive cells using FACS.

FDA positive non-cultivable glucose-grown (G18) *Rbx. benzoatilyticus* cells were enumerated using flow cytometry. Malate grown cells and heat killed malate grown cells of same age (M18) were taken as positive and negative controls respectively. Nearly 36.8 % G18 cells were observed to be FDA positive (Fig. 3.5 A) which is quite comparable to malate

grown (M18) cells (43.4 %). Heat killed malate grown M18 cells did not show any FDA positive signal (Fig. 3.5).

3.1.10. Viability analysis using vital dye staining.

The viability of G18 cells was assessed using vital dye staining also. Cells of *Rbx. benzoatilyticus* were stained with resazurin (which stains cells based on the redox state of the cell thus, an indicator of metabolic activity inside the cell) and PI which enters the cells through damaged membrane (membrane compromised cells) and binds to DNA. Positive signal was observed with both the stains resazurin as well as PI under the microscope (Fig. 3.6).

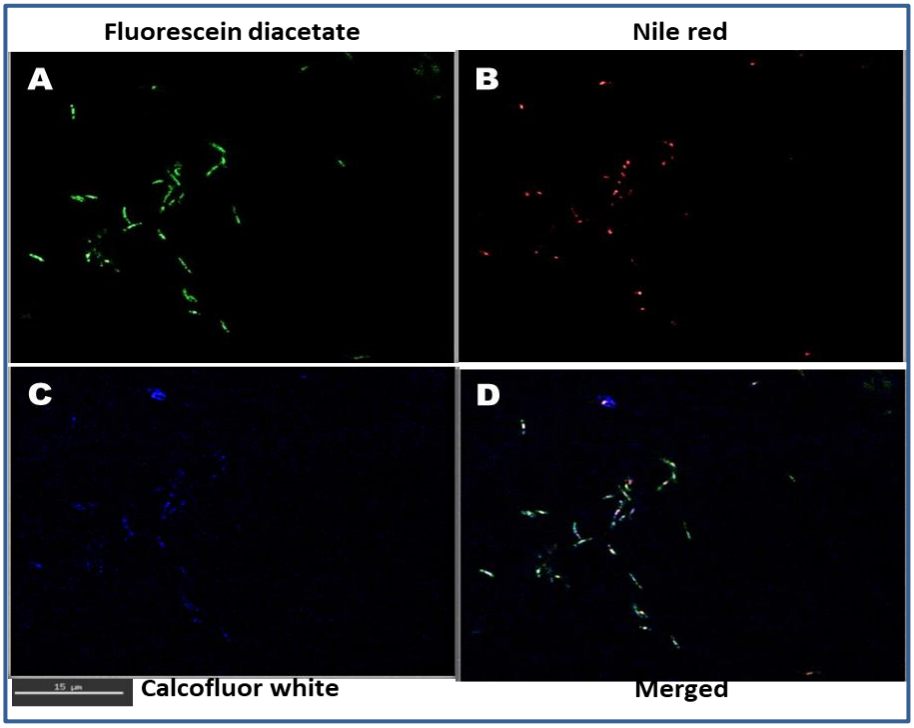

Fig. 3. 4: Confocal laser scanning microscopic (CLSM) images of late stationary phase glucose grown *Rbx. benzoatilyticus* cells.

*Confocal image of cells stained with FDA (**A**), nile red (**B**), calcofluor white (**C**) and merged image (**D**). Darkly stained red colour bodies indicate PHA granules.*

Cells were grown as described under Fig. 3.1, except for cells grown on glucose were harvested at 18 days after inoculation and stained with FDA (for assessing viability), nile red (for PHAs) and calcofluor white (for polysaccharides) and analysed for fluorescence under confocal microscope. FDA, fluorescein diacetate; PHA, polyhydroxy alkanoate.

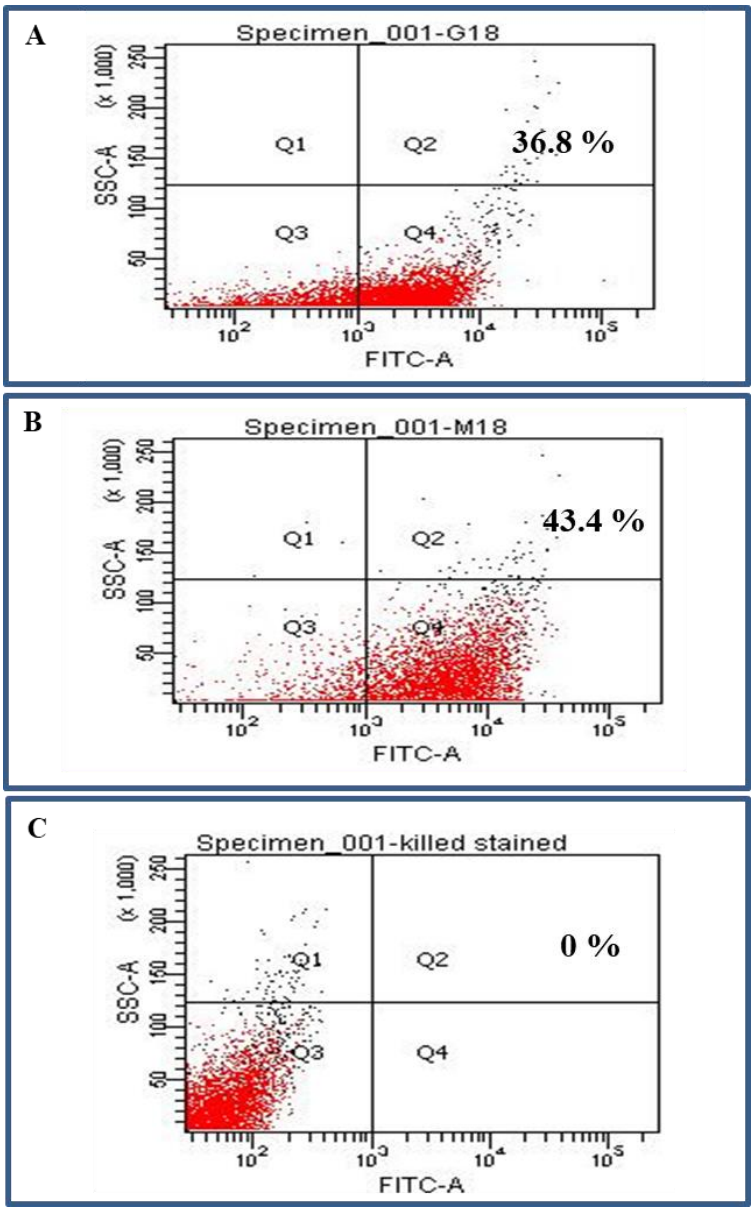

Fig. 3. 5: Enumeration of FDA positive stationary phase *Rbx. benzoatilyticus* cells by flow cytometric analysis.

*FACS analysis of stationary phase glucose grown (**A**), malate grown (**B**) and heat killed malate grown (**C**) cells.*

Cells were grown as described under Fig. 3.1, except for cells harvested at 18 days after inoculation were stained with FDA. The FDA positive cells were enumerated by FACS. Malate grown and heat killed malate grown cells were taken respectively as positive and negative controls for glucose grown cells. FDA, fluorescein diacetate; FACS, fluorescence activated cell sorter.

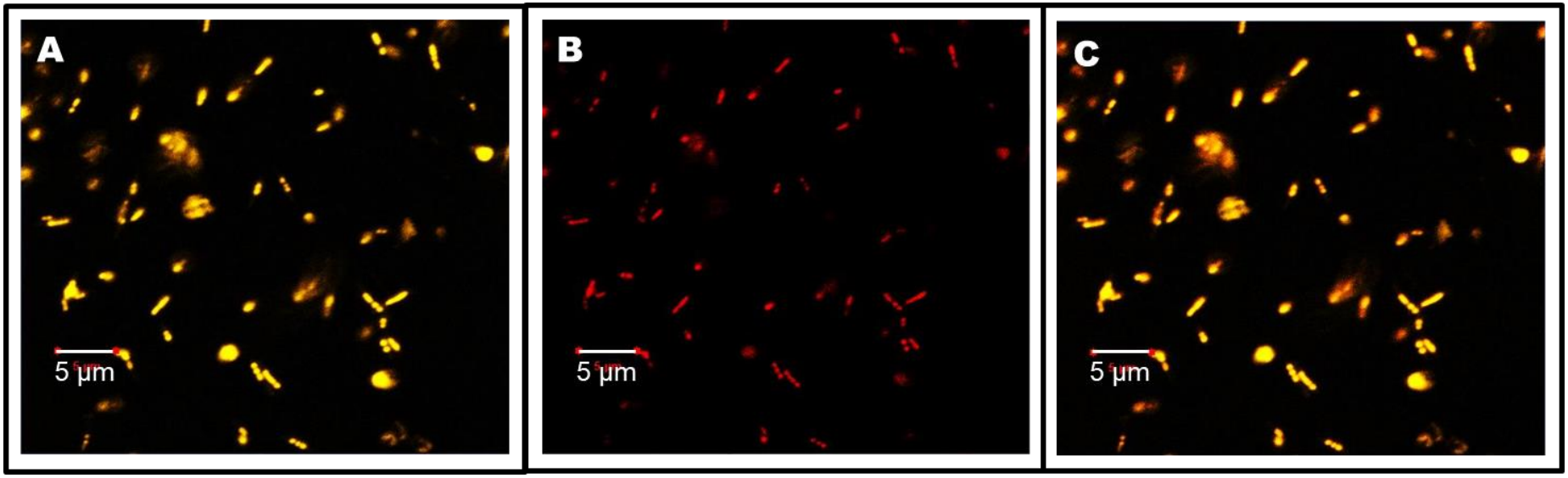

Fig. 3. 6: Viability assessment of non-cultivable glucose grown *Rbx. benzoatilyticus* cells.

*Confocal image of cells stained with resazurin (**A**), propidium iodide (PI) (**B**), and merged image (**C**) to assess the viability of non-cultivable stationary phase glucose grown (G18) Rbx. benzoatilyticus cells.*

Cells were grown as described under Fig. 3.1, except for cells grown on glucose were harvested at 18 days after inoculation and stained with resazurin (which stains based on the redox status of the cell), PI (stains membrane compromised cells) and analysed for fluorescence under confocal microscope. PI, propidium iodide.

3.1.11. Not only growing cells, resting cells are also under the influence of glucose.

To examine whether the effect of glucose is restricted to growing cells only or to the resting cells as well, resting cells (prepared as described in the methods) were transferred to fresh medium (same volume) and incubated phototrophically for 18 days. Surprisingly, resting cells transferred to glucose medium gradually lost their pigmentation without any detectable change in turbidity. On the contrary, resting cells transferred to fresh malate medium sustained pigmentation as well as turbidity.

3.1.12. Glucose tolerance test.

Glucose (as reducing sugar) was estimated from the spent media to quantify the amount of glucose consumed by *Rbx. benzoatilyticus* in 18 days. Nearly 40% (accounting to 8.8 mM) sugar was observed in the spent media of late stationary phase culture (G18). This provoked another question- is it the characteristic of the organism to metabolise less sugar than what is provided or 22 mM is itself high enough for *Rbx. benzoatilyticus*. To rule out the possibilities, glucose tolerance test was performed ranging from 0-10 mM (which is more than 8.8 mM) glucose. *Rubrivivax benzoatilyticus* retained pigmentation with dose dependent turbidity (growth) and consumed the sugar almost entirely upto 10 mM concentration (Fig. 3.7). At higher concentrations of glucose (upto 100 mM) also, the final growth $OD_{660\ nm}$ was same as that of 20 mM glucose (0.44) with loss in pigmentation. Thus, it was inferred that not merely glucose but higher concentration (22 mM or higher) of glucose is toxic to *Rbx. benzoatilyticus*.

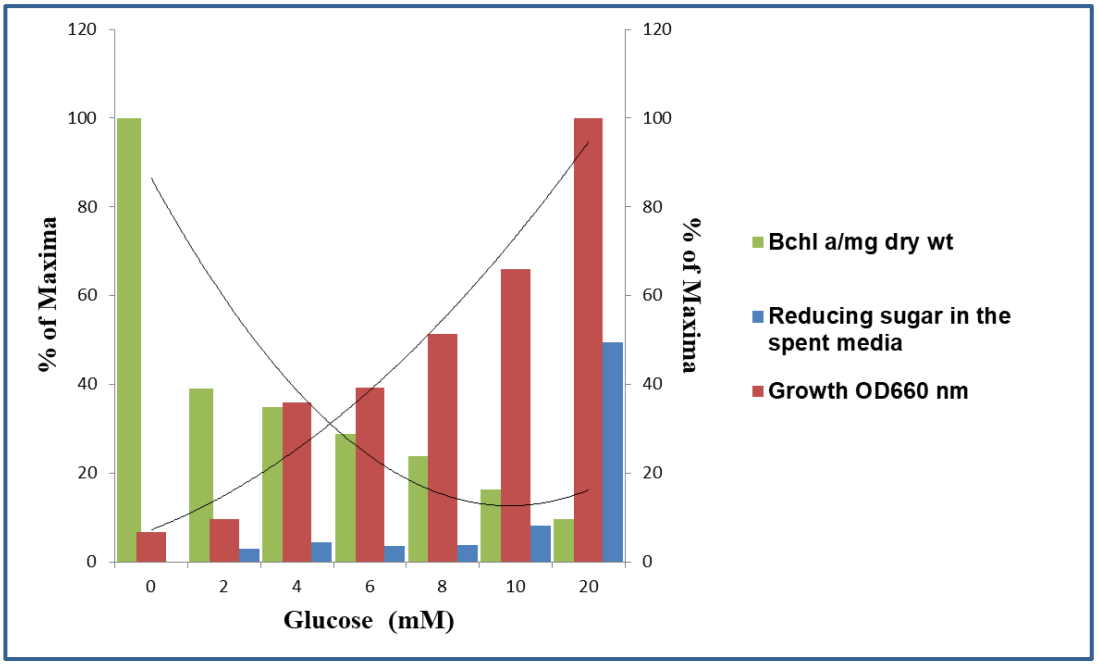

Fig. 3. 7: Glucose tolerance test of *Rbx. benzoatilyticus*.

Malate grown mid exponential phase culture ($OD_{660\ nm}$ 0.25) of Rbx. benzoatilyticus was used as inoculum (10%) and the culture was photoheterotrophically grown on glucose (0-20 mM). After 18 d of incubation, growth was monitored as turbidity at $OD_{660\ nm}$ against uninoculated media blank and the culture was harvested. Pigments were quantitated from the cell pellet and reducing sugar from spent media. 100% growth corresponds to 0.44 $OD_{660\ nm}$; 100% pigment corresponds to 2.6 µg.mg dry wt^{-1}.

3.1.13. Influence of oxygen on the growth, pigmentation and cultivability of *Rbx. benzoatilyticus* in presence of glucose.

To assess the role of oxygen as stimulant to the non-cultivable state of *Rbx. benzoatilyticus*, cells were grown on malate/glucose in presence of ample oxygen (in Erlenmeyer flask, under shaking) or under oxygen limited conditions (completely filled screw cap test tubes). The growth turbidity under aerobic mode was less as compared to respective turbidity under anaerobic growth mode. In contrast to anaerobic photoheterotrophic conditions, where *Rbx. benzoatilyticus* lost its complete pigmentation and cultivability after 18 days of incubation on glucose (Fig. 3.8 A,C), the cells were able to retain pigmentation as well as cultivability under dark aerobic conditions on glucose (Fig. 3.8 B,D). Malate grown cells retained pigmentation and cultivability under anaerobic as well as aerobic growth mode (Fig. 3.8).

3.1.14. Reactive oxygen species (ROS) evaluation.

Glucose is well known for the generation of intracellular ROS (Luo et al., 2018). Thus, cells of *Rbx. benzoatilyticus* were stained with CM-H_2DCFDA to estimate the ROS production at 3rd (G3, M3), 9th (G9, M9) and 18th (G18, M18) days after inoculation. CM-H_2DCFDA passively diffuses into cells where it is retained after cleaving the acetate groups by intracellular esterases. Subsequently, oxidation yields a fluorescent adduct, trapped inside the cell, facilitating the measurement of fluorescence (Salma et al., 2013). Mean intensity of 0.07, 1.5 and 2.6 was observed respectively at stained G3, G9 and G18 *Rbx. benzoatilyticus* cells (Fig. 3.9). While mean intensity of 0.07, 0.8 and 1.18 was observed at M3, M9 and M18 cells respectively (Fig. 3.9) which is much less than that from glucose grown cells. Thus, we suspected more ROS generation in glucose grown cells.

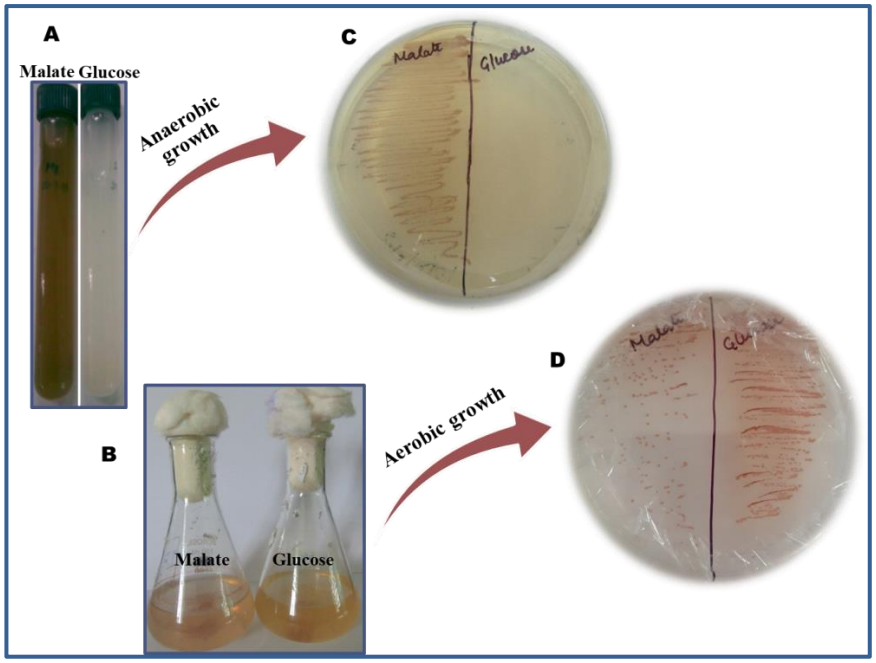

Fig. 3. 8: Influence of oxygen on glucose metabolism by *Rbx. benzoatilyticus*.

Cells were grown on malate/glucose media under oxygen limiting (A) or in the presence of ample oxygen under shaking (B) conditions. After 18 days of incubation, using sterile inoculating loop, cells from anaerobically and aerobically grown culture were streaked on nutrient agar (C, D) under sterile conditions to assess the cultivability.

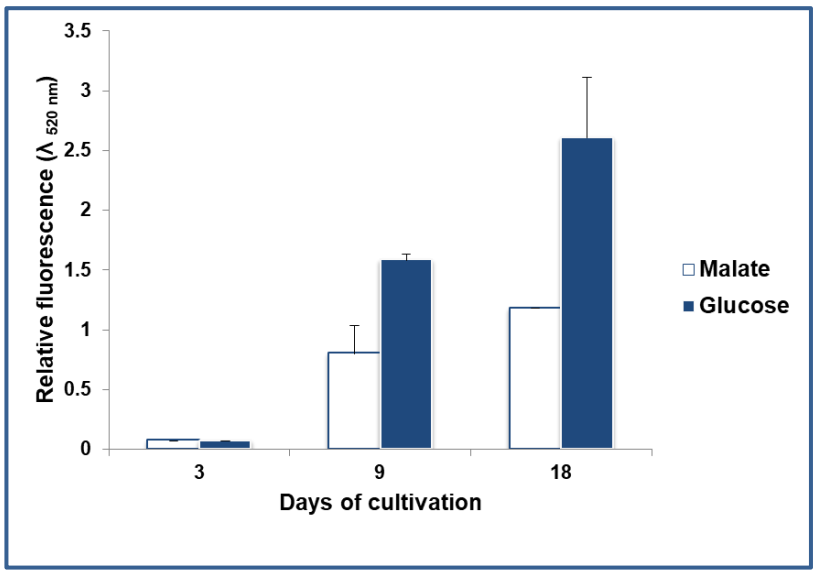

Fig. 3. 9: ROS analysis from *Rbx. benzoatilyticus* cells.

Cells were grown as described under Fig. 3.1, except for cells were harvested at 3rd (exponential phase), 9th (early stationary phase) and 18th (late stationary phase) days of growth and using the stain CM-H2DCFDA, the ROS accumulation was quantitated. CM-H2DCFDA, 5-(and-6)-chloromethyl-2',7'-dichlorodihydrofluorescein diacetate; ROS, reactive oxygen species.

3.2. Biochemical studies

3.2.1. Fatty acid profiling of malate/glucose-grown *Rbx. benzoatilyticus* cells.

FAME analysis of malate/glucose-grown logarithmic or stationary phase cells was carried out separately to study the variation in the fatty acid composition. The analysis revealed deviation in the composition of G18 cells. Glucose-grown stationary phase cells displayed decrease in unsaturated fatty acid content from 54 to 12 mol% and an increase in the saturated fatty acid content from 37 to 79 mol% (Fig. 3.10 B). Thereby, resulting in a ten-fold increase in the saturated to unsaturated fatty acid ratio of glucose-grown stationary phase cells compared to logarithmic phase cells (Table 3.3). The most influenced fatty acid species include, $C_{16:0}$ (increased from 27.3 to 54.9%), $C_{16:1}\omega7c/C_{16:1}\omega6c$ (decreased from 37.7 to 4%) and $C_{10:0}3OH$ (increased from 5.5 to 8.6%) (Table 3.3). On the other hand, *Rbx. benzoatilyticus* upheld its fatty acid composition as well as the saturated to unsaturated fatty acid ratio (similar to logarithmic phase) even during stationary phase (Table 3.3, Fig. 3.10 A) when grown on malate.

3.2.2. Pigment kinetics of glucose grown *Rbx. benzoatilyticus* cells.

Rubrivivax benzoatilyticus contains sphaeroidene (sph), spirilloxanthin (spr) and bacteiochlorophyll *a* (bchl) as pigment system (Gupta et al., 2019; Ramana et al., 2006). HPLC analysis of pigments extracted from stationary phase malate/glucose-grown cultures revealed depletion of both sph, spr as well as bchl in presence of glucose (Fig. 3.11). To understand whether loss in bchl in *Rbx. benzoatilyticus* follows the loss in carotenoids under the influence of glucose or vice-versa, growth and pigments kinetics was carried out using spectrophotometer and HPLC respectively. Growth kinetics of glucose grown *Rbx. benzoatilyticus* cells revealed a lag phase of 24 h attaining stationary phase after 9 days (G9) of phototrophic incubations (Fig. 3.12 B). Also, it was observed that the peak intensity of sph decreased in the time dependent manner (Fig. 3.12 A). Contrariwise, intensity of spr peak

augmented initially till 9 days (G9) and thereafter it also decreased finally attaining a straight line without any peak at G18 (Fig 3. 12 A). In the similar fashion, bchl peak was constant until 9 days (G9) and subsequently it also decreased (Fig. 3.12 A). Thus, the samples at three time points: exponential phase (G3), early stationary phase (G9) and late stationary phase (G18) were taken forward for studying the dynamics of metabolite (footprint) and proteome (fingerprint) analysis.

3.2.3. Effect of glucose on the photosystems of *Rbx. benzoatilyticus*.

Photosystems were isolated from late stationary phase malate/glucose grown *Rbx. benzoatilyticus* cells by sucrose density gradient ultracentrifugation. Differential ultracentrifugation resulted in the separation of two bands corresponding to reaction center-light harvesting complex I (RC-LHC I) and light harvesting complex II (LHC II). Spectral analysis of the bands isolated from stationary phase cells revealed the complete absence of RC-LHC I, (Fig. 3.13 A) and very low quantities of LHC II (Fig. 3.13 B) in glucose grown cells.

3.2.4. Effect of glucose on the quinones of *Rbx. benzoatilyticus*.

Quinones were extracted from late stationary phase malate/glucose grown *Rbx. benzoatilyticus* cells by preparative TLC and analysed by HPLC. HPLC analysis of quinones revealed 16-20 fold lower levels of ubiquinone (Q8) at stationary phase glucose grown cells (compared with that of malate grown cells) of *Rbx. benzoatilyticus* (Fig. 3.14). However, no significant change in the levels of menaquinone (MK-8) was observed.

Table 3. 3: Fatty acid profiling of exponential and late stationary phase malate/glucose grown cells of *Rbx. benzoatilyticus*

Cellular fatty acid	Percentage (%) in Malate grown culture		Percentage (%) in Glucose grown culture	
	3 D	18 D	3 D	18 D
$C_{10:0}$	0.6 ± 0.0	0.7 ± 0.0	0.8 ± 0.0	1.05 ± 0.35
$C_{10:0}$ 3OH	6.2 ± 0.0	6.95 ± 0.95	5.45 ± 0.55	8.65 ± 3.85
$C_{12:0}$	7 ± 1.2	8.5 ± 0.6	6 ± 0.2	9.8 ± 2.3
$C_{14:0}$	5 ± 0.9	6.5 ± 0.9	2.55 ± 0.15	5.0 ± 0.8
$C_{16:1}$ ω9c	No	No	2.8 ± 0.0	No
$C_{16:1}$ω7c/$C_{16:1}$ω6c	41.1 ± 2.9	36.1 ± 1.5	37.7 ± 0.0	4.0 ± 2
$C_{16:1}$ ω 5c	0.4 ± 0.0	No	0.6 ± 0.0	0.1 ± 0.0
$C_{16:0}$	2.15 ± 0.5	28.8 ± 0.0	27.3 ± 1.9	54.95 ± 3.45
iso-$C_{17:1}$ω9c	1.2 ± 0.0	0.8 ± 0.0	1 ± 0.0	0.5 ± 0.0
$C_{17:0}$ 10-methyl	1 ± 0.0	No	2.5 ± 0.0	No
$C_{18:1}$ ω9c	No	No	0.2 ± 0.2	3.4 ± 2.6
$C_{18:1}$ ω7c	4.55 ± 1.2	4.8 ± 0.6	12.05 ± 1.45	2.6 ± 0.0
$C_{18:0}$	7.8 ± 3.9	1.3 ± 0.0	0.9 ± 0.1	3.6 ± 1.7
$C_{18:1}$ω7c11-methyl	No	1.8 ± 0.0	0.7 ± 0.1	No
iso-$C_{19:0}$	No	No	No	1.0 ± 0.0
$C_{20:0}$	No	No	No	0.1 ± 0.0
$C_{20:1}$ω7c	No	No	No	2.5 ± 0.0
Ratio of SFA/UFA	0.94	1.09	0.68	6.6

no; not observed.

Malate grown mid exponential phase culture (OD_{660} = 0.25) of *Rbx. benzoatilyticus* was used as inoculum (10%) and the culture was grown on malate/glucose media under photoheterotrophic conditions for 18 days. Culture was harvested at 3rd day and 18th day of growth, lyophilised and analysed for fatty acid profiling by gas chromatography.

Datum represents mean ± standard deviation of two independent experiments. 3D, at 3rd day of growth; 18D, at 18th day of growth; No, not observed; SFA, total saturated fatty acid; UFA, total unsaturated fatty acid.

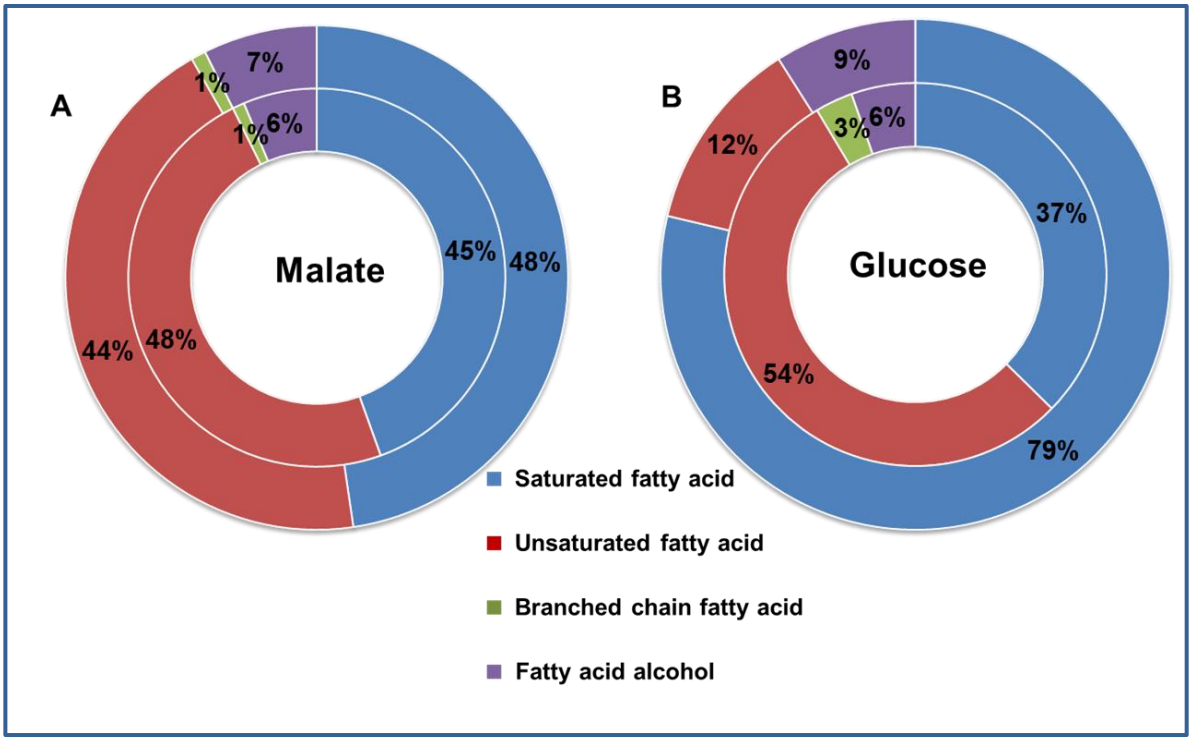

Fig. 3. 10: Whole cell fatty acid profiling of malate/glucose grown cells of *Rbx. benzoatilyticus*.

*Fatty acid composition of malate grown (**A**) or glucose grown (**B**) cells.*

Malate grown mid exponential phase culture ($OD_{660\ nm}$ 0.25) of Rbx. benzoatilyticus was used as inoculum (10%). Cells were grown photoheterotrophically on malate/glucose media for 18 days. Cells were harvested after 3^{rd} (exponential phase) and 18^{th} (late stationary phase) day of growth, lyophilised and analysed by gas chromatography. Inner circle represents fatty acid profiling of exponential phase cells and outer circle represents that of stationary phase cells.

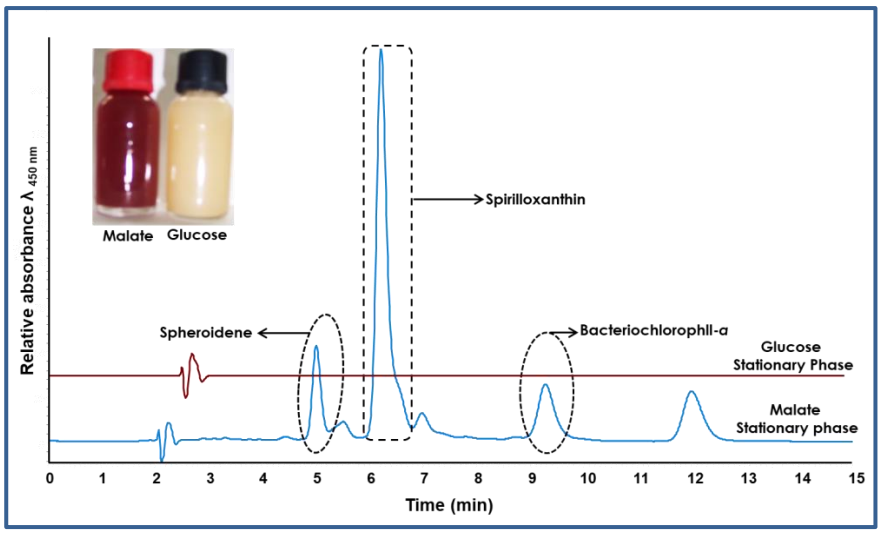

Fig. 3. 11: Photosynthetic pigments of *Rbx. benzoatilyticus* under the influence of glucose.

HPLC chromatogram of photosynthetic pigments from stationary phase cells. Experimental conditions were similar as described under Fig. 3.10, except for cells harvested after 18 days, pigments were extracted in methanol acetone (2:7 v/v) from cell pellet and analysed by HPLC. Inset represents the culture image just before harvesting. HPLC, high performance liquid chromatography.

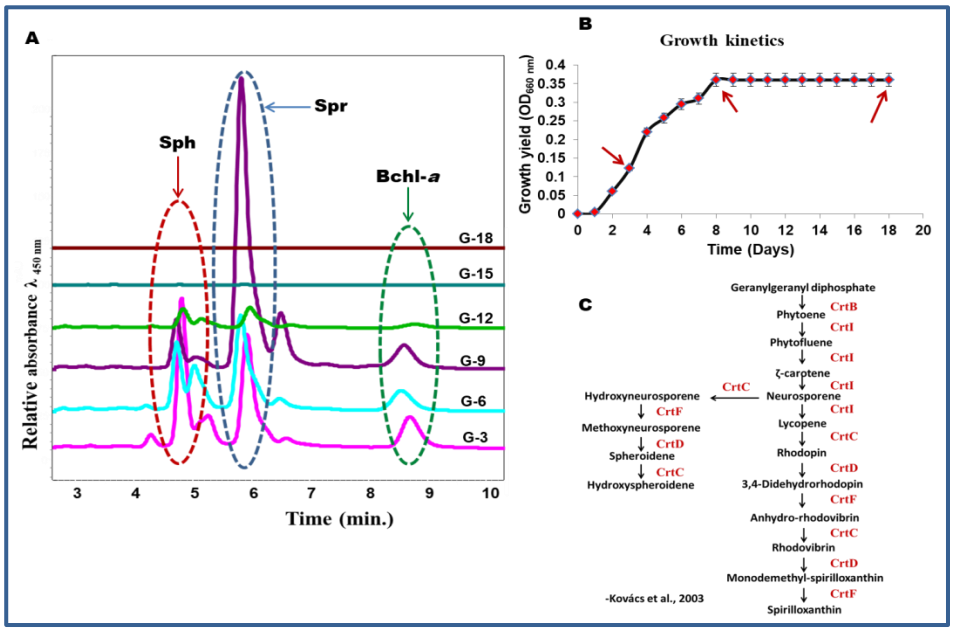

Fig. 3. 12: Pigment kinetics of *Rbx. benzoatilyticus*.

*Pigment (**A**) and growth (**B**) kinetics of glucose grown cells and well-reported carotenoid biosynthetic pathway (**C**)*

Experimental conditions were similar as described under Fig. 3.11, except for cells were periodically (every third day) harvested only from glucose grown culture. Red bold arrows in panel B represents the time points taken forward for metabolite and protein dynamic studies. Sph, spheroidene; spr, spirilloxanthin; bchl a, bacteriochlorophll-a.

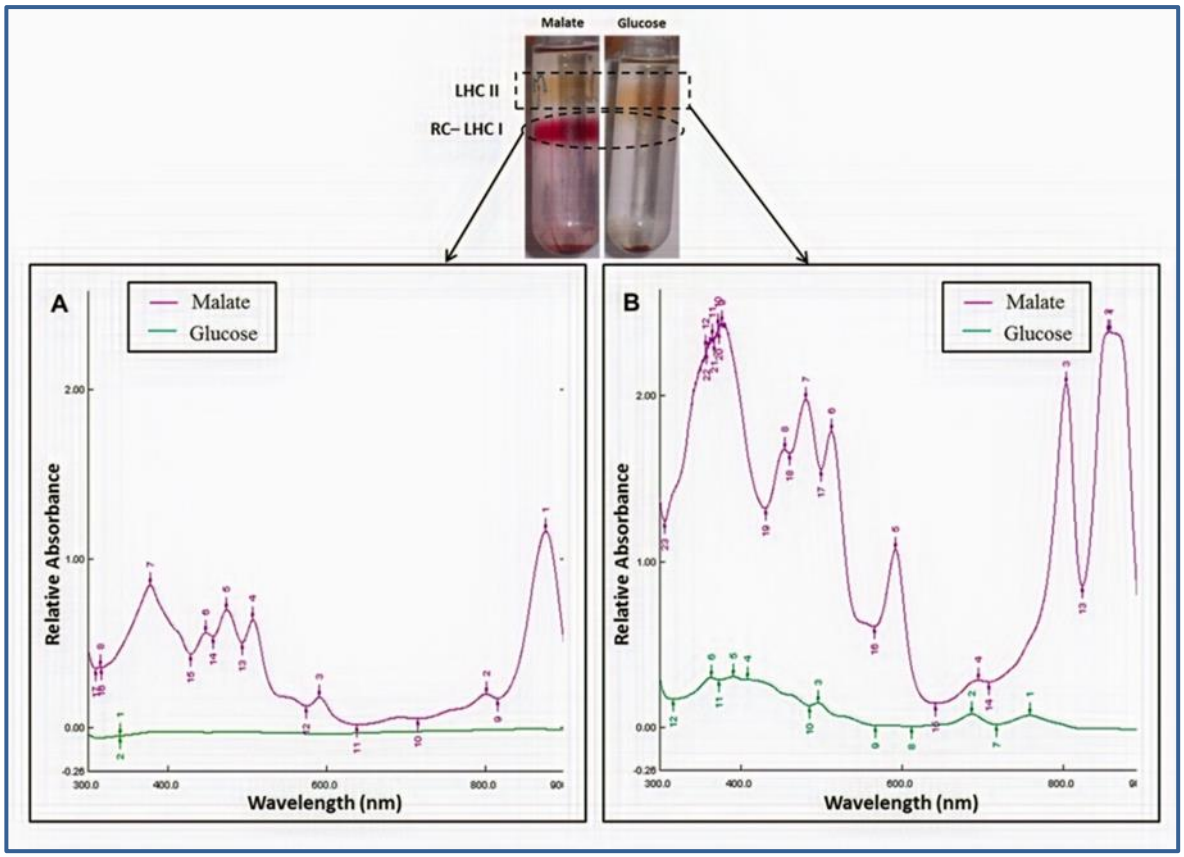

Fig. 3. 13: Absorption spectra of photo systems isolated from *Rbx. benzoatilyticus*.

*Absorption spectra of RC-LHC I (**A**) and LHC II (**B**).*

Experimental conditions were similar as described under Fig. 3.10, except for photosystems were isolated from cell biomass after 18 d of phototrophic growth using sucrose density gradient ultra-centrifugation and the bands were thus collected to read the absorption spectra. Inset represents the photograph of bands corresponding to RC-LHC I and LHC II. RC-LHC I, reaction centre-light harvesting complex I; LHC II, light harvesting complex II.

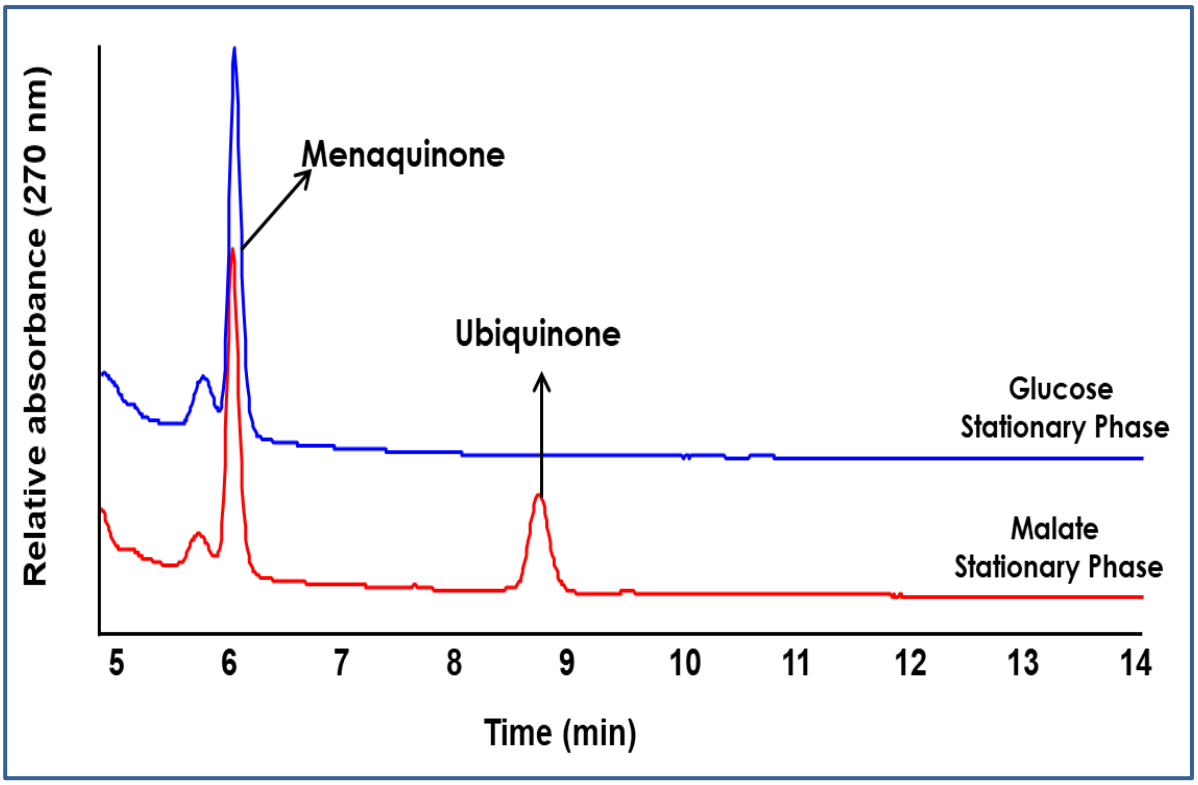

Fig. 3. 14: Chromatogram of quinones from *Rbx. benzoatilyticus*.

HPLC chromatogram of the quinones extracted from stationary phase malate/glucose grown cells.

Experimental conditions were similar as described under Fig. 3.10, except for quinones were extracted by preparative TLC from cell biomass of 18 d incubated culture and analysed by HPLC. TLC, thin layer chromatography; HPLC, high performance liquid chromatography.

3.3. Metabolite footprints of malate and glucose grown cultures of *Rbx. benzoatilyticus*

Exogenous metabolites excreted by the cell under specified conditions are referred to as the 'metabolic footprint' or exometabolome. Often, fluctuations in the exometabolome mirror the changes happening inside the cell reflecting its metabolic state (Fu et al., 2014; Pinu et al., 2018). We aimed in characterizing the exometabolome of *Rbx. benzoatilyticus* on longer incubations (up to 18 days) of glucose by conducting global analysis of metabolites from the spent-media samples using GC-MS.

3.3.1. Comparative footprint analysis of malate/glucose grown *Rbx. benoatilyticus*.

Gas chromatography mass spectrometry (GC-MS) based metabolomics approach was employed to interpret the metabolic responses of *Rbx. benzoatilyticus* to glucose. Extracellular metabolites from spent-media of malate/glucose grown cells were extracted and derivatised (silylation; BSTFA + TMCS) before GC-MS analysisWe compared the mass spectrum of metabolites to national institute of standards and technology (NIST) library or Golm metabolome database (*www.gmd.mpimp-golm.mpg.de*) for their identification. Relative metabolite concentration was predicted by comparing the respective metabolite's peak area. To identify the hidden patterns, datum was normalised and subjected to multivariate statistical analysis t. Complete experimental scheme is illustrated in Fig. 2.1**.**

To understand the physiological states of *Rbx. benzoatilyticus*, exometabolome of cells grown on either malate or glucose were compared at exponential phase (M3 or G3) and late stationary phase (M18 or G18) separately. Gas chromatography mass spectrometric analysis of exometabolome listed two hundred metabolites from each sample. Based on the mass spectrum similarity in the data base, we were able to identify 102, 102, 63 and 77 metabolites from M3, M18, G3 and G18 samples respectively while rest of the metabolites remained unidentified. Those that were identified includes aromatics, organic acids, sugars,

nucleotides, fatty acids, amines and amino acids. The counts of metabolites common and unique to each sample are represented as Venn-diagram in Fig. 3.15.

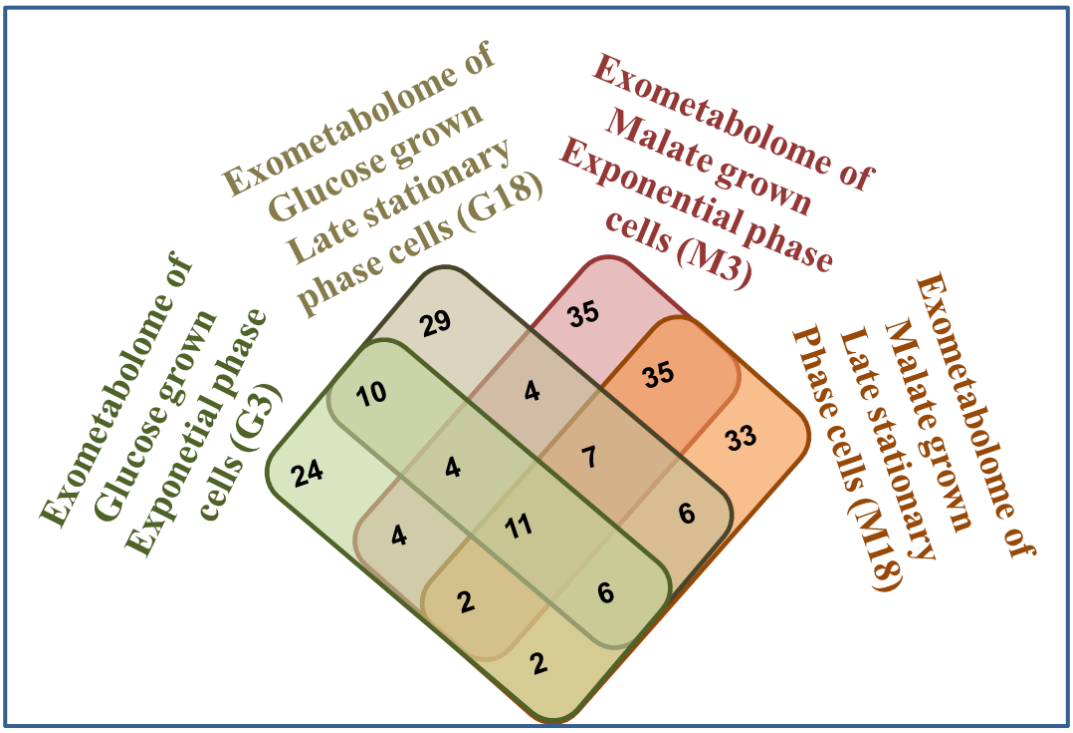

Fig. 3. 15: Venn-diagram representing common and unique metabolites from footprint of malate/glucose grown *Rbx. benzoatilyticus* cells.

Metabolites from spent media of glucose grown cells are shaded green while those from malate grown cells are shaded red in the Venn-diagram.

Malate grown mid exponential phase culture ($OD_{660\ nm}$ 0.25) of Rbx. benzoatilyticus was used as inoculum (10%). Cells of Rbx. benzoatilyticus were grown photoheterotrophically on malate/glucose media for 18 days. Cells were harvested after 3 (exponential phase) and 18 (late stationary phase) days of growth and supernatant was evaporated to dryness.

Extracellular metabolites were extracted from spent media, derivatised and analysed by GC-MS. Metabolites were identified by comparing the spectra to the NIST library (similarity $>$ 700) and Golm metabolome database (http://gmd.mpimpgolm.mpg.de/). GC-MS, gas chromatography- mass spectrometry.

3.3.1.1. Normalization of exometabolome datum obtained from GC-MS analysis.

To identify the significantly different metabolic features, datum was subjected to multivariate statistical analysis using MetaboAnalyst 4.0. Exometabolome datum gathered from GC-MS analysis, which comprised of two hundred and fifty eight identified metabolites along with their peak area at respective time points, was submitted to the software. Before performing the statistical analyses, datum was normalized by log transforming and mean centered data scaling. Figure 3.16 displays the datum before and after normalization.

3.3.1.2. Heatmap and hierarchical clustering analysis (HCA) of metabolites.

Hierarchical cluster analysis is an unsupervised multivariate statistical method used to illustrate the metabolite's concentration pattern. The HCA of metabolites from all the four samples (M3, M18, G3, and G18) of *Rbx. benzoatilyticus* was performed to detect the response pattern and is represented as heatmap (Fig. 3.17). Groups or metabolites with similar response pattern clustered together in the HCA analysis. Metabolomes from the four samples separated from each other creating four distinct clusters wherein both the metabolomes from malate grown cells (M3, M18) clustered together. Similarly, both the metabolomes from glucose grown cells (G3, G18) clustered together (Fig. 3.17). also, metabolites were clustered into six groups based on their response patterns. Group I comprises metabolites with high concentration in G3 sample, group II consist of metabolites with high concentration in G18 sample and group III, IV include metabolites whose concentration was high in M3 and M18 samples respectively. Group V, VI comprised of metabolites with differential expression in the four samples wherein concentration of group V metabolites was high in stationary phase samples (M18 and G18) while concentration of group VI metabolites was high in exponential phase samples (M3 and G3) (Fig. 3.17). HCA provided the overview of metabolic dissimilarity amongst malate and glucose grown cells.

3.3.1.3. Principal component analysis (PCA)

Normalised exometabolome datum as described in section 3.3.1.1 was submitted for PCA to identify the significant metabolic dissimilarities between the four samples (M3, M18, G3, and G18). It is an unsupervised, reductive statistical method used in metabolomics to interpret the metabolic variance in the data set, separating samples from each other. Samples clustering closely suggest metabolically similar and those stood away specify metabolic dissimilarity. Five component PCA analyses explained the variance amongst the four samples wherein 41.9 % variance was explained by principal component1 (PC1), 31.4% and 26.8% by PC2 and PC3 respectively (Fig. 3.18 A). The samples were visibly separated from each other in the PCA scatter plot (Fig. 3.18 B and C) suggesting the different metabolic states of the samples.

3.3.1.4. Partial least square discrimination analysis (PLS-DA)

Partial least square discrimination analysis was employed to further confirm the metabolic variations and to recognize the key metabolic features responsible for the dissimilarity in metabolic state of the samples. It is a supervised statistical method executed to differentiate the groups based on pre-assigned class and to identify the statistically significant metabolites contributing to group separation. The exometabolome samples were seen well separated in three principal components by PLS-DA analysis (Fig. 3.19). The R^2 value for this model was 0.9, indicating goodness of fit and Q^2 was 0.85, indicating goodness of predictability. High R^2 and Q^2 values specify that this model illustrates true differences in the metabolomes.

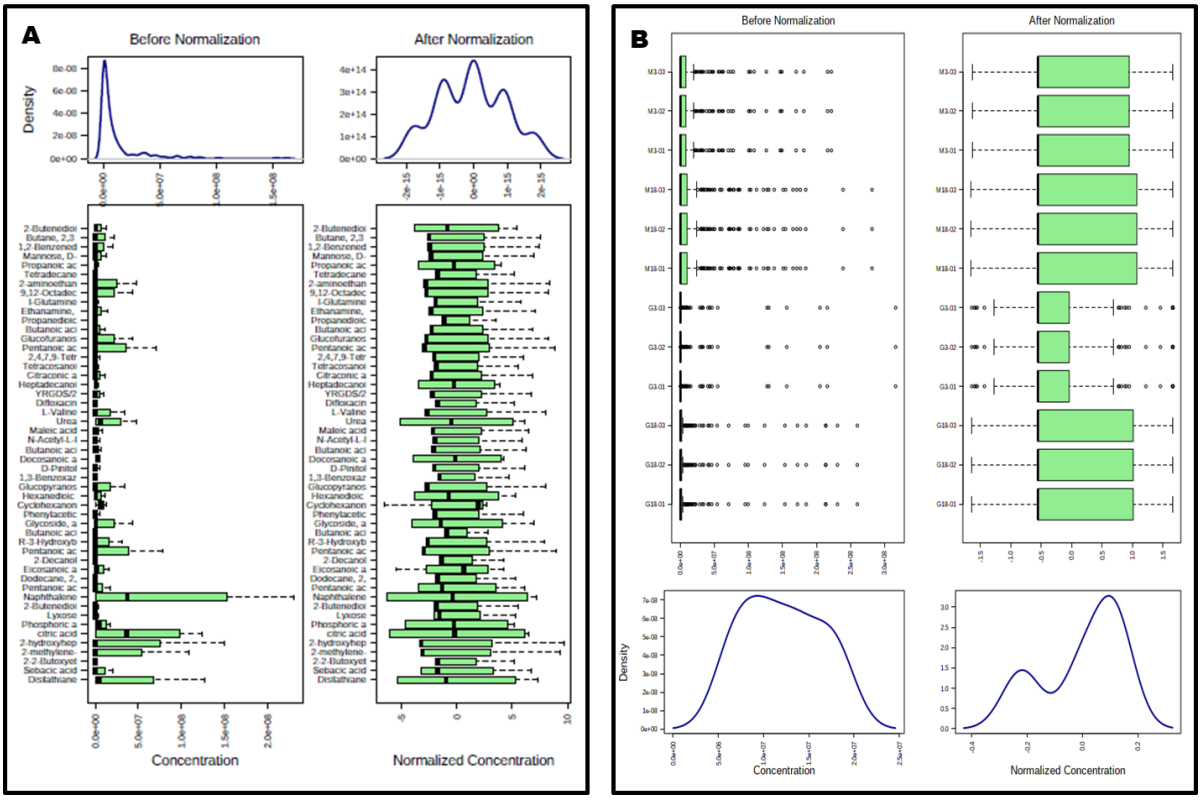

Fig. 3. 16: Box plots and kernel density plots before and after normalization of exometabolome data from malate/glucose grown *Rbx. benzoatilyticus* cells.

Feature view (A) and sample view (B) of the datum before and after normalization.

Datum obtained from GC-MS analysis as described under Fig. 3.15 was normalized before performing statistical analysis. Statistical normalisation of datum was done with row-wise normalisation and log (log_2) transformation.

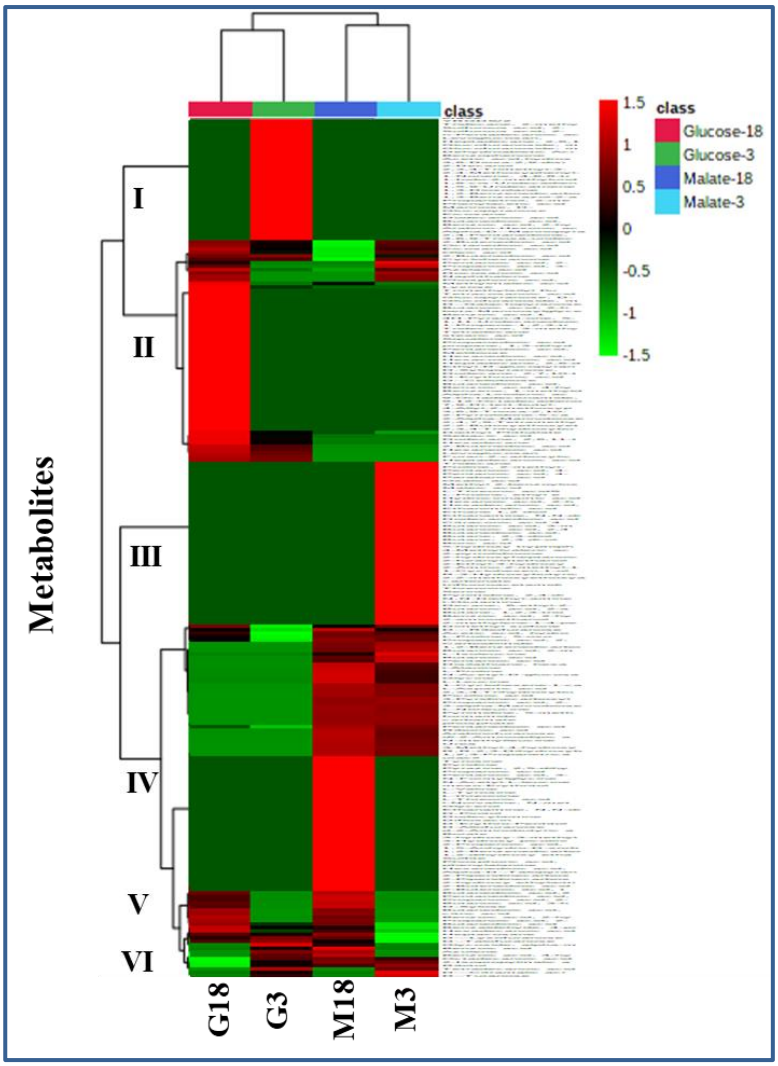

Fig. 3. 17: Hierarchical clustering analysis (HCA) of metabolites associated with malate/glucose grown *Rbx. benzoatilyticus* cells.

Metabolites from exponential/stationary phase malate/glucose grown cell's spent media are represented as heatmap. Clustering was performed using Pearson correlation as distance matrix by MetaboAnalyst online software. Metabolites in red represent higher concentration and green as low concentration.

Normalised datum obtained from GC-MS analysis as described under Fig. 3.16 was used for HCA and heatmap analysis. Datum was log transformed (log_2) and normalization was carried by quantile approach using MetaboAnalyst. M3, sample from 3rd day growth on malate; M18, sample from 18th day growth on malate; G3, sample from 3rd day growth on glucose; G18, sample from 18th day growth on glucose.

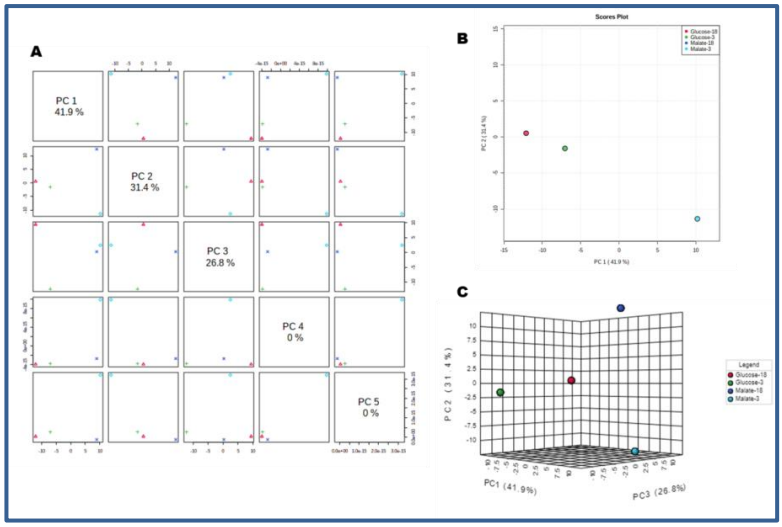

Fig. 3. 18: Principal component analysis (PCA) of exometabolome from malate/glucose grown *Rbx. benzoatilyticus* cells.

Pairwise score plots between the selected PCs (A). 2-D (B) and 3-D (C) scores plot between selected PCs.

Normalised datum obtained from GC-MS analysis as described under Fig. 3.16 was subjected to PCA using MetaboAnalyst. Metabolome at M3, M18, G3 and G18 are seen in light blue, dark blue, green and red colour respectively. PC, principal component; PCA, principal component analysis. M3, sample from 3rd day growth on malate; M18, sample from 18th day growth on malate; G3, sample from 3rd day growth on glucose; G18, sample from 18th day growth on glucose.

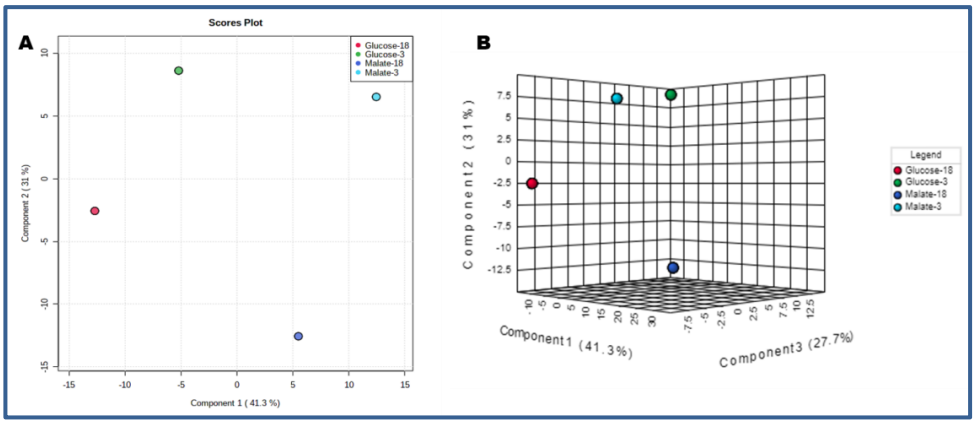

Fig. 3. 19: Partial least square discriminant (PLS-DA) scatter plot analysis of exometabolome from malate/glucose grown *Rbx. benzoatilyticus* cells.

2-D (A) and 3-D (B) scores plot between selected PCs.

Normalised datum obtained from GC-MS analysis as described under Fig. 3.16 was subjected to PLS-DA analysis using MetaboAnalyst. Metabolome at M3, M18, G3 and G18 are seen in light blue, dark blue, green and red colour respectively. PC, principal component; PLS-DA, partial least square discriminant analysis. M3, sample from 3rd day growth on malate; M18, sample from 18th day growth on malate; G3, sample from 3rd day growth on glucose; G18, sample from 18th day growth on glucose.

3.3.1.5. Identification of key metabolic features

The key metabolic features significant for group separation were identified based on the variable importance projection (VIP) scores obtained from PLS-DA model. Hundred and forty-three metabolites with VIP score > 1 were identified as the significant contributors for metabolic variation in the model (Fig. 3.20). These metabolites were categorized based on their structure. Carbohydrates, fatty acids, organic acids, amino acid and their derivatives were principally responsible for group separation in model. Amino acids and amines were specifically observed in the exometabolome of malate grown samples (M3, M18) while discrepancy in alkanes and fatty acids was more in the exometabolome of glucose grown samples as compared to the respective malate grown samples (Fig 3.21 A,B).

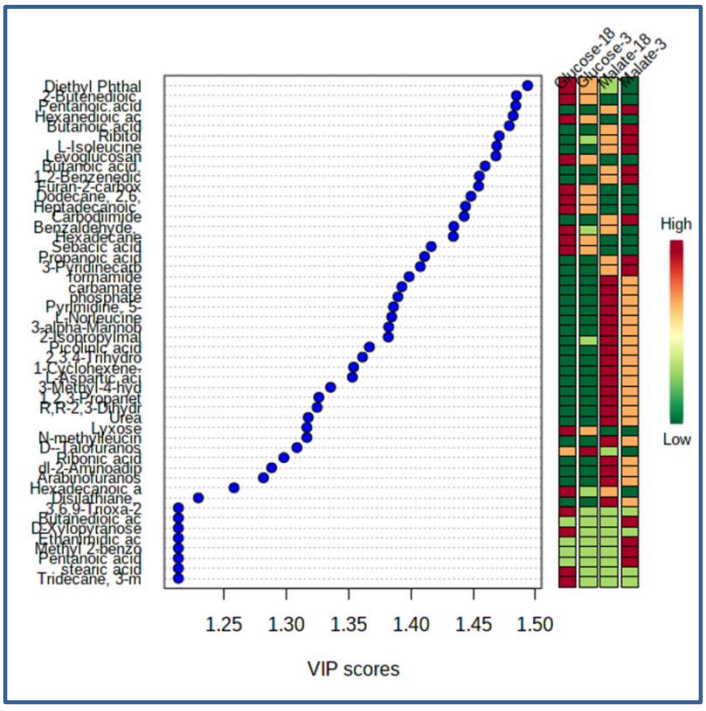

Fig. 3. 20: Variable importance on projection (VIP) scores of the metabolites obtained from PLS-DA analysis of malate/glucose grown *Rbx. benzoatilyticus* cells.

Coloured boxes on right side indicate relative abundance of metabolites between the samples. Metabolites with $VIP \geq 1.0$ was considered to be significant statistically.

Data processing parameters were same as described under Fig. 3.19 and the same data was subjected to VIP analysis by using MetaboAnalyst.

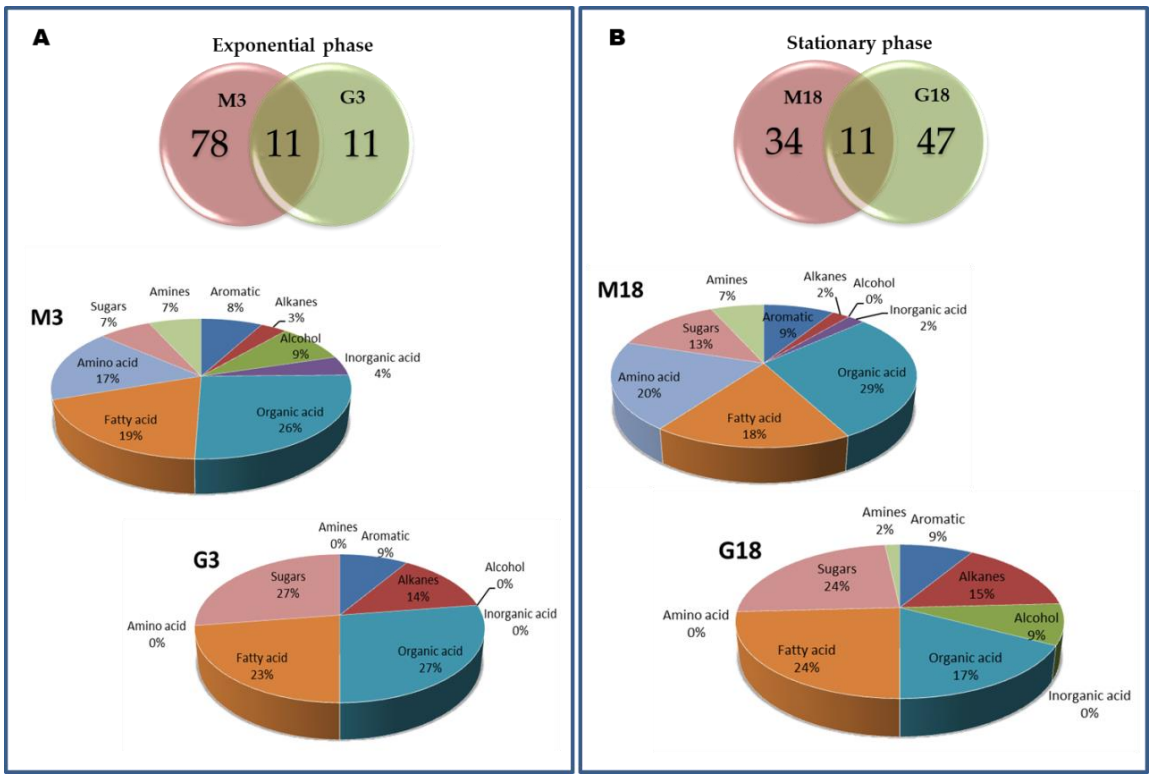

Fig. 3. 21: Structural categorization of metabolites from malate/glucose grown *Rbx. benzoatilyticus* cells.

Metabolites obtained as described under Fig. 3.20 were classified based on their structure according to the functional group they carried. The count of metabolites observed as common or unique is represented as Venn-diagram.

3.3.2. Metabolite dynamic studies from glucose grown cultures of *Rbx. benzoatilyticus*.

To study the dynamic changes in metabolites, GC-MS analysis of exometabolome from spent media of glucose grown cells was carried out at three time points- exponential phase (G3), early (G9) and late (G18) stationary phase. Analysis listed 200 metabolite peaks at each time point, of which 149 metabolic features were identified based on mass spectra comparison in the database (NIST similarity >700, Golm database) at one and/or other time point while other metabolites remained unidentified.

3.3.2.1. Normalization of dynamic exometabolome data of glucose grown Rbx. benoatilyticus.

Identified metabolic features along with their respective peak area at G3, G9 and G18 were recorded and submitted to MetaboAnalyst 4.0 online software to identify significant metabolic pattern and variation. Prior to performing multivariate statistical analyses, datum was subjected to sample specific normalization (dry weight of the sample), log transformation and auto scaling (mean centred and divided by standard deviation of each variable). Figure 3.22 illustrates the effect before and after normalization.

3.3.2.2. Hierarchical clustering analysis (HCA)

Hierarchical Clustering analysis (HCA) was performed considering Euclidean distance similarity measure and Ward's linkage clustering algorithm. The result of the HCA is represented as heatmap (Fig. 3.23). Metabolites clustered into five groups based on the response patterns. Group I, II and V comprises metabolites with high concentration in G18, G9 and G3 samples respectively, group III and IV includes metabolites whose concentration was high in two of the three samples (Fig. 3.23). HCA specified the metabolic dissimilarity between the three samples.

3.3.2.3. Principal Component Analysis (PCA) plot

Principal component analysis (PCA) is an unsupervised method intended to identify the directions best explaining the variance in a data set without referring to class labels. Pairwise score plot provided an overview of the separation pattern amongst the most significant principal components (PCs). Fifty one percent accumulated variance was explained by five PCs (Fig. 3.24 A) wherein 17.1%, 11.1% and 8.6% was explained by PC 1, 2 and 3 respectively (Fig. 3.24 B and C).

3.3.2.4. Partial Least Squares - Discriminant Analysis (PLS-DA)

To assess the significance of class discrimination, partial least squares - discriminant analysis (PLS-DA) was performed. The latter is a supervised method that uses multivariate regression techniques to extract, the information predicting the class membership via linear combination of original variables. The exometabolome samples were seen clearly separated by PLS-DA analysis (Fig. 3.25). The R^2 and Q^2 value of 0.95 and 0.4 respectively indicated goodness of fit and predictability, suggesting representative model for the difference in metabolomes.

3.3.2.5. Important metabolic feature identification

The VIP scores derived from PLS-DA model was used to ascertain key metabolic features significant for group separation. Metabolites with VIP score >1 were considered to have statistically contributed to the model. Forty metabolites were identified as statistically significant contributors to the model (Fig. 3.26 A) and were mainly accountable for group separation in the model. Metabolites were classified based on their chemical structure as alkanes (20%), sugars (28%), organic acid (17%), amino acid (10%), fatty acid (8%), nucleotide (3%) and others (5%) (Fig. 3.26 B). Amongst these forty metabolites, a total of 19, 25 and 33 were detected in G3, G9 and G18 samples respectively (Fig. 3.27). The count of common and unique metabolites is displayed as Venn-diagram and their structural

classification as pie-chart in Fig. 3.27. These metabolites were also enriched to their respective pathways in Kyoto Encyclopedia of Genes and Genomes (KEGG) database (Fig. 3.28).

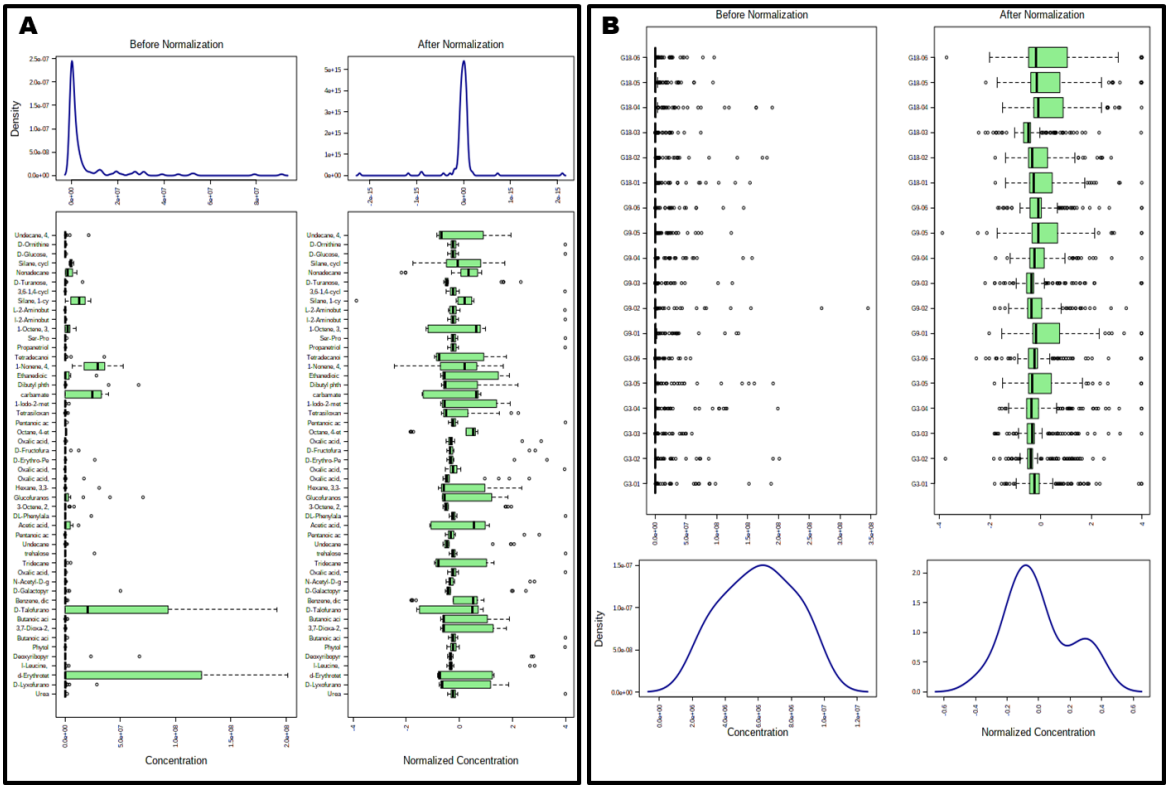

Fig. 3. 22: Box plots and kernel density plots before and after normalization of footprint data from glucose grown *Rbx. benzoatilyticus* cells at three time points.

Feature view (A) and sample view (B) of the exometabolome data before and after normalization.

Experimental conditions were similar to those described under Fig. 3.15, except for glucose grown cells were harvested at 3rd (G3), 9th (G9) and 18th (G18) day of growth. Metabolites extracted from spent media were derivatized and analysed by GC-MS. Datum generated was log transformed (log_2) and sample specific normalization (dry weight of the sample) was carried out before performing statistical analysis.

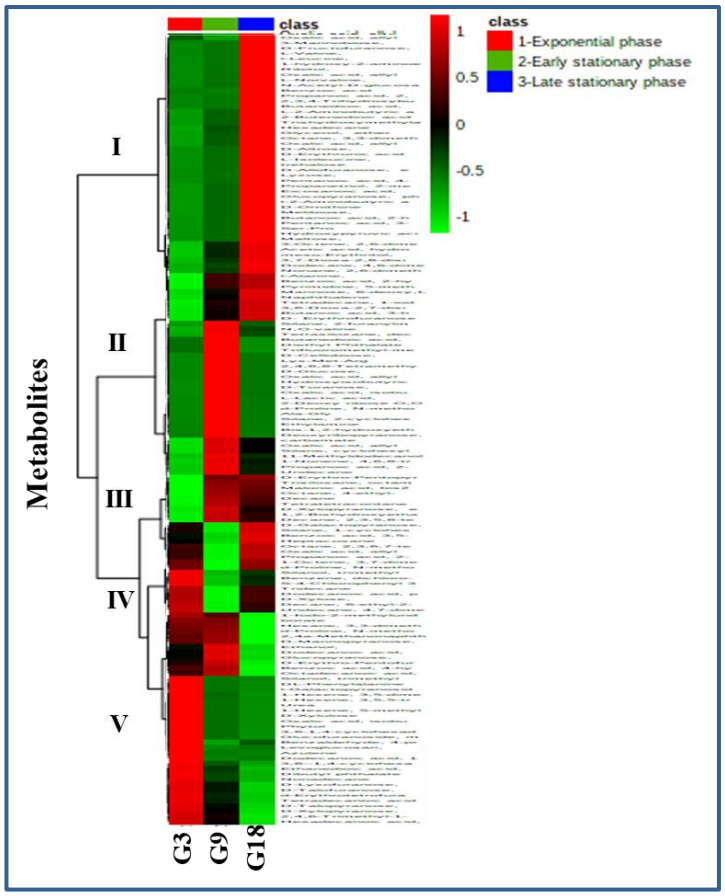

Fig. 3. 23: Hierarchical clustering analysis of dynamic metabolites from glucose grown *Rbx. benzoatilyticus* cells.

Metabolites from spent media of glucose grown cells at three different time points are represented as heatmap. Clustering was performed with Pearson correlation as distance matrix using MetaboAnalyst online software. Metabolites in red represent higher concentration and those in green as low concentration.

Normalised datum obtained as described under Fig. 3.22 was subjected to hierarchical clustering analysis using MetaboAnalyst. G3, sample from 3rd day growth on glucose; G9, sample from 9th day growth on glucose; G18, sample from 18th day growth on glucose.

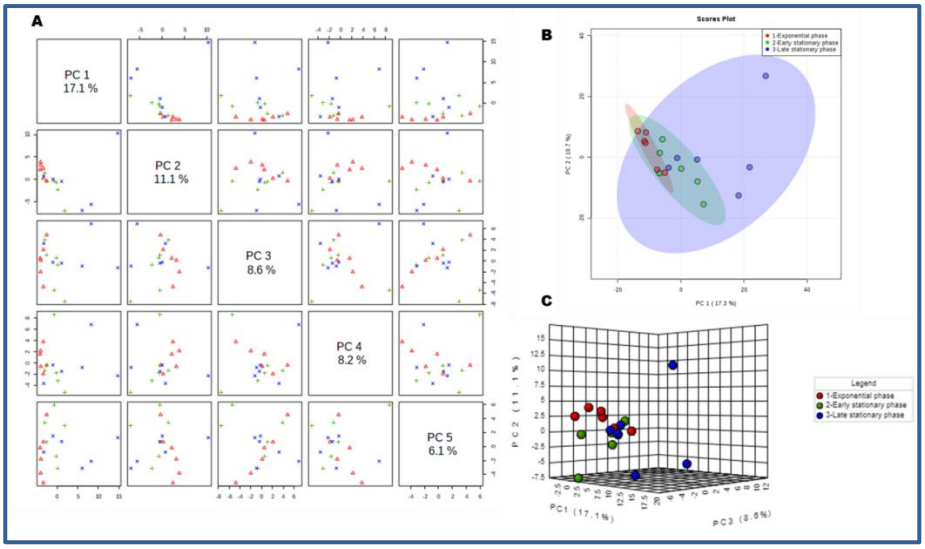

Fig. 3. 24: Principal component analysis (PCA) of exometabolome from glucose grown *Rbx. benzoatilyticus* cells.

Pairwise score plots between the selected PCs (A). 2-D (B) and 3-D (C) scores plot between selected PCs.

Normalised datum obtained from GC-MS analysis as described under Fig. 3.22 was subjected to PCA using MetaboAnalyst. Metabolome from G3, G9 and G18 samples are represented in red, green and blue colour respectively. PC, principal component; PCA, principal component analysis.

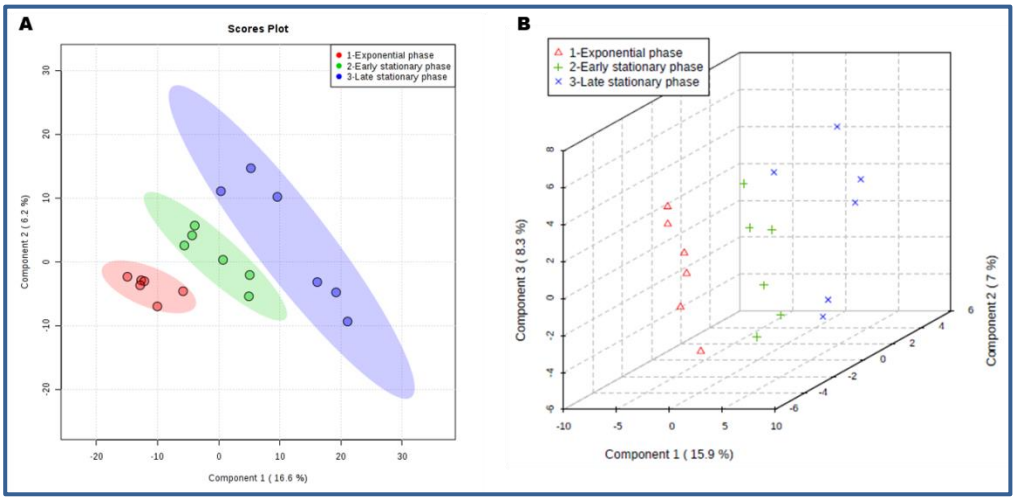

Fig. 3. 25: Partial least square discriminant (PLS-DA) scatter plot analysis of exometabolome from glucose grown *Rbx. benzoatilyticus* cells.

2-D (A) and 3-D (B) scores plot between selected PCs.

Normalised datum obtained from GC-MS analysis as described under Fig. 3.22 was subjected to PLS-DA analysis using MetaboAnalyst. Metabolome from G3, G9 and G18 samples are represented in red, green and blue colour respectively. PC, principal component; PLS-DA, partial least square discriminant analysis.

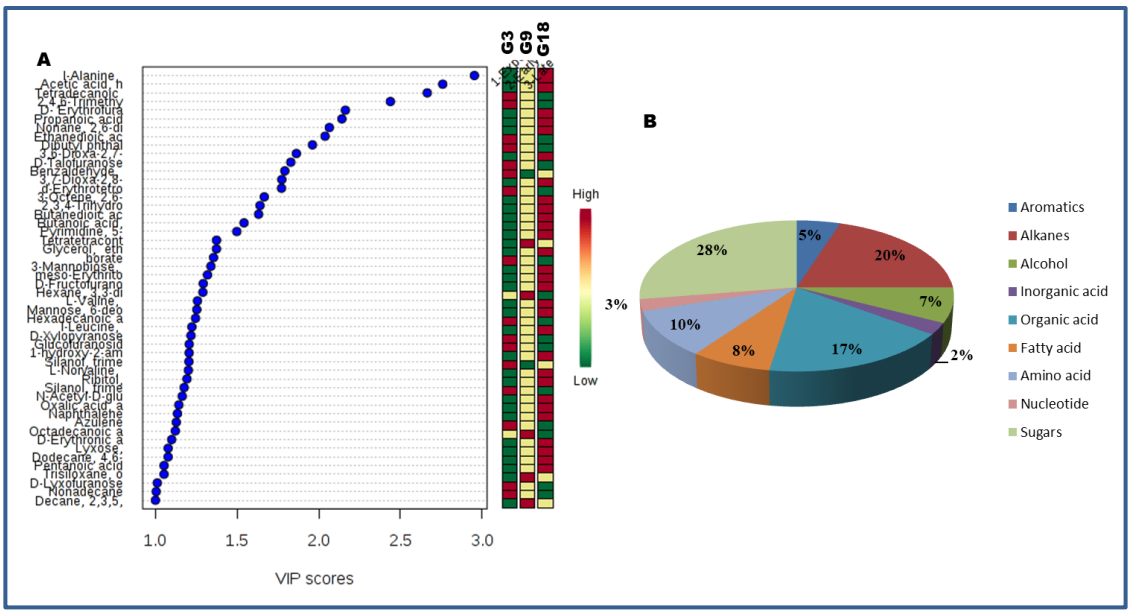

Fig. 3. 26: Variable importance on projection (VIP) scores of the metabolites obtained from PLS-DA analysis of glucose grown *Rbx. benzoatilyticus* cells.

Coloured boxes on right side indicate relative abundance of metabolites at different time points. Metabolites with VIP ≥ 1.0 *was considered to be statistically significant.*

Data processing parameters were same as described under Fig. 3.25 and the same datum was subjected to VIP analysis by using MetaboAnalyst. G3, sample from 3rd day growth on glucose; G9, sample from 9th day growth on glucose; G18, sample from 18th day growth on glucose.

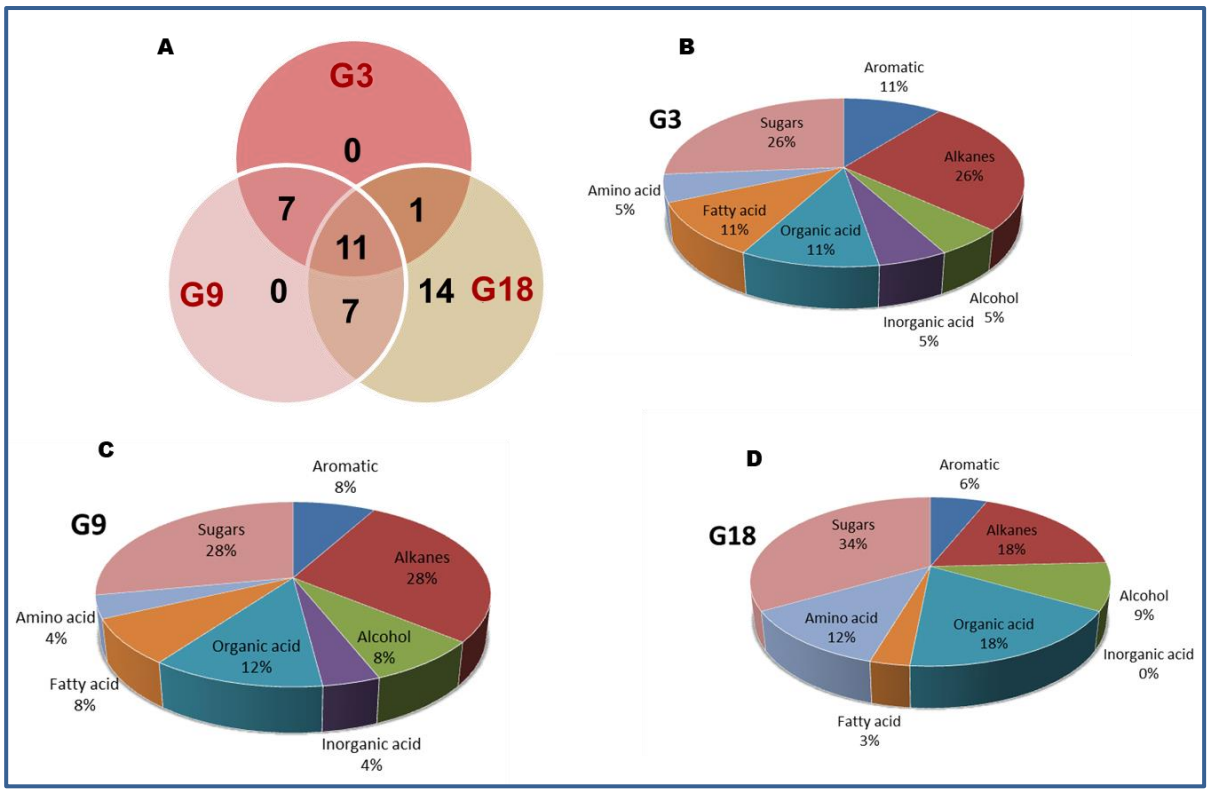

Fig. 3. 27: Structural categorization of metabolites from glucose grown *Rbx. benzoatilyticus* cells.

Venn-diagram presenting unique and shared metabolites between the three time points of glucose grown of Rbx. benzoatilyticus cells (A). Pie-chart representing structural categorization of metabolites from spent media of exponential phase (B), early stationary phase (C) and late stationary phase cells (D).

Metabolites obtained as described under Fig. 3.26 were classified based on their structure and according to the functional group they carried. G3, sample from 3rd day growth on glucose; G9, sample from 9th day growth on glucose; G18, sample from 18th day growth on glucose.

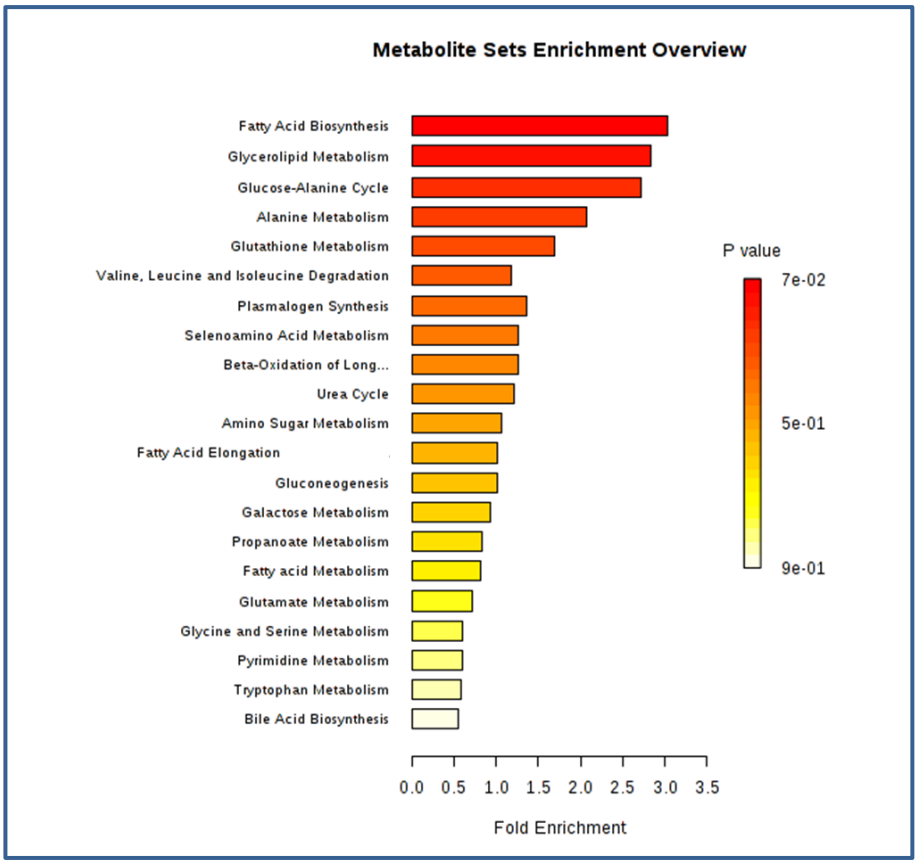

Fig. 3. 28: Metabolite enrichment based on KEGG pathway map.

Metabolites obtained as described under Fig. 3.26 were enriched to different pathways based on their function in KEGG database.

3.4. Proteomic insights of glucose grown *Rbx. benzoatilyticus* cells

To decipher the functional response of glucose photometabolism on *Rbx. benzoatilyticus*, Isobaric Tag for Relative and Absolute Quantification (iTRAQ) technique was employed. Proteome was isolated from three samples grown on glucose (G3, G9 and G18) in duplicate (see materials and methods). Proteome from malate grown sample (M3) was used for comparison. Proteomic inventory of the iTRAQ identified proteins was studied (refer to section 3.4.1). The fold change (FC) ratio for each protein at each time point was calculated separately for downstream analysis. To get the holistic view, firstly we compared the abundance of proteins at early stationary phase of glucose grown cells (G9) with that of malate grown ones (refer to section 3.4.2). Further, dynamics of protein abundance in glucose grown cells was studied where the protein abundance at G9 and G18 were compared with those at G3 (refer to section 3.4.3).

3.4.1. Proteomic inventory of *Rbx. benzoatilyticus*.

Proteome isolated from all the samples were subjected to SDS-PAGE analysis before iTRAQ profiling to check the quality. *Rbx. benzoatilyticus* contains 3898 protein-coding genes (Mohammed et al., 2011) of which, 2431 proteins were detected in the iTRAQ analysis (accounting to 62% of theoretical proteome of *Rbx. benzoatilyticus*) (Fig. 3.29). These detected proteins were subjected to *in silico* analysis to determine their physico-chemical properties (molecular mass, isoelectric point (pI) and grand average hydropathy (GRAVY)) using online tool ProtParam (www.expasy.org). The 3D scatter plot of molecular mass *vs*. pI *vs*. hydropathy indicated two clusters of proteins, in the pI range of 3.8 to 7.0 and 8.0 to 11.0 respectively (Fig. 3.30). A computed pI value less than 7 indicates protein to be acidic and greater than 7 represents basic. Based on the computed pI values, 63.7% proteins were observed to be acidic, and 36.2% were basic. The GRAVY value for a protein is calculated as the sum of hydropathy values of all the amino acids divided by the number of residues. A

positive value indicates hydrophobicity and a negative value indicates hydrophilicity. Based on the computed GRAVY values, 35.9% proteins were hydrophobic, 63.9% were hydrophilic while a few (0.2%) were neutral. These results suggest a broad coverage of proteome. Detected proteins were filtered based on the cut-off values of unused prot score > 2, peptides ≥ 2 and a false discovery rate of $< 1.0\%$ to give a total of 1935 proteins (which corresponds to 49.6% of the total proteome). Theses 1935 filtered proteins were subjected to statistical analysis and proteome profiling.

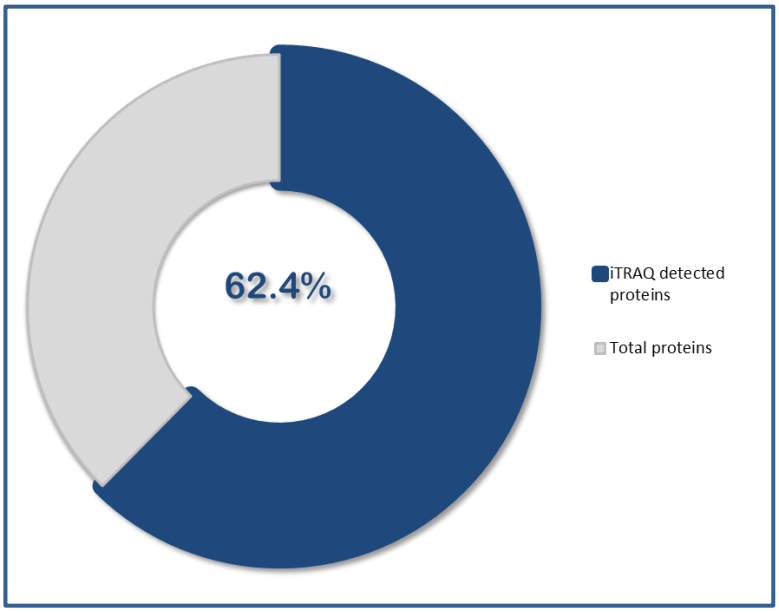

Fig. 3. 29: Proteome from malate/glucose grown cells of *Rbx. benzoatilyticus*.

Fraction of proteins detected by iTRAQ analysis.

Experimental conditions were same as described under Fig. 3.15, except for the culture was harvested and proteins were isolated from cell biomass, lyophilised and analysed by iTRAQ (isobaric tags relative and absolute quantitation). Proteins were identified and quantified by using ProteinPilot 5.0.

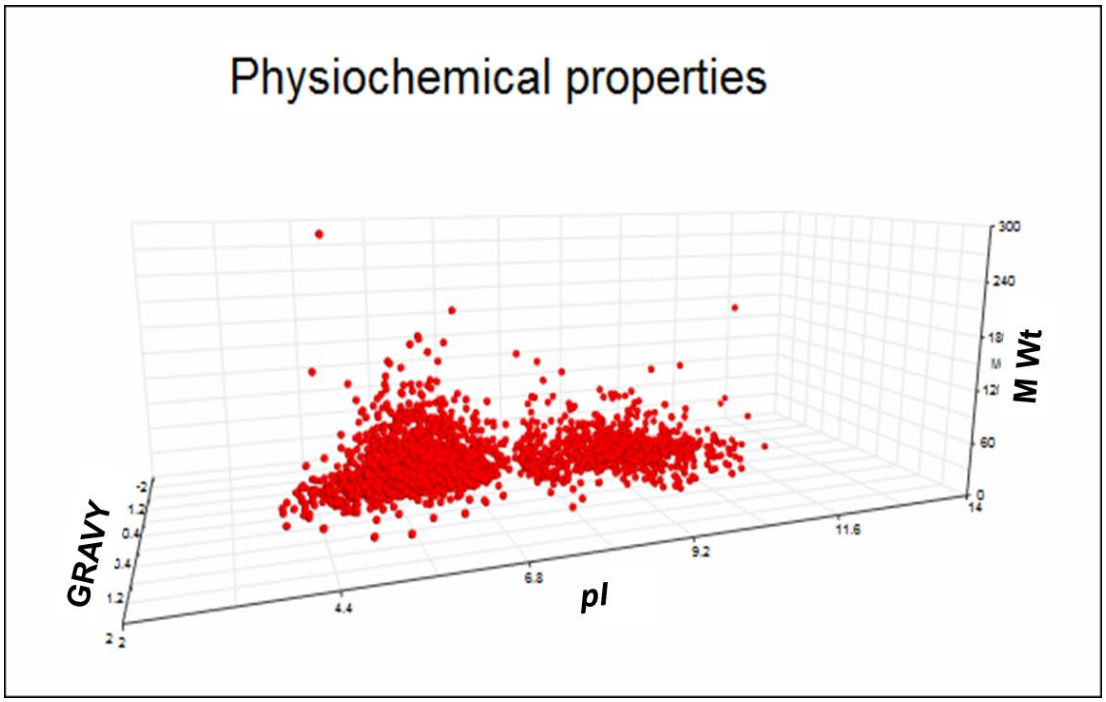

Fig. 3. 30: Scatter plot of molecular weight versus isoelectric point versus hydropathy of proteins detected by iTRAQ analysis.

Proteins identified by iTRAQ analysis as described under Fig. 3.29 were subjected to pI, M wt analysis by ExPASy tool (www.expasy.org), and GRAVY by Sequence Manipulation Suite (www.bioinformatics.org/sms2/protein_gravy). The values were plotted as 3-D scatter plot of GRAVY versus pI versus M wt. GRAVY, grand average of hydropathy; pI, isoelectric point; M wt, molecular weight.

3.4.2. Cellular responses of glucose-grown cells of *Rbx. benzoatilyticus* with respect to malate grown cells.

To capture the events associated with the metabolic rewiring, early stationary phase glucose-grown (9 days incubated, G9) cells were selected. The FC value of a protein, expressed as ratio, was calculated by comparing its abundance in glucose grown cells with that of respective protein in malate grown cells. The FC values were $\log_2$ transformed and considered for the pathway enrichment and other analyses.

3.4.2.1. Statistical analysis and identification of differentially regulated proteins.

Correlation and linear regression analysis of the $\log_2$ FC values of identified 1935 proteins from two biological replicates was carried out to evaluate their reproducibility. The analysis exhibited a correlation coefficient value of $R = 0.9, R^2 = 0.827$ (Fig. 3.31), indicating the reproducibility of the datum with line equation of $y = 0.97x - 0.0092$ (slope $=$ 0.97 and intercept $=$ -0.0092; Fig. 3.31).

Proteins with error factor (EF) $\leq$ 2 were identified and subjected to volcano plot analysis to identify the statistically significant differentially expressed proteins, DEPs (Fig. 3.32). A protein with a fold change (FC) cut-off value $|\log_2 FC| \geq 0.26$ and p value $\leq$ 0.05 in at least two of the four expression ratio values was considered as significantly affected differentially expressed protein (DEP) or dysregulated. A total of 378 proteins were identified as significantly DEPs of which 162 were up-regulated and 216 were down-regulated (Table S1). The average of $\log_2$ fold change of up-regulated proteins was 0.73 and that of down-regulated proteins was -0.88.

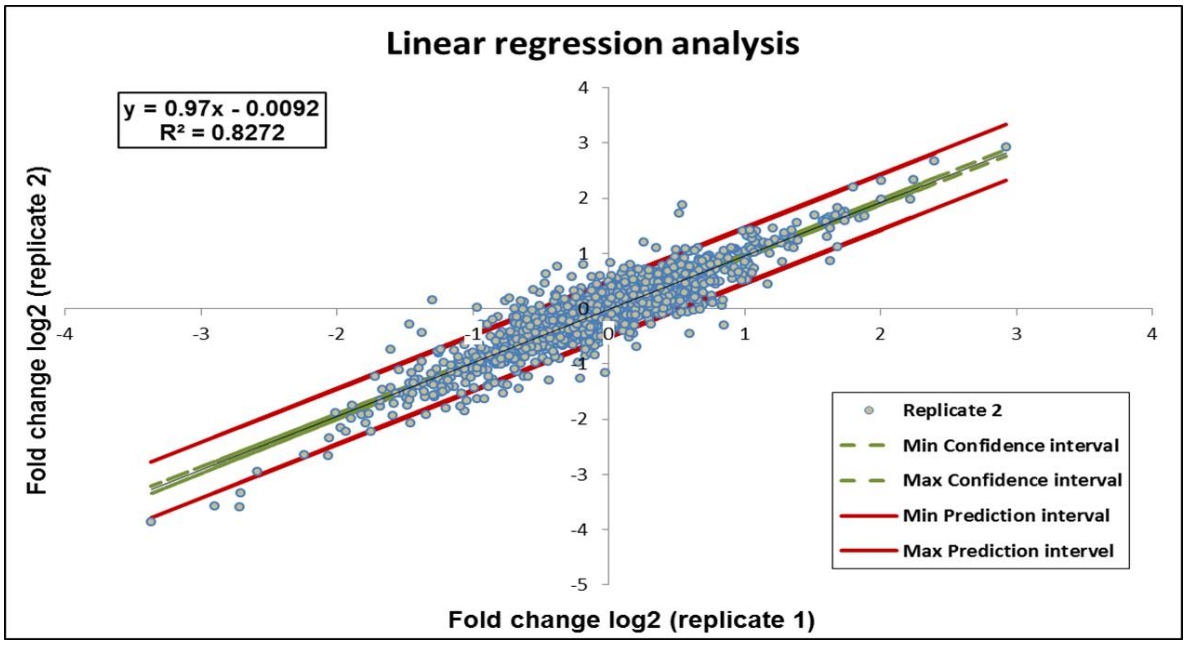

Fig. 3. 31: Correlation analysis of iTRAQ identified proteins from two biological replicates of stationary phase *Rbx. benzoatilyticus* cells.

Liner regression analysis of iTRAQ identified proteins. Each blue dot corresponds to single protein. Area between red lines represents the prediction band and that between green lines represents the confidence band. R^2, correlation coefficient value.

Proteins from early stationary phase samples identified by iTRAQ analysis as described under Fig. 3.29 were selected for linear regression analysis. Fold change, corresponding to the ratio of protein abundance (glucose grown/malate grown), of two biological replicates from iTRAQ analysed samples were log transformed (log_2) and plotted as scatter plot.

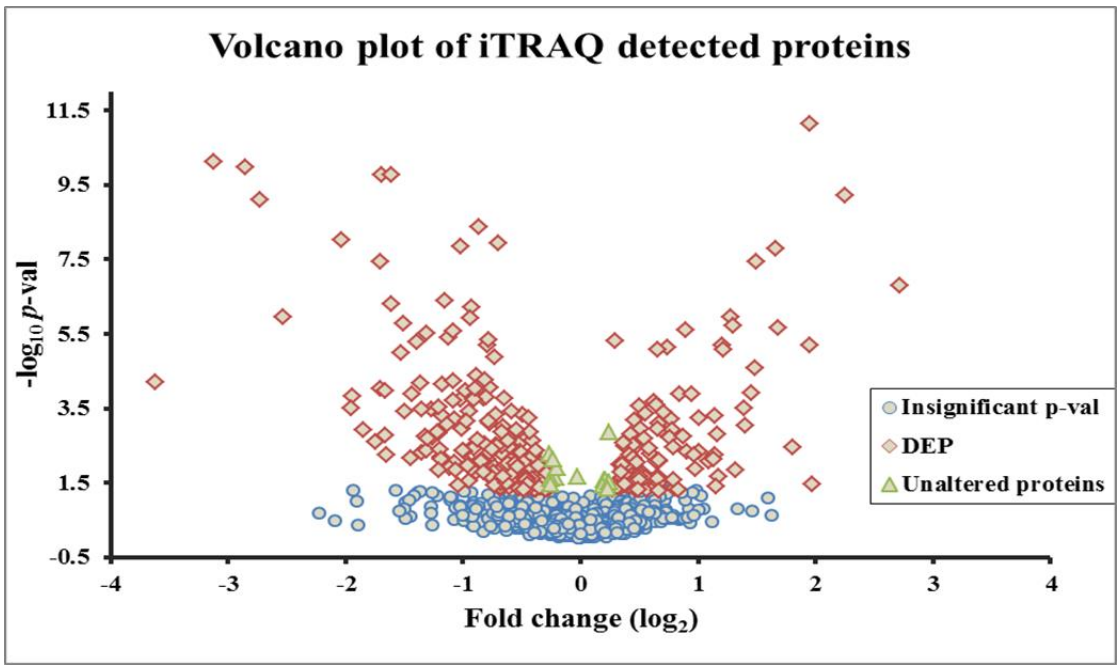

Fig. 3. 32: Volcano plot analysis of stationary phase iTRAQ identified proteins from *Rbx. benzoatilyticus*.

Volcano plot analysis representing fold change (log_2) value versus p-value (log_{10}) of iTRAQ identified proteins.

Data processed as described under Fig. 3.31 was subjected to volcano plot analysis. Red diamonds stipulate statistically significant (p-value≤ 0.05) dysregulated proteins, positive and negative values on X-axis represents up-regulated and down-regulated protein respectively. Green triangles indicate proteins with unaltered expression and blue circles specify statistically insignificant (p-value> 0.05) proteins. Proteins with $log_2 FC \geq 0.26$ value were considered up-regulated ($FC\ ratio \geq 1.2$) and those with a value of $log_2 FC \leq 0.26$ were considered down-regulated ($FC\ ratio \leq 0.83$). FC, fold change.

3.4.2.2. Functional classification of differentially regulated proteins.

To identify the major pathways modulated, DEPs were enriched to different pathways based on their function in gene ontology (GO) and KEGG database. The GO analysis demonstrated 1582, 811 and 2260 protein categories amongst biological process (BP), cellular component (CC) and molecular function (MF) respectively. The most representative GO terms (associated with BP, CC and MF) are depicted in Fig. 3.33.

KEGG database (http://www.genome.jp/kegg) was used to assign DEPs to specific pathways which are discussed in detail in the next section. Differentially expressed proteins were categorized into 22 pathways under 5 broad categories based on their function in KEGG database mainly comprising of general cellular metabolism, genetic information processing, environmental information processing, cellular process and uncharacterised proteins (Fig. 3.34, Table S1). Count of DEPs enriched under membrane transport was highest followed by central carbon metabolism, hypothetical proteins, energy metabolism, amino acid metabolism, folding, sorting and degradation of proteins (Fig. 3.34).

Amongst the up-regulated proteins, 27%, 22%, 19%, 10% and 22% enriched under metabolism, genetic information processing, environmental information processing, cellular process and uncharacterised respectively (Fig. 3.35 A). Majority of up-regulated proteins were related to membrane transport (17%), followed by hypothetical proteins (11%). Lipid and fatty acid metabolism, amino acid metabolism, transcription, regulatory proteins, quorum sensing and signal transduction, porin/pilus/cell division related protein were up-regulated by 5%.

Amongst the down-regulated proteins, 41%, 15%, 15%, 4% and 25% were related to metabolism, genetic information processing, environmental information processing, cellular process and uncharacterised respectively. More specifically, major contributing pathways included glycolysis (7%), electron transport chain (ETC; 7%), amino acid metabolism (5%),

pigment biosynthesis and photosynthesis (7%) amongst metabolism (Fig. 3.35 B). Protease/peptidase (5%), chaperone (3%), and replication (3%) were the major contributor enriched under genetic information processing. Amongst down-regulated proteins enriched under environmental information processing (15 %), membrane transport/translocation (14 %) comprised of major category.

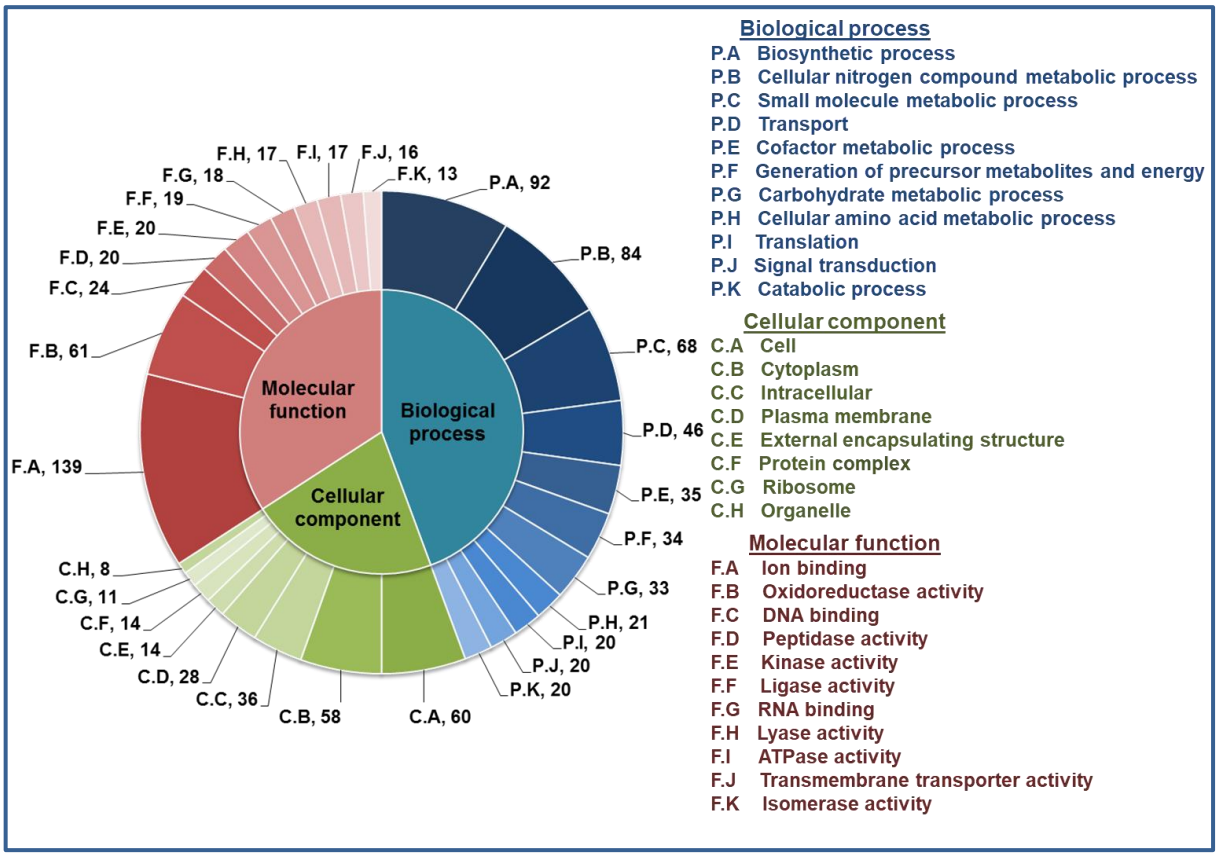

Fig. 3. 33: Functional categorization of differentially regulated proteins based on their function in GO.

Statistically significant differentially regulated proteins obtained from volcano plot analysis as described under Fig. 3.32, were functionally categorized based on GO under the head of biological process, cellular component and molecular function. GO, gene ontology.

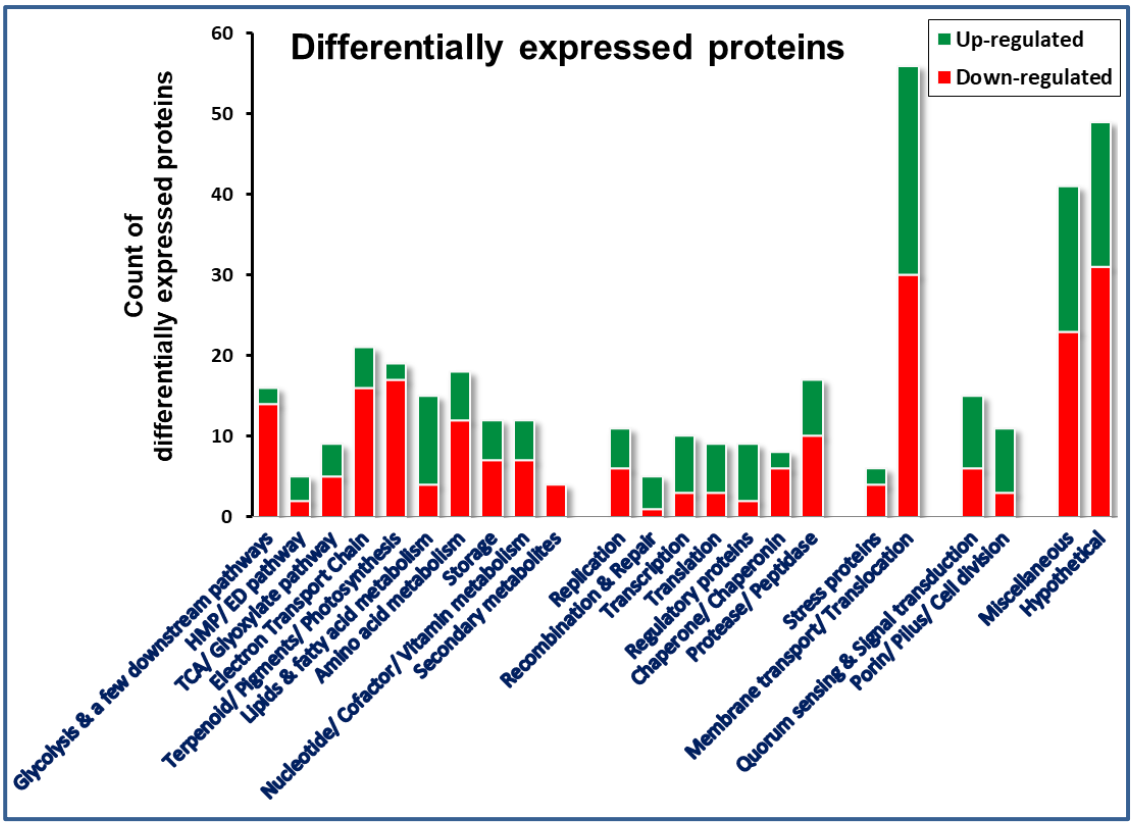

Fig. 3. 34: Functional classification of differential regulated proteins of *Rbx. benzoatilyticus* identified by iTRAQ analysis.

Functional classification was carried according to KEGG (Kyoto Encyclopedia of Genes and Genomes database, www.genome.jp/kegg/) database.

Differential regulated proteins identified by volcano plot analysis as described under Fig. 3.32 were functionally annotated. Datum is plotted as bar chart representing the count of proteins related to different pathways of metabolism (A), genetic information processing (B), environmental information processing (C), cellular process (D) and uncharacterised (E).

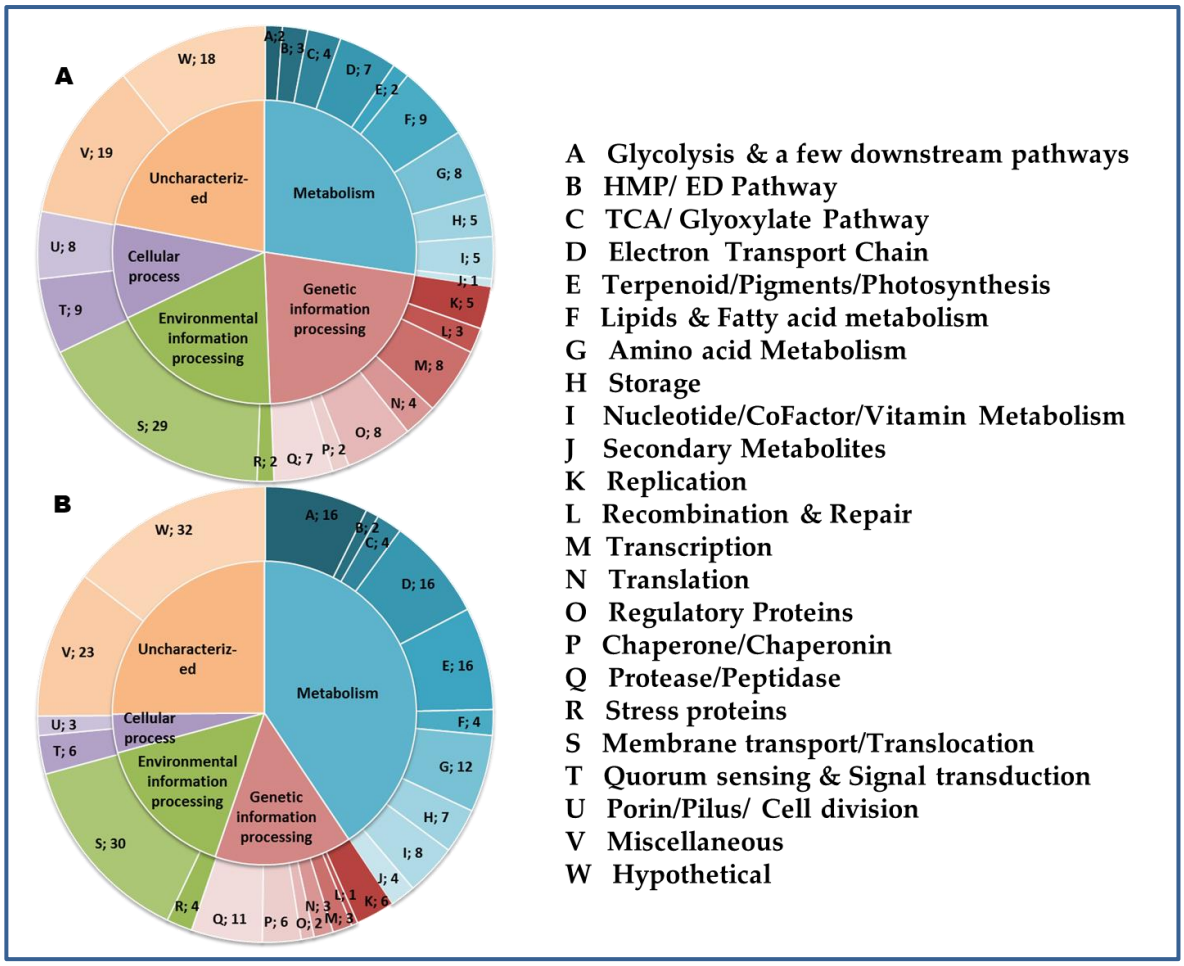

Fig. 3. 35: Functional categorization of differentially regulated proteins based on their function in KEGG database.

*Functional categories of up-regulated proteins (**A**) and down-regulated proteins (**B**).*

Up-regulated and down-regulated proteins stipulated from the volcano plot analysis as described under Fig. 3.32 were categorized based on their function in KEGG database. Count of DEPs belonging to each pathway is given next to it. KEGG, Kyoto Encyclopedia of Genes and Genomes.

3.4.2.3. Metabolic adaptations glucose-grown Rbx. benzoatilyticus cells.

Proteins related to Embden-Meyerhof-Parnas (EMP) pathway such as, 6-phosphofructokinase (RBXJA2T_16767), fructose-1,6-bisphosphate aldolase (RBXJA2T_06270, RBXJA2T_18668), glyceraldehyde-3-phosphate dehydrogenase (RBXJA2T_02647), phosphoglycerate kinase (RBXJA2T_06250; unaltered expression), phosphoglycerate mutase (RBXJA2T_00150) and enolase (RBXJA2T_12387) (Table S1) of EMP pathway were down-regulated. Proteins involved in gluconeogenesis (PEP carboxy kinase (RBXJA2T_05268) and fructose-1,6-bisphosphatase (RBXJA2T_18688)) and non-oxidative phase of pentose phosphate pathway (transketolase (RBXJA2T_18678)) were also down-regulated in glucose-grown cells.

3.4.2.4. Glucose-grown cells displayed extensive rewiring of central carbon metabolism.

The proteins related to ED pathway like glucokinase (RBXJA2T_07368) and glucose-6-phosphate-1-dehydrogenase (RBXJA2T_00995) were up-regulated while phosphogluconate dehydratase (RBXJA2T_14896) was unaffected in glucose-grown cells (Table S1). Further, down-regulation of pyruvate dehydrogenase subunit-E (RBXJA2T_04798) and pyruvate flavodoxin/ferredoxin oxidoreductase (RBXJA2T_04953), involved in the conversion of pyruvate to acetyl CoA, along with down-regulation of lactate dehydrogenase (RBXJA2T_08560) and alcohol dehydrogenase (RBXJA2T_16662) suggests that pyruvate is not metabolized through either of these routes. Additionally, aldehyde dehydrogenase (Aldh) (RBXJA2T_18613) involved in pyruvate catabolism leading to acetate production was highly up-regulated in glucose-grown cells (Table S1).

3.4.2.5. Activation of lipid/fatty acid β-oxidation and glyoxalate shunt in glucose-grown cells.

Proteins involved in lipid catabolism, viz., putative phospholipase A1 (PldA) (RBXJA2T_03603), Phospholipase D/transphosphatidylase (RBXJA2T_07115) protein and

esterase/lipase-like protein (RBXJA2T_02347) were up-regulated in glucose-grown cells. The study also revealed up-regulation of proteins related to β-oxidation of fatty acids (Table S1) such as acyl CoA dehydrogenase (RBXJA2T_05028), enoyl CoA hydratase/isomerase (RBXJA2T_03031), putative long-chain-fatty-acid-CoA ligase protein (RBXJA2T_13294; unaltered expression), acetyl-CoA acetyl transferase (RBXJA2T_02991) and short-chain dehydrogenase/reductase sdr (RBXJA2T_10314) in glucose-grown cells. We observed up-regulation of key enymes of glyxoylate cycle– citrate synthase (RBXJA2T_09894), isocitrate lyase (RBXJA2T_08565) and malate synthase (RBXJA2T_00704; expression unaltered) along with down-regulation of TCA pathway protein (isocitrate dehydrogenase (RBXJA2T_10419) in the glucose-grown cells (Table S1).

3.4.2.6. Impaired oxidative-phosphorylation in glucose-grown cells.

Although, NADH dehydrogenase (Complex I) (RBXJA2T_12717, RBXJA2T_12682) and succinate dehydrogenase (complex II) (RBXJA2T_09909) of electron transport chain (ETC) were up-regulated in glucose-grown cells, other ETC related proteins such as oxidoreductase FAD/NAD(P)-binding domain protein (RBXJA2T_04988), cytochrome c prime (RBXJA2T_11046), class I cytochrome c (RBXJA2T_18799), electron transfer flavoproteinα/β-subunit (RBXJA2T_19081, RBXJA2T_19086) and FoF1 ATP synthase subunit β (RBXJA2T_16907) were down-regulated suggesting differential regulation of ETC. Further, we observed up-regulation of membrane-bound proton-translocating pyrophosphatase (RBXJA2T_19256) (Table S1), which is known to express under low energy (ATP) conditions (Lo and Pe, 2004).

3.4.2.7. Repression of photosynthetic machinery in glucose-grown cells.

Proteins involved in isoprene and carotenoid biosynthesis were down-regulated, which includes proteins such as 4-hydroxy-3-methylbut-2-enyl diphosphate reductase (RBXJA2T_18493), and spheroidene monooxygenase (RBXJA2T_09487) (Table S1).

Additionally, chlorophyll/heme biosynthetic proteins, delta-aminolevulinic acid dehydratase (RBXJA2T_16272), porphobilinogen deaminase (RBXJA2T_17559), uroporphyrinogen decarboxylase (RBXJA2T_16937), glutamate-1-semialdehyde aminotransferase (RBXJA2T_12137), (Table S1) were also down-regulated.

3.4.2.8. Molecular responses of glucose-grown cells.

Though DNA gyrase subunit A (RBXJA2T_16527) and DNA topoisomerase IV subunit A (RBXJA2T_18233), which are involved in unwinding and decatenation of DNA, were unaffected in the proteome datum, DNA-directed DNA polymerase (RBXJA2T_09347) was down-regulated but DNA polymerase III subunit epsilon (RBXJA2T_04543) that has proof-reading and editing function (Koonin and Deutscher, 1993) was up-regulated (Table S1). Also, DNA repair protein RadA (RBXJA2T_18874), Holliday junction DNA helicase RuvB (RBXJA2T_16317), transcription-repair coupling factor (RBXJA2T_03364) and HhH-GPD family protein (RBXJA2T_10469) that are known to be involved in recombination and repair were up-regulated (Table S1).

Although, the expression of DNA-directed RNA polymerase subunit β (RBXJA2T_03267) was unaltered, several transcriptional regulators such as Crp/FNR family (RBXJA2T_04128), HTH-type (RBXJA2T_01345), TetR family (RBXJA2T_15433), RpiR family (RBXJA2T_01000), histone-like nucleoid-structuring protein H-NS (RBXJA2T_09122) and histidine kinase transcription regulator protein (RBXJA2T_01165) were up-regulated in glucose grown cells (Table S1). Furthermore, poly(A) polymerase (PAP I) (RBXJA2T_10736), polynucleotide phosphorylase (PNPase)/polyadenylase (RBXJA2T_12657), ribonuclease E (RNase E) (RBXJA2T_07978) and ribonuclease R (RBXJA2T_17981) were up-regulated (Table S1).

Proteins involved in translation, initiation and fidelity like 30S ribosomal proteins S1 (RBXJA2T_16502), S3 (RBXJA2T_02145), S4 (RBXJA2T_02245), S5 (RBXJA2T_02205), S8 (RBXJA2T_02190), S21 (RBXJA2T_12532) were unaffected, while elongation factors Ts (RBXJA2T_18006), Tu (RBXJA2T_03242) and G (RBXJA2T_03247) were down-regulated. However, 50S ribosomal proteins L2 (RBXJA2T_02130), L14 (RBXJA2T_02170), L16 (RBXJA2T_02150), L20 (RBXJA2T_08785) and L29 (RBXJA2T_02155) along with peptidyl-tRNA hydrolase (RBXJA2T_15518) were up-regulated (Table S1). Moreover, we observed up-regulation of heat shock protein Hsp20 (RBXJA2T_02095, RBXJA2T_02100, RBXJA2T_02105) and other proteases such as peptidase U32 (RBXJA2T_13014), peptidase M24 (RBXJA2T_10831), protease Do (RBXJA2T_11997) and protease IV (RBXJA2T_16957)(Table S1) which are involved in maintaining the protein quality control of the cells (Molière and Turgay, 2009). Proteome datum revealed up-regulation of Ppx/GppA phosphatase (RBXJA2T_09377) which is involved in the interconversions of guanosine penta to tetra poly phosphates [pppGpp/ppGpp; known as alarmone](Choi et al., 2012).

Proteins involved in signal transduction and chemotaxis such as methyl-accepting chemotaxis sensory transducer (RBXJA2T_13604, RBXJA2T_12107, RBXJA2T_13914), chemotaxis response regulator (RBXJA2T_18538) and CheW protein (RBXJA2T_11777) were up-regulated (Table S1). Moreover, our study revealed up-regulation of Acetyl-CoA acetyltransferase (RBXJA2T_02991) (Table S1) involved in the pol-β-hydroxyalkanoate (PHA) biosynthesis (Kim and Copeland, 1997). Apart from this, a large number of hypothetical proteins and membrane transport proteins were differentially regulated along with lysophospholipid transporter LplT (RBXJA2T_18889) and toluene tolerance protein (RBXJA2T_01010) which might have plausible function in cell survival under glucose induced stressed condition.

3.4.3. Proteome dynamics: From exponential phase to pigment loss state to growth arrest/ non-cultivable state.

Dynamics of protein was studied considering 3 time points: exponential phase (G3), early stationary phase (G9) and late stationary phase (G18). Comparing the abundance of protein(s) at G9 and G18 with those of respective protein(s) at G3, FC values were calculated. The calculated FC values were log transformed ($\log_2$) and considered for downstream analyses.

3.4.3.1. Statistical analyses and differentially expressed proteins (DEPs) identification.

To evaluate the reproducibility of the datum, correlation and linear regression analysis of the $\log_2$ FC values of iTRAQ identified 1935 proteins from two biological replicates was carried out. The analysis exhibited a correlation coefficient value of $R = 0.8, R^2 = 0.642$ at G9 (Fig. 3.36 A), indicating the reproducibility of the datum with line equation of $y = 0.74x - 0.0131$ (slope $= 0.74$ and intercept $= -0.0131$; Fig. 3.36 A). The analysis of G18 proteome exhibited a correlation coefficient value of $R = 0.73, R^2 = 0.532$ (Fig. 3.36 B), representing the reproducibility of the datum with line equation of $y = 0.71x - 0.0235$ (slope $= 0.71$ and intercept $= -0.0235$; Fig. 3.36 B).

To identify the statistically significant DEPs, iTRAQ detected proteins were subjected to volcano plot analysis (Fig. 3.37). Based on the applied cut-off (see materials and methods), 321 filtered proteins met the criteria of statistical significance. Out of these 321 proteins, 312 proteins were observed as significantly dysregulated ($|\log_2 FC| \geq 0.26$) at single and/or both the time points. Figure 3.38 represents the dynamics of DEPs as heatmap.

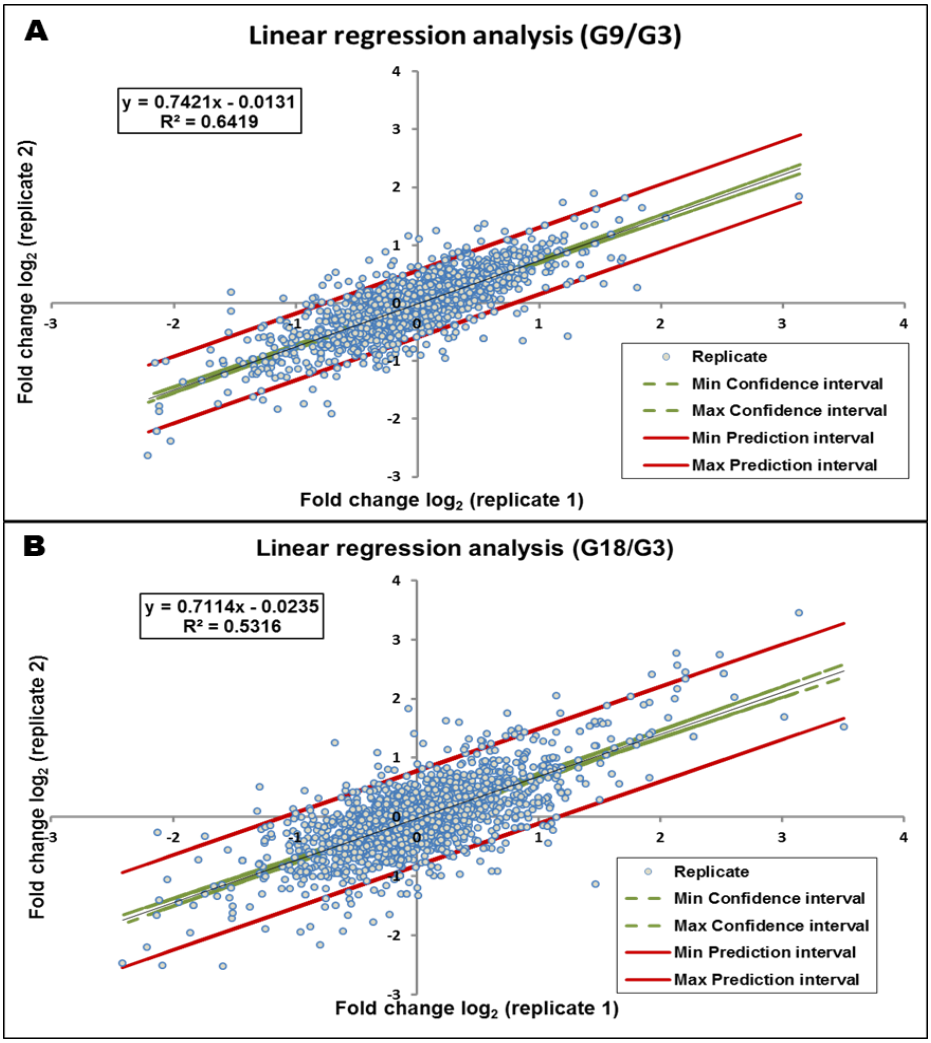

Fig. 3. 36: Correlation analysis of iTRAQ identified proteins from glucose grown *Rbx. benzoatilyticus* cells.

*Liner regression analysis of G9 (**A**) and G18 (**B**) iTRAQ identified proteins.*

Proteins from glucose grown samples identified by iTRAQ analysis as described under Fig. 3.29 were selected for linear regression analysis. Proteome of early and late stationary phase cells (G9 and G18 respectively) were compared with those of exponential phase cells (G3). Fold change, corresponding to the ratio of protein abundance (either G9/G3 or G18/G3 separately), of two biological replicates from iTRAQ analysed samples were log transformed (log_2) and plotted as scatter plot. Each blue dot corresponds to single protein. Area between red lines represents the prediction band and that between green lines represents the confidence band. R^2, correlation coefficient value; G3, proteome extracted at 3^{rd} day of growth on glucose (exponential phase cells); G9, proteome extracted at 9^{th} day of growth on glucose (early stationary phase cells); G18, proteome extracted at 18^{th} day of growth on glucose (late stationary phase cells).

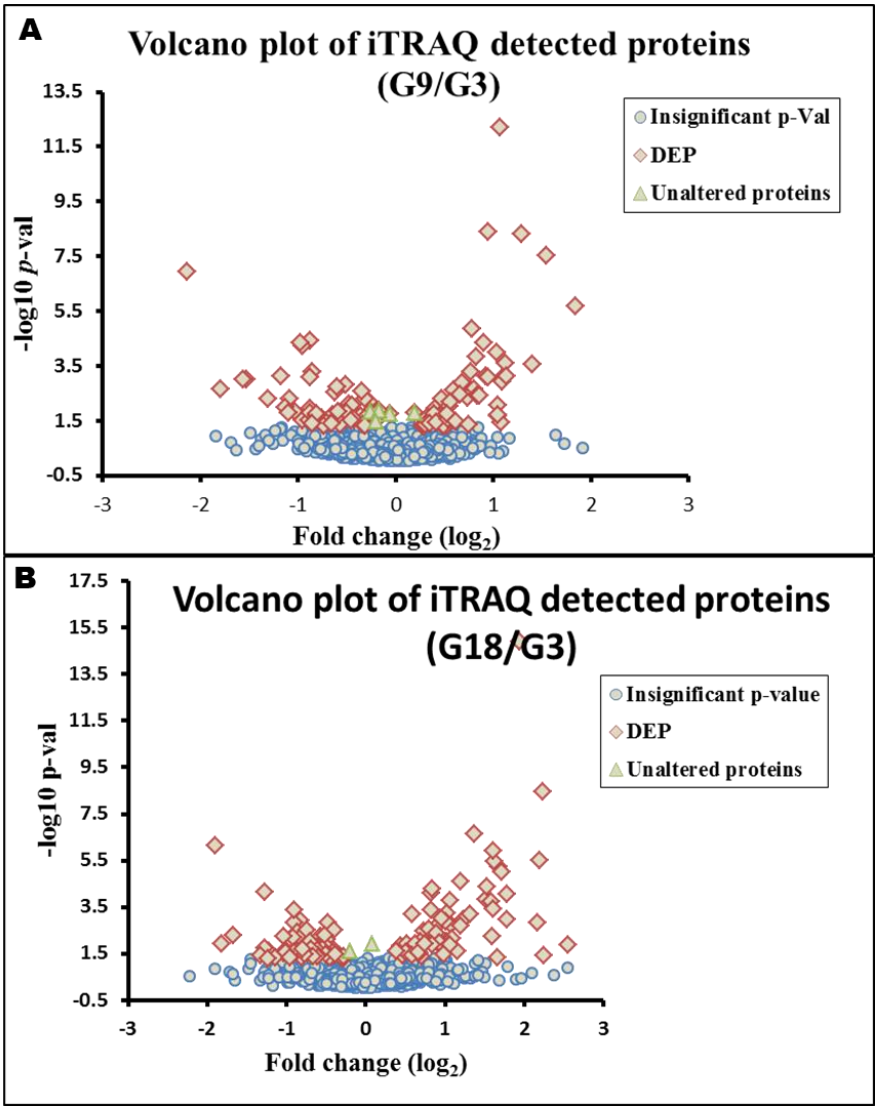

Fig. 3. 37: Dynamics of volcano plot analysis of iTRAQ identified proteins from glucose grown *Rbx. benzoatilyticus* cells.

*Volcano plot analysis representing fold change (log_2) value versus p-value (log_{10}) at G9 (**A**) and G18 (**B**) of iTRAQ identified proteins.*

Datum processed as described under Fig. 3.36 was subjected to volcano plot analysis. Red diamonds specify statistically significant ($p\text{-value} \leq 0.05$) dysregulated proteins, positive and negative values on X-axis represents up-regulated and down-regulated protein respectively. Green triangles indicate proteins with unaltered expression and blue circles specify statistically insignificant ($p\text{-value} > 0.05$) proteins. Proteins with $log_2 FC \geq 0.26$ value were considered up-regulated ($FC\ ratio \geq 1.2$) and those with a value of $log_2 FC \leq 0.26$ were considered down-regulated ($FC\ ratio \leq 0.83$). FC, fold change.

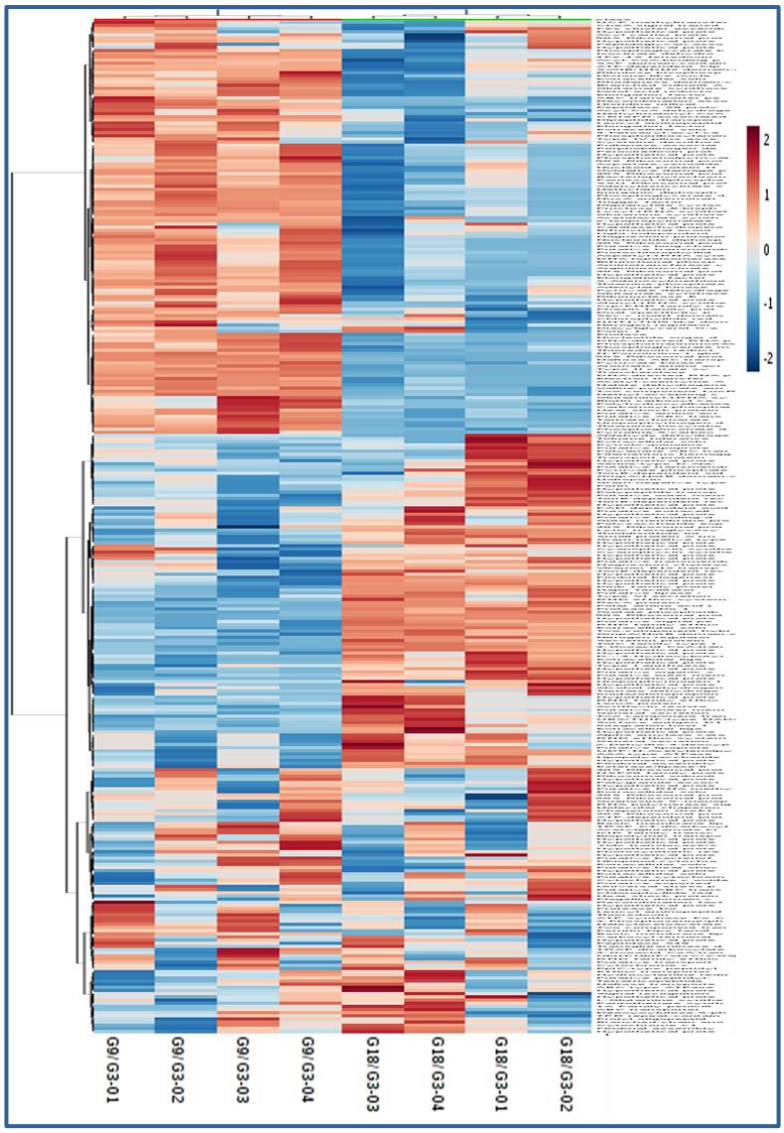

Fig. 3. 38: Heatmap representing dynamics of differentially expressed proteins.

Heatmap representing the dynamics of iTRAQ identified proteins.

Statistically significant DEPs at one or the other time point obtained as described under Fig. 3. 37 were plotted as heat map. Tan colour represents up-regulated proteins and blue represents down-regulated proteins. DEP, differentially expressed protein.

3.4.3.2. Overview of proteome dynamics.

Comparing with the control (G3), we observed that the abundance of hundred twenty one proteins increased and hundred and two proteins decreased at G9 while that of hundred fifteen proteins increased and hundred sixty nine proteins reduced at G18. Moreover, out of three hundred twenty one statistically significant proteins, hundred seventy six showed similar abundance at both the time points (G9 and G18) wherein ninety one DEPs up-regulated and eighty five down-regulated as compared with G3 (Fig. 3.39). However, nineteen DEPs showed dissimilar pattern wherein twelve DEPs were up-regulated at G9 but down-regulated at G18; contrariwise 7 proteins were down-regulated at G9 but up-regulated at G18. Additional twenty-eight proteins observed as DEP at G9, were unaltered at G18. Conversely, eighty nine proteins which were unaltered at G9, expressed differentially at G18 (Fig. 3.39).

3.4.3.3. Rippling effect and dynamics of relative protein levels

KEGG database was used to classify and group these 312 DEPs into 23 biological pathways (assigned under metabolism, genetic information processing, environmental information processing, cellular process and uncharacterised) with membrane transport/ translocation being most prominent followed by hypothetical, miscellaneous and amino acid metabolism (Fig. 3.40). In addition, other enriched pathways were also observed such as “porphyrin and chlorophyll metabolism”, “ETC”, “translation”, “chaperone/chaperonin”, “protease/peptidase” and “stress related proteins”. Dynamic proteome study (of DEPs) illustrates that their count at G18, categorised under each pathway, was more as compared with G9 (Fig. 3.40).

Just as ripples spread out when a single pebble is dropped in water, glucose has created an incremental effect on the metabolism of *Rbx. benzoatilyticus* transforming its phenotype (Fig. 41). The figure demonstrates the snapshot of increment in the ripples in

response to glucose wherein three ripples at G9 corresponds to up-regulated, down-regulated and unaffected proteins respectively (Fig. 3.41 A). Each ripple is segmented based on the count of proteins in the particular pathway, as their function in KEGG database. The number of ripples increased from 3 at G9 to 9 at G18 (Fig. 3.41 B) where each of up-regulated, down-regulated or unaffected ripple was further sub-divided into three ripples (up-regulated, down-regulated or unaffected) based on the FC value it displayed at G9. Overall, the analysis gave a brief idea about proteins/ pathways that differentially regulated only at a later stage (G18) and also the DEPs/ pathways that were initially differentially regulated but are in the process of recovery at the later stage.

To study the depth of glucose influence, filtered proteins were categorized as unaffected ($|\log_2 FC| < 0.26$), least affected ($0.26 \leq |\log_2 FC| < 0.58$), moderately affected ($0.58 \leq |\log_2 FC| < 1.0$), and most affected ($1.0 \leq |\log_2 FC|$). Analysis suggested that the count of proteins most affected and moderately affected raised while that of unaffected and least affected proteins declined at G18 as compared with G9 (Table 3.4). The count of most affected DEPs increased from 34 at G9 to 63 at G18 (Table 3.4). Similarly, count of moderately affected DEPs also increased from 75 at G9 to 109 at G18. Conversely, the count of least affected proteins decreased from 114 at G9 to 112 at G18. Likewise, the count of unaffected proteins decreased from 98 at G9 to 37 at G18. Thus, suggesting a stepwise increase in the DEPs. Overall, the higher number (284) of DEPs (115 up-regulated and 169 down-regulated) were detected at G18 as compared with 223 DEPs (121 up-regulated and 102 down-regulated) at G9 (Table 3.4). Also, count of up-regulated proteins was higher than the count of down-regulated proteins at G9 whereas, count of down-regulated proteins was more than that of up-regulated proteins at G18.

3.4.3.4. Functional categorization of differentially expressed proteins (DEPs) along the growth.

The identified proteins were categorized based on their function in the gene ontology (GO) consortium database. GO analysis demonstrated membrane, metabolic process and binding functional categories amongst cellular component (CC), biological process (BP) and molecular function (MF) respectively (Fig. 3.42). Figure 3.42 represents the top 10 enriched GO terms associated with CC, BP and MF. The terms of metabolic process, cellular process, biosynthetic process; membrane, cell, cytoplasm and binding, transferase activity, hydrolase activity made up the majority amongst BP; CC and MF respectively.

To further classify DEPs, KEGG enrichment analyses were performed on up or down-regulated proteins separately at both the time points. Amongst down-regulated proteins, the pathway of membrane transport, amino acid metabolism and pigment biosynthesis/photosynthesis were significantly enriched. In contrast, amongst up-regulated proteins, stress related proteins were also observed apart from significantly enriched pathways of membrane transport/ translocation. Figure 3.43 suggests that amongst down-regulated, percentage of proteins enriched under metabolism increased from 33.3 % at G9 to 45 % at G18. Also, genetic information processing increased from 9.8 % to 16.6 % (Fig 3.43 A,B). Whereas environmental information processing and uncharacterised proteins decreased from 23.5 % and 28.4 % to 14.8 % and 18.3 % respectively (Fig 3.43 A,B). On the contrary, amongst up-regulated percentage of proteins enriched under metabolism, genetic information processing and cellular process decreased from 19.8 %, 20.6 % and 7.4 % to 11.3 %, 20 % and 5 % respectively (Fig 3.43 C,D). Additionally, proteins enriched under environmental information processing and uncharacterised increased from 26.4 % and 25.6 % to 30.4 % and 33 % respectively (Fig 3.43 C,D).

In addition, to provide a global view of biochemical pathways, KEGG IDs of DEPs and metabolites at both the time points were submitted separately to the online software

Interactive Pathways (iPath 3; https://pathways.embl.de/) and mapped to different pathways. Figure 3.44 depicts the snapshot of the biochemical pathways mapped to general metabolism. The green, blue or red lines specified whether the expression of proteins involved in that particular pathway were up-regulated, unaffected or down-regulated respectively at that instant as compared with the exponential phase. Down-regulation of carbohydrate metabolism, oxidative phosphorylation, photosynthesis and fatty acid metabolism was observed at G9 as well as at G18 (Fig. 3.44 A;B). While, citrate cycle, terpenoid backbone biosynthesis, nucleotide metabolism, amino acid (alanine, aspartate, glutamate) metabolism and urea cycle down-regulated at G18 only (Fig. 3.44 B). This suggested that glucose has influenced the proteins/pathways related to primary metabolism prior to those related to secondary metabolism.

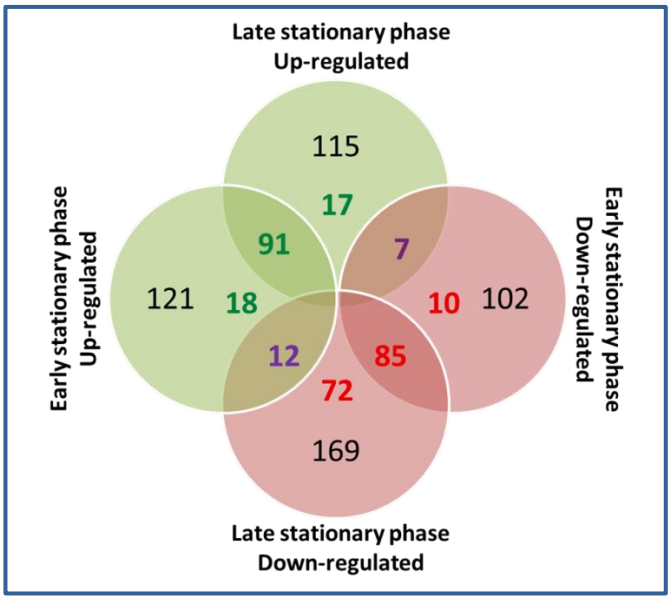

Fig. 3. 39: Venn-diagram representing the shared and unique DEPs of glucose grown *Rbx. benzoatilyticus* cells.

Venn-diagram constructed based on the count of statistically significant DEPs obtained from volcano plot analysis as described under Fig. 3.37. Green and red fill or numerals represent up-regulated and down-regulated protein counts respectively. Purple numerals represents the count of proteins up-regulated at one time point but down-regulated at the other or vice-versa. Numerals in black represent the total count of protein at that instant. G9, abundance of DEP at 9th day of growth on glucose as compared with 3rd day growth; G18, abundance of DEP at 18th day of growth on glucose as compared with 3rd day growth.

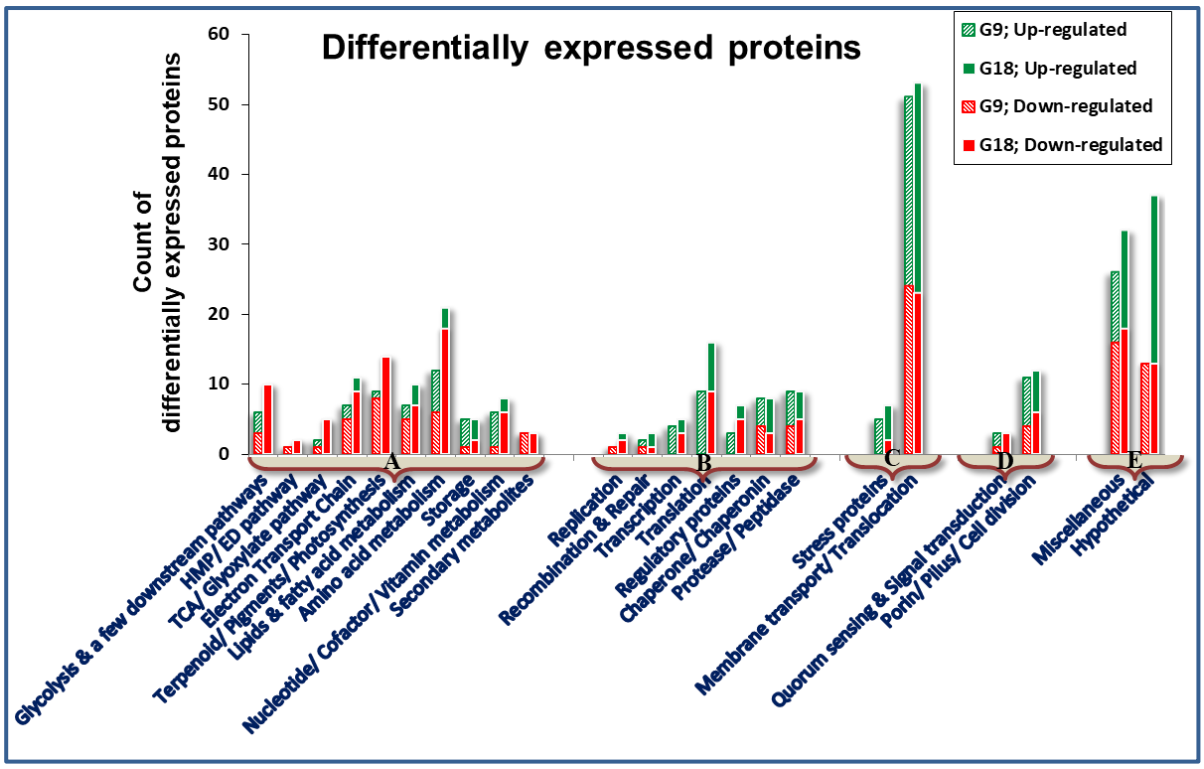

Fig. 3. 40: Functional classification of differentially regulated proteins of *Rbx. benzoatilyticus* cells grown on glucose as identified by iTRAQ analysis.

Functional classification was carried according to KEGG (Kyoto Encyclopedia of Genes and Genomes database, www.genome.jp/kegg/) database.

Differentially regulated proteins identified by volcano plot analysis as described under Fig. 3.37 were functionally annotated. Datum is plotted as bar chart representing the count of proteins related to different pathways of metabolism (A), genetic information processing (B), environmental information processing (C), cellular process (D) and uncharacterised (E).

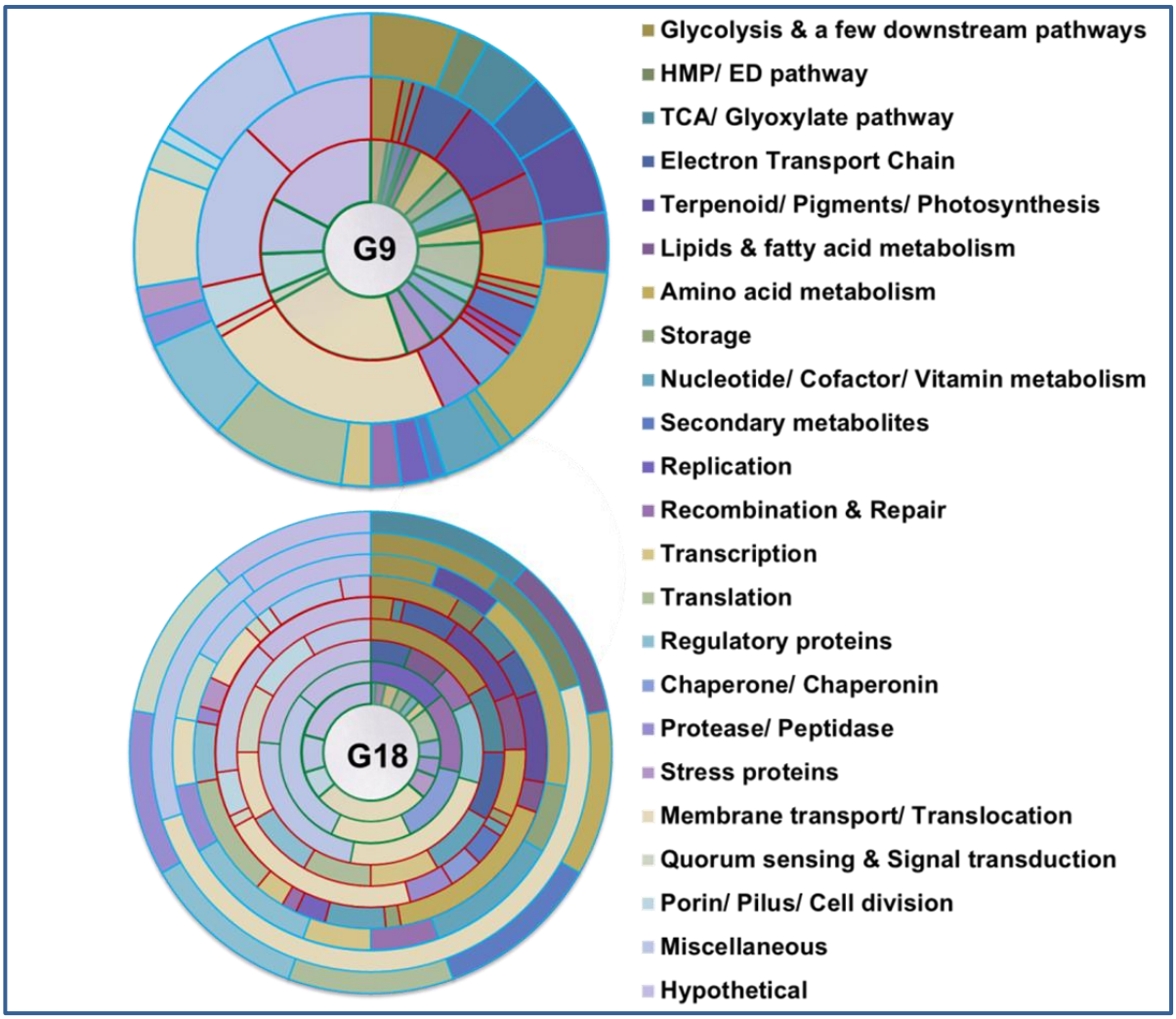

Fig. 3. 41: Rippling effect of glucose on *Rbx. benzoatilyticus*.

*Pie-graph representing statistically significant proteins identified by iTRAQ analysis at G9 (**A**) and G18 (**B**).*

DEPs obtained from volcano plot analysis, as described under Fig. 3.37, were plotted as pie-graph wherein each ripple (circle) corresponded to up-regulated, down-regulated and unaffected proteins respectively from center. Further, each ripple was sub-divided wherein each segment is based on the count of DEPs belonging to particular KEGG pathway map. Green, red and blue circle/stroke represents up-regulated, down-regulated and unaffected protein/pathway respectively. DEP, differentially expressed protein; G9, abundance of DEP at 9th day of growth on glucose as compared with 3rd day growth; G18, abundance of DEP at 18th day of growth on glucose as compared with 3rd day growth.

Table 3. 4: Dynamics of protein count at early and late stationary phase observed in iTRAQ based proteome analysis of glucose grown *Rbx. benzoatilyticus* cells

Significantly affected proteins	Early stationary phase (G9)			Late stationary phase (G18)		
	Up-regulated	Down-regulated	Total	Up-regulated	Down-regulated	Total
Unaffected ($\|log_2FC\|< 0.26$)	–	–	98	–	–	47
Least affected ($0.26 \leq \|log_2FC\| < 0.58$)	69	45	114	27	85	112
Moderately affected ($0.58 \leq \|log_2FC\| < 1.0$)	34	41	75	48	61	109
Most affected ($1.0 \leq \|log_2FC\|$)	18	16	34	40	23	63
Total	121	102	321	115	169	321

G3, proteome extracted at 3rd day of growth; G9, proteome extracted at 9th day of growth; G18, proteome extracted at 18th day of growth; FC, fold change.

Proteome from early (G9) and late (G18) stationary phase glucose grown *Rbx. benzoatilyticus* cells was compared with that of exponential phase (G3) cells. Fold change values were log transformed (log_2). Based on the fold change values, proteins were categorized as up-regulated, down-regulated or unaffected. Further, proteins were sub-categorized as unaffected, least affected, moderately affected or most affected based on the range their fold change value attains and the count of such proteins is presented in the table.

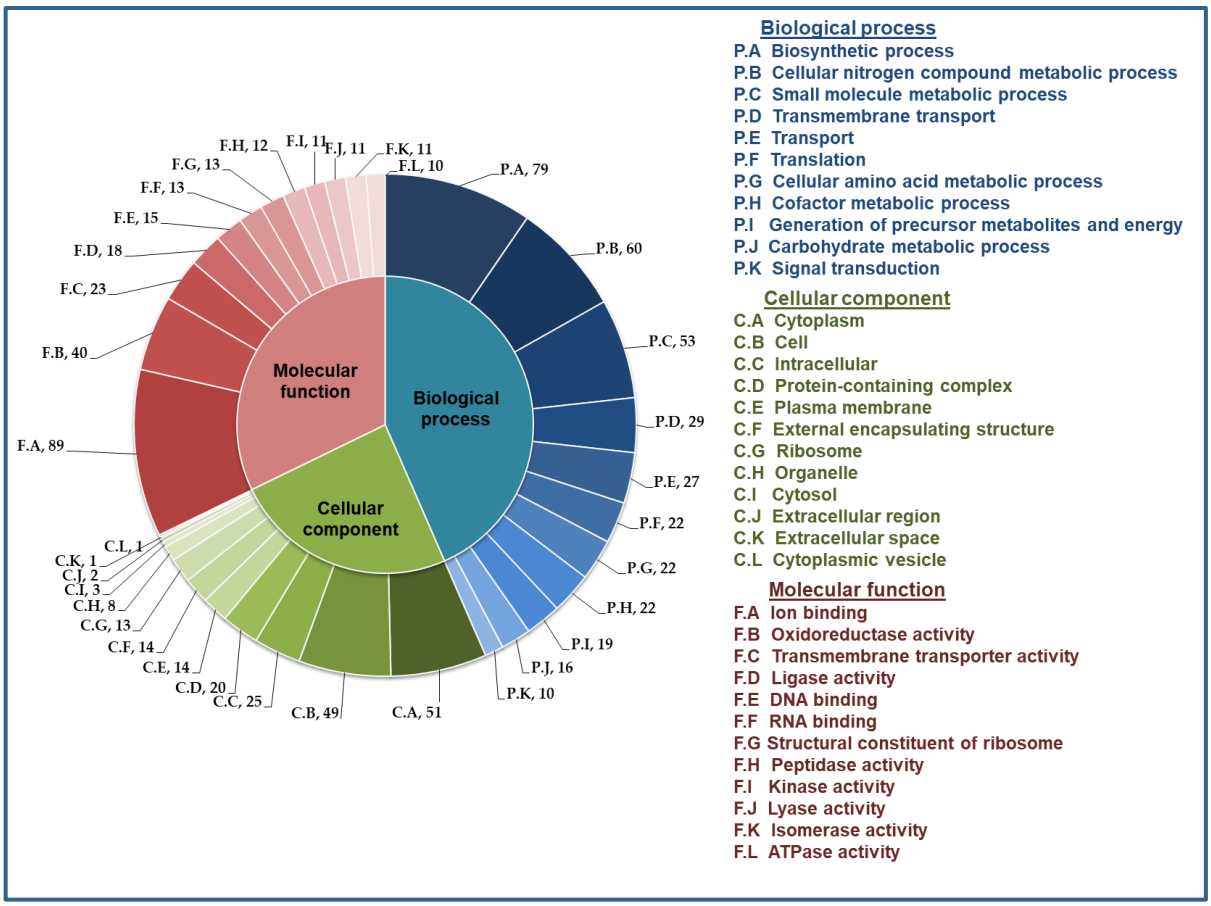

Fig. 3. 42: Functional categorization of differentially regulated proteins based on their function in Gene Ontology.

Statistically significant differentially regulated proteins obtained from volcano plot analysis as described under Fig. 3.37, were functionally categorized based on GO under the head of biological process, cellular component and molecular function. GO, gene ontology.

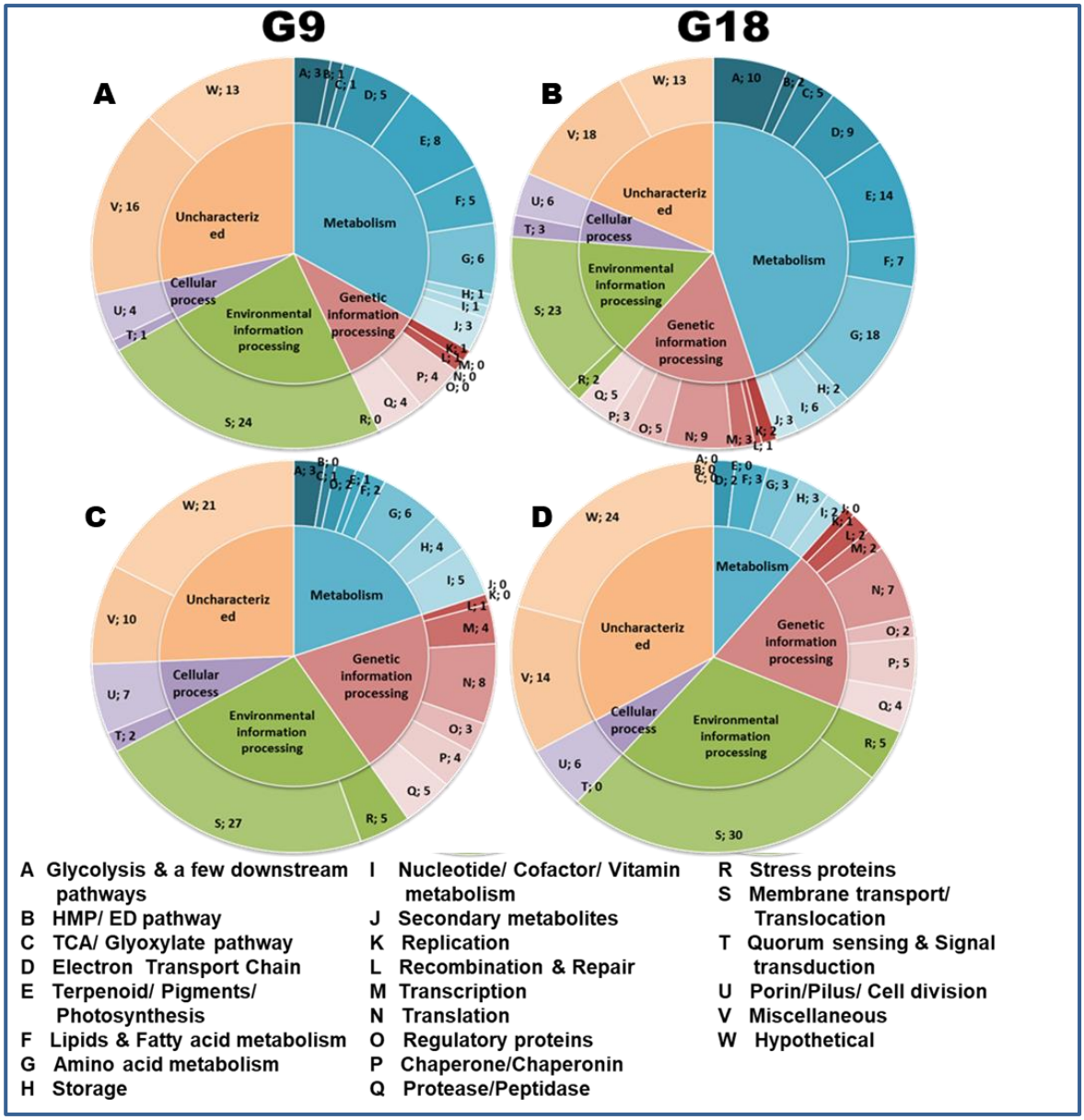

Fig. 3. 43: Functional categorization of differentially regulated proteins based on their function in KEGG.

*Functional categories of down-regulated proteins (**A, B**) and up-regulated proteins (**C, D**).*

DEPs obtained from volcano plot analysis, as described under Fig. 3.37, were enriched based on their function in KEGG database. Each segment represents the count of proteins in that particular category/pathway. Count of DEPs belonging to each pathway is given next to it. DEP, differentially expressed protein; KEGG, Kyoto Encyclopedia of Genes and Genomes; G9, abundance of DEP at 9th day of growth on glucose as compared with 3rd day growth; G18, abundance of DEP at 18th day of growth on glucose as compared with 3rd day growth.

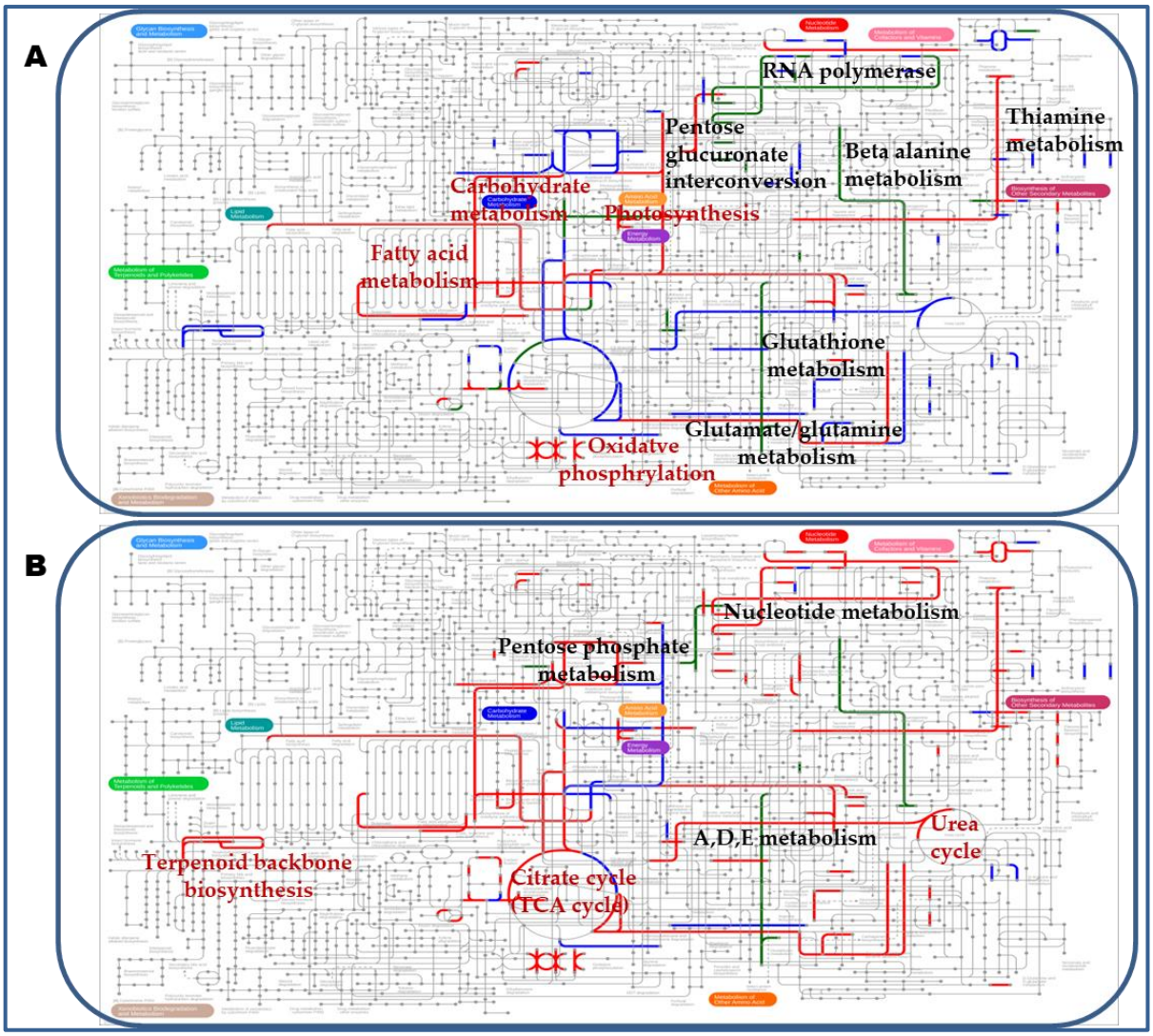

Fig. 3. 44: Overview of altered biochemical pathways of *Rbx. benzoatilyticus* under the influence of glucose.

*Differentially regulated biochemical pathways under the influence of glucose at G9 (**A**) and G18 (**B**).*

Datum processed as described under Fig. 3.43 was subjected to iPath online software. Lines connecting the nodes represent the pathway. Green, red or blue lines represents the pathways up-regulated, down-regulated or unaltered at that instant. G9, abundance of DEP at 9th day of growth on glucose as compared with 3rd day growth; G18, abundance of DEP at 18th day of growth on glucose as compared with 3rd day growth.

3.4.3.5. Dynamics of key metabolic pathways along growth

Identified DEPs were involved in different cellular and metabolic processes with a preferential distribution to membrane transport/ translocation and amino acid metabolism categories apart from hypothetical proteins. Results provide new insights into the potentially tight protein regulatory network controlling transcription of proteins related to metabolic processes.

Amongst the DEPs, certain proteins related to membrane transport/ translocation up-regulated: ImpA, putative lipoprotein (RBXJA2T_17871, RBXJA2T_18428); TonB dependent receptor (RBXJA2T_03319, RBXJA2T_04738, RBXJA2T_12407); type I antifreeze protein, HlyD family secretion protein (RBXJA2T_05793); OmpA/MotB domain-containing protein (RBXJA2T_05158, RBXJA2T_16532); TolC family type I secretion outer membrane protein (RBXJA2T_18363); polyamine ABC transporter system, substrate-binding protein (RBXJA2T_08615); transport protein (RBXJA2T_05103) and polypeptide-transport-associated domain-containing protein (RBXJA2T_06380s) (Fig. 3.43; Table S2). The FC value of these proteins was higher at G18 as compared with G9 (Table S2) indicating a stepwise increase in the abundance of these proteins. On the other hand, certain other membrane transport/ translocation related proteins down-regulated: extracellular solute-binding protein (RBXJA2T_03873, RBXJA2T_12882); extracellular solute-binding protein family 1 (RBXJA2T_07035); Yidc translocase/secretase (RBXJA2T_07513); polar amino acid transporter substrate-binding protein (RBXJA2T_00774); TRAP C4-dicarboxylate transport system permease subunit DctP (RBXJA2T_12507); maltose transporter membrane protein (RBXJA2T_07343); biopolymer transport ExbD protein (RBXJA2T_14856); branched-chain amino acid ABC transporter periplasmic amino acid-binding protein (RBXJA2T_04288) and putative amino acid ATP-binding ABC transporter protein (RBXJA2T_09242). The FC value of these proteins was lower at G18 as compared with G9

(Table S2) indicating a stepwise decline in the abundance of these proteins. In general efflux related proteins were observed up-regulated while import related proteins down-regulated and transporters differently regulated.

Also, we observed down-regulation of proteins related to replication– DNA topoisomerase III (RBXJA2T_02627) and protein synthesis: Elongation factor G (RBXJA2T_03247); SSU Ribosomal protein S2P (RBXJA2T_18001); 30S Ribosomal protein S1 (RBXJA2T_16502); 30S Ribosomal protein S5 (RBXJA2T_02205); 50S Ribosomal protein L25/general stress protein Ctc (RBXJA2T_15523); elongation factor Tu (RBXJA2T_03242) and elongation factor G (RBXJA2T_01710) at G18 that were unaffected at G9 (Table S2). Further, amino acid transport and metabolism related proteins down-regulated at G9 as well as G18 suggesting decelerated cellular protein synthesis machinery for *Rbx. benzoatilyticus* in the presence of glucose.

Apart from this, we observed up-regulation of several putative stress related response proteins such as universal stress protein (RBXJA2T_13976), ferritin Dps family protein (RBXJA2T_05183), HSP20 family protein (RBXJA2T_02095), heat shock protein Hsp20 (RBXJA2T_02105), putative heat shock protein (RBXJA2T_18136) and putative organic solvent tolerance transmembrane protein (RBXJA2T_02907) at both the time points G9 and G18 (Table S2).

3.4.3.6. Gradual transit to less energy requiring state

We observed the down-regulation of all the proteins involved in pigments including bacteriochlorophyll biosynthesis at both the time points G9 and G18 (Fig. 3.40, 3.43; Table S2). Though, observed unaffected at G9, proteins involved in glycolysis and TCA cycle were down-regulated at G18. These include enolase (RBXJA2T_12387); fructose-1,6-bisphosphate aldolase (RBXJA2T_06270); pyruvate kinase (RBXJA2T_06260)

phosphoenolpyruvate carboxykinase (RBXJA2T_05268); isocitrate dehydrogenase (RBXJA2T_10419) and type II citrate synthase (RBXJA2T_09894) (Table S2). Also, phosphogluconate dehydratase (RBXJA2T_14896) and transketolase (RBXJA2T_02652) displayed similar accumulation suggesting down-regulation of PPP as well. This indicates that the cells gradually transited to a less energy requiring or non-growing state.

3.4.3.7. Storage filling in the transition from exponential phase to PHA synthesis and accumulation

Differentially expressed proteins associated with storage granules such as phasin family (RBXJA2T_17372), cyanophycin synthetase (RBXJA2T_07833, RBXJA2T_07838) and poly granule-associated protein (RBXJA2T_06865) accumulated maximally at both G9 and G18 (Table S2). Also, α amylase (RBXJA2T_07353), which is responsible for hydrolysing α-1,4 glycosidic bonds, down-regulated suggesting inhibition of polysaccharide hydrolysis. Apart from this, arginosuccinate synthase (RBXJA2T_10059), which catalyses the synthesis of arginosuccinate from citrulline and aspartate, was down-regulated at G18. Taken together, this suggests the accumulation of storage granules highlighting the transition from exponential phase to storage filling stage.

3.4.3.8. Protein expression characteristics during non-cultivable state

The dynamic proteome analysis suggested the down-regulation of oxidative damage protection protein (RBXJA2T_01425) (which was unaffected at G9) at G18 (Table S2) indicating the accumulation of ROS. Replication and repair related proteins, though observed down-regulated at G9, were up-regulated at G18 perhaps to maintain the genomic stability. Also the analysis demonstrated that almost all the DEPs involved in proteolysis (9 of 11 proteins) exhibited differential accumulation (Table S2). Enormous DEPs related to protein synthesis (16 of 17 proteins) and transport (53 of 59 proteins) displayed similar accumulation pattern to that of proteolysis-related proteins. This could be attributed for the protein turnover

in order to maintain the quality of proteins and amino acid pool along with the stability of genetic material. Apart from this, significant number of hypothetical proteins was differentially expressed indicating their crucial involvement to combat the stressed condition generated as a result of glucose photometabolism by *Rbx. benzoatilyticus*.

3.5. Genomic insights of glucose grown *Rbx. benzoatilyticus* cells

Differences in physiological, biochemical, metabolomic and proteomic analyses of malate/glucose grown cells encouraged to look for the variation(s) in the genome (if any) since glucose causes base modification and mis-match pairing (Zhang et al., 2007). For this we have used the gDNA of stationary phase cultures of *Rbx. benzoatilyticus* which were either fed with glucose (G15) or malate (M15). We were not successful in the isolation of gDNA from G18 cells. Despite following both conventional and various non-conventional kit methods, DNA could not be isolated from G18 cells (Fig. 3.45). Thus, gDNA from G15 and M15 cells was taken forward to study the genomic analysis.

3.5.1. Genomic features of both malate and glucose grown cells of *Rbx. benzoatilyticus*

DNA samples from M15 and G15 cells of *Rbx. benzoatilyticus* were out-tasked to AgriGenome Pvt. Ltd. (Kochi, India) for *de novo* whole genome sequencing (WGS). Any possible contamination in the genome sequence thus obtained was checked with the ContEst service (EZBiocloud) which gave single 16S rRNA gene sequence in both the samples, indicating that the WGS was free from any contaminating sequences of other sample. The WGS of *Rbx. benzoatilyticus* grown on malate (mal) and glucose (glc) were deposited at DDBJ/ENA/GenBank under the accession number JAAOCD000000000 and JAAOCE000000000 respectively. The version described in this study is version JAAOCD010000000 and JAAOCE010000000 respectively.

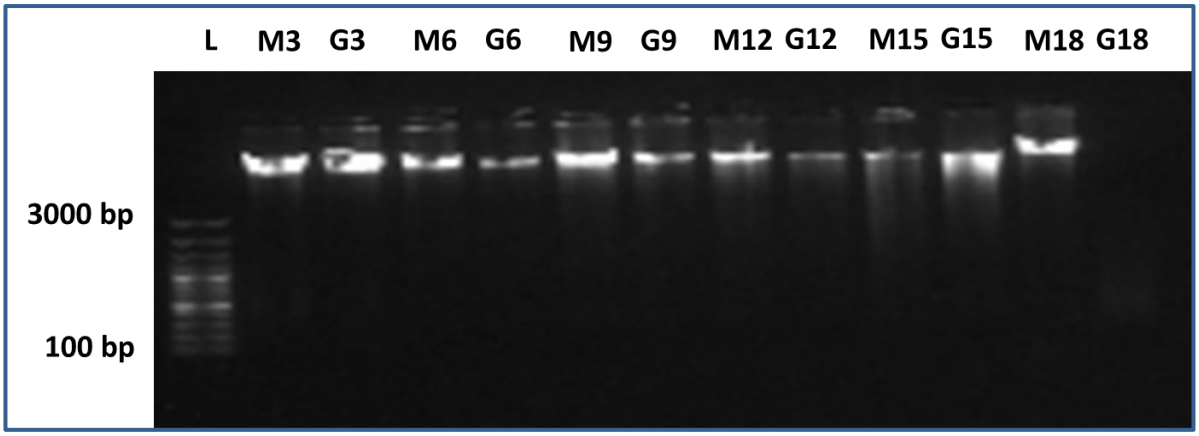

Fig. 3. 45: Agarose gel electrophoresis of DNA isolated temporally from malate/glucose grown *Rbx. benzoatilyticus*.

Gel image of DNA isolated at regular intervals from malate/glucose grown cells.

Malate grown mid exponential phase culture ($OD_{660\ nm}$ 0.25) of Rbx. benzoatilyticus was used as inoculum (10%). Cells were grown photoheterotrophically on either malate or glucose medium for 18 days. Cells were harvested periodically (every third day) and genomic DNA was isolated from the cell biomass using kit method. DNA, deoxyribonucleic acid; L, DNA ladder; M3, M6, M9, M12, M15 and M18, DNA samples isolated at 3^{rd}, 6^{th}, 9^{th}, 12^{th}, 15^{th} and 18^{th} day of growth from malate grown Rbx. benzoatilyticus cells respectively; G3, G6, G9, G12, G15 and G18, DNA samples isolated at 3^{rd}, 6^{th}, 9^{th}, 12^{th}, 15^{th} and 18^{th} day of growth from glucose grown Rbx. benzoatilyticus cells respectively.

The genomic G+C content of *Rbx. benzoatilyticus* was 71.6 mol% for both malate and glucose grown cells. The genome size of DNA samples from mal and glc grown cells were 4,157,967 nt and 4,149,196 nt with 35 and 36 contigs respectively. The N50 and L50 value for the genome from malate-grown *Rbx. benzoatilyticus* cells (mal-genome) was 427788 and 4 respectively whereas it was 375635 and 5 respectively for genome from glucose grown cells of *Rbx. benzoatilyicus* (glc-genome). The genome average nucleotide identity (ANI) score and digital DNA–DNA hybridization (dDDH) values between mal-genome and glc-genome were 99.99 and 100 %, respectively, which was as anticipated. NCBI data analysis of the genomes indicated that the total number of coding sequences (CDS) was 3807 for mal-genome and 3801 for glc-genome. Amongst them 3769 and 38 coded for proteins and pseudogenes respectively in case of mal-genome whereas 3764 and 37 respectively for glc-

genome. Both the genomes indicated presence of single rRNA (5S, 16S, 23S) gene cluster, 46 tRNAs and 3 non-coding RNAs thus a total of 52 RNA genes (Table 3.5) along with 3 CRISPR arrays.

Table 3. 5: Comparison of genomic information from mal-genome and glc-genome

Genomic features	Mal-genome	Glc-genome
Sequence size (bp)	4157967	4149196
Number of contigs	35	36
GC content (%)	71.6	71.6
Shortest contig size	106	106
Median sequence size	4122	5327
Mean sequence size	118799.1	115255.4
Longest contig size	961299	585015
N50 value	427788	375635
L50 value	4	5
Genes (total)	3859	3853
Coding sequences (total)	3807	3801
Genes (coding)	3769	3764
Genes (RNA)	52	52
rRNA (5S, 16S, 23S)	1,1,1	1,1,1
tRNAs	46	46
ncRNAs	3	3
Pseudogenes (total)	38	38
CRISPR Arrays	3	3

Mal-genome; genome isolated from *Rbx. benzoatilyticus* cells grown on malate, Glc-genome; genome isolated from *Rbx. benzoatilyticus* cells grown on glucose.

Genomic DNA was isolated from malate/glucose grown cells after 15 days of phototrophic incubations. Genome was sequenced by Illumina- Hiseq platform and annotated using RAST.

3.5.2. Nucleotide variation analysis between mal-genome and glc-genome of *Rbx. benzoatilyticus*

To identify the nucleotide sequence variations (including SNPs and indels) in the genomes, variation analysis service of PATRIC was utilised. Using the raw reads of mal-genome and glc-genome reference based assembly was created. The reference genome for the assembly was taken as *Rbx. benzoatilyticus* genome that was sequenced ten years back (in the year 2011; NCBI accession number AEWG00000000.1). The analyses resulted in 99.4% and 99.2% mapped reads with 702.2 and 324.3 mean base coverage for mal-genome and glc-

genome respectively. A total of 158 variants have been found in the analysis. Based on score > 50 criteria, 128 variants filtered out. The nucleotide variations observed in both the genomes were considered to be due to passaging the cells for a decade and those observed only in glc-genome were considered to be due to the glucose effect.

3.5.2.1. Nucleotide variations observed in Rbx. benzoatilyticus genome as a result of several passages

A total of 57 out of 128 filtered variants were identified in both the read libraries. Thus, this might be a consequence of several passages that *Rbx. benzoatilyticus* cells underwent during the past ten years. Nearly fifty percent (29 of 57) variations were observed in the intergenic regions. Apart from this, silent or synonymous substitutions were observed at 4 CDS positions. Nonsynonymous substitutions were observed at 16 positions amongst which, a non-sense substitution was observed at single CDS on the other hand, mis-sense substitutions at the remaining 15 CDSs positions. Also, indels of single nucleotide at 8 CDSs resulted in frame shift effect (Table S3).

3.5.2.2. Nucleotide variations observed Rbx. benzoatiyticus genome as a result of glucose effect

We observed 69 variations unique to glc-genome. Perhaps, these variations are the result of substrate (glucose) effect. At none of these positions, nucleotide base substitution was observed; only insertion or deletions (Indels) were observed. Nearly seventy eight percent (54 of 69) indels were in the intergenic regions. Amongst the remaining 15 indels that were in the CDS, insertion of 18 nt was observed at single position, resulting in inframe insertion. However, insertion or deletion of single nucleotide was observed at the remaining 14 positions accounting for frame shift effect (Table S3).

3.5.3. Mauve alignment suggests shuffling of DNA sequences

We aligned DNA sequences of mal-genome and glc-genome using Mauve to identify the multiple maximal matches (MMM) and locally collinear blocks (LCBs). The DNA sequence of mal-genome was used as reference. Mauve alignment displayed 25 LCBs with a minimum weight of 221 (Fig. 3.46). The alignment also facilitated detection of homologous regions that are shuffled or inverted due to DNA rearrangement or recombination. Apart from this, gaps in the alignment were observed at a few places, which suggest that the sequences are truncated at those places.

3.5.4. Comparative genomics of glucose and malate grown cells of *Rbx. benzoatilyticus*

The proteome comparison service of the PATRIC server (https://www.patricbrc.org/) compared the two genomes based on their protein sequence identity. The results pointed out that that most of the proteins were 100% identical however, nearly 20 proteins shared 97-99% similarity (Fig. 3.47). Circular map of glc-genome was constructed using freely available online CGView server (http://cgview.ca/). The map was blasted against mal-genome (outer blue circle Fig. 3.48). The resulting map suggests presence of the identical genes in both the genomes with single rRNA gene cluster (highlighted as single green band within the orange bands of CDS). Several transposases, seen in the genome (labelled in purple), were unevenly scattered across the genome (Fig 3.48).

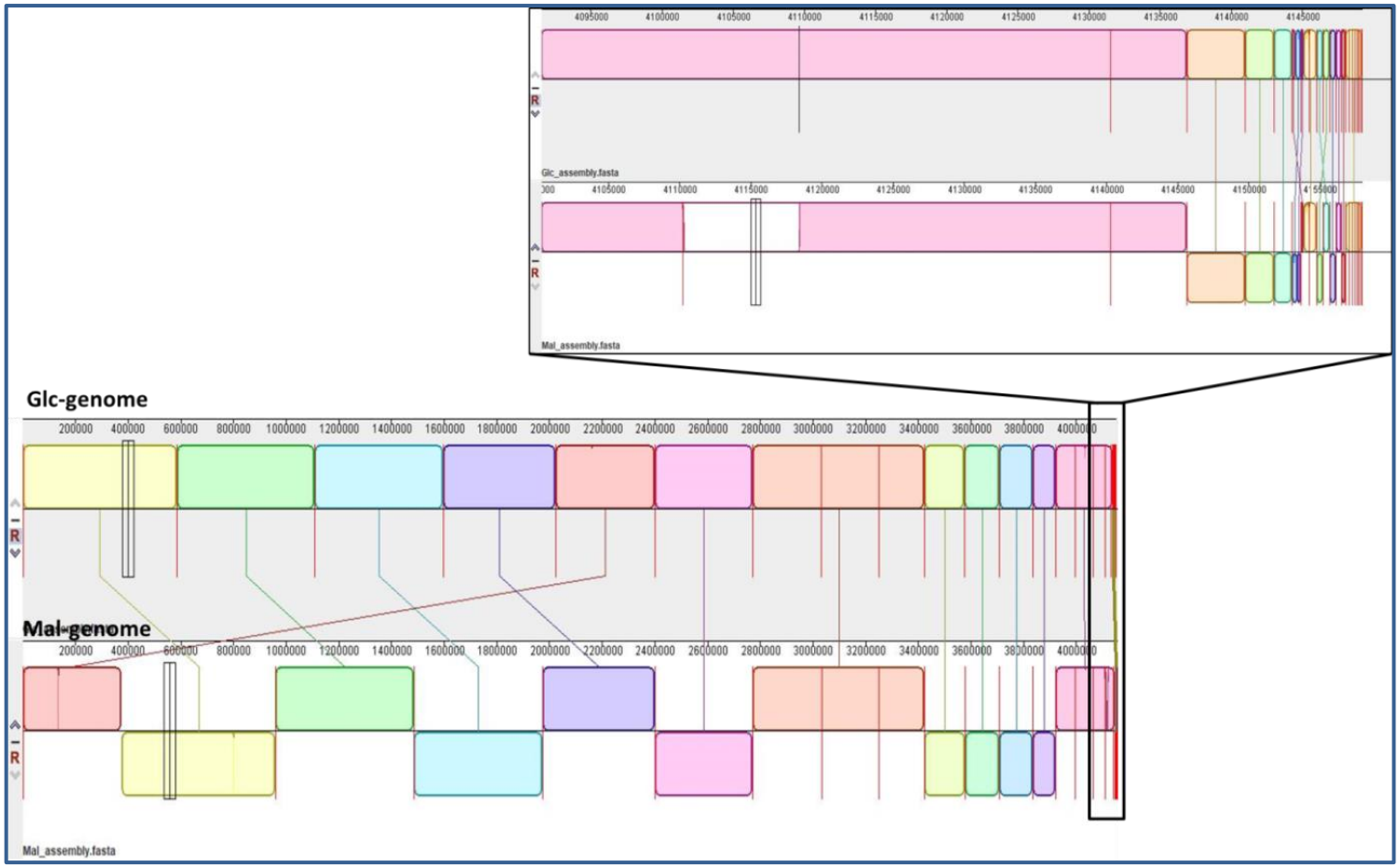

Fig. 3. 46: Mauve alignment of mal-genome and glc-genome.

Genomic data obtained as described under Fig. 3.46 were aligned using Mauve to identify the shuffling and rearrangement of sequences. The inset represents the gap observed in the alignment. mal-genome, genomic DNA isolated frommalate grown Rbx. benzoatilyticus cells; glc-genome, genomic DNA isolated from glucose grown Rbx. benzoatilyticus cells.

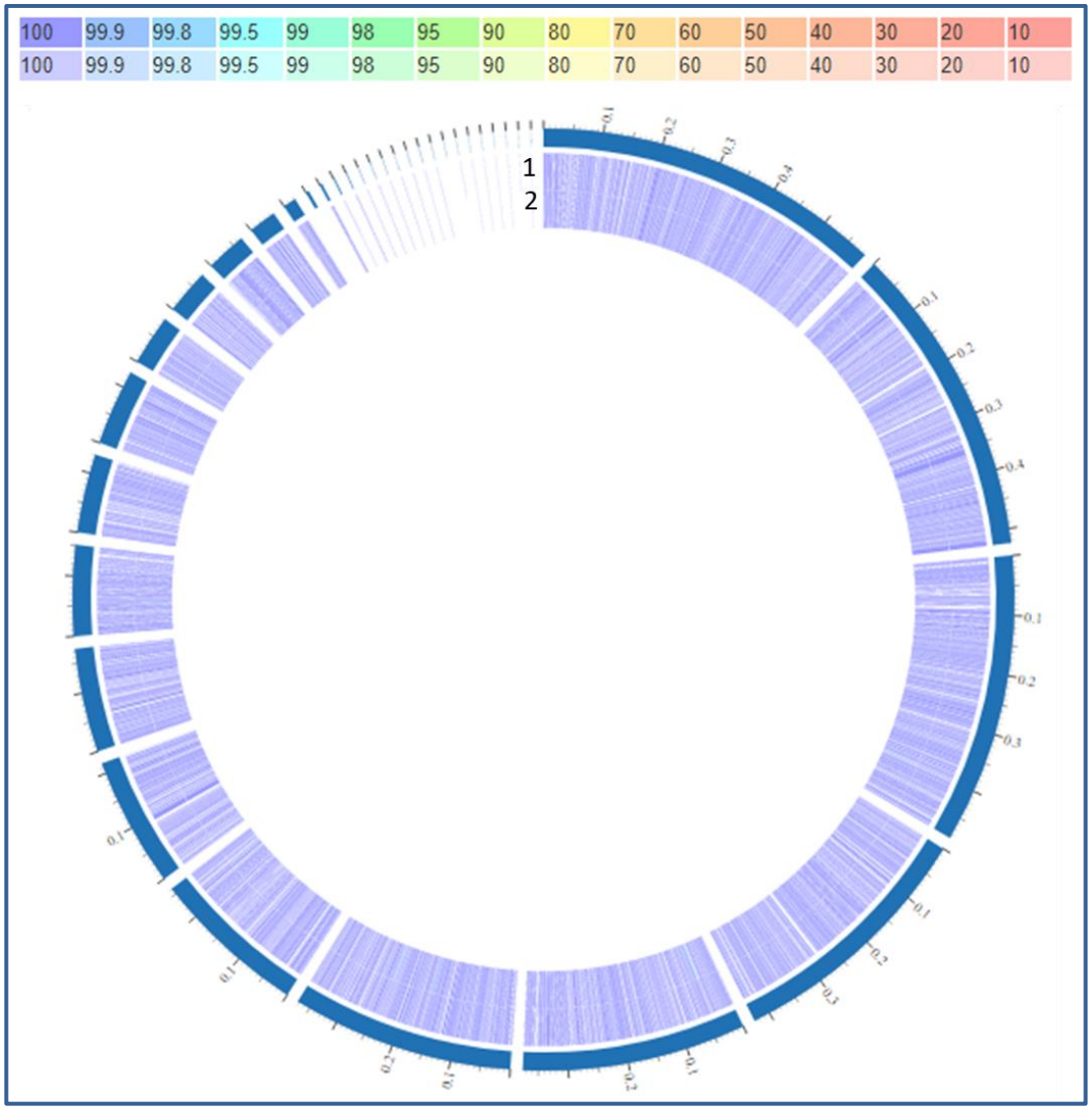

Fig. 3. 47: Protein sequence identity between mal-genome and glc-genome.

Genome map based on protein sequence identity between mal-genome and glc-genome.

M15 and G15 DNA samples obtained as described under Fig. 3.45 were taken forward for WGS by Illimina HIseq. Genome sequences were subjected to the proteome comparison service of the PATRIC server. List of track from outside to inside 1- Glc-genome, 2- Mal-genome. DNA, deoxyribonucleic acid; mal-genome, genomic DNA of Rbx. benzoatilyticus isolated from stationary phase culture fed with malate (M15); glc-genome, genomic DNA of Rbx. benzoatilyticus isolated from stationary phase culture fed with glucose (G15).

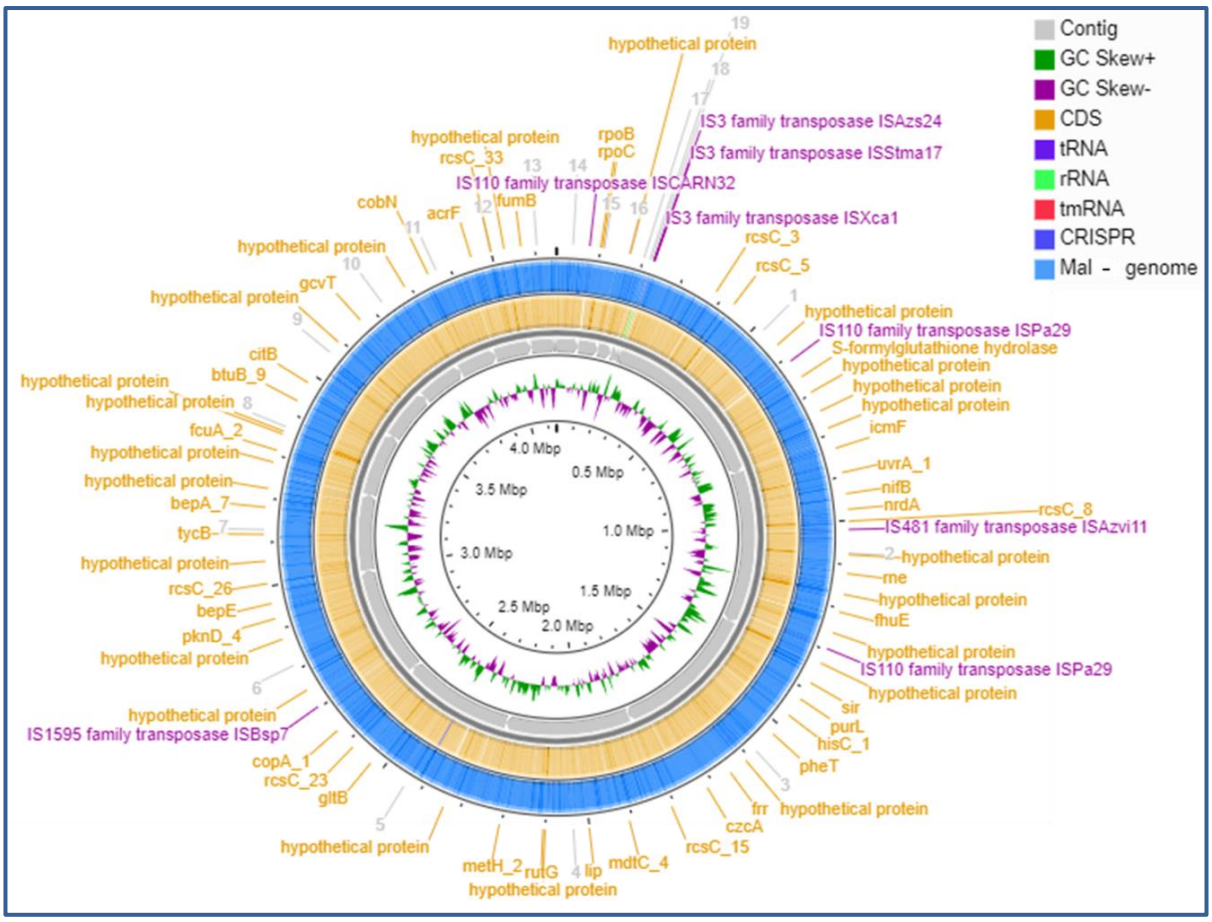

Fig. 3. 48: Circular map of glc-genome.

Glc-genome data obtained as described under Fig. 3.46 was subjected to CGviewer, annotated and blasted against mal-genome to look for the homologous proteins. Transposases, labelled in purple, were unevenly scattered across the genome. CDS, coding sequences; mal-genome, genomic DNA isolated from malate grown Rbx. benzoatilyticus cells; glc-genome, genomic DNA isolated from glucose grown Rbx. benzoatilyticus cells.

3.5.5. Genome annotation and analysis

The RAST annotated file of both the genomic DNA was downloaded from the server for further analysis. Mal-genome displayed presence of 4103 genes of which 2196 genes were coded by forward (+ strand sense) strand and 1907 genes by reverse strand (- strand sense) (Table 3.6). On the other hand, glc-genome showed existence of 4099 genes amongst which 2087 and 2012 genes were coded by forward and reverse strands respectively. Detailed analysis of the count of genes from mal-genome or glc-genome coded by same strand or opposite strand is given in Table 3.6. Few genes were uniquely present in mal-genome/glc-genome as listed in table 3.7. In addition, the copy number of few genes was also observed to be different in the two genomes (Table 3.7). Also, eleven transposase genes were observed in both which were spread across the genome. Perhaps these are accountable for the shuffling of LCBs as observed in the Mauve alignment (Fig. 3.46).

3.5.6. Inconsistencies, at the 5' end, of a few selected genes from glc-genome as compared to those from mal-genome

Nucleotide length of all the genes from mal-genome/glc-genome was calculated from the annotation file by subtracting the position of stop coding nt from start coding nt of the respective gene. Nearly eighteen genes were identified which differ in their nucleotide length between the two genomes. The nucleotide sequence of these 18 genes was subjected to pair-wise alignment naively using ClustalW with character count. It was observed that nine genes from glc-genome were truncated at their 5' end only while eight genes were extended/prolonged only at their 5' end as compared with their mal-genome counterpart (Table 3.8). Apart from this, no mutational variation (miss or gap) was observed in any of these 18 genes thus, declining any possibility for degeneracy of codon usage as well.

Contrariwise, a gene 'putative exported protein of unknown function with OmpA family domain' from mal-genome was trimmed into three regions in the glc-genome (Fig. 3.49). The gene, comprising of 1218 nucleotides, is located on contig 1 of mal-genome. But,

it was observed pruned to three fragments in the glc-genome. The first fragment, comprising of 492 nucleotides from 5' end, transposed to contig 5 of glc-genome retaining only the last fragment, covering stretch of 558 nucleotides from 3' end, at contig 1. The middle snippet of 168 nucleotides was not at all observed in the glc-genome (Table 3.8).

3.5.7. Inconsistencies at the first amino acid position of a few selected proteins from glc-genome as compared with mal-genome

The observed variation in the nucleotide length of 18 genes directed to look for the pairwise alignment of amino acid sequence of their proteins as well. As seen in Table 3.8, methionine at 1st position (M1) of nine proteins from glc-genome aligned with methionine or valine or leucine at positions other than M1 of corresponding protein from mal-genome without any gap or miss thereafter. On the contrary, valine or leucine or methionine at positions other than 1st position of eight proteins from glc-genome aligned with M1 of respective protein from mal-genome and continued thereafter without any gaps or miss. All the 18 proteins from glc-genome concluded with the same amino acid as that from the respective protein of mal-genome. Exception being 'putative exported protein of unknown function with OmpA family domain' as observed in the pairwise alignment of nucleotide also. Though M1 of this protein from glc-genome aligned with M1 of corresponding protein from mal-genome but terminated at D164. Thereafter, R221 of same protein from mal-genome aligned freshly at R1 of the protein from glc-genome and the alignment continued till end of the protein sequence. This indicates that the protein is truncated in glc-genome and partly transposed to a different location with middle stretch of nearly 57 amino acid found missing (Fig. 3.49).

3.5.8. Comparison of photosynthetic gene cluster (PGC) in the two genomes

Physiological analysis along with proteomic analysis implicated the loss of entire photosynthetic machinery of *Rbx. benzoatilyticus* in the presence of glucose. Thus,

comparison of PGC between the two genomes was carried out and it was observed that entire PGC (comprising of 35 genes) was oriented reverse (as suggested by the position of start and stop codon and also by strand sense) i.e. coded by opposite strands in the two genomes (Fig. 3.50). Two genes from the entire cluster 'spheroidene monooxygenase (EC 1.14.15.9)' and 'chlorophyll *a* synthase (ChlG; EC 2.5.1.62)' were truncated in glc-genome as indicated by the calculated nucleotide length of the respective genes from the two genomes. Pairwise alignment of the amino acid sequences suggested truncation at N-terminal end in both the proteins of glc-genome as compared with mal-genome (Fig. 3.50, Table 3.8). Apart from this, no difference in any other genes of PGC was observed. But, most of the proteins related to pigment biosynthesis and LHC were down-regulated in the glucose grown cells (as compared with malate grown ones), as highlighted in the physiological and proteome analyses (refer to section 3.1.3, 3.2.3 and 3.4.2.7).

Table 3. 6: Count of genes observed on each strand of the genome isolated from malate/glucose grown cells of *Rbx. benzoatilyticus*

Genome under consideration (total count)	Strand sense (total count)	Genome to be compared (strand sense)	Count of genes on forward/reverse strand of the DNA
Mal-genome = 4103	Strand sense (+) = 2196	Glc-genome (+) Glc-genome (-) Glc-genome (absent)	1175 1012 9
	Strand sense (-) = 1907	Glc-genome (+) Glc-genome (-) Glc-genome (absent)	905 994 8
Glc-genome = 4099	Strand sense (+) = 2087	Mal-genome (+) Mal-genome (-) Mal-genome (absent)	1197 879 11
	Strand sense (-) = 2012	Mal-genome (+) Mal-genome (-) Mal-genome (absent)	993 1013 6

Absent, not observed in this genome but detected in the other; Mal-genome; genome isolated from *Rbx. benzoatilyticus* cells grown on malate, Glc-genome; genome isolated from *Rbx. benzoatilyticus* cells grown on glucose.

Genomic data obtained as described under Table 3.5 were analysed manually based on the orientation of genes.

Table 3. 7: Genes differing in copy number amongst mal-genome and glc-genome

Gene name	Nucleotide length of the gene (bp)	Copy number	
		Mal-genome	Glc-genome
Aldehyde dehydrogenase (EC 1.2.1.3)	1233	4	3
Aspartate aminotransferase (EC 2.6.1.1)	1161	2	1
Biotin synthesis protein BioC	1725	no	1
Cell division protein FtsK	1713	1	no
CRISPR region with repeat 5'cgcgcttgtcgtaggtctgctgcagcgggttcgggatcgggccgtcctcg3'	221	no	1
CRISPR repeat with sequence 5'agcgcttgtcgtaggtctgctgcagcgggttcgggatcgggccgtcctcg3'	50	no	1
CRISPR repeat with sequence 5'cgcgcttgtcgaaggtctgctgcagcgggttcgggatcgccggcccctcg3'	50	no	1
CRISPR repeat with sequence 5'cgcgcttgtcgtaggtctgctgcagcgggttcgggatcgggccgtcctcg3'	50	no	1
CRISPR spacer	34	no	1
CRISPR spacer	37	no	1
Cys regulon transcriptional activator CysB	945	1	no
Cytosol aminopeptidase PepA (EC 3.4.11.1)	1482	1	no
DNA polymerase III chi subunit (EC 2.7.7.7)	435	1	no
Exonuclease SbcC	702	no	1
FIG00799555: hypothetical protein	510	no	1
FIG00931595: hypothetical protein	702	1	no
GGDEF domain protein	1095	5	6
Hypothetical protein	978	1	no
Hypothetical protein	1479	1	no
Hypothetical protein	510	1	no
Hypothetical protein	891	1	no
Hypothetical protein	936	1	no
Hypothetical protein	1305	1	no
Hypothetical protein	1434	no	1
Hypothetical protein	438	no	1
Hypothetical protein	1053	no	1
Hypothetical protein	147	no	1
Hypothetical protein	693	no	1
Hypothetical protein	327	no	1
InterPro IPR002797 COGs COG2244	1488	no	1
Lipopolysaccharide biosynthesis protein WzxC	1488	1	no
Lipopolysaccharide export system permease protein LptF	1095	1	no
Lipopolysaccharide export system permease protein LptG	1113	1	no
methyltransferase, FkbM family domain protein	1725	2	1
Sirohydrochlorin cobaltochelatase CbiX(small) (EC 4.99.1.3)	372	1	no

no, not observed.

Mal-genome, genome isolated from *Rbx. benzoatilyticus* cells grown on malate; Glc-genome, genome isolated from *Rbx. benzoatilyticus* cells grown on glucose.

Genomic data obtained as described under Table 3.5 were examined manually based on the length and copy number of genes.

Table 3. 8: Clustal analysis of selected genes from mal-genome and glc-genome

Contig		Gene/Protein[$]	Nuceleotide length in bp (strand sense)		Dissimilarity in pairwise alignment of glc-genome from mal-genome	
Mal-genome	Glc-genome		Mal-genome	Glc-genome	Nucleotide sequence	Amino acid sequence
3	3	Arylesterase precursor (EC 3.1.1.2)	543 (-)	645 (+)	Extended at 5' end	M1 aligned with V35
12	13	ATP-binding region, ATPase-like	993 (-)	891 (+)	Truncated at 5' end	M35 aligned with M1
7	8	ATP-dependent Clp protease adaptor protein ClpS	360 (-)	333 (-)	Truncated at 5' end	V10 aligned with M1
5	6	Chlorophyll *a* synthase ChlG (EC 2.5.1.62)	885 (-)	822 (+)	Truncated at 5' end	M22 aligned with M1
11	12	Cytosolic long-chain acyl-CoA thioester hydrolase family protein	501 (-)	531 (+)	Extended at 5' end	M1 aligned with V11
11	12	D-alanyl-D-alanine carboxypeptidase-like protein	516 (+)	456 (-)	Truncated at 5' end	V21 aligned with M1
3	3	DNA-directed RNA polymerase specialized sigma subunit, sigma24-like	567 (-)	588 (+)	Extended at 5' end	M1 aligned with L8
2	2	FeoA	345 (+)	348 (+)	Extended at 5' end	M1 aligned with M2
3	3	FIG00537881: hypothetical protein	990 (+)	1074 (-)	Extended at 5' end	M1 aligned with M29
13	14	FIG01005060: hypothetical protein	1002 (-)	975 (-)	Truncated at 5' end	L10 aligned with M1
13	14	Fumarate reductase flavoprotein subunit (EC 1.3.5.4)	1665 (-)	1770 (-)	Extended/prolonged at 5' end	M1 aligned with V36
1	1	Histone acetyltransferase HPA2 and related acetyltransferases	213 (+)	321 (-)	Extended at 5' end	M1 aligned with M37
5	6	Methyl-accepting chemotaxis protein I (serine chemoreceptor protein)	1695 (-)	1545 (+)	Truncated at 5' end	V51 aligned with M1
3	3	Murein endolytic transglycosylase MltG	966 (+)	963 (-)	Truncated at 5' end	L2 aligned with M1
7	8	Peptidyl-prolyl cis-trans isomerase PpiB (EC 5.2.1.8)	501 (+)	489 (+)	Truncated at 5' end	V5 aligned with M1
8	9	Protein of unknown function DUF86, SO_3166 group	414 (+)	429 (+)	Extended at 5' end	M1 aligned with L6
1	1	Putative exported protein of unknown function with OmpA family domain	1218 (+)	558 (-)	Truncated at 5' end	R221 aligned with R1
	5			492 (+)	Truncated at 3' end	M1 aligned with M1 but terminated at D164
5	6	Spheroidene monooxygenase (EC 1.14.15.9)	771 (-)	696 (+)	Truncated at 5' end	L26 aligned with M1

Mal-genome; genome isolated from *Rbx. benzoatilyticus* cells grown on malate, Glc-genome; genome isolated from *Rbx. benzoatilyticus* cells grown on glucose.

[$]Protein of mal-genome in red font was observed to be trimmed into three parts in glc-genome, two were detected at separate locations but one (middle fragment) was observed missing.

Nucleotide and amino acid sequences of selected genes retrieved from the genomic data as obtained in Table 3.5 were aligned separately using ClustalO.

Fig. 3. 49: Pairwise alignment of 'putative exported protein of unknown function with OmpA family domain'.

Genomic data obtained as described under Fig. 3.46 were annotated using RAST. Annotated amino acid sequence for protein 'putative exported protein of unknown function with OmpA family domain' from mal-genome and glc-genome was aligned pairwise using ClustalO. Mal-genome, genome from malate-grown Rbx. benzoatilyticus cells; glc-genome, genome from glucose-grown Rbx. benzoatilyticus cells.

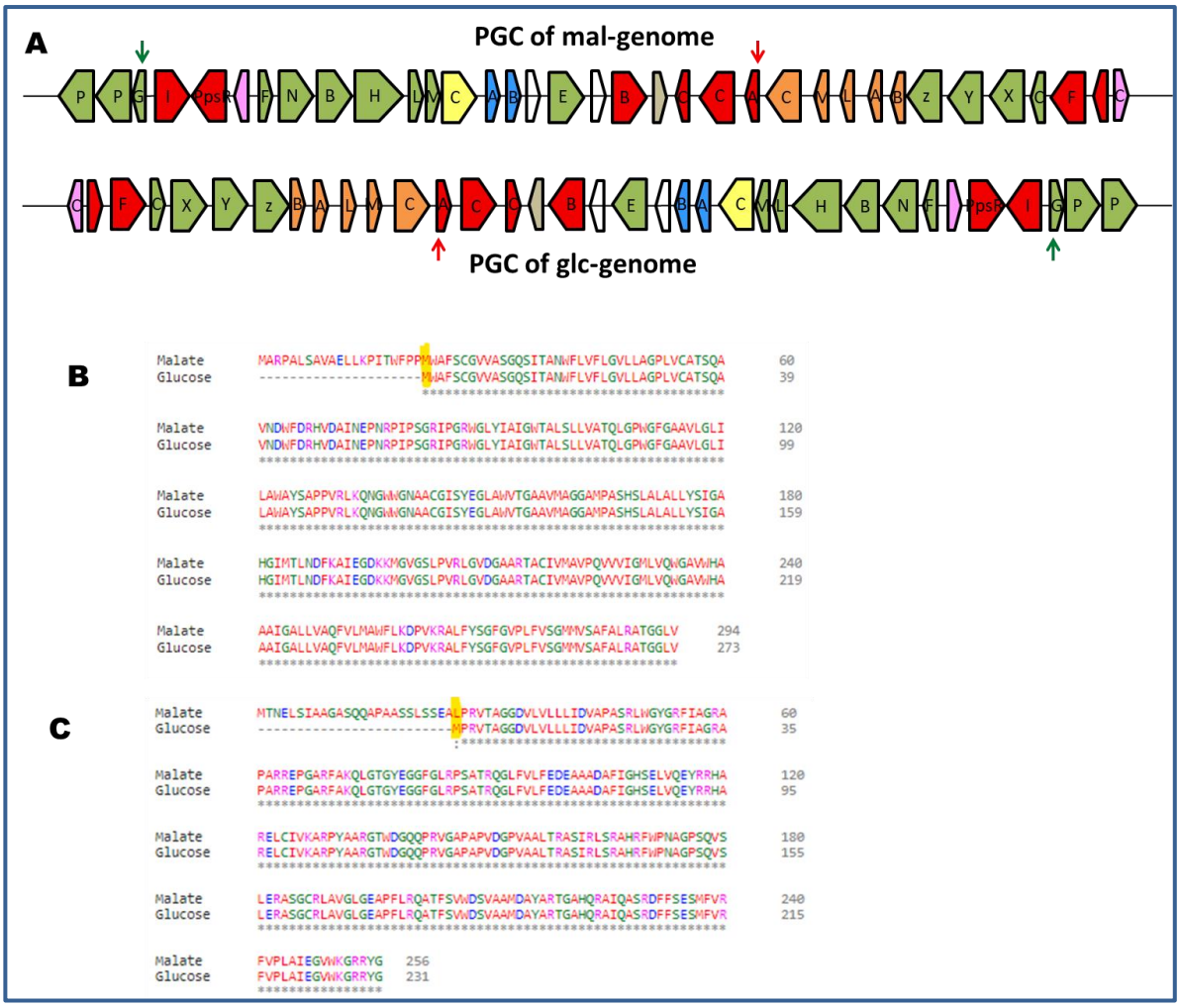

Fig. 3. 50: Arrangement of photosynthetic gene cluster in the two genomes of *Rbx. benzoatilyticus*.

*Orientation and arrangement of PGC in mal-genome and glc-genome (**A**), pairwise alignment of the amino acid sequence of chlorophyll a synthase ChlG (**B**) and spheroidene monooxygenase (**C**) from mal-genome and glc-genome.*

PGC genes were extracted from the annotation file obtained as described under Fig. 3.46. Genes are represented as arrows pointing in the direction of their transcription. Green, bacterial chlorophyll genes; orange, puf genes; blue, puh genes; red, carotenoid and regulatory genes, pink, hem and cyc genes; yellow, lha gene; blank, uncertain genes; gray, hypothetical gene. PGC, photosynthetic gene cluster; Mal-genome, genome from malate-grown Rbx. benzoatilyticus cells; glc-genome, genome from glucose-grown Rbx. benzoatilyticus cells.

Chapter 4: Discussion

4. Discussion

Bacteria are constantly exposed to the dynamic environment and they counter these changes for their survival by initiating a cascade of cellular events which adapt them to a particular environment (Boller and Felix, 2009). Carbon source is one such external factor which influences growth and physiology of the organism. Thus understanding how carbon source modulates metabolic phenotype is of interest in basic as well as applied point of view. Facultative phototrophic bacterium, *Rubrivivax benzoatilyticus* has shown a paradigm shift, reflected as phenotypic perturbation, when grown on glucose as carbon source. Here, in this study, employing systems approach we performed iTRAQ proteome profiling in conjunction with the physiological studies to elucidate its metabolic adaptations when grown on glucose as compared with malate. Also, we attempted to understand the variation in genome under the influence of glucose and concluded the study with an inventory of differences and commonalities between hyperglycaemia in micro and macro-organisms.

Present study started with the inventory of glucose photometabolism by different APB. We observed that many APB are able to photometabolize glucose in the same fashion as other carbon sources while a few can't be cultivated at all on glucose. A few others can grow on glucose but, the latter has a toxic effect on them at 18 days or longer incubations and *Rbx. benzoatilyticus* is one amongst them (Table 3.1). This gives an impression that though majority of APB members can photometabolize glucose yet, it is not a preferred carbon source for all APB; rather it has some deleterious effect on certain spp. Not only APB, glucose intolerance was also reported in chemotrophs like *Salmonella*, yeast like *Saccharomyces* and other microorganisms (Morishige et al., 2014).

Rbx. benzoatilyticus has a chimeric pathway for carotenoid biosynthesis that is both spirilloxanthin as well as spheroidene biosynthetic pathway (Ramana et al., 2006). On the other hand, this is not the case with other APB which have either of the two pathways. Also, genomic information of *Rbx. benzoatilyticus* is available (Mohammed et al., 2011). Consequently, *Rbx. benzoatilyticus* perfectly fits for this study, the cells of which were photo-bleached as a result of longer incubations on glucose. *Rbx. benzoatilyticus* cells, when attempted to grow on different sugars as carbon sources phototrophically, the cells were photo-bleached losing their pigmentation and thus affecting photosynthesis. However, cells retained pigmentation on non-sugar carbon sources (Table 3.2). This concluded that not only glucose but sugars in general have a kind of toxic effect on *Rbx. benzoatilyticus* when used as carbon source phototrophically. Accordingly, we selected glucose, a preferred carbon source for many bacteria, for experimentation against malate (a non-sugar organic carbon source) as control.

4.1. Glucose modulated growth characteristics and pigmentation of *Rbx. benzoatilyticus*

Rubrivivax benzoatilyticus cells increased their doubling time on glucose as compared with malate. This implicated malate a preferred carbon source over glucose for *Rbx. benzoatilyticus* since it is well documented that faster the growth rate or lesser the doubling time, higher the hierarchy for preference of carbon source (Aidelberg et al., 2014).

Rubrivivax benzoatilyticus contains sphaeroidene, spirilloxanthin and bacteriochlorophyll *a* as pigment system (Gupta et al., 2019; Ramana et al., 2006) but it lost its entire pigment and pigment synthesizing machinery upon longer incubations on glucose (Table S1, Fig. 4.1). To examine the interdependency, pigment kinetics was studied. Results demonstrated that sphaeroidene peak diminished in time dependent manner (Fig. 3.12). In contrast, spirilloxanthin peak augmented till 9^{th} day, possibly to recover the loss of

sphaeroidene function thereafter, it also reduced to negligible (Fig. 3.12). In the similar fashion, bacteriochlorophyll *a* peak, which was constant until 9th day, started declining thereafter. Thus, we predicted that loss in bacteriochlorophyll *a* is somewhat correlated with loss in spirilloxanthin but not with sphaeroidene and there is no interdependency between loss in spirilloxanthin and sphaeroidene. This concluded that the loss in-bacteriochlorophyll *a* correlated with the loss in spirilloxanthin and not sphaeroidene for *Rbx. benzoatilyticus*.

Not only pigments, glucose has influenced photosystems and quinones also. *Rbx. benzoatilyticus* contains menaquinone-8 (MK-8) and ubiquinone-8 (Q8) as the two major quinones. Same are also observed previously from closely related *Rubrivivax gelatinosus* (Agalidis et al., 1990). Though, MK-8 was unaffected, Q8 along with RC and LHC of photosystems were greatly affected under the influence of glucose. Thus, implicating that glucose has affected not only pigments but also the entire photosynthesizing machinery and photosynthesis, the major energy driving route for *Rbx. benzoatilyticus* (Ramana et al., 2006).

To get the holistic view, three time points- G3 (exponential or actively growing phase), G9 (the state where pigments start disappearing) and G18 (a non-cultivable state) were taken forward for dynamic studies of protein and metabolites.

4.2. Glucose grown cells displayed altered cell size and membrane adaptation

Rubrivivax benzoatilyticus reduced its cellular size in presence of glucose on longer incubations. Morphological variation is commonly observed in response to external perturbations acting as a survival strategy to conserve energy and better absorption of nutrients during unfavorable circumstances (Krebs and Taylor, 2011). Similarly, reduction in size of glucose grown *Rbx. benzoatilyticus* cells may have same kind of fitness benefits to survive during growth on glucose.

Rubrivivax benzoatilyticus modulated its membrane composition in response to longer incubations on glucose by increasing its saturated to unsaturated fatty acid ratio. Cytoplasmic membranes separate cellular content from external environment regulating the entry and exit of substances either by altering physical properties or lipid composition of the membranes (Denich et al., 2003). This membrane management strategy probably helps the cells to acclimate with the alterations in cellular metabolism as a consequence of growth on a non-preferred carbon source and also it might be the reason for shrinkage in cell size.

4.3. Resuscitation occurred for a limited duration

Cultivability analysis of *Rbx. benzoatilyticus* cells under the influence of glucose suggested that 18 days and longer incubated cells transited to a state of non-cultivability (section 3.1.6; Fig. 3.3). In other words, 15 d or lesser incubated glucose grown cells multiplied on sub-culturing while 18 d or longer incubated cells failed to do so. This suggests that either there was a progressive reduction in the number of cultivable or resuscitable cells (Pinto et al., 2013) (which is in correlation with the loss of pigments (Fig 3.1) and the duration of incubation on glucose (Fig. 3.3)) or the cells might be triggered to a death phase. At the same time, we also observed that the effect of glucose on repeated sub-culturing of exponential phase cells was inefficacious wherein, though cells lost their pigmentation but still were able to grow on glucose as well as malate media after such transferring's (refer to section 3.1.7).

Another aspect that grabbed the attention of researchers is 'resuscitation window' that was described for *Micrococcus luteus*, *Vibrio cholera* and *Escherichia coli* (Pinto et al., 2013). Resuscitation window is the limited time period during which cells resuscitates in response to the stimulus under study and it varies with the stimulus, age of the cells and the species (Pinto et al., 2013). Taking together our results suggest that (1) resuscitation event occurred only till 15 days glucose incubated *Rbx. benzoatilyticus* cells, in other words, their

resuscitation window is less than 18 days for glucose and (2) longer incubations on glucose in batch culture contributes to the said non-cultivable state of *Rbx. benzoatilyticus* rather than mere glucose *per se* as unfavourable substrate. To gain comprehensive understandings into the growth arrested state of *Rbx. benzoatilyticus* in the presence of glucose, cell biomass and spent media were used to analyse proteome and metabolome profiling respectively.

Viability of non-cultivable cells was assessed using vital dye staining like DAPI, PI and resazurin. *Rbx. benzoatilyticus* failed to stain with DAPI, this could be due to high GC content of *Rbx. benzoatilyticus* (76.1 mol%) (Ramana et al., 2006) and DAPI stains AT rich regions of the DNA (Silva and Guerra, 2010). Thus, another stain FDA, in replacement, was used in this study. Small neutral molecules and positively charged molecules can pass through viable cell membranes and remain inside the cells, depending on their reactivity or hydrophilicity. Esters like fluorescein diacetate (FDA) suits for staining viable cells as it can permit through the viable cell membranes and is hydrolyzed by intracellular esterases into negatively charged fluorescein analogs under physiological pH, emitting green fluorescence. These fluorescent products, because of their negative charges, are retained by the cells. FDA is a non-fluorescent dye which on entering the cells cleaves into fluorescein that fluoresces and the fluorescence can be measured at 514 nm (Salma et al., 2013). Green fluorescence of G18 cells detected in CLSM (Fig. 3.4) and 37 % FDA positive glucose grown cells (Fig. 3.5) detected in FACS analysis (which is comparable with 43 % malate grown cells) indicates that perhaps G18 cells are in viable but non-cultivable (VBNC) state which subsequently might be triggered to death phase. Positive signal with both resazurin as well as PI indicates that G18 cells are probably metabolically active with damaged membrane and this might be the reason for G18 cells being in a non-growing state.

4.4. *Rbx. benzoatilyticus* cells rewired their central carbon metabolism extensively and adopted alternate energy driving routes

Three glycolytic pathways were reported in bacteria- Embden-Meyerhof-Parnas (EMP) pathway, pentose phosphate pathway (PPP) and the Entner Doudoroff (ED) pathway (Chen et al., 2016). Complete set of genes encoding enzymes for all the three pathways are present in the genome of *Rbx. benzoatilyticus* (Mohammed et al., 2011). The EMP pathway is undoubtedly the most common route for the catabolism of glucose to pyruvate (Flamholz et al., 2013). Yet, in glucose-grown cells, we observed that proteins related to EMP pathway along with gluconeogenesis were down-regulated.

The first two proteins of ED pathway were up-regulated while phosphogluconate dehydratase (RBXJA2T_14896) was unaffected in our iTRAQ datum of glucose-grown cells. This suggests that glucose is catabolised to pyruvate *via* ED pathway (or yet unknown pathway) and not through EMP since most of the enzymes of EMP were down-regulated (Table S1). As ED pathway is less efficient in ATP synthesis compared to EMP pathway (Flamholz et al., 2013), the active ED pathway in glucose-grown cells of *Rbx. benzoatilyticus* might have resulted in the generation of less ATP thereby leading to the reduced cellular ATP pool. Further, iTRAQ analysis indicated repression of pyruvate conversion to acetyl CoA, lactate or ethanol as well in the glucose-grown cells.

Furthermore, aldehyde dehydrogenase (Aldh) (RBXJA2T_18613) involved in pyruvate catabolism leading to acetate production was highly up-regulated in glucose-grown cells (Table S1). Although pyruvate decarboxylase (involved in conversion of pyruvic acid to acetaldehyde) was not covered in our iTRAQ datum, highly expressed Aldh indicates possible flux of pyruvate to acetate formation, thereby, leading to acetate accumulation in glucose-grown cells. Excess of acetate ion acidifies the cytoplasm which is toxic to cell and to prevent this, possibly acetate is excreted out leading to rapid extracellular acidification

(Thomas et al., 2014) (Fig. 4.1). In agreement with this, we observed a decrease in extracellular pH from neutral (6.8) to acidic (4.4) in glucose-grown culture supporting acid fermentation. In contrast, malate grown cultures did not show such decrease in pH (section 3.1.4). Considering these results, we hypothesize that down-regulation of pyruvate, lactate and alcohol dehydrogenase along with low oxygen levels (microaerophilic) might have resulted in metabolic shift towards acid fermentation (acetate) in glucose-grown cells. Up-regulation of acetyl CoA synthetase (RBXJA2T_05903)/AMP dependent synthetase-ligase (RBXJA2T_17162) which converts acetate to acetyl CoA (Wolfe, 2005) suggests activation of an alternative route for acetyl CoA synthesis in glucose-grown cells. Acetate switch enables bacteria to utilize acetate as a carbon source under nutrient limiting conditions (Wolfe, 2005), and it's up-regulation in glucose-grown cells implies acetate assimilation.

The study also revealed up-regulation of proteins related to lipid catabolism and β-oxidation of fatty acids. Taken together, these results suggest an active lipid/fatty acid degradation in glucose-grown cells consequently cells might be obtaining energy by catabolizing endogenous phospholipids as alternative energy source. Similar metabolic adaptation was observed in *Escherichia coli* and *Vibrio* sp., wherein cells showed active lipid and fatty acid catabolism to survive under energy deficient conditions (Bergkessel et al., 2016). Fatty acid β-oxidation generates acetyl CoA which is further metabolized through glyoxylate pathway when TCA pathway is repressed to generate important TCA pathway intermediates for cell survival. In line with this, we found up-regulation of key enzymes of glyoxylate pathway indicating an active glyoxylate shunt along with down-regulation of TCA pathway protein (isocitrate dehydrogenase (RBXJA2T_10419) in the glucose-grown cells (Table S1). Carbon flux through the glyoxylate pathway is reported to be a key metabolic adaptation displayed by stressed cells to sustain the metabolic activity under nutrient/energy limiting conditions (Bergkessel et al., 2016). Similarly, activation of glyoxylate pathway may

provide an adaptive benefit under glucose induced energy limiting conditions by preventing the loss of carbon in the form of CO_2 at the same time generating important TCA pathway intermediates and reducing equivalents (NADH/FADH). We speculate that bypassing the two CO_2 evolution steps of Kreb's cycle might be a cause or consequence of loss in photosynthesis. β-oxidation of odd or branched chain fatty acids generates acetyl CoA and propionyl CoA. Excessive propionyl CoA accumulation is toxic to cell and bacteria overcomes this by metabolizing propionyl CoA to succinate using methyl citrate or methyl malonyl CoA pathway (Gengenbacher and Kaufmann, 2012). Consistent with this, we observed up-regulation of propionyl CoA carboxylase (RBXJA2T_03021) and methylmalonyl CoA mutase (RBXJA2T_09869) (Table S1) which converts propionyl CoA to succinyl CoA via methylmalonyl CoA (Gengenbacher and Kaufmann, 2012).

Active ATP synthesis requires a fully functional ETC but down-regulation of proteins related to ETC except complex-I and II indicates impaired electron transport and ATP synthesis, thereby leading to energy limitation state in glucose-grown cells. Furthermore, the low energy state of the cell was evident from up-regulation of membrane-bound proton-translocating pyrophosphatase (RBXJA2T_19256) (Table S1), which is known to express under low energy (ATP) conditions to compensate the energy deficiency by maintaining the proton motive force (PMF) (Lo and Pe, 2004). Impaired photo and oxidative phosphorylation in glucose-grown cells may have activated proton-translocating pyrophosphatase, an alternative PMF maintaining mechanism to survive (Fig. 4.1).

Rbx. benzoatilyticus contains MEP pathway for IPP biosynthesis (Ramana et al., 2006). Proteins related to IPP biosynthesis and chlorophyll/ heme biosynthetic pathway were down-regulated. This is further supported by the gradual loss of pigments over a period of time in glucose-grown culture (Fig. 3.1A,B). *Rbx. benzoatilyticus* contains sphaeroidene as well as spirilloxanthin (Ramana et al., 2006) series of carotenoids. HPLC analysis of

pigments revealed gradual depletion of both sphaeroidene, spirilloxanthin as well as bacteriochlorophyll *a* (Fig. 3.12) in stationary phase glucose-grown cultures (G-18). Thus, suggesting that starting from IPP biosynthesis to quinones, pigments along with photosynthetic reaction centre and the entire photosynthetic machinery is down-regulated. Similar to this, down-regulation in the number of thylakoid membrane and photosynthetic pigments by externally added glucose is reported in *Galdieria sulphuraria* and *G. partita* (Graverholt and Eriksen, 2007; Oesterhelt et al., 2007; Stadnichuk et al., 1998). Also, presence of exogenous sugars limiting photosynthesis and preventing proper development of photosynthetic apparatus has been well reported in higher plants (Eckstein et al., 2012; Hdider and Desjardins, 1994; Huylenbroeck and Debergh, 1996; Rybczyński et al., 2007). Moreover, photosynthetic reaction centre cytochrome *c* subunit (RBXJA2T_09482) and reaction centre subunit H (RBXJA2T_09532) were down-regulated in our proteome analysis also (Table S1).

In correlation with proteome datum, differential ultracentrifugation and spectral analysis of photosystems isolated from stationary phase cells revealed the complete absence of RC-LHC I, (Fig. 3.13A) and very low quantities of LHC II (Fig. 3.13B) in glucose grown cells. Menaquinone-8 (MK-8) and ubiquinone-8 (Q8) are the two major quinones of *Rbx. benzoatilyticus* has also observed previously for *Rbx. gelatinosus* (Agalidis et al., 1990). HPLC analysis of quinones revealed 16-20 fold lower levels of Q8 in stationary phase glucose grown cells (compared with that of malate grown cells) of *Rbx. benzoatilyticus* (Fig. 3.14) which is in line with impaired ETC observed in the proteome analysis. Down-regulation of pigments involved in photosynthesis (chlorophyll/carotenoids) and reaction centre-light harvesting complex proteins strongly suggests repression of entire photosynthetic machinery in glucose grown cells. In APB light and oxygen tension regulates the expression of genes related to photosynthetic machinery (Roh et al., 2004; Steunou et al., 2004) thereby,

modulating the growth modes. For the first time, this study reported a plausible carbon source (glucose) mediated regulation of photosynthesis in APB. Interestingly, excess of glucose is known to repress the photosynthetic processes (pigment synthesis, photophosphorylation, CO_2 fixation) by feedback regulation in higher plants, algae and cyanobacteria (Oesterhelt et al. 2007; Stadnichuk et al. 1998; Lebedeva et al. 2005; Jang and Sheen 1994). Similarly, in our study down-regulation of genes related to photosynthesis (Table S1) and loss of pigmentation in glucose-grown cells suggest a possible glucose mediated-repression of the photosynthetic machinery. Furthermore, repression of photosynthetic machinery may have resulted in low ATP pools and thus cells may have shifted to other growth mode(s) to obtain energy.

4.5. Molecular response of glucose grown cells

Down-regulation of DNA replication, as observed in proteome datum (Table S1), may be an energy conserving mechanisms displayed by glucose-grown *Rbx. benzoatilyticus* cells during their transition period and this phenomenon is also observed as stringent response by *Escherichia coli* (Carneiro et al., 2016). The epsilon subunit of DNA polymerase III has the editing function and is a 3'-5' proofreading exonuclease (Koonin and Deutscher, 1993). An enhanced level of DNA polymerase III and DNA repair proteins could be attributed to the maintenance of the genetic material in response to the stress generated during the growth on glucose.

Our datum suggested unaltered expression of RNA polymerase subunit β and up-regulation of transcription factors. This suggests active transcription and the selective gene expression to adapt to the changing circumstances. PAP I synthesizes poly(A) at 3' end of RNAs while RNase E/R and PNPase are components of the multienzyme complex, RNA degradosome, involved in the degradation of RNA (Mackie, 2013). Thus up-regulation of RNA degradation machinery may be a molecular adaptation to maintain the condition-

specific mRNAs and proteins (Mackie, 2013) in glucose-grown culture which needs further evaluation.

Efficient translation requires a full complement of ribosomal proteins, down-regulation of elongation factors suggests reduced or repressed translation in the glucose-grown cells. Further, the impaired translation is evident from up-regulation of peptidyl-tRNA hydrolase (RBXJA2T_15518) (Table S1), an enzyme known to up-regulate in response to translational stalling and it cleaves the nascent peptide releasing peptidyl-tRNAs and allowing rescue/reuse of the ribosomes (Das and Varshney, 2006). We speculate that impaired or stalled translation along with other physiological stress may have resulted in the accumulation of immature or denatured polypeptides and to combat this, glucose grown cells activated the protein quality control system. Up-regulation of proteins related to protein quality control (Table S1) ensures degradation of dispensable proteins to provide amino acid pools under nutrient limiting conditions.

Two component signal transduction and chemotaxis proteins sense changes in the environment and orchestrate the expression of genes essential for cell survival and up-regulation of these proteins in glucose grown cells may help in better adaptation to the changing milieu. Moreover, our study revealed up-regulation of Acetyl-CoA acetyltransferase (RBXJA2T_02991) (Table S1) involved in the polyhydroxyalkanoate (PHA) synthesis (Kim and Copeland, 1997). This suggests an accumulation of PHAs in glucose-grown cells and it is further supported by TEM analysis showing more PHA granules in glucose-grown cells (Fig. 3.2 G,H). Alarmone activates stringent response in bacteria, which represses the translation, cell division/replication while activates the selective transcription to cope with starvation (Gaca et al., 2015). In accordance with this idea, we observed up-regulation of alarmone along with down-regulation of translation, cell-

division/replication and activation of selective transcription and stress response possibly indicating stringent response like mechanism in glucose-grown cells.

A large number of hypothetical proteins were differentially regulated (Fig. 3.34, Table S1) and this suggests their plausible functional role in cell survival under glucose-grown condition and this needs further investigation which will provide more clues to their functions. Remarkably, membrane transport proteins were the most abundant differentially regulated proteins in glucose-grown cells (Fig. 3.34, Table S1) and such regulation of transport proteins enable cell survival under resource-limited conditions by the acquisition of nutrients and prevention of the key metabolites leakage (Denich et al., 2003). Proteome analysis also revealed up-regulation of proteins related to membrane targeting complexes, secretion system, outer membrane/lipoproteins, pili/fimbriae assembly and cell wall modifying proteins (Table S1) involved in remodelling or repairing of the envelope (Grabowicz and Silhavy, 2017). Maintaining the envelope integrity is crucial for cell survival as it carries vital cellular functions; envelope perturbation activates envelope biogenesis and homeostasis factors (Grabowicz and Silhavy, 2017). We argue that reduction in size of glucose-grown cells warrants an extensive envelope remodelling and this is achieved by activating the envelope homeostasis system. Furthermore, up-regulation of lysophospholipid transporter LplT (RBXJA2T_18889) (Table S1) (which acts as a flippase for trans-bilayer movement of lysophospholipids and plays vital role in maintaining membrane integrity and stability (Lin et al., 2016)) along with toluene tolerance protein (RBXJA2T_01010) (presumed to be involved in modifying lipid/fatty acids) strongly suggests active remodelling of cell envelope in glucose-grown cells. Based on the prior knowledge and findings of the current study, we propose a model to showcase the events associated with rewiring of cellular processes in glucose-grown cells of *Rbx. benzoatilyticus* under photoheterotrophy (Fig. 4.1).

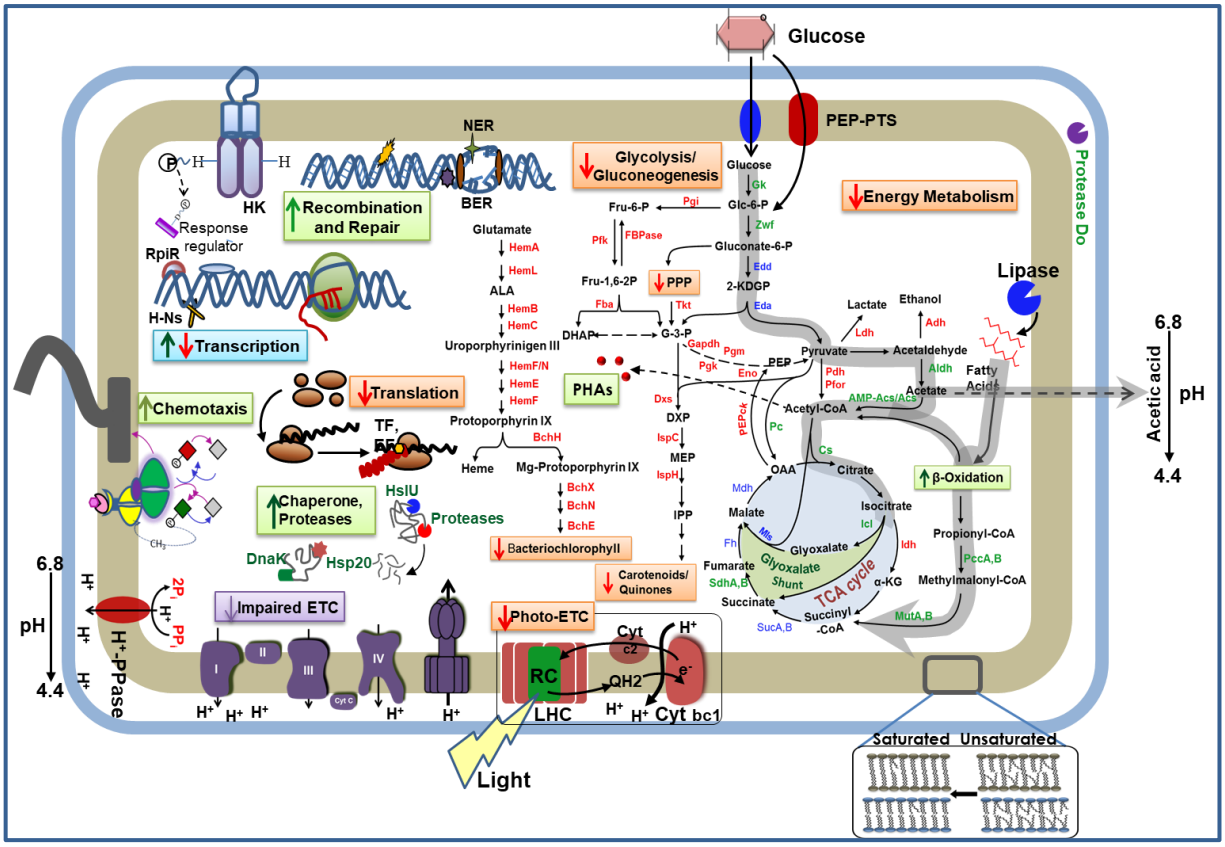

Fig. 4. 1: Model depicting cellular events taking place in glucose grown *Rbx. benzoatilyticus* cells (Gupta et al., 2019)

Model was generated by integrating physiological, biochemical, metabolomic and proteomic data. Metabolic pathways were constructed based on bacterial metabolic pathways of KEGG and genome analysis of Rbx. benzoatilyticus JA2.

Solid up arrows in green indicate up-regulation; solid down arrows in red indicate down-regulation of a cellular process. Proteins represented in green font indicate up-regulated, red indicates down-regulated, and blue indicates unaltered expression. Proteins with p-value < 0.05 represented in the bold letter while p-value > 0.05 are unbold, Dotted arrows denote multiple steps in a pathway. Pathway(s) shaded in gray indicate carbon flux.

Gk, Glucokinase; Zwf, glucose-6-phosphate dehydrogenase; Edd, Phosphogluconate dehydratase; Eda, 2-Keto-3-deoxy-6-phosphogluconate aldolase; Gapdh, Glyceraldehyde 3-phosphate dehydrogenase; Pgk, Phosphoglycerate kinase; Pgm, Phosphoglyceromutase; Eno, Enolase; Dxs, 1-deoxy-D-xylulose-5-phosphate synthase; IspC, 1-deoxy-D-xylulose-5-phosphate reductoisomerase; IspH, 4-hydroxy-3-methylbut-2-enyl diphosphate reductase; Tkt, Transketolase; Pgi, glucose-6-phosphate isomerise; Pfk, 6-phosphofructokinase; FBPase, Fructose 1,6-bisphosphatase; Fba, Fructose 1,6-bisphosphate aldolase; Pdh, Pyruvate dehydrogenase; Pfor, pyruvate-ferredoxin/flavodoxinoxidoreductase; PccA,B, Propionyl CoA carboxylase A, B; MutA,BMethylmalonyl CoA mutase A, B; Ldh, Lactate dehydrogenase; Aldh, Aldehyde dehydrogenase; Adh, Alcohol dehydrogenase; AMP-Acs, AMP dependentsynthetase-ligase; Acs, Acetyl CoA synthetase; Cs, Citrate synthase; Icl, Isocitratelyase; Idh, Isocitrate Dehydrogenase; SucC, SucD, succinate synthase subunits; SdhA,Bsuccinate dehydrogenase A, B; Fh, fumaratehydratase; Mdh, malate dehydrogenase; Mls, malate synthase;PEPck, Phosphoenol pyruvatecarboxykinase; HemA,glutamyl-tRNA reductase; HemL, glutamate-1-semialdehyde 2,1-aminomutase; HemB,porphobilinogen synthase; HemC, hydroxymethylbilane

synthase/porphobilinogendeaminase; HemF/N, oxygen-independentcoproporphyrinogen III oxidase; HemE, uroporphyrinogen decarboxylase; HemF, coproporphyrinogen III oxidase; BchH, magnesium chelatase subunit I; BchX, Bacteriochlorophyllide reductase; BchN, Light-independent protochlorophyllide reductase; BchEProtoporphyrinmonomethylestercyclise; RC, Reaction center; LHC, Light harvesting complex; KDPG, 2-Keto-3-deoxy-6-phosphogluconate; Glc-6-P, glucose-6-phosphate; Fru-6-P, fructose-6-phosphate; Fruc-1,6-2P, fructose-1,6-bisphosphate; PEP, phosphoenol pyruvate; OAA, oxaloacetate; α-KG, α-ketoglutarate;DXP, 1-deoxy-D-xylulose-5-phosphate; MEP, methyl erythrytol-4-phosphate; IPP, ALA, Amino levulinic acid; Isopentenylpyrophosphate; PEP-PTS, PEP-phosphotransferase system;H^+PPase, Membrane-bound proton-translocatingpyrophosphatase; PPP, pentose phosphate pathway; ETC, oxidative electron transport chain; Photo-ETC, photo phosphorylation;PPi, inorganic pyrophosphate; HK, Histidine kinase; H-Ns, Histone-like nucleoid-structural protein;RpiR, RpiR family transcriptional regulator; DnaK, Molecular chaperone DnaK; NER, Nucleotide Excision repair; BER, Base excision repair; TF, Termination Factor; EF, Elongation Factor; Hsp20, Heat shock protein Hsp20; HslU, ATP-dependent protease ATP-binding subunit HslU.

4.6. Dynamic studies: a paradigm shift from exponential phase to pigment loss to non-cultivable state.

Our analysis revealed that not mere glucose but the longer incubations of glucose is responsible for the toxic effect on *Rbx. benzoatilyticus*. This provoked us to study the dynamics starting from exponential phase to early stationary phase to late stationary phase. In this aspect dynamics of pigments, metabolites and proteins was carried out. Metabolomic and proteomic changes were examined during longer incubations (selecting 3 time points - exponential phase or actively growing state (G3); pigment loss state (G9) and non-cultivable/growth arrested state (G18)) to elucidate the metabolic adaptations leading to a transition in the physiology of the organism. Temporal increase in the metabolites and differentially expressed proteins (DEPs) as seen in the exometabolome and iTRAQ analysis respectively, revealed gradual exaggerated condition. Dynamic proteome analysis suggested that proteins associated with primary metabolism down-regulated prior to those related to secondary metabolism as discussed below.

Our study exhibited lower levels of proteins involved in the metabolism and protein synthesizing machinery. As non-cultivable state have limited demand for energy resources (Bergkessel et al., 2016), it was not surprising to observe lower levels of proteins related to

the metabolic activities and energy production. This includes oxidative phosphorylation and photophosphorylation.

4.6.1. Pigment kinetics ravelled gradual repression of carotenoids and bacteriochlorophyll a

Our pigment kinetic study by HPLC revealed that sphaeroidene peak diminished in a time dependent way paradoxically, spirilloxanthin peak augmented (Fig. 3.12). We speculate this augmentation of spirilloxanthin is to recover the vacuous of sphaeroidene till 9th day of growth curve. But, thereafter glucose influenced spirilloxanthin also resulting in its loss. The bacteriochlorophyll *a* peak showed similar behaviour. This suggested that glucose influenced loss of sphaeroidene prior which is followed by loss of spirilloxanthin and bacteriochlorophyll *a*.

Phototrophy is the preferred growth mode and energy generating route for APB including *Rbx. benzoatilyticus* (Ramana et al., 2006). But in this study, we observed loss of pigmentation along with down-regulation of all the proteins involved in pigment (carotenoid as well as chlorophyll) biosynthesis even at G9. This also supports that *Rbx. benzoatilyticus* knocked off (arrested) its phototrophic growth mode and switched to an alternate energy driving route or less energy demanding state right from the early phase of growth curve.

iTRAQ proteome analysis suggested down regulation of 4-hydroxy-3-methylbut-2-enyl diphosphate (engaged in terpenoid biosynthetic process), spheroidene monooxygenase (involved in pigment biosynthesis). The proteins related to photosynthesis (RuBP carboxylase, photosynthetic reaction Centre cytochrome c subunit and electron transfer flavoprotein) (Table S1, S2) were also under-expressed indicating absence of pigment biosynthesis and photosynthesis. Hence, it was predicted that pigments are not degraded instead its biosynthesis is hampered. Further, we attempted to look for pigment degradation products/isoprene units in the exometabolome datum of GC-MS but, terpenoid/isoprene units

were not observed in the data. We speculate that this could be either due to metabolites not detected by the instrument or short half-life of the metabolite, they disappeared instead of getting degraded.

4.6.2. Storage filling in the transition from exponential phase to PHA synthesis and accumulation

Strikingly, DEPs related to EMP pathway and TCA cycle (energy metabolism) were rapidly down-regulated even at exponential phase glucose grown cells compared to malate grown ones (Gupta et al., 2019). The PPP is central to the carbon metabolism and involves in generating reducing power (in the oxidative part of PPP) and pentose phosphates for numerous metabolic pathways. Phosphogluconate dehydratase, which participates in ox PPP and transketolase, which is involved in the non-oxidative part of PPP showed similar accumulation as that of glycolysis or TCA cycle proteins suggesting down-regulation of PPP as well.

Meanwhile, at the mid stage of growth phase (early stationary phase) where cells exhibited loss of pigmentation (Fig. 3.12), storage material (PHAs) began to be rapidly synthesized and accumulated. As a result, DEPs associated with storage granules (4 of 6 proteins), such as phasin family and poly granule-associated protein showed maximal accumulation at this stage. Also, α amylase which is responsible for hydrolysing α-1,4 glycosidic bonds was down-regulated suggesting inhibition of polysaccharide hydrolysis. Apart from this, arginosuccinate synthase which catalyses the synthesis of arginosuccinate from citrulline and aspartate was down-regulated at G18. Thus, reflecting the transition from exponential phase to storage filling.

4.6.3. Protein expression characteristics during non-cultivable state

The late stationary phase, G18, is characterized by complete loss of pigments where glucose grown *Rbx. benzoatilyticus* cells gradually go into a quiescent/nonproliferating

dormant state. The molecular chaperones control folding of nascent polypeptides into mature protein (Molière and Turgay, 2009). In line with this, a substantial percentage of DEPs involved in protein folding/ modification e.g. HSP and chaperones/ chaperonins concomitantly expressed along with storage proteins. These proteins are noteworthy candidates for investigating the folding and assembly of storage proteins. Remarkably, many DEPs (5 of 8 proteins) related to chaperone significantly accumulated at this stage apart from HSPs.

During the non-cultivable state (late stationary phase), other noticeable feature is the maximum number of DEPs involved in stress (5 of 6 proteins). The increased expression of stress proteins have also been observed in spore formation and other non-growing states (Hecker and Völker, 1990). The existence and accumulation of stress proteins correlated with loss in pigmentation and in response to dormant states of growth.

Glucose is well reported to cause ROS production, instability of DNA and base modifications (Lindahl, 1993; Zhang et al., 2007; Lee et al., 2012). When ROS production greatly exceeds the capacity of endogenous antioxidant systems, ROS levels increase further. In accordance with this, we observed oxidative damage protection protein, which was unaffected at G9, down-regulated at G18 in our proteome datum further adding up to the accumulation of ROS. ROS is associated with induction of oxidative stress as also observed in this study or signal transduction and is characterized by damaging effects on biomolecules like proteins and DNA leading to loss of function (Kashmiri and Mankar, 2014) contributing to the physiology of aging . In line with this, we observed elevated levels of proteins involved in replication and repair at G18 though they were down-regulated at G9 possibly to maintain the genomic stability.

Active protein turnover was also observed during early and late stationary phase stage. Hitherto, our analysis highlighted that almost all the DEPs involved in proteolysis (9 of 11 proteins) exhibited differential accumulation. Few of these DEPs are significant component of the ubiquitination or proteasome pathway. Apart from this, a huge number of DEPs involved in protein synthesis (16 of 17 proteins) and transport (53 of 59 proteins) showed similar accumulation pattern to that of proteolysis-related ones. In nut shell, these results suggested that protein turnover and rearrangements aere also essential for maintaining the quality of proteins and amino acid pool along with the stability of genetic material.

4.7. Change in life style might be a key player in inducing a state of non-cultivability in *Rbx. benzoatilyticus*.

Glucose tolerance test suggested cells of *Rbx. benzoatilyticus* were able to resuscitate when grown on glucose with concentrations up to 10 mM. But, failed to grow when incubated at the concentration of 20 mM and above. This implies that not merely glucose but a concentration of 22 mM or higher under phototrophic growth mode is unfavourable to *Rbx. benzoatilyticus* (Fig. 3.7). This suggested that 22 mM glucose, used in this study, was hyperglycemic and not normoglycemic to *Rbx. benzoatilyticus*. When literature survey was carried out, it was observed that 22 mM glucose is hyperglycemic to mammalian cells as well (Koziel et al., 2012) and is termed ‘Diabetes’ for this case. Further, the study with resting cells indicated that the mechanism of pigment and cultivability loss is confined not only to growing cells but to resting cells as well.

Also, the study suggested an increase in the levels of ROS generation. And this might be playing a crucial role in the transition of *Rbx. benzoatilyticus* to a non-cultivable state. Apart from this, glucose grown cells retained pigmentation and viability under chemotrophic growth mode (Fig. 3.8). This indicated that the preferred growth mode for *Rbx. benzoatilyticus* on glucose is chemoheteroorganotrophy rather than photoheteroorganotrophy.

Thus, specifies that perhaps a physiological stress (oxygen limitation) might have led to the switch from phototrophic growth to a non-cultivable state in *Rbx. benzoatilyticus*. In other words, *Rbx. benzoatilyticus* can grow chemotrophically when glucose is provided as electron donor but a change in life style *i.e.* when forced to grow phototrophically, cells switched to a non-cultivable state. A condition similar to the diabetes of higher organisms, where diet along with the sedentary life style is considered to be the prime culprit (Ssewanyana et al., 2018).

4.8. Genome wide variation analysis of glucose grown cells

Rbx. benzoatilyticus was isolated from flooded paddy soil near Eluru, Andhra Pradesh, India and culture is also available at different culture collections (=ATCC BAA-35T=JCM 13220T=MTCC 7087T) (Ramana et al., 2006). The gDNA of *Rbx. benzoatilyticus*, sequenced in the year 2011, is available in NCBI database with GenBank accession number AEWG00000000 (Mohammed et al., 2011). Over the years, *Rbx. benzoatilyticus* underwent several passages under the sterile laboratory conditions and thus prone to metabolic or genomic adaptation as passaging effect.

Glucose is well reported to cause DNA base instability and modifications (Lindahl, 1993). Here, we hypothesized that glucose might have modified the nucleotide bases of *Rbx. benzoatilyticus* also. To test this hypothesis, we isolated and sequenced gDNA from late stationary phase malate and glucose grown *Rbx. benzoatilyticus* cells (respectively called as mal-genome and glc-genome). To rule out the possibility of passaging effect and to study the genotypic effect, genomic information obtained from mal-genome and glc-genome was compared with those from gDNA sequenced 10 years back. For the same reason, the mother culture for the isolation of both the DNA samples (mal-genome and glc-genome) was kept same.

Our data showed that both the genomes contain single rRNA gene cluster, 46 tRNAs, 3 non-coding RNAs and 3 CRISPR arrays (Table 3.5). The genome average nucleotide

identity (ANI) score and digital DNA–DNA hybridization (dDDH) values between mal-genome and glc-genome were 99.99 and 100 %, respectively. This was as expected since both the genomes were isolated from same strain, but grown on two different carbon sources. As anticipated, comparative genome map also revealed that majority of proteins from the two genomes shared 100% identity while only a few shared 97-99% similarity (Fig. 3.47).

Our nucleotide variation analyses revealed dissimilarities at 57 loci in both the genomes (Table S3). Since, they were observed in both the genomes, we presumed them to be generated as a result of passaging effect rather than glycemic effect. Further, we searched for the nucleotide variations confined only to glc-genome and considered them to be the consequence of glycemic effect (Table S3). These variations, comprising of indels, were mostly in the intergenic regions and only a few were in the CDS that have perhaps resulted in truncated or elongated gene (Table 3.10). Also, several transposases observed scattered across the genome (Fig. 3.48) which probably resulted in the shuffling and reverse orientation of the genes, as observed in Mauve alignment (Fig. 3.46; Table 3.6).

Our omics analyses unravelled hampered photosynthetic machinery of glucose grown *Rbx. benzoatilyticus* cells thus we were interested to examine the effect of glucose on photosynthetic gene cluster (PGC) at genetic level. To achieve this, we extracted and compared the PGC from the two genomes. PGC of *Rbx. benzoatilyticus* encompasses 35 genes (Fig. 3.50). The entire genes of the PGC were oriented reverse in the two genomes. Also, two genes from the entire cluster ‘spheroidene monooxygenase (EC 1.14.15.9)’ and ‘chlorophyll *a* synthase (ChlG; EC 2.5.1.62)’ were truncated in glc-genome (Fig. 3.50). Apart from this, there wasn’t any difference in the PGC. But since, we observed down-regulation of most of the proteins related to LHC, pigment biosynthesis and photosynthesis in our iTRAQ analysis, we speculate that several of the PGC genes exhibited epigenetic changes.

4.9. Comparative study between the hyperglycemic effect of microorganism and macroorganism

For the first time, we tried to compare the hyperglycemic effect that we observed with reference to *Rbx. benzoatilyticus* and those reported from other microorganisms with that of eukaryotic system. Figure 4.2 illustrates commonalities and differences between prokaryotic and eukaryotic hyperglycemia. In our analysis, we observed that the findings of hyperglycemic effect on microorganisms are quite comparable with those of macroorganisms as discussed below.

a) Foremost, we observed photo-bleaching of cells on longer phototrophic incubations of glucose, resulting in loss of pigmentation and photosynthesis. Similar inhibition of photosynthesis, in presence of high glucose, is also reported from red algae and higher plants (Koch, 1996; Graverholt and Eriksen, 2007; Oesterhelt et al., 2007).

b) Our study has also shown impaired oxidative phosphorylation as glycemic effect. Similar to this, reports from cell lines suggests mitochondrial dysfunctioning as an effect of hyperglycemia which results in the accumulation of reactive oxygen species (ROS). ROS in turn, is reported to affect the genetic material by generating single nucleotide polymorphism (SNP) and finally resulting in apoptosis/autophagy. Such mechanisms are not yet reported from prokaryotic system and need to be explored.

c) Cells combat to the changing milieu by modulating their membrane. In agreement to this, our results have shown a decrease in unsaturated fatty acid (UFA) and an increase in the saturated fatty acid (SFA) content as membrane adaptation. Similar to this, conversion of UFA to SFA and an increase in the SFA:UFA ratio is also reported from erythrocyte membrane (Bakan et al., 2006).

d) Our biochemical and proteome analysis showed that glucose is catabolised to pyruvate which is converted to acetate. Excess of acetate ion is toxic to the cells (Wolfe,

2005) and is thus excreted out. In the muscle cells of diabetic patients, under hypoxic conditions, pyruvate is converted to lactate which is also excreted out (Schurr, 2017).

e) During hyperglycemia, hexokinase that has high affinity for glucose becomes saturated thus excess glucose is sequestered through Aldose Reductase pathway resulting in reduction of glucose to sorbitol and the accumulation of sorbitol (Pasupulati et al., 2019). In contrast to this, we observed pyruvate flux to acetate and acetyl CoA which is channelized to the accumulation of PHA granules in glucose grown *Rbx. benzoatilyticus* cells (Fig. 4.1).

f) Under normal conditions, glucose is converted to glucose-6-phosphate immediately after it is taken up by the cell. But, during "diabetic" settings, glucose-6-phosphate gets dephosphorylated to glucose and returns to the circulation thus creating hyperglycemic condition (Pasupulati et al., 2019). As a result, glucose is not available to the cell to be used as an energy source. Cells in turn, adapt to use Acetyl-CoA derived from burning of accumulated fats which in turn contributes to the loss in weight. In the same way, our analyses revealed up-regulation of proteins related to lipid catabolism and β-oxidation of fatty acids suggesting that glucose grown *Rbx. benzoatilyticus* cells are deriving energy by catabolising endogenous phospholipids and perhaps resulted in the reduction of cellular size.

g) In diabetic patients, inadequate insulin avoids the body from receiving blood glucose into the cells for use as energy. As a consequence, the body onsets burning muscle and stored fat for energy, which causes loss in the overall body weight. In agreement with this, present study also revealed siphoning of pigments and size of *Rbx. benzoatilyticus* cells. This raises a question 'Is *Rbx. benzoatilyticus* diabetic?' as the Greek word 'diabetes' means 'siphoning'.

In nut shell, our data demonstrated that high glucose levels not only affected the photosynthetic gadgetry of *Rbx. benzoatilyticus* but also rewired the entire metabolism and the expression of several genes. Nevertheless, variation was not detected at the genetic level. Thus, we presume that several of these genes exhibited epigenetic changes.

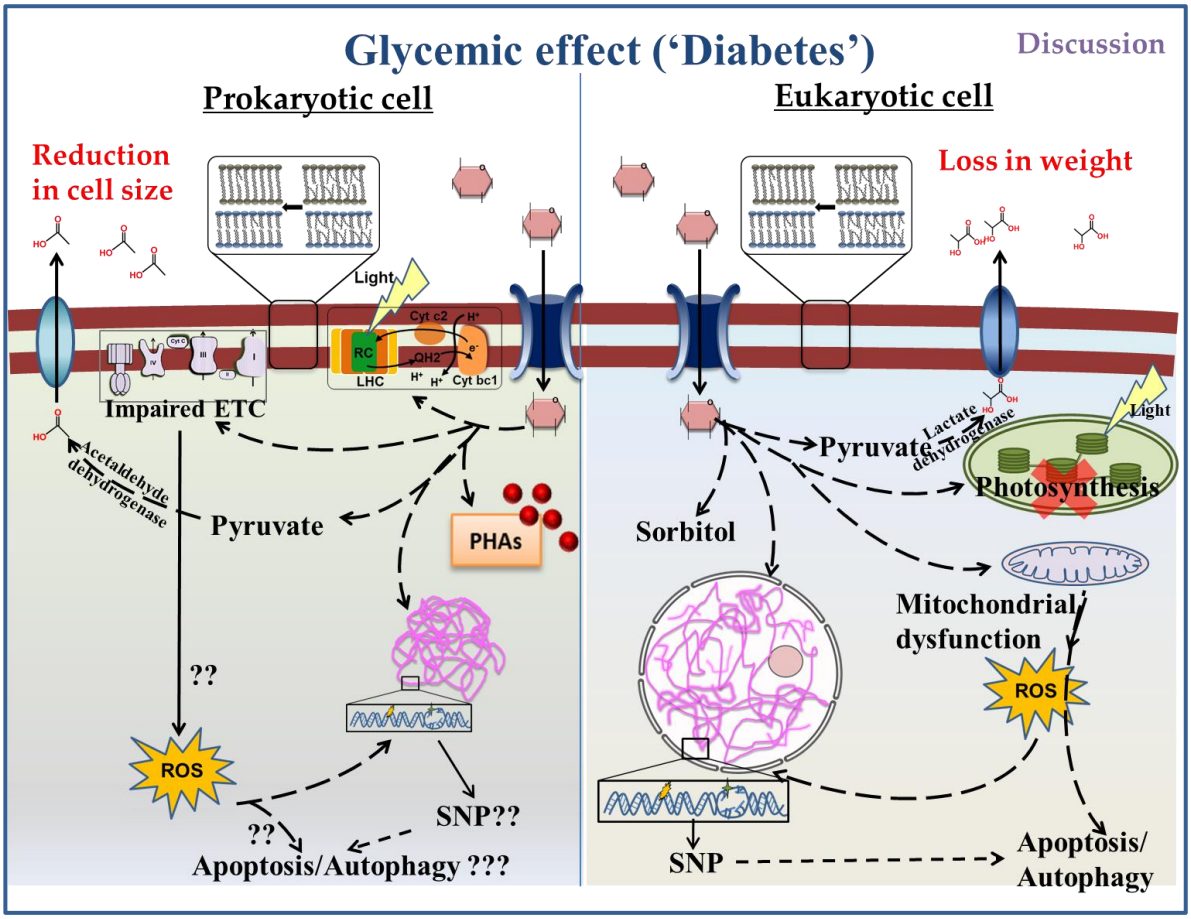

Fig. 4. 2: Commonalities and differences between prokaryotic and eukaryotic hyperglycemia

Model depicting resemblance and variation of prokaryotic hyperglycemia from eukaryotic hyperglycemia.

Based on the findings of present study and knowledge gained from literature review, an attempt is made to understand the toxic effect of glucose on bacteria/ glucose intolerance in bacteria which is quite comparable with 'diabetes' of eukaryotic system. Dotted line(s) and '?' represent multistep and not yet known pathway(s) respectively. PHA, polyhydroxyalkanoate; ROS, reactive oxygen species; SNP, single nucleotide polymorphism.

Quick glance…

Quick glance

Summary of objective I:

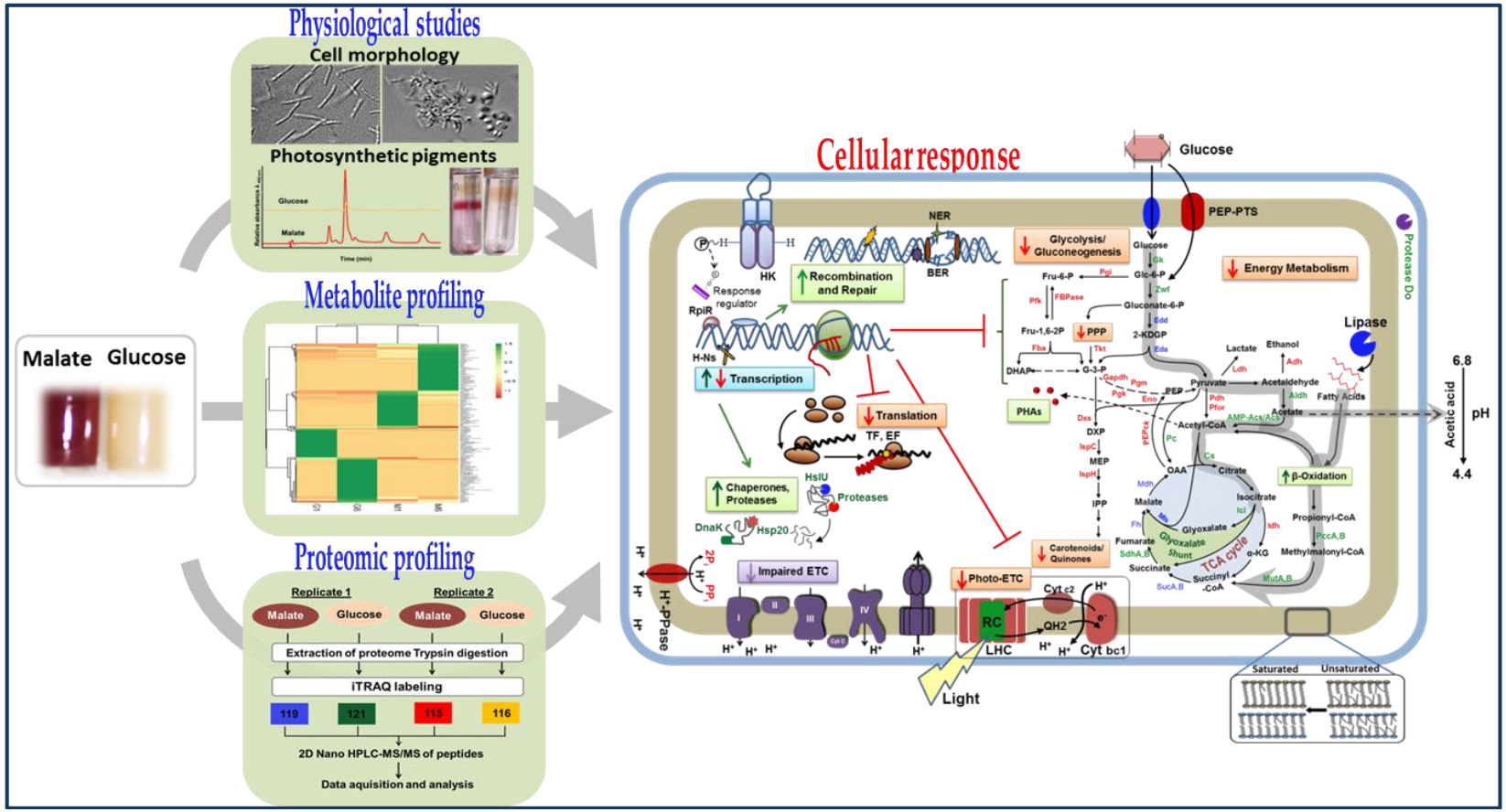

Fig. 5. 1: Graphical representation summarizing objective I of the present study

Graphical summary of objective I based on the observations of the present study illuminating the metabolic adaptations of Rbx. benzoatilyticus as a consequence of hyperglycemic effect. Data taken from Gupta et al. (2019)

Summary of objective II:

Loss in spirilloxanthin and not spheroidene correlated with the loss in bacteriocholrophyll *a.*
Longer incubations on glucose in batch culture contributes to the non-cultivable state rather than glucose *per se* as unfavourable substrate.
Change in life style might be a key player.
Protein dynamics suggests proteins related to primary metabolism down-regulated prior to those of secondary metabolism.

Major findings

The major findings of this study are as listed below:

- Glucose is not the preferred substrate for photometabolism by some of the APB.
- "Life style" and nature of the microorganism does affect its metabolic state.
- Longer incubations on glucose in batch culture contributes to the non-cultivable state rather than glucose *per se* as an unfavourable substrate for *Rbx. benzoatilyticus*.
- Metabolic adaptation
    - Our results suggest an extensive remodelling of metabolic and molecular functions during photometabolism of glucose by *Rbx. benzoatilyticus*.
- Loss in spirilloxanthin and not spheroidene correlated with the loss in bacteriocholrophyll *a* for *Rbx. benzoatilyticus.*
- Coping with changing milieu
    - Though, the organism rewired its biological process to cope with the changing milieu but not to an extent to which it can resuscitate.
- Change in life style might be a key player.
- Protein dynamics suggests proteins related to primary metabolism of *Rbx. benzoatilyticus* down-regulated prior to those of secondary metabolism.
- Studies of glucose toxicity on microorganisms need due attention.
- The study concludes with an open question: Are microorganisms also diabetic?

Supplementary data

Supplementary data

Table S 1: iTRAQ identified proteins from glucose grown cells of *Rbx. benzoatilyticus* compared with those from malate grown cells.

Gene ORF (locus)	Accession number	Protein name*	Number of unique peptides	Unused Prot score	Percent sequence coverage (% Cov)	log_2 (FC)#	SD
Glycolysis & a few downstream pathways							
RBXJA2T_06270	gi|332108687	Fructose-1,6-bisphosphate aldolase	119	55.32	94.92	-1.697	0.24
RBXJA2T_02647	gi|332107970	Glyceraldehyde-3-phosphate dehydrogenase	75	46.82	72.81	-1.081	0.198
RBXJA2T_18668	gi|332112580	Fructose-1,6-bisphosphate aldolase	9	9.94	45.7	-0.997	0.045
RBXJA2T_18688	gi|332112584	Fructose-1,6-bisphosphatase class 1 2	21	19.85	40.66	-1.088	0.065
RBXJA2T_04248	gi|332108287	Zn-dependent alcohol dehydrogenase	284	76.35	96.71	-0.89	0.078
RBXJA2T_10514	gi|332110123	Phosphoenolpyruvate carboxylase	44	62.69	51.75	-0.923	0.015
RBXJA2T_18683	gi|332112583	Phosphoribulokinase	21	16.11	48.98	-0.931	0.041
RBXJA2T_11031	gi|332110531	Aldose 1-epimerase	11	13.47	35.69	-0.453	0.248
RBXJA2T_05268	gi|332108491	Phosphoenolpyruvate carboxykinase	79	59.59	66.72	-0.797	0.128
RBXJA2T_04953	gi|332108428	Pyruvate flavodoxin/ferredoxin oxidoreductase domain protein	50	70.05	36.87	-0.436	0.128
RBXJA2T_12207	gi|332110911	Zinc-binding alcohol dehydrogenase	19	26.29	70.61	-0.406	0.146
RBXJA2T_12387	gi|332111092	Enolase	89	56.72	84.07	-0.399	0.107
RBXJA2T_08560	*gi|332109441*	*L-Lactate dehydrogenase*	18	20.23	58.09	-0.272	0.032
RBXJA2T_16767	gi|332112017	6-Phosphofructokinase	31	30.08	59.6	-0.288	0.119
RBXJA2T_04798	gi|332108397	Pyruvate dehydrogenase subunit E1	115	100.24	69.11	-0.26	0.036
RBXJA2T_06250	gi|332108683	Phosphoglycerate kinase	50	38.68	70.03	-0.2	0.197
RBXJA2T_00150	*gi|332107479*	*Phosphoglycerate mutase 1 family protein*	26	21.38	60.89	-0.195	0.125
RBXJA2T_05903	gi|332108616	Acetyl-coenzyme A synthetase	68	54.34	56.36	0.208	0.073
RBXJA2T_18086	gi|332112464	Phosphoenolpyruvate synthase	16	21.06	32.38	-0.172	0.037
RBXJA2T_17067	*gi|332112078*	*Pyruvate carboxylase*	56	75.78	53.27	0.172	0.057

RBXJA2T_12252	gi|332110920	Hydroxyacylglutathione hydrolase	4	6.12	36.33	0.54	0.036
RBXJA2T_11241	gi|332110573	2-Oxoacid dehydrogenase subunit E1	14	19.79	28.24	0.609	0.011
HMP/ ED pathway							
RBXJA2T_14891	gi|332111640	2-Dehydro-3-deoxyphosphogluconate aldolase/4-Hydroxy-2-oxoglutarate aldolase	21	18.22	66.67	-0.746	0.13
RBXJA2T_18678	gi|332112582	Transketolase	38	34.37	60.87	-0.769	0.036
RBXJA2T_14896	*gi|332111641*	*Phosphogluconate dehydratase*	25	26.07	59.6	-0.076	0.058
RBXJA2T_07368	gi|332109206	Glucokinase	14	20.96	51.92	0.645	0.41
RBXJA2T_00995	gi|332107644	Glucose-6-phosphate 1-dehydrogenase	17	23.9	45.53	0.663	0.053
RBXJA2T_07373	gi|332109207	Bifunctional glucokinase/RpiR family transcriptional regulator	20	24.44	30.19	1.097	0.09
TCA/ Glyoxylate pathway							
RBXJA2T_01525	gi|332107750	Aconitase	37	49.56	50.55	-0.777	0.025
RBXJA2T_10419	gi|332110104	Isocitrate dehydrogenase	68	53.26	69.14	-0.52	0.142
RBXJA2T_18328	gi|332112512	Succinate semialdehyde dehydrogenase	37	36.7	67.07	-0.655	0.055
RBXJA2T_09879	*gi|332109996*	*Succinyl-CoA synthetase subunit beta*	40	36.2	65.54	-0.54	0.119
RBXJA2T_07858	gi|332109304	Tartrate dehydrogenase	17	26.73	54.6	-0.522	0.117
RBXJA2T_05893	*gi|332108614*	*Tartrate/fumarate subfamily Fe-S type hydro-lyase subunit alpha*	35	35.87	59.84	0.115	0.045
RBXJA2T_09929	*gi|332110006*	*Malate dehydrogenase*	100	50.95	87.8	0.21	0.084
RBXJA2T_00704	*gi|332107587*	*Malate synthase G*	12	18.19	26.06	0.16	0.005
RBXJA2T_08565	gi|332109442	Isocitrate lyase	25	28.23	49.65	0.285	0.01
RBXJA2T_09894	gi|332109999	Type II citrate synthase	79	39.83	64.91	0.436	0.014
RBXJA2T_02986	gi|332108037	Bifunctional isocitrate dehydrogenase kinase/phosphatase protein	10	10.99	31.49	0.466	0.124
RBXJA2T_09904	gi|332110001	Succinate dehydrogenase subunit B	14	13.88	38.46	0.521	0.048
Electron Transport Chain							
RBXJA2T_11046	gi|332110534	Cytochrome c prime	29	15.33	72.3	-1.45	0.559
RBXJA2T_06965	gi|332109127	Ubiquinol-cytochrome c reductase, iron-sulfur subunit	11	13.15	32.83	-1.947	0.194

RBXJA2T_06975	gi|332109129	Cytochrome c1	15	13.97	41.02	-1.743	0.14
RBXJA2T_18799	gi|332112605	Class I cytochrome c	10	11.38	52.87	-1.203	0.117
RBXJA2T_04488	gi|332108335	Cytochrome c	12	15.31	46.8	-1.207	0.165
RBXJA2T_19086	gi|332112662	Electron transfer flavoprotein alpha/beta-subunit	61	33.41	81.93	-0.704	0.237
RBXJA2T_19081	gi|332112661	Electron transfer flavoprotein subunit alpha	42	23.59	73.23	-0.668	0.195
RBXJA2T_04988	gi|332108435	Oxidoreductase FAD/NAD(P)-binding domain protein	10	8.75	54.04	-0.617	0.113
RBXJA2T_16662	gi|332111996	Alcohol dehydrogenase	16	19.93	47.4	-0.676	0.025
RBXJA2T_10384	gi|332110097	Cytochrome c oxidase, cbb3-type subunit III	14	18.33	57.89	-0.791	0.127
RBXJA2T_02427	gi|332107926	Periplasmic protein thiol	8	13.81	55.17	-0.533	0.161
RBXJA2T_19019	gi|332112649	FAD linked oxidase	12	17.14	52.75	-0.552	0.198
RBXJA2T_17454	gi|332112155	Putative iron sulfur binding protein	24	24.98	63.84	-0.415	0.084
RBXJA2T_00055	gi|332107460	UbiH/UbiF/VisC/COQ6 family ubiquinone biosynthesis hydroxylase	8	11.33	38.95	-0.424	0.019
RBXJA2T_16907	gi|332112046	F0F1 ATP synthase subunit beta	194	63.59	87.55	-0.33	0.056
RBXJA2T_12697	gi|332111154	Putative NADH dehydrogenase I (chain E) oxidoreductase protein	9	7.62	47.83	-0.295	0.035
RBXJA2T_17322	gi|332112129	4Fe-4S ferredoxin iron-sulfur-binding domain-containing protein	11	11.87	55.14	0.18	0.449
RBXJA2T_16347	gi|332111932	Pyrrolo-quinoline quinone	22	31.16	29.89	0.309	0.008
RBXJA2T_12717	gi|332111158	NADH dehydrogenase subunit I	5	7.07	28.48	0.515	0.286
RBXJA2T_09909	gi|332110002	Succinate dehydrogenase subunit A	39	38.35	57.96	0.357	0.028
RBXJA2T_12682	gi|332111151	NADH dehydrogenase subunit B	5	3.39	26.58	0.509	0.141
RBXJA2T_19256	gi|332112696	Membrane-bound proton-translocating pyrophosphatase	20	20.38	25.66	1.006	0.037
RBXJA2T_12607	gi|332111136	FeS cluster assembly scaffold iscu	9	10.42	58.21	1.322	0.134
Terpenoid/ Pigments/ Photosynthesis							
RBXJA2T_18708	gi|332112588	Ribulose bisophosphate carboxylase	61	49.76	62.07	-1.608	0.09
RBXJA2T_18703	gi|332112587	Ribulose-bisphosphate carboxylase	20	17.16	52.78	-1.659	0.096

RBXJA2T_09552	gi|332109933	Magnesium chelatase subunit H	14	16.11	20.31	-1.111	0.272
RBXJA2T_18493	gi|332112545	4-Hydroxy-3-methylbut-2-enyl diphosphate reductase	14	18.28	50.77	-0.975	0.125
RBXJA2T_04628	gi|332108363	Magnesium-protoporphyrin IX monomethyl ester anaerobic oxidative cyclase	68	80.01	74.23	-0.865	0.166
RBXJA2T_09482	gi|332109919	Photosynthetic reaction center cytochrome c subunit	140	37.93	56.66	-1.173	0.171
RBXJA2T_09402	gi|332109903	Oxygen-independent coproporphyrinogen III oxidase	14	22.3	45.78	-0.612	0.019
RBXJA2T_09437	gi|332109910	2-Desacetyl-2-hydroxyethyl bacteriochlorophyllide A dehydrogenase, putative	57	33.31	82.87	-0.586	0.035
RBXJA2T_09487	gi|332109920	Spheroidene monooxygenase	9	11.77	52.81	-0.448	0.044
RBXJA2T_09532	gi|332109929	Photosynthetic reaction center subunit H	137	48.5	77.87	-0.356	0.059
RBXJA2T_12137	gi|332110897	Glutamate-1-semialdehyde aminotransferase	35	26.17	51.16	-0.504	0.145
RBXJA2T_00590	gi|332107567	Deoxyxylulose-5-phosphate synthase	22	29.04	39.17	-0.614	0.026
RBXJA2T_16937	gi|332112052	Uroporphyrinogen decarboxylase	42	26.82	56.99	-0.546	0.059
RBXJA2T_16272	gi|332111917	Delta-aminolevulinic acid dehydratase	29	20.9	55.48	-0.606	0.123
RBXJA2T_17569	gi|332112178	Uroporphyrin-III C-methyltransferase	12	23.22	61.94	-0.464	0.011
RBXJA2T_09447	gi|332109912	Chlorophyllide reductase subunit Y	16	21.26	38.43	-0.296	0.05
RBXJA2T_17559	*gi|332112176*	*Porphobilinogen deaminase*	27	31.86	72.82	-0.32	0.057
RBXJA2T_17916	gi|332112430	4-Hydroxy-3-methylbut-2-en-1-yl diphosphate synthase	35	35.73	80.47	0.421	0.07
RBXJA2T_10409	gi|332110102	Coproporphyrinogen III oxidase	29	26.66	46.21	0.647	0.027
Lipids & fatty acid metabolism							
RBXJA2T_18989	gi|332112643	Glycerol kinase	10	14.55	32.42	-0.843	0.001
RBXJA2T_15423	gi|332111746	Diacylglycerol O-acyltransferase	7	8.02	24.84	-0.587	0.151
RBXJA2T_04088	gi|332108255	Basic membrane lipoprotein	99	43.66	67.27	-0.908	0.021
RBXJA2T_14881	gi|332111638	Short-chain dehydrogenase/reductase sdr	19	28.52	70.23	-0.498	0.049
RBXJA2T_12577	*gi|332111130*	*Polyhydroxyalkanoate depolymerase, intracellular*	22	18.89	44.66	-0.174	0.334

RBXJA2T_13294	*gi|332111321*	*Putative long-chain-fatty-acid--CoA ligase protein*	69	57.39	57.12	0.216	0.02
RBXJA2T_02991	*gi|332108038*	*Acetyl-CoA acetyltransferase*	35	24.09	59.69	0.444	0.143
RBXJA2T_10314	gi|332110083	Short-chain dehydrogenase/reductase sdr	23	22.64	84.13	0.442	0.11
RBXJA2T_03391	gi|332108116	Propionyl-CoA carboxylase subunit alpha	47	56.55	64.5	0.543	0.058
RBXJA2T_07115	gi|332109157	Phospholipase D/Transphosphatidylase protein	7	9.16	39.29	0.489	0.014
RBXJA2T_03031	gi|332108046	Enoyl-CoA hydratase/isomerase	6	4.62	41.38	0.472	0.073
RBXJA2T_03021	gi|332108044	Propionyl-CoA carboxylase	12	16.62	36.19	0.649	0.116
RBXJA2T_03603	gi|332108158	Putative phospholipase A1 (PldA)	5	8.02	31.17	0.656	0.018
RBXJA2T_09869	gi|332109994	Methylmalonyl-CoA mutase	32	41.34	41.91	0.893	0.017
RBXJA2T_17162	gi|332112097	AMP-dependent synthetase and ligase	12	16.18	26.85	0.789	0.078
RBXJA2T_18889	*gi|332112623*	*Lysophospholipid transporter LplT*	3	0.28	11.75	*1.254*	*0.186*
RBXJA2T_01010	gi|332107647	Toluene tolerance	30	19.2	70.39	1.947	0.012
Amino acid metabolism							
RBXJA2T_12902	gi|332111195	Glycine cleavage system T protein	38	36	68.34	-1.707	0.065
RBXJA2T_19181	gi|332112681	2-Isopropylmalate synthase	55	42.95	72.12	-1.312	0.082
RBXJA2T_03436	gi|332108125	Aspartate-semialdehyde dehydrogenase	119	61.8	87.77	-1.123	0.042
RBXJA2T_05073	gi|332108452	Phospho-2-dehydro-3-deoxyheptonate aldolase	14	22.08	37.53	-1.185	0.077
RBXJA2T_12892	gi|332111193	Glycine dehydrogenase	38	42.69	41.95	-0.822	0.081
RBXJA2T_08800	gi|332109489	Threonyl-tRNA synthetase	27	43.78	45.83	-0.735	0.055
RBXJA2T_01035	gi|332107652	Glutamate synthase subunit beta	44	45.92	62.7	-0.716	0.004
RBXJA2T_01040	gi|332107653	Glutamate synthase (NADH) large subunit	117	118.27	52.47	-0.696	0.026
RBXJA2T_01470	gi|332107739	Urocanate hydratase	437	120.74	90.59	-0.487	0.088
RBXJA2T_10991	gi|332110523	Serine hydroxymethyltransferase	34	34.81	58.41	-0.415	0.203
RBXJA2T_16512	gi|332111966	Prephenate dehydrogenase	8	8.73	33.79	-0.274	0.099
RBXJA2T_15133	gi|332111688	L-Asparaginase II	13	13.8	45.56	-0.526	0.311
RBXJA2T_01055	gi|332107656	3-Dehydroquinate synthase	10	15.18	41.05	0.218	0.043

RBXJA2T_08775	gi|332109484	Phenylalanyl-tRNA synthetase subunit beta	47	54.88	56.1	0.204	0.02
RBXJA2T_01485	gi|332107742	Imidazolonepropionase	57	44.37	61.5	0.478	0.062
RBXJA2T_08225	gi|332109374	Maleylacetoacetate isomerase	6	10.54	36.97	0.499	0.096
RBXJA2T_10821	gi|332110489	Kynureninase	14	16.27	52.03	0.462	0.161
RBXJA2T_08780	gi|332109485	Phenylalanyl-tRNA synthetase subunit alpha	18	21.93	49.86	0.355	0.229
RBXJA2T_19196	gi|332112684	Acetolactate synthase 3 regulatory subunit	17	18.57	69.94	0.494	0.045
RBXJA2T_11061	gi|332110537	Valine-pyruvate aminotransferase	19	22.56	55.78	0.709	0.13
Storage							
RBXJA2T_03723	gi|332108182	Glucose-1-phosphate adenylyltransferase	43	37.81	57.48	-0.939	0.048
RBXJA2T_17402	gi|332112145	Aalpha,alpha-trehalose-phosphate synthase	20	28.48	36.67	-0.946	0.044
RBXJA2T_05783	gi|332108592	Trehalose synthase	11	18.09	25.81	-0.802	0.141
RBXJA2T_07353	gi|332109203	Alpha amylase catalytic region	10	14.49	27.58	-0.583	0.009
RBXJA2T_03718	gi|332108181	ADP-glucose type glycogen/starch synthase	15	24.58	43.38	-0.456	0.032
RBXJA2T_17397	gi|332112144	Trehalose-phosphatase	9	14.67	51.17	-0.587	0.06
RBXJA2T_09287	gi|332109881	UTP-glucose-1-phosphate uridylyltransferase	23	23.98	54.17	-0.305	0.032
RBXJA2T_05763	gi|332108588	UDP-N-acetyl-D-galactosamine dehydrogenase	14	22.4	41.78	0.386	0.004
RBXJA2T_03733	gi|332108184	1,4-Alpha-glucan branching protein	14	22.51	30.71	0.663	0.168
RBXJA2T_03728	gi|332108183	Glycogen/starch/alpha-glucan phosphorylase	80	70.09	59.9	0.847	0.166
RBXJA2T_07838	gi|332109300	Cyanophycin synthetase	46	53.59	50.07	1.495	0.017
RBXJA2T_07833	gi|332109299	Cyanophycin synthetase	66	77.74	62.14	1.949	0.054
Nucleotide/ Cofactor/ Vitamin metabolism							
RBXJA2T_00065	gi|332107462	Thiamine-phosphate pyrophosphorylase	10	11.53	43.44	-0.961	0.13
RBXJA2T_00070	gi|332107463	Hydroxyethylthiazole kinase	34	12.32	39.13	-1.189	0.083
RBXJA2T_02532	gi|332107947	Cobalamin biosynthesis protein CobW	11	14.29	37.64	-0.486	0.022
RBXJA2T_12132	gi|332110896	Hydroxymethylpyrimidine kinase	8	12.01	45.76	-0.777	0.014
RBXJA2T_11787	gi|332110827	3-methyl-2-oxobutanoate hydroxymethyltransferase	10	15.1	50.35	-0.485	0.046
RBXJA2T_00060	gi|332107461	Phosphomethylpyrimidine kinase	24	26.05	71.43	-0.584	0.051

RBXJA2T_09062	gi|332109836	Alkaline phosphatase	80	39.73	58.55	-0.26	0.041
RBXJA2T_11763	gi|332110823	Putative biotin carboxylase protein	21	25.74	53.23	-0.238	0.033
RBXJA2T_10304	gi|332110081	Vitamin B12 transporter btuB precursor, putative	631	179.84	92.47	0.295	0.113
RBXJA2T_00550	gi|332107559	Coenzyme A synthetase-like protein	12	20.62	42.44	0.369	0.086
RBXJA2T_18603	gi|332112567	Thiamine biosynthesis protein ThiC	45	50.17	59.43	0.455	0.032
RBXJA2T_04183	gi|332108274	NMT1/THI5-like domain-containing protein	19	27.3	69.16	0.659	0.024
RBXJA2T_00595	gi|332107568	GTP cyclohydrolase	5	4.96	31.2	0.539	0.026
Secondary metabolites							
RBXJA2T_01090	gi|332107663	1A Family penicillin-binding protein	22	34.88	44.77	-0.898	0.062
RBXJA2T_16822	gi|332112028	Glutamate--cysteine ligase	9	14.01	22.9	-0.54	0.061
RBXJA2T_10841	gi|332110493	Metallo-beta-lactamase family protein	17	21.81	45.23	-0.46	0.104
RBXJA2T_15348	gi|332111731	Indolepyruvate ferredoxin oxidoreductase	15	26.54	26.17	-0.68	0.464
RBXJA2T_07723	gi|332109277	CRISPR-associated Csd2 family protein	45	36.71	76.57	0.234	0.038
Replication							
RBXJA2T_06275	gi|332108688	Phosphoribosylaminoimidazole-succinocarboxamide synthase	50	42.8	80.33	-1.02	0.155
RBXJA2T_11733	gi|332110817	Ribonucleotide-diphosphate reductase subunit alpha	20	29.01	36.11	-1.021	0.155
RBXJA2T_08390	gi|332109407	N5-Glutamine S-adenosyl-L-methionine-dependent methyltransferase	4	8.01	26.99	-0.442	0.148
RBXJA2T_07663	gi|332109265	Orotate phosphoribosyltransferase	19	20.14	67.7	-0.36	0.039
RBXJA2T_06285	gi|332108690	Phosphoribosylaminoimidazole carboxylase, catalytic subunit	11	10.01	72.35	-0.425	0.204
RBXJA2T_09347	gi|332109892	DNA-directed DNA polymerase	26	37.81	39.13	-0.365	0.029
RBXJA2T_16527	*gi|332111969*	*DNA gyrase subunit A*	44	52.9	44.07	*-0.151*	*0.009*
RBXJA2T_18233	*gi|332112493*	*DNA topoisomerase IV subunit A*	18	23.78	34.89	*0.164*	*0.053*
RBXJA2T_17791	gi|332112222	S-Adenosyl-L-homocysteine hydrolase	29	40.17	56.9	0.369	0.062
RBXJA2T_00180	gi|332107485	Phosphoribosyltransferase	10	15.41	54.49	0.389	0.046
RBXJA2T_06470	gi|332108727	Putative ATP-dependent RNA helicase 2	22	35.52	48.86	0.309	0.157

RBXJA2T_04543	gi|332108346	DNA polymerase III subunit epsilon	6	12.78	34.42	0.456	0.067
RBXJA2T_17272	gi|332112119	Ribonucleoside-diphosphate reductase, adenosylcobalamin-dependent	22	33.6	38.45	0.778	0.04
Recombination & Repair							
RBXJA2T_13534	gi|332111369	RecA protein	57	40.78	72.7	-0.281	0.21
RBXJA2T_16317	*gi|332111926*	*Holliday junction DNA helicase RuvB*	9	14.04	40.4	*0.373*	*0.239*
RBXJA2T_18874	gi|332112620	DNA repair protein RadA	4	4.97	20	0.472	0.226
RBXJA2T_10469	gi|332110114	HhH-GPD family protein	4	8.04	34.4	0.371	0.026
RBXJA2T_03364	gi|332108111	Transcription-repair coupling factor	21	26.17	28.56	0.581	0.204
Recombination & Repair							
RBXJA2T_19656	gi|332112774	Ribonuclease activity regulator protein RraA	13	18.01	72.39	-0.747	0.004
RBXJA2T_19296	gi|332112704	NusA antitermination factor	46	45.9	51.22	-0.381	0.091
RBXJA2T_02812	gi|332108003	Ferric uptake regulator family protein	16	10.11	58.04	-0.482	0.013
RBXJA2T_03267	gi|332108092	DNA-directed RNA polymerase subunit beta'	171	167.31	72.6	0.246	0.023
RBXJA2T_17981	gi|332112443	Ribonuclease R	20	28.59	35.18	0.341	0.007
RBXJA2T_12657	gi|332111146	Polynucleotide phosphorylase/polyadenylase	85	73.18	59.56	0.275	0.021
RBXJA2T_01345	gi|332107714	HTH-type transcriptional regulator	4	5.39	39.2	0.387	0.062
RBXJA2T_01165	gi|332107678	Transmembrane sensor histidine kinase transcription regulator protein	10	16.1	34.16	0.412	0.162
RBXJA2T_10736	gi|332110472	Poly(A) polymerase	27	28.21	43.11	0.446	0.066
RBXJA2T_11703	gi|332110811	Signal recognition particle protein	24	27.23	50.91	0.662	0.077
RBXJA2T_07978	gi|332109326	Ribonuclease E	41	48.69	54.66	0.654	0.128
Translation							
RBXJA2T_03242	gi|332108087	Elongation factor Tu	237	90.51	90.38	-0.607	0.043
RBXJA2T_03247	gi|332108088	Elongation factor G	161	88.76	82.74	-0.438	0.117
RBXJA2T_18006	gi|332112448	Elongation factor Ts	66	44.18	74.51	-0.258	0.174
RBXJA2T_16502	gi|332111964	30S Ribosomal protein S1	87	61.61	56.39	-0.209	0.09
RBXJA2T_02190	*gi|332107881*	*30S Ribosomal protein S8*	25	20.59	82.44	*-0.044*	*0.071*
RBXJA2T_02205	*gi|332107884*	*30S Ribosomal protein S5*	22	23.73	62.21	*0.152*	*0.046*

RBXJA2T_02145	gi|332107872	30S ribosomal protein S3	39	30.57	68.86	0.215	0.09
RBXJA2T_12532	*gi|332111121*	*30S Ribosomal protein S21*	9	8.2	52.86	*0.153*	*0.153*
RBXJA2T_02245	*gi|332107892*	*30S Ribosomal protein S4*	37	36.11	71.98	*0.122*	*0.081*
RBXJA2T_15518	*gi|332111765*	*Peptidyl-tRNA hydrolase*	12	14.96	62.91	*0.266*	*0.055*
RBXJA2T_02130	gi|332107869	50S Ribosomal protein L2	23	18.82	48.91	0.327	0.163
RBXJA2T_02170	gi|332107877	50S Ribosomal protein L14	24	20.23	72.13	0.355	0.133
RBXJA2T_08785	*gi|332109486*	*50S Ribosomal protein L20*	17	16.31	54.24	*0.465*	*0.157*
RBXJA2T_02155	gi|332107874	50S Ribosomal protein L29	9	8.41	72.31	0.474	0.434
RBXJA2T_02150	*gi|332107873*	*50S Ribosomal protein L16*	17	8.05	61.59	*0.493*	*0.061*
Regulatory proteins							
RBXJA2T_19236	gi|332112692	Nitrogen regulatory protein P-II	25	16.18	73.21	-1.214	0.138
RBXJA2T_06980	gi|332109130	Putative transcription modulator protein	35	24.88	71.92	-0.613	0.091
RBXJA2T_01475	gi|332107740	Histidine utilization repressor	27	27.62	64.71	0.214	0.087
RBXJA2T_11196	gi|332110564	Nitrogen regulatory protein P-II	18	11.82	74.11	0.531	0.056
RBXJA2T_13539	gi|332111370	Two component transcriptional regulator	7	7.81	44.39	0.542	0.028
RBXJA2T_04128	gi|332108263	Crp/FNR family transcriptional regulator	22	24	71.31	0.42	0.001
RBXJA2T_15433	gi|332111748	TetR family transcriptional regulator	3	3.05	28.44	0.514	0.023
RBXJA2T_01000	gi|332107645	RpiR family transcriptional regulator	9	17.93	31.66	0.876	0.135
RBXJA2T_09122	gi|332109848	Histone-like nucleoid-structuring protein H-NS	28	14.81	82.41	1.141	0.129
RBXJA2T_18418	gi|332112530	Two component transcriptional regulator	23	26.32	53.42	1.403	0.167
Chaperone/ Chaperonin							
RBXJA2T_07898	gi|332109310	Urease accessory protein UreE	15	19.36	35.86	-1.393	0.185
RBXJA2T_12642	gi|332111143	Putative transporter signal peptide protein	11	8.89	34.81	-1.253	0.09
RBXJA2T_02902	gi|332108021	PpiC-type peptidyl-prolyl cis-trans isomerase	14	16.2	35.78	-1.258	0.057
RBXJA2T_04468	gi|332108331	Co-chaperonin GroES	43	17.08	86.46	-0.825	0.143
RBXJA2T_13444	gi|332111351	Putative signal peptide protein	13	22.22	51.34	-0.887	0.074
RBXJA2T_04473	gi|332108332	Chaperonin GroEL	347	116.39	87.8	-0.406	0.178

RBXJA2T_09377	*gi|332109898*	*Ppx/GppA phosphatase*	15	25.1	47.2	*0.206*	*0.06*
RBXJA2T_18131	gi|332112473	Molecular chaperone DnaK	93	77.73	71.85	0.465	0.108
RBXJA2T_02095	gi|332107862	HSP20 family protein	8	8.02	45.83	1.137	0.054
Protease/ Peptidase							
RBXJA2T_15188	gi|332111699	Carboxyl-terminal protease	21	31.24	54.91	-1.27	0.198
RBXJA2T_10561	gi|332110437	Peptidase U32	16	19.92	41.3	-0.556	0.153
RBXJA2T_14191	gi|332111501	Dienelactone hydrolase family protein	36	51.39	55.21	-0.783	0.075
RBXJA2T_17152	gi|332112095	Putative zinc protease	70	89.58	67.69	-0.494	0.028
RBXJA2T_06855	gi|332109105	Carboxypeptidase Taq	33	35.26	58.47	-0.542	0.058
RBXJA2T_09687	gi|332109960	Membrane protease FtsH catalytic subunit	35	41.48	50.95	-0.347	0.067
RBXJA2T_16247	gi|332111912	Serine-type D-Ala-D-Ala carboxypeptidase	15	16.57	53.81	-0.51	0.046
RBXJA2T_01565	gi|332107758	Peptidyl-dipeptidase Dcp	29	38.53	42.22	-0.384	0.13
RBXJA2T_17956	gi|332112438	Putative serine protease transmembrane protein	33	33.04	69.7	-0.434	0.037
RBXJA2T_01550	gi|332107755	Prolyl oligopeptidase family protein	22	33.42	43.81	-0.452	0.022
RBXJA2T_13014	gi|332111217	Peptidase U32	9	11.12	30.32	0.288	0.142
RBXJA2T_10831	gi|332110491	Peptidase M24	19	25.45	40.23	0.53	0.017
RBXJA2T_10434	gi|332110107	ATP-dependent Clp protease, ATP-binding subunit clpA	36	51.08	50.65	0.502	0.148
RBXJA2T_01770	gi|332107797	ATP-dependent protease ATP-binding subunit HslU	25	34.11	54.67	0.423	0.08
RBXJA2T_16957	gi|332112056	Protease IV	14	16.23	43.71	0.649	0.076
RBXJA2T_03758	gi|332108189	Leucyl aminopeptidase	19	29.41	46.83	1.485	0.028
RBXJA2T_11997	gi|332110869	Protease Do	91	56.32	78.57	2.72	0.007
Stress proteins							
RBXJA2T_14346	gi|332111533	Heat shock protein HtpX	19	10.35	36.24	-1.955	0.101
RBXJA2T_15328	gi|332111727	YceI family protein	6	8.32	46.03	-1.357	0.438
RBXJA2T_05183	gi|332108474	Ferritin Dps family protein	22	18.92	72.46	-0.706	0.61
RBXJA2T_13976	gi|332111458	Universal stress protein	32	28.03	72.88	-0.675	0.043

RBXJA2T_02100	gi|332107863	Heat shock protein Hsp20	6	7.46	76.38	1.386	0.113
RBXJA2T_02105	gi|332107864	Heat shock protein Hsp20	12	12.1	62	1.459	0.069
Membrane transport/ Translocation							
RBXJA2T_03668	gi|332108171	Extracellular ligand-binding receptor	88	53.31	86.32	-3.121	0.48
RBXJA2T_15748	gi|332111811	Extracellular solute-binding protein	80	53.16	84.75	-2.855	0.438
RBXJA2T_11423	gi|332110755	Putative binding-dependent transport protein	24	25.25	37.21	-2.534	0.275
RBXJA2T_00774	gi|332107601	Polar amino acid transporter substrate-binding protein	26	31.08	67.41	-2.039	0.421
RBXJA2T_12832	gi|332111181	Secretion protein HlyD	14	19.03	50.91	-1.527	0.002
RBXJA2T_08295	gi|332109388	Import inner membrane translocase subunit Tim44	22	16.28	50.16	-1.5	0.189
RBXJA2T_07628	gi|332109258	Putative binding protein component of ABC transporter	19	32.01	43.7	-1.437	0.007
RBXJA2T_03873	gi|332108212	Extracellular solute-binding protein	30	23.97	45.97	-1.367	0.225
RBXJA2T_09707	gi|332109964	Putative phosphate-binding periplasmic (pbp) ABC transporter protein	19	25.39	69.65	-1.082	0.422
RBXJA2T_12237	gi|332110917	RND family efflux transporter MFP subunit	15	22.11	48.92	-1.353	0.004
RBXJA2T_07175	gi|332109169	Translocation protein TolB	43	56.16	79.49	-1.151	0.071
RBXJA2T_07035	gi|332109141	Extracellular solute-binding protein family 1	52	34.57	63.39	-1.173	0.201
RBXJA2T_14856	gi|332111633	Biopolymer transport ExbD protein	9	11.29	52.74	-1.061	0.02
RBXJA2T_07608	gi|332109254	ABC type ATPase	23	30.08	54.87	-1.07	0.034
RBXJA2T_01420	gi|332107729	Extracellular solute-binding protein	6	8.81	31.12	-0.926	0.099
RBXJA2T_12232	gi|332110916	Acriflavin resistance protein	18	29.94	37.02	-0.895	0.004
RBXJA2T_07185	gi|332109171	Putative transmembrane protein	32	31.88	73.28	-0.605	0.133
RBXJA2T_07513	gi|332109235	Yidc translocase/secretase	13	15.84	26.45	-0.946	0.024
RBXJA2T_12882	gi|332111191	Extracellular solute-binding protein	46	40.11	63.94	-0.426	0.342
RBXJA2T_08945	gi|332109518	Putative exported isomerase	36	38.55	74.44	-0.806	0.154
RBXJA2T_10951	gi|332110515	ABC transporter permease and ATP-binding protein	6	6.02	20.55	-0.618	0.099
RBXJA2T_18278	gi|332112502	Putative transmembrane protein	30	33.33	60.58	-0.59	0.074

RBXJA2T_06185	gi|332108672	Preprotein translocase subunit SecD	37	38.32	53.79	-0.659	0.075
RBXJA2T_12787	gi|332111172	TRAP dicarboxylate transporter subunit DctP	29	24.64	68.99	-0.811	0.309
RBXJA2T_02817	gi|332108004	Small protein A (tmRNA-binding)-like protein	8	12.02	49.15	-0.608	0.085
RBXJA2T_02362	gi|332107915	Efflux transporter RND family, MFP subunit	22	27.99	59.66	-0.784	0.005
RBXJA2T_06995	gi|332109133	Preprotein translocase subunit SecA	68	74.61	56.24	-0.582	0.083
RBXJA2T_08955	gi|332109520	Putative ABC transporter ATP-binding protein	61	56.04	73.47	-0.544	0.116
RBXJA2T_17312	gi|332112127	TonB-dependent siderophore receptor	71	71.31	62.22	-0.338	0.052
RBXJA2T_12507	gi|332111116	TRAP C4-dicarboxylate transport system permease subunit DctP	34	27.33	53.89	-0.283	0.122
RBXJA2T_16532	gi|332111970	OmpA/MotB domain-containing protein	55	37.72	69.16	0.255	0.198
RBXJA2T_07488	gi|332109230	Surface antigen (D15)	7	7.75	24.49	0.201	0.06
RBXJA2T_18363	gi|332112519	TolC family type I secretion outer membrane protein	40	38.77	69.84	0.245	0.056
RBXJA2T_12407	gi|332111096	TonB-dependent receptor	61	71.34	85.71	0.319	0.016
RBXJA2T_06385	gi|332108710	Filamentous hemagglutinin outer membrane protein	143	130.23	46.15	0.479	0.063
RBXJA2T_04103	gi|332108258	Putative sugar ATP binding ABC transporter protein	11	16.84	42.51	0.464	0.003
RBXJA2T_13149	gi|332111292	Putative transmembrane protein	15	20.23	78.79	0.413	0.004
RBXJA2T_06480	gi|332108729	Polysaccharide export protein	26	29.88	58.96	0.385	0.053
RBXJA2T_17871	gi|332112238	Putative lipoprotein	20	16.46	57.64	0.549	0.019
RBXJA2T_18041	gi|332112455	Outer membrane protein assembly complex, YaeT protein	71	68.09	71.43	0.432	0.109
RBXJA2T_12867	gi|332111188	ABC transporter-like protein	8	6.12	34.39	0.568	0.445
RBXJA2T_06380	gi|332108709	Polypeptide-transport-associated domain-containing protein	77	57.3	73.44	0.591	0.131
RBXJA2T_04738	gi|332108385	TonB-dependent receptor	16	29.92	39.7	0.756	0.078
RBXJA2T_06930	gi|332109120	Sec-independent translocase	6	7.3	30.91	0.716	0.02
RBXJA2T_17077	gi|332112080	General secretion pathway protein D	15	15.31	44.33	0.69	0.13

RBXJA2T_05798	gi|332108595	Putative outer membrane transport protein involved in copper (silver) tolerance (cusC)	27	34.43	54.97	0.624	0.049
RBXJA2T_12352	gi|332111085	Extracellular solute-binding protein	80	39.69	69.82	0.687	0.135
RBXJA2T_15323	gi|332111726	Extracellular solute-binding protein, family 7	51	39.09	74.26	0.476	0.04
RBXJA2T_03319	gi|332108102	TonB-dependent receptor	49	64.6	53.09	1.209	0.03
RBXJA2T_05793	gi|332108594	Type I antifreeze protein:HlyD family secretion protein	24	34.13	67.13	0.67	0.081
RBXJA2T_07943	gi|332109319	Putative outer membrane protein	16	25.28	59.33	0.905	0.031
RBXJA2T_01725	gi|332107788	ABC transporter-like protein	7	8.89	48.71	0.937	0.238
RBXJA2T_07843	gi|332109301	Putative ABC transporter	14	16.92	33.29	1.163	0.009
RBXJA2T_01735	gi|332107790	RND efflux system outer membrane lipoprotein	23	29.76	53.43	1.146	0.097
RBXJA2T_07333	gi|332109199	ABC transporter	14	17.34	41.8	1.131	0.185
RBXJA2T_06010	gi|332108637	Iron transporter	10	4.3	33.52	0.575	0.028
RBXJA2T_07338	gi|332109200	Maltose ABC transporter periplasmic protein	127	67.35	77.58	1.662	0.156
RBXJA2T_03748	gi|332108187	Extracellular ligand-binding receptor	29	26.01	66.84	0.552	0.302
RBXJA2T_01730	gi|332107789	RND family efflux transporter MFP subunit	35	34.63	57.8	1.683	0.014
Quorum sensing & Signal transduction							
RBXJA2T_06820	gi|332109098	Two component LuxR family transcriptional regulator	18	20.02	68.72	-1.01	0.061
RBXJA2T_17439	gi|332112152	Multi-sensor signal transduction histidine kinase	4	2.79	25.8	-1.097	0.103
RBXJA2T_05813	gi|332108598	Two component transcriptional regulator, winged	9	9.58	35.53	-0.661	0.049
RBXJA2T_13419	gi|332111346	PAS/PAC sensor signal transduction histidine kinase	24	31.67	37.05	-0.261	0.062
RBXJA2T_15588	gi|332111779	Two-component hybrid sensor and regulator	29	44.01	34.22	-0.508	0.182
RBXJA2T_13414	gi|332111345	MCP methyltransferase/methylesterase, CheR/CheB with PAS/PAC sensor	29	44.71	36.38	-0.272	0.116
RBXJA2T_02782	gi|332107997	DNA-binding domain-containing protein, excisionase family	8	7.08	32.37	0.221	0.049
RBXJA2T_13604	gi|332111383	Methyl-accepting chemotaxis sensory	8	13.72	33.08	0.663	0.128

		transducer					
RBXJA2T_12107	gi|332110891	Methyl-accepting chemotaxis sensory transducer	48	51.58	66.93	0.367	0.045
RBXJA2T_18538	*gi|332112554*	*Chemotaxis response regulator*	10	9.76	36.46	*0.722*	*0.037*
RBXJA2T_05113	gi|332108460	Twitching motility protein	16	14.87	38.62	0.471	0.077
RBXJA2T_16302	gi|332111923	Two component LuxR family transcriptional regulator	16	19.03	71.03	0.477	0.247
RBXJA2T_02572	gi|332107955	Putative two component response regulator transcription regulator protein	8	7.6	34.2	0.536	0.184
RBXJA2T_11777	gi|332110825	CheW protein	6	8.32	45.95	1.146	0.05
RBXJA2T_13914	gi|332111446	Methyl-accepting chemotaxis sensory transducer	7	8.73	30.12	0.987	0.132
RBXJA2T_18413	gi|332112529	Histidine kinase	17	23.1	52.77	0.969	0.048
Porin/ Pilus/ Cell division							
RBXJA2T_08940	gi|332109517	BolA-like protein	8	10.41	88.51	-0.784	0.421
RBXJA2T_01075	gi|332107660	Fimbrial assembly protein	16	20.28	58.95	-0.902	0.18
RBXJA2T_19141	gi|332112673	Trigger factor	73	52.38	76.38	-0.438	0.045
RBXJA2T_18939	gi|332112633	Gram-negative type outer membrane porin protein	598	132.76	89.19	0.373	0.063
RBXJA2T_12337	gi|332111082	Porin	433	108.82	92.11	0.367	0.009
RBXJA2T_11588	gi|332110788	Type IV-A pilus assembly ATPase PilB	16	20.55	41.36	0.362	0.084
RBXJA2T_04483	gi|332108334	GTP-binding protein YsxC	12	16.91	56.19	0.313	0.038
RBXJA2T_18338	gi|332112514	Gram-negative type outer membrane porin protein	184	76.69	83.15	0.516	0.112
RBXJA2T_01065	gi|332107658	Fimbrial biogenesis protein	56	60.65	55.63	0.944	0.13
RBXJA2T_04083	gi|332108254	Porin	64	30.34	63.29	1.006	0.046
RBXJA2T_07363	gi|332109205	Maltoporin	281	90.33	86.08	2.253	0.188
Miscellaneous							
RBXJA2T_02507	gi|332107942	6-Aminohexanoate-dimer hydrolase	14	20.5	49.76	-1.658	0.087
RBXJA2T_17826	gi|332112229	Lytic transglycosylase, catalytic	29	42.29	62.96	-1.611	0.091

RBXJA2T_00475	gi|332107544	Putative peptidyl-prolyl cis-trans isomerase transmembrane protein	33	45.31	61.57	-1.7	0.069
RBXJA2T_13564	gi|332111375	EvpB	8	11.65	27.68	-1.04	0.094
RBXJA2T_00779	gi|332107602	Glutathione S-transferase domain-containing protein	18	18.11	55.92	-1.311	0.09
RBXJA2T_17836	gi|332112231	Glutathione S-transferase domain-containing protein	11	12.74	35.24	-1.133	0.028
RBXJA2T_17342	gi|332112133	Putative nitrite/sulfite reductase	21	30.16	41.75	-1.076	0.085
RBXJA2T_03126	gi|332108065	Saccharopine dehydrogenase	17	16.53	34.34	-1.349	0.312
RBXJA2T_10459	gi|332110112	Tetratricopeptide repeat family protein	7	11.68	42.17	-1.296	0.01
RBXJA2T_09412	gi|332109905	Molybdopterin oxidoreductase, iron-sulfur binding subunit	5	4.3	20.56	-0.996	0.074
RBXJA2T_03943	gi|332108226	TPR repeat-containing protein	7	14.41	31.46	-0.735	0.028
RBXJA2T_13244	gi|332111311	Thiol:disulfide interchange protein	11	14.93	53.95	-0.753	0.047
RBXJA2T_13204	gi|332111303	3-Oxoacid CoA-transferase subunit B	20	17.75	66.67	-1.19	0.132
RBXJA2T_11907	gi|332110851	Sulfate adenylyltransferase, large subunit	34	42.9	48.11	-0.646	0.038
RBXJA2T_08415	gi|332109412	Acetyl-CoA C-acetyltransferase	70	44.94	85.06	-0.509	0.006
RBXJA2T_18663	gi|332112579	HAD-superfamily hydrolase, subfamily IA, variant 3	14	20.29	70.08	-0.483	0.01
RBXJA2T_13189	gi|332111300	Glutathione S-transferase domain-containing protein	4	2.97	31.7	-0.514	0.25
RBXJA2T_02417	gi|332107924	TPR repeat-containing protein	11	13.15	46.27	-0.629	0.164
RBXJA2T_18693	gi|332112585	AAA type ATPase	5	7.8	29.65	-0.568	0.061
RBXJA2T_19076	gi|332112660	Putative acyl-CoA dehydrogenase oxidoreductase protein	49	46.43	56.35	-0.439	0.026
RBXJA2T_12907	gi|332111196	Putative CoA ligase	16	26.99	48.18	-0.424	0.123
RBXJA2T_16932	gi|332112051	LemA protein	16	18.04	57.5	-0.667	0.228
RBXJA2T_13199	gi|332111302	3-Oxoacid CoA-transferase	20	18.76	54.7	-0.793	0.005
RBXJA2T_10536	gi|332110432	Putative dehydrogenase	19	30.66	43.96	0.164	0.042
RBXJA2T_18358	gi|332112518	Protein-L-isoaspartate(D-aspartate) O-methyltransferase	15	17.69	52.68	0.345	0.054

RBXJA2T_04633	gi|332108364	Basic membrane lipoprotein	22	21.07	50.76	0.544	0.252
RBXJA2T_12602	gi|332111135	Cysteine desulfurase	17	16.64	54.95	0.558	0.054
RBXJA2T_01225	gi|332107690	Diguanylate cyclase	14	22.46	32.84	0.28	0.124
RBXJA2T_12192	gi|332110908	PhoH family protein	21	29.67	56.59	0.277	0.03
RBXJA2T_01095	gi|332107664	Iron donor protein CyaY	13	10.09	72.97	0.665	0.225
RBXJA2T_01220	gi|332107689	Sensory box/Response regulator	13	19.64	39.02	0.483	0.133
RBXJA2T_11698	gi|332110810	Signal recognition particle-docking protein FtsY	17	22.04	51.21	0.343	0.093
RBXJA2T_10571	gi|332110439	Sterol-binding domain-containing protein	9	11.71	75.33	0.57	0.073
RBXJA2T_00664	gi|332107581	Carboxyl transferase	24	22.49	36.4	0.541	0.134
RBXJA2T_09859	gi|332109992	Carboxyl transferase	29	30.83	53.33	0.583	0.019
RBXJA2T_02347	gi|332107912	Esterase/lipase-like protein	11	16	38.91	0.666	0.063
RBXJA2T_03026	gi|332108045	Dinb family protein	4	4.36	29.78	0.862	0.118
RBXJA2T_04028	gi|332108243	PrkA family serine protein kinase	57	66.59	67.66	0.743	0.04
RBXJA2T_17801	gi|332112224	Putative outer membrane signal peptide protein	40	10.85	57	1.387	0.148
RBXJA2T_18613	gi|332112569	Aldehyde dehydrogenase	97	56.98	71.15	1.281	0.137
RBXJA2T_07358	gi|332109204	Pullanase-associated protein	15	10	51.27	1.158	0.295
RBXJA2T_14421	gi|332111548	Iron-sulfur cluster insertion protein ErpA	11	8.37	50	1.34	0.018
Hypothetical							
RBXJA2T_14391	gi|332111542	Hypothetical protein RBXJA2T_14391	74	46.46	82.66	-2.724	0.626
RBXJA2T_16062	gi|332111875	Hypothetical protein RBXJA2T_16062	10	8.86	72.64	-1.686	0.026
RBXJA2T_10499	gi|332110120	Hypothetical protein RBXJA2T_10499	10	14.4	55	-1.325	0.353
RBXJA2T_13559	gi|332111374	Hypothetical protein RBXJA2T_13559	10	13.68	68.6	-1.201	0.244
RBXJA2T_06125	gi|332108660	Hypothetical protein RBXJA2T_06125	5	6.24	33.2	-1.572	0.122
RBXJA2T_16312	gi|332111925	Hypothetical protein RBXJA2T_16312	6	7.23	44.23	-1.251	0.082
RBXJA2T_01560	gi|332107757	Hypothetical protein RBXJA2T_01560	7	8.67	46.67	-1.279	0.484
RBXJA2T_13569	gi|332111376	Hypothetical protein RBXJA2T_13569	37	17.61	77.33	-0.903	0.534
RBXJA2T_17731	gi|332112210	Hypothetical protein RBXJA2T_17731	31	29.51	79.32	-1.51	0.085

RBXJA2T_14606	gi|332111585	Hypothetical protein RBXJA2T_14606	36	25.85	64.17	-1.211	0.097
RBXJA2T_05878	gi|332108611	Hypothetical protein RBXJA2T_05878	9	7.4	52.63	-1	0.2
RBXJA2T_05208	gi|332108479	Hypothetical protein RBXJA2T_05208	10	16.31	41.41	-0.897	0.144
RBXJA2T_05278	gi|332108493	Hypothetical protein RBXJA2T_05278	12	11.8	43.57	-0.989	0.3
RBXJA2T_16522	gi|332111968	Hypothetical protein RBXJA2T_16522	30	19.61	83.58	-0.764	0.285
RBXJA2T_10309	gi|332110082	Hypothetical protein RBXJA2T_10309	4	6.01	55.83	-0.991	0.064
RBXJA2T_09252	gi|332109874	Hypothetical protein RBXJA2T_09252	7	8.2	28.79	-0.9	0.345
RBXJA2T_14866	gi|332111635	Hypothetical protein RBXJA2T_14866	22	29.71	76.13	-0.723	0.156
RBXJA2T_03339	gi|332108106	Hypothetical protein RBXJA2T_03339	22	24.34	66.09	-0.954	0.004
RBXJA2T_17926	gi|332112432	Hypothetical protein RBXJA2T_17926	16	18.11	74.67	-0.965	0.052
RBXJA2T_06450	gi|332108723	Hypothetical protein RBXJA2T_06450	6	10.02	50.82	-0.826	0.073
RBXJA2T_12317	gi|332111078	Hypothetical protein RBXJA2T_12317	31	32.56	68.63	-0.993	0.436
RBXJA2T_04823	gi|332108402	Hypothetical protein RBXJA2T_04823	5	6	33.91	-0.784	0.021
RBXJA2T_17187	gi|332112102	Hypothetical protein RBXJA2T_17187	16	25.36	42.72	-0.666	0.002
RBXJA2T_09522	gi|332109927	Hypothetical protein RBXJA2T_09522	11	12	62.99	-0.875	0.086
RBXJA2T_18323	gi|332112511	Hypothetical protein RBXJA2T_18323	22	18.68	70.95	-0.809	0.115
RBXJA2T_09467	gi|332109916	Hypothetical protein RBXJA2T_09467	20	6.49	66.67	-0.735	0.017
RBXJA2T_01885	gi|332107820	Hypothetical protein RBXJA2T_01885	22	33.19	49.72	-0.324	0.038
RBXJA2T_16782	gi|332112020	Hypothetical protein RBXJA2T_16782	9	10	36.97	-0.629	0.127
RBXJA2T_13159	gi|332111294	Hypothetical protein RBXJA2T_13159	26	31.84	48.79	-0.48	0.113
RBXJA2T_17931	gi|332112433	Hypothetical protein RBXJA2T_17931	27	34.46	64.4	-0.327	0.036
RBXJA2T_06955	gi|332109125	Hypothetical protein RBXJA2T_06955	30	42.31	42.06	-0.348	0.05
RBXJA2T_05308	gi|332108499	Hypothetical protein RBXJA2T_05308	6	6.4	32.78	-0.239	0.058
RBXJA2T_19039	gi|332112653	Hypothetical protein RBXJA2T_19039	6	5.86	25.13	-0.153	0.11
RBXJA2T_13484	gi|332111359	Hypothetical protein RBXJA2T_13484	13	13.56	51.82	0.328	0.115
RBXJA2T_09802	gi|332109981	Hypothetical protein RBXJA2T_09802	17	10.6	74.58	0.379	0.056
RBXJA2T_04048	gi|332108247	Hypothetical protein RBXJA2T_04048	19	30.78	43.31	0.324	0.008
RBXJA2T_06300	gi|332108693	Hypothetical protein RBXJA2T_06300	21	19.58	45.17	0.502	0.088

RBXJA2T_04638	gi|332108365	Hypothetical protein RBXJA2T_04638	6	10.05	57.04	0.446	0.206
RBXJA2T_15178	gi|332111697	Hypothetical protein RBXJA2T_15178	9	9.64	29.19	0.797	0.08
RBXJA2T_00255	gi|332107500	Hypothetical protein RBXJA2T_00255	16	13.89	45.29	0.57	0.088
RBXJA2T_00005	gi|332107450	Hypothetical protein RBXJA2T_00005	12	15.85	37.46	0.657	0.315
RBXJA2T_14366	gi|332111537	Hypothetical protein RBXJA2T_14366	36	33.69	49.77	0.77	0.065
RBXJA2T_00090	gi|332107467	Hypothetical protein RBXJA2T_00090	3	5.5	51.61	0.681	0.266
RBXJA2T_16917	gi|332112048	Hypothetical protein RBXJA2T_16917	10	10.88	51.7	0.497	0.088
RBXJA2T_07848	gi|332109302	Hypothetical protein RBXJA2T_07848	10	16.13	85.99	0.977	0.224
RBXJA2T_05053	gi|332108448	Hypothetical protein RBXJA2T_05053	11	16.09	46.03	0.802	0.346
RBXJA2T_03788	gi|332108195	Hypothetical protein RBXJA2T_03788	7	12.64	51.65	0.747	0.177
RBXJA2T_08990	gi|332109527	Hypothetical protein RBXJA2T_08990	24	33.15	41.29	1.301	0.008
RBXJA2T_00015	gi|332107452	Hypothetical protein RBXJA2T_00015	23	28.42	40.65	1.221	0.124
RBXJA2T_01190	gi|332107683	Hypothetical protein RBXJA2T_01190	18	7.19	86.27	1.156	0.166
RBXJA2T_18423	gi|332112531	Hypothetical protein RBXJA2T_18423	54	22.66	74.18	1.809	0.002

Proteins listed were sorted out by considering the following parameters from the raw result file generated by Protein Pilot 5.0:

Unused prot score >2.0 with minimum two unique peptides for each protein and *p*- value < 0.05 in atleast two of four fold change expression values (Italicised proteins are not *p*-value significant but discussed in the text).

[#]Protein fold change (FC) ratios (glucose/malate) of identified proteins were $\log_2$ transformed, and the values represented are average of four FC ratios generated from two experiments (as described in the materials and methods).

Proteins with FC expression ratios and unused prot score >2, $|\log_2 FC| \geq 0.26$, p-value ≤ 0.05 were considered as dysregulated and are presented in the table.

[#]FC values shaded in red represents down-regulated proteins and the ones shaded green represents up-regulated proteins. Intensity of colour is proportional to the fold change value.

*Protein names in red font represents down-regulated proteins, green font represents up-regulated and ones in blue represents proteins with unaltered expression.

Protein names in italics are the ones with insignificant *p*-value but discussed in the text.

Table S 2: Dynamics of proteins extracted from glucose grown cells of *Rbx. benzoatilyticus* identified based on iTRAQ analysis.

Gene names (ORF)	Accession	Name	log_2 (G9/G3)	SD	log_2 (G18/G3)	SD
Glycolysis & a few downstream pathways						
RBXJA2T_04798	gi|332108397	Pyruvate dehydrogenase subunit E1	-0.332	0.030	-0.433	0.054
RBXJA2T_07403	gi|332109213	Pyruvate phosphate dikinase	-0.374	0.004	*-0.339*	*0.022*
RBXJA2T_06250	gi|332108683	Phosphoglycerate kinase	0.385	0.083	*0.056*	*0.110*
RBXJA2T_00150	gi|332107479	Phosphoglycerate mutase 1 family protein	0.355	0.135	*-0.270*	*0.138*
RBXJA2T_08555	gi|332109440	Alcohol dehydrogenase	-0.387	0.101	*-0.090*	*0.060*
RBXJA2T_05268	gi|332108491	Phosphoenolpyruvate carboxykinase	*-0.067*	*0.235*	-0.606	0.114
RBXJA2T_18373	gi|332112521	Phosphomannomutase	*0.006*	*0.146*	-0.554	0.040
RBXJA2T_12387	gi|332111092	Enolase	*-0.006*	*0.123*	*-0.505*	*0.075*
RBXJA2T_06270	gi|332108687	Fructose-1,6-bisphosphate aldolase	*0.022*	*0.040*	*-0.627*	*0.194*
RBXJA2T_05903	gi|332108616	Acetyl-coenzyme A synthetase	*0.356*	*0.029*	*-0.486*	*0.125*
RBXJA2T_06260	gi|332108685	Pyruvate kinase	0.068	0.073	*-0.441*	*0.053*
RBXJA2T_07060	gi|332109146	Nucleotide sugar dehydrogenase	*0.005*	*0.111*	*-0.610*	*0.037*
HMP/ ED pathway						
RBXJA2T_14891	gi|332111640	2-Dehydro-3-deoxyphosphogluconate aldolase/4-hydroxy-2-oxoglutarate aldolase	-0.588	0.151	*-0.225*	*0.352*
RBXJA2T_02652	gi|332107971	Transketolase	*-0.018*	*0.022*	*-0.486*	*0.013*
RBXJA2T_14896	gi|332111641	Phosphogluconate dehydratase	*-0.027*	*0.124*	*-0.498*	*0.066*
TCA/ Glyoxylate pathway						
RBXJA2T_09929	gi|332110006	Malate dehydrogenase	0.389	0.028	*-0.329*	*0.058*
RBXJA2T_07858	gi|332109304	Tartrate dehydrogenase	-0.658	0.062	*-0.538*	*0.068*
RBXJA2T_10419	gi|332110104	Isocitrate dehydrogenase	*-0.094*	*0.035*	-0.615	0.247
RBXJA2T_09939	gi|332110008	Bifunctional aconitate hydratase 2/2-methylisocitrate dehydratase	*0.015*	*0.105*	*-0.234*	*0.167*

RBXJA2T_09894	gi|332109999	Type II citrate synthase	*0.102*	*0.059*	*-0.686*	*0.047*
RBXJA2T_05893	gi|332108614	Tartrate/fumarate subfamily Fe-S type hydro-lyase subunit alpha	*-0.116*	*0.045*	*-0.339*	*0.003*
Electron Transport Chain						
RBXJA2T_10384	gi|332110097	Cytochrome c oxidase, cbb3-type subunit III	-1.306	0.231	-1.215	0.113
RBXJA2T_04488	gi|332108335	Cytochrome c	-0.959	0.126	*-0.903*	*0.078*
RBXJA2T_06975	gi|332109129	Cytochrome c1	-1.527	0.315	-1.328	0.252
RBXJA2T_06965	gi|332109127	Ubiquinol-cytochrome c reductase, iron-sulfur subunit	-1.558	0.234	-1.677	0.155
RBXJA2T_12607	gi|332111136	Fes cluster assembly scaffold iscu	0.848	0.230	*0.742*	*0.369*
RBXJA2T_02677	gi|332107976	UbiH/UbiF/VisC/COQ6 family ubiquinone biosynthesis hydroxylase	-0.144	0.484	*-0.310*	*0.304*
RBXJA2T_16347	gi|332111932	Pyrrolo-quinoline quinone	*0.120*	*0.127*	0.692	0.368
RBXJA2T_17322	gi|332112129	4Fe-4S ferredoxin iron-sulfur-binding domain-containing protein	*0.189*	*0.101*	-1.008	0.437
RBXJA2T_19081	gi|332112661	Electron transfer flavoprotein subunit alpha	*0.322*	*0.083*	*-0.379*	*0.107*
RBXJA2T_19251	gi|332112695	Inorganic diphosphatase	*0.112*	*0.096*	*-0.695*	*0.156*
RBXJA2T_16882	gi|332112041	ATP synthase Fo C subunit	*-1.251*	*0.440*	*-1.905*	*0.460*
Terpenoid/ Pigments/ Photosynthesis						
RBXJA2T_18708	gi|332112588	Ribulose bisophosphate carboxylase	-0.518	0.145	-0.867	0.121
RBXJA2T_09482	gi|332109919	Photosynthetic reaction center cytochrome c subunit	-0.721	0.231	*-0.821*	*0.206*
RBXJA2T_09442	gi|332109911	Chlorophyllide reductase iron protein subunit X	-0.517	0.023	-0.545	0.170
RBXJA2T_00590	gi|332107567	Deoxyxylulose-5-phosphate synthase	-0.461	0.077	*-0.524*	*0.149*
RBXJA2T_09447	gi|332109912	Chlorophyllide reductase subunit Y	-0.428	0.016	*-0.538*	*0.110*
RBXJA2T_09552	gi|332109933	Magnesium chelatase subunit H	-0.848	0.266	*-0.566*	*0.013*
RBXJA2T_15892	gi|332111841	Putative bacterioferritin	-0.574	0.251	*-0.935*	*0.136*
RBXJA2T_17564	gi|332112177	Uroporphyrinogen III synthase	-0.731	0.004	*-0.565*	*0.236*
RBXJA2T_04628	gi|332108363	Magnesium-protoporphyrin IX monomethyl ester anaerobic oxidative cyclase	*-0.100*	*0.103*	-0.578	0.117

RBXJA2T_09557	gi|332109934	Light-independent protochlorophyllide reductase subunit B	*-0.168*	*0.088*	-0.389	0.120
RBXJA2T_09547	gi|332109932	Protochlorophyllide reductase iron-sulfur ATP-binding protein	*-0.013*	*0.128*	-0.521	0.102
RBXJA2T_17559	gi|332112176	Porphobilinogen deaminase	*0.294*	*0.139*	*-0.257*	*0.109*
RBXJA2T_16937	gi|332112052	Uroporphyrinogen decarboxylase	*-0.071*	*0.051*	*-0.403*	*0.023*
RBXJA2T_00585	gi|332107566	Farnesyl-diphosphate synthase	*0.211*	*0.098*	*-0.559*	*0.262*
RBXJA2T_15273	gi|332111717	Bacteriophytochrome-like protein	*-0.221*	*0.136*	*-1.020*	*0.282*
Lipids & fatty acid metabolism						
RBXJA2T_04088	gi|332108255	Basic membrane lipoprotein	-1.177	0.286	-1.275	0.342
RBXJA2T_01010	gi|332107647	Toluene tolerance	1.405	0.081	1.600	0.283
RBXJA2T_06420	gi|332108717	Acyl carrier protein	0.745	0.066	0.621	0.165
RBXJA2T_08250	gi|332109379	3-Ketoacyl-(acyl-carrier-protein) reductase	*-0.135*	*0.173*	-0.701	0.397
RBXJA2T_12577	gi|332111130	Polyhydroxyalkanoate depolymerase, intracellular	*-0.413*	*0.208*	-0.867	0.060
RBXJA2T_08325	gi|332109394	Acyl-CoA dehydrogenase domain-containing protein	*-0.383*	*0.114*	-0.684	0.093
RBXJA2T_13294	gi|332111321	Putative long-chain-fatty-acid--CoA ligase protein	*0.032*	*0.125*	*-0.496*	*0.078*
RBXJA2T_09869	gi|332109994	Methylmalonyl-CoA mutase	*0.045*	*0.092*	*-0.165*	*0.063*
RBXJA2T_06620	gi|332108757	Lipopolysaccharide biosynthesis protein	*-0.062*	*0.188*	*0.417*	*0.148*
RBXJA2T_15423	gi|332111746	Diacylglycerol O-acyltransferase	*-0.327*	*0.222*	*-0.344*	*0.674*
RBXJA2T_11768	gi|332110824	Biotin carboxyl carrier protein	*-0.431*	*0.248*	-0.844	0.028
Amino acid metabolism						
RBXJA2T_01040	gi|332107653	Glutamate synthase (NADH) large subunit	-0.265	0.031	-0.479	0.068
RBXJA2T_18318	gi|332112510	Alanyl-tRNA synthetase	-0.053	0.144	*-0.421*	*0.008*
RBXJA2T_19201	gi|332112685	Acetolactate synthase 3 catalytic subunit	-0.460	0.002	-0.755	0.243
RBXJA2T_06555	gi|332108744	Phosphoglycerate dehydrogenase and related dehydrogenase	0.426	0.075	*0.012*	*0.105*
RBXJA2T_18253	gi|332112497	FAD dependent oxidoreductase	0.520	0.109	0.704	0.115

RBXJA2T_08605	gi|332109450	L-Glutamine synthetase	-0.789	0.194	*-0.661*	*0.190*
RBXJA2T_08225	gi|332109374	Maleylacetoacetate isomerase	0.298	0.104	*0.234*	*0.080*
RBXJA2T_11782	gi|332110826	Pantothenate synthetase	0.391	0.110	*0.464*	*0.104*
RBXJA2T_19191	gi|332112683	Ketol-acid reductoisomerase	*-0.224*	*0.134*	-0.810	0.277
RBXJA2T_01035	gi|332107652	Glutamate synthase subunit beta	*-0.046*	*0.161*	-0.517	0.211
RBXJA2T_01485	gi|332107742	Imidazolonepropionase	*0.418*	*0.075*	0.699	0.076
RBXJA2T_06715	gi|332108776	Lysyl-tRNA synthetase	*-0.335*	*0.000*	-0.481	0.041
RBXJA2T_17766	gi|332112217	S-Adenosylmethionine synthetase	*0.063*	*0.131*	-0.918	0.298
RBXJA2T_05228	gi|332108483	Pyrroline-5-carboxylate reductase	*-0.057*	*0.107*	-0.397	0.016
RBXJA2T_10044	gi|332110029	3-Phosphoserine/phosphohydroxythreonine aminotransferase	*-0.346*	*0.211*	-0.663	0.179
RBXJA2T_16847	gi|332112033	Glutamine synthetase	*0.238*	*0.081*	*-0.663*	*0.241*
RBXJA2T_03436	gi|332108125	Aspartate-semialdehyde dehydrogenase	*-0.164*	*0.043*	*-0.501*	*0.192*
RBXJA2T_07095	gi|332109153	Aspartyl-tRNA synthetase	*-0.016*	*0.152*	*-0.469*	*0.094*
RBXJA2T_19181	gi|332112681	2-Isopropylmalate synthase	*-0.369*	*0.000*	*-0.596*	*0.113*
RBXJA2T_12582	gi|332111131	Aromatic amino acid aminotransferase	*0.092*	*0.054*	*-0.356*	*0.034*
RBXJA2T_01495	gi|332107744	N-Formimino-L-glutamate deiminase	*0.155*	*0.060*	*-0.552*	*0.009*
RBXJA2T_10861	gi|332110497	Glutaminyl-tRNA synthetase	-0.219	0.170	*-0.552*	*0.058*
RBXJA2T_16242	gi|332111911	Branched subunit Amino acid: 2-keto-4-methylthiobutyrate aminotransferase	0.114	0.103	*-0.129*	*0.112*
RBXJA2T_09197	gi|332109863	Thioredoxin reductase	-0.051	0.067	*-0.402*	*0.051*
RBXJA2T_11061	gi|332110537	Valine-pyruvate aminotransferase	0.444	0.056	*0.087*	*0.063*
Storage						
RBXJA2T_07833	gi|332109299	Cyanophycin synthetase	0.942	0.357	1.030	0.035
RBXJA2T_07838	gi|332109300	Cyanophycin synthetase	0.787	0.272	0.843	0.056
RBXJA2T_17372	gi|332112139	Phasin family protein	0.546	0.062	*0.055*	*0.236*
RBXJA2T_07353	gi|332109203	Alpha amylase catalytic region	-1.792	0.385	-1.272	0.413
RBXJA2T_10059	gi|332110032	Argininosuccinate synthase	*0.171*	*0.118*	*-0.409*	*0.100*
RBXJA2T_06865	gi|332109107	Polygranule-associated protein	*0.454*	*0.285*	*0.729*	*0.288*

Nucleotide/ Cofactor/ Vitamin metabolism						
RBXJA2T_10304	gi|332110081	Vitamin B12 transporter btuB precursor, putative	1.064	0.505	1.943	0.132
RBXJA2T_18603	gi|332112567	Thiamine biosynthesis protein ThiC	-0.392	0.051	-0.907	0.038
RBXJA2T_10319	gi|332110084	Adenylate kinase	0.582	0.036	*-0.069*	*0.366*
RBXJA2T_04183	gi|332108274	NMT1/THI5-like domain-containing protein	0.552	0.143	*0.246*	*0.146*
RBXJA2T_09312	gi|332109886	Guanosine 5'-monophosphate oxidoreductase	0.345	0.082	*0.349*	*0.088*
RBXJA2T_06835	gi|332109101	Bifunctional phosphoribosylaminoimidazolecarboxamide formyltransferase/IMP cyclohydrolase	*-0.055*	*0.140*	-0.470	0.119
RBXJA2T_00065	gi|332107462	Thiamine-phosphate pyrophosphorylase	*-0.079*	*0.065*	-0.481	0.117
RBXJA2T_09657	gi|332109954	Carbamoyl-phosphate synthase large subunit	*-0.072*	*0.104*	*-0.326*	*0.002*
RBXJA2T_17971	gi|332112441	Adenylosuccinate synthetase	*-0.061*	*0.129*	*-0.509*	*0.171*
RBXJA2T_17896	gi|332112426	Nucleoside diphosphate kinase	*0.631*	*0.242*	*-0.956*	*0.275*
Secondary metabolites						
RBXJA2T_18478	gi|332112542	Catalase/hydroperoxidase HPI(I)	0.024	0.192	*-0.238*	*0.168*
RBXJA2T_01090	gi|332107663	1A Family penicillin-binding protein	-0.742	0.148	*-0.415*	*0.438*
RBXJA2T_06875	gi|332109109	Acetylglutamate kinase	-0.384	0.091	*-0.476*	*0.093*
RBXJA2T_07723	gi|332109277	CRISPR-associated Csd2 family protein	*-0.477*	*0.000*	-0.691	0.062
Replication						
RBXJA2T_06275	gi|332108688	Phosphoribosylaminoimidazole-succinocarboxamide synthase	*-0.096*	*0.182*	-0.558	0.174
RBXJA2T_02627	gi|332107966	DNA topoisomerase III	*0.032*	*0.118*	*-0.353*	*0.084*
RBXJA2T_07663	gi|332109265	Orotate phosphoribosyltransferase	*-0.295*	*0.033*	*0.422*	*0.086*
Recombination & Repair						
RBXJA2T_13534	gi|332111369	RecA protein	-0.578	0.079	0.587	0.192
RBXJA2T_09222	gi|332109868	Recombination factor protein RarA	0.299	0.138	*0.245*	*0.059*
RBXJA2T_16387	gi|332111940	Recombination associated protein	*-0.149*	*0.144*	-0.630	0.039
RBXJA2T_08770	gi|332109483	Integration host factor alpha-subunit	*-0.187*	*0.127*	*0.729*	*0.314*

Transcription						
RBXJA2T_03272	gi|332108093	DNA-directed RNA polymerase subunit beta	0.330	0.042	*-0.323*	*0.000*
RBXJA2T_07978	gi|332109326	Ribonuclease E	0.297	0.057	*0.047*	*0.082*
RBXJA2T_03267	gi|332108092	DNA-directed RNA polymerase subunit beta'	*0.005*	*0.078*	-0.375	0.030
RBXJA2T_19296	gi|332112704	NusA antitermination factor	*-0.056*	*0.070*	-0.493	0.123
RBXJA2T_09637	gi|332109950	RNA polymerase sigma S (sigma-38) factor transcription regulator protein	*0.491*	*0.146*	0.562	0.148
RBXJA2T_13264	gi|332111315	Putative RNA methylase	*0.573*	*0.199*	0.604	0.210
Translation						
RBXJA2T_02245	gi|332107892	30S Ribosomal protein S4	0.700	0.044	*0.533*	*0.200*
RBXJA2T_02145	gi|332107872	30S Ribosomal protein S3	0.483	0.171	*0.684*	*0.000*
RBXJA2T_03252	gi|332108089	30S Ribosomal protein S7	0.517	0.164	*-0.388*	*0.171*
RBXJA2T_03277	gi|332108094	50S Ribosomal protein L7/L12	0.886	0.020	*0.644*	*0.259*
RBXJA2T_02170	gi|332107877	50S Ribosomal protein L14	0.750	0.041	*0.619*	*0.241*
RBXJA2T_02155	gi|332107874	50S Ribosomal protein L29	0.864	0.010	1.085	0.000
RBXJA2T_12532	gi|332111121	30S Ribosomal protein S21	0.771	0.216	*0.568*	*0.266*
RBXJA2T_03247	gi|332108088	Elongation factor G	*-0.134*	*0.066*	-0.571	0.156
RBXJA2T_18001	gi|332112447	SSU Ribosomal protein S2P	*-0.088*	*0.127*	-0.763	0.263
RBXJA2T_02205	gi|332107884	30S Ribosomal protein S5	*0.035*	*0.196*	-1.170	0.142
RBXJA2T_15523	gi|332111766	50S Ribosomal protein L25/general stress protein Ctc	*0.023*	*0.070*	-1.175	0.022
RBXJA2T_03242	gi|332108087	Elongation factor Tu	*-0.013*	*0.044*	*-0.400*	*0.103*
RBXJA2T_01710	gi|332107785	Elongation factor G	*-0.096*	*0.095*	*-0.420*	*0.096*
RBXJA2T_16502	gi|332111964	30S Ribosomal protein S1	*-0.121*	*0.094*	*-0.483*	*0.138*
RBXJA2T_02120	gi|332107867	50S Ribosomal protein L4	*0.171*	*0.190*	*-0.395*	*0.221*
RBXJA2T_02235	gi|332107890	30S Ribosomal protein S13	*0.250*	*0.203*	*0.245*	*0.176*
RBXJA2T_10781	gi|332110481	Ribosomal subunit Interface protein	*0.714*	*0.317*	*0.567*	*0.345*

Regulatory proteins						
RBXJA2T_18418	gi|332112530	Two component transcriptional regulator	0.739	0.298	*0.208*	*0.406*
RBXJA2T_09122	gi|332109848	Histone-like nucleoid-structuring protein H-NS	0.567	0.150	*0.033*	*0.161*
RBXJA2T_04808	gi|332108399	Two component LuxR family transcriptional regulator	*0.318*	*0.000*	*-0.443*	*0.087*
RBXJA2T_01475	gi|332107740	Histidine utilization repressor	*-0.026*	*0.099*	*-0.633*	*0.006*
RBXJA2T_19171	gi|332112679	IclR family transcriptional regulator	*0.038*	*0.106*	*-0.142*	*0.140*
RBXJA2T_10404	gi|332110101	Crp/FNR family transcriptional regulator	*0.141*	*0.235*	*-0.492*	*0.166*
RBXJA2T_19236	gi|332112692	Nitrogen regulatory protein P-II	*-0.011*	*0.112*	*0.489*	*0.078*
RBXJA2T_01415	gi|332107728	Nucleoid protein H-NS	*0.009*	*0.133*	*-1.000*	*0.496*
RBXJA2T_11196	gi|332110564	Nitrogen regulatory protein P-II	*0.082*	*0.613*	*-0.399*	*0.317*
RBXJA2T_15723	gi|332111806	Two component transcriptional regulator	*-0.021*	*0.147*	*0.593*	*0.211*
Chaperone/ Chaperonin						
RBXJA2T_04473	gi|332108332	Chaperonin GroEL	0.493	0.103	0.481	0.156
RBXJA2T_18131	gi|332112473	Molecular chaperone DnaK	0.533	0.149	0.572	0.154
RBXJA2T_02902	gi|332108021	PpiC-type peptidyl-prolyl cis-trans isomerase	-1.126	0.240	-0.946	0.234
RBXJA2T_12642	gi|332111143	Putative transporter signal peptide protein	-0.858	0.328	*-0.620*	*0.226*
RBXJA2T_02095	gi|332107862	HSP20 family protein	1.048	0.363	1.075	0.330
RBXJA2T_09767	gi|332109976	Thioredoxin	-1.175	0.345	*-1.472*	*0.251*
RBXJA2T_13444	gi|332111351	Putative signal peptide protein	*-0.433*	*0.183*	*0.380*	*0.099*
RBXJA2T_15183	gi|332111698	UBA/THIF-type NAD/FAD-binding protein	*0.456*	*0.071*	1.000	0.256
Protease/ Peptidase						
RBXJA2T_11997	gi|332110869	Protease Do	1.837	0.498	1.582	0.490
RBXJA2T_06070	gi|332108649	Protease Do	0.774	0.046	1.059	0.032
RBXJA2T_01770	gi|332107797	ATP-dependent protease ATP-binding subunit HslU	0.379	0.097	*0.388*	*0.095*
RBXJA2T_01550	gi|332107755	Prolyl oligopeptidase family protein	-0.644	0.252	-0.636	0.144
RBXJA2T_15188	gi|332111699	Carboxyl-terminal protease	-0.428	0.059	*-0.481*	*0.083*

RBXJA2T_03758	gi|332108189	Leucyl aminopeptidase	1.136	0.358	0.963	0.327
RBXJA2T_16247	gi|332111912	Serine-type D-Ala-D-Ala carboxypeptidase	-0.540	0.039	-0.437	0.110
RBXJA2T_07958	gi|332109322	Peptidase S49	-0.807	0.171	*-0.827*	*0.151*
RBXJA2T_13814	gi|332111426	Leucyl aminopeptidase	0.597	0.168	*0.112*	*0.111*
RBXJA2T_08078	gi|332109346	Peptidase S9 prolyl oligopeptidase	*0.052*	*0.035*	*-0.187*	*0.032*
RBXJA2T_19136	gi|332112672	ATP-dependent Clp protease, proteolytic subunit ClpP	*0.020*	*0.027*	*-0.747*	*0.599*
Stress proteins						
RBXJA2T_13976	gi|332111458	Universal stress protein	0.578	0.183	0.595	0.157
RBXJA2T_05183	gi|332108474	Ferritin Dps family protein	0.844	0.264	*0.711*	*0.296*
RBXJA2T_02105	gi|332107864	Heat shock protein Hsp20	0.943	0.294	1.322	0.357
RBXJA2T_18136	gi|332112474	Putative heat shock protein	0.534	0.073	*0.323*	*0.535*
RBXJA2T_02907	gi|332108022	Putative organic solvent tolerance transmembrane protein	*0.404*	*0.015*	0.726	0.096
RBXJA2T_01425	gi|332107730	Oxidative damage protection protein	*0.158*	*0.044*	-0.659	0.318
RBXJA2T_14451	gi|332111554	Heat shock protein 90	*-0.049*	*0.085*	*-0.403*	*0.058*
Membrane transport/ Translocation						
RBXJA2T_06385	gi|332108710	Filamentous hemagglutinin outer membrane protein	0.502	0.187	0.829	0.440
RBXJA2T_12407	gi|332111096	TonB-dependent receptor	0.730	0.225	1.375	0.263
RBXJA2T_17312	gi|332112127	TonB-dependent siderophore receptor	0.448	0.039	0.525	0.168
RBXJA2T_18041	gi|332112455	Outer membrane protein assembly complex, YaeT protein	0.478	0.177	0.834	0.189
RBXJA2T_03319	gi|332108102	TonB-dependent receptor	0.817	0.457	1.673	0.402
RBXJA2T_06380	gi|332108709	Polypeptide-transport-associated domain-containing protein	0.598	0.223	1.621	0.277
RBXJA2T_03668	gi|332108171	Extracellular ligand-binding receptor	-0.468	0.051	*-0.083*	*0.083*
RBXJA2T_15748	gi|332111811	Extracellular solute-binding protein	-0.875	0.240	-0.817	0.176
RBXJA2T_12352	gi|332111085	Extracellular solute-binding protein	0.820	0.255	1.058	0.315
RBXJA2T_18363	gi|332112519	TolC family type I secretion outer	0.451	0.077	1.192	0.063

		membrane protein				
RBXJA2T_08945	gi|332109518	Putative exported isomerase	-0.980	0.216	-0.897	0.188
RBXJA2T_16532	gi|332111970	OmpA/MotB domain-containing protein	1.040	0.284	1.711	0.497
RBXJA2T_01730	gi|332107789	RND family efflux transporter MFP subunit	1.119	0.285	1.072	0.281
RBXJA2T_07035	gi|332109141	Extracellular solute-binding protein family 1	-0.617	0.187	-0.824	0.159
RBXJA2T_05798	gi|332108595	Putative outer membrane transport protein involved in copper (silver) tolerance (cusC)	0.466	0.088	1.022	0.162
RBXJA2T_05793	gi|332108594	Type I antifreeze protein:HlyD family secretion protein	0.454	0.182	0.819	0.122
RBXJA2T_00774	gi|332107601	Polar amino acid transporter substrate-binding protein	-0.804	0.009	-0.540	0.023
RBXJA2T_07608	gi|332109254	ABC type ATPase	-0.562	0.041	*-0.503*	*0.091*
RBXJA2T_04738	gi|332108385	TonB-dependent receptor	0.623	0.214	1.012	0.199
RBXJA2T_06480	gi|332108729	Polysaccharide export protein	0.736	0.262	1.231	0.257
RBXJA2T_01735	gi|332107790	RND efflux system outer membrane lipoprotein	1.087	0.217	1.610	0.223
RBXJA2T_02362	gi|332107915	Efflux transporter RND family, MFP subunit	-0.857	0.207	-0.714	0.218
RBXJA2T_12507	gi|332111116	TRAP C4-dicarboxylate transport system permease subunit DctP	-0.589	0.210	-0.737	0.179
RBXJA2T_07180	gi|332109170	Peptidoglycan-associated lipoprotein	1.042	0.311	*0.994*	*0.295*
RBXJA2T_03748	gi|332108187	Extracellular ligand-binding receptor	-1.786	0.077	-0.716	0.680
RBXJA2T_07943	gi|332109319	Putative outer membrane protein	0.482	0.121	0.924	0.352
RBXJA2T_11423	gi|332110755	Putative binding-dependent transport protein	-0.503	0.154	*-0.306*	*0.164*
RBXJA2T_12787	gi|332111172	TRAP dicarboxylate transporter subunit DctP	-0.876	0.405	-1.035	0.148
RBXJA2T_03873	gi|332108212	Extracellular solute-binding protein	-0.295	0.083	-0.728	0.178
RBXJA2T_12832	gi|332111181	Secretion protein HlyD	-0.615	0.012	*-0.331*	*0.051*
RBXJA2T_07843	gi|332109301	Putative ABC transporter	0.832	0.153	0.845	0.163
RBXJA2T_07513	gi|332109235	Yidc translocase/secretase	-0.758	0.301	-1.005	0.248
RBXJA2T_07343	gi|332109201	Maltose transporter membrane protein	-0.883	0.235	-0.813	0.178

RBXJA2T_13579	gi|332111378	Type VI secretion protein	-0.777	0.076	*-0.488*	*0.132*
RBXJA2T_02817	gi|332108004	Small protein A (tmRNA-binding)-like protein	-0.736	0.109	*-0.374*	*0.086*
RBXJA2T_03441	gi|332108126	Putative transmembrane protein	0.634	0.006	0.748	0.103
RBXJA2T_14856	gi|332111633	Biopolymer transport ExbD protein	-0.720	0.110	*-0.876*	*0.114*
RBXJA2T_04288	gi|332108295	Branched-chain amino acid ABC transporter periplasmic amino acid-binding protein	-0.805	0.258	*-0.674*	*0.276*
RBXJA2T_07140	gi|332109162	Dipeptide transporter ATP-binding subunit	0.730	0.007	*-0.056*	*0.463*
RBXJA2T_07338	gi|332109200	Maltose ABC transporter periplasmic protein	*0.289*	*0.000*	-0.926	0.056
RBXJA2T_12882	gi|332111191	Extracellular solute-binding protein	*-0.190*	*0.188*	-0.662	0.157
RBXJA2T_07593	gi|332109251	RND family efflux transporter MFP subunit	*0.095*	*0.053*	0.394	0.035
RBXJA2T_08615	gi|332109452	Polyamine ABC transporter system, substrate-binding protein	*0.466*	*0.197*	0.670	0.395
RBXJA2T_18046	gi|332112456	Putative transmembrane protein	*0.036*	*0.348*	0.809	0.232
RBXJA2T_09242	gi|332109872	Putative amino acid ATP-binding ABC transporter protein	*-0.114*	*0.082*	-0.613	0.059
RBXJA2T_17871	gi|332112238	Putative lipoprotein	*0.573*	*0.135*	1.057	0.362
RBXJA2T_08088	gi|332109348	Surface antigen (D15)	*0.292*	*0.044*	0.752	0.176
RBXJA2T_17077	gi|332112080	General secretion pathway protein D	*0.466*	*0.099*	1.163	0.324
RBXJA2T_11226	gi|332110570	General secretion pathway protein D	*0.161*	*0.266*	0.667	0.289
RBXJA2T_10951	gi|332110515	ABC transporter permease and ATP-binding protein	*-0.056*	*0.107*	-0.330	0.040
RBXJA2T_08955	gi|332109520	Putative ABC transporter ATP-binding protein	*0.003*	*0.090*	*-0.305*	*0.040*
RBXJA2T_03898	gi|332108217	Extracellular solute-binding protein	*0.528*	*0.155*	*0.909*	*0.503*
RBXJA2T_12232	gi|332110916	Acriflavin resistance protein	*-0.337*	*0.066*	*-0.025*	*0.166*
RBXJA2T_12237	gi|332110917	RND family efflux transporter MFP subunit	*-0.379*	*0.035*	*0.155*	*0.307*
RBXJA2T_05103	gi|332108458	Transport protein	*0.506*	*0.183*	*0.847*	*0.394*
RBXJA2T_04533	gi|332108344	Major facilitator superfamily transporter	*-0.001*	*0.151*	*0.846*	*0.137*
RBXJA2T_02377	gi|332107916	RND efflux system outer membrane	*-0.382*	*0.193*	*0.890*	*0.403*

		lipoprotein				
RBXJA2T_07020	gi|332109138	ABC transporter	*-0.268*	*0.198*	*0.022*	*0.501*
RBXJA2T_01420	gi|332107729	Extracellular solute-binding protein	*-0.353*	*0.050*	*-0.056*	*0.021*
Quorum sensing & Signal transduction						
RBXJA2T_13414	gi|332111345	MCP methyltransferase/methylesterase, CheR/CheB with PAS/PAC sensor	-0.243	0.119	*-0.371*	*0.079*
RBXJA2T_13474	gi|332111357	Methylation	0.490	0.000	*-0.988*	*0.402*
RBXJA2T_13604	gi|332111383	Methyl-accepting chemotaxis sensory transducer	0.593	0.057	*-0.018*	*0.066*
RBXJA2T_13594	gi|332111381	CheA signal transduction histidine kinase	-0.759	0.438	*-1.447*	*0.507*
RBXJA2T_15588	gi|332111779	Two-component hybrid sensor and regulator	*-0.212*	*0.087*	*0.249*	*0.075*
Porin/ Pilus/ Cell division						
RBXJA2T_18939	gi|332112633	Gram-negative type outer membrane porin protein	1.294	0.282	2.230	0.242
RBXJA2T_12337	gi|332111082	Porin	0.923	0.177	1.518	0.290
RBXJA2T_07363	gi|332109205	Maltoporin	1.544	0.365	2.200	0.635
RBXJA2T_18338	gi|332112514	Gram-negative type outer membrane porin protein	1.067	0.268	1.784	0.382
RBXJA2T_01065	gi|332107658	Fimbrial biogenesis protein	0.801	0.317	1.527	0.037
RBXJA2T_04083	gi|332108254	Porin	1.092	0.160	1.097	0.251
RBXJA2T_01075	gi|332107660	Fimbrial assembly protein	-1.087	0.195	*-0.779*	*0.156*
RBXJA2T_13684	gi|332111400	Flagellin domain-containing protein	-1.475	0.424	-1.146	0.633
RBXJA2T_01070	gi|332107659	Fimbrial assembly protein	-0.655	0.129	*-0.389*	*0.095*
RBXJA2T_01085	gi|332107662	Type IV pilus assembly protein PilM	*-0.501*	*0.140*	-0.743	0.158
RBXJA2T_19141	gi|332112673	Trigger factor	*0.318*	*0.051*	*-0.412*	*0.098*
RBXJA2T_00979	gi|332107642	Putative transmembrane protein	*0.055*	*0.105*	*-0.421*	*0.101*
Miscellaneous						
RBXJA2T_00475	gi|332107544	Putative peptidyl-prolyl cis-trans isomerase transmembrane protein	-1.176	0.185	-0.857	0.200
RBXJA2T_16137	gi|332111890	Hydroxylamine reductase	-2.138	0.258	-1.903	0.310

RBXJA2T_17826	gi|332112229	Lytic transglycosylase, catalytic	-0.176	0.069	*0.315*	*0.047*
RBXJA2T_02000	gi|332107843	Putative cytochrome c peroxidase	-0.552	0.186	*-0.522*	*0.117*
RBXJA2T_04633	gi|332108364	Basic membrane lipoprotein	0.568	0.063	*0.338*	*0.204*
RBXJA2T_10666	gi|332110458	TPR repeat-containing protein	-1.029	0.064	-1.035	0.321
RBXJA2T_05158	gi|332108469	OmpA/MotB domain-containing protein	0.556	0.151	1.219	0.090
RBXJA2T_13199	gi|332111302	3-Oxoacid CoA-transferase	-0.805	0.033	*-0.324*	*0.030*
RBXJA2T_13204	gi|332111303	3-Oxoacid CoA-transferase subunit B	-0.775	0.376	*-0.922*	*0.153*
RBXJA2T_02347	gi|332107912	Esterase/lipase-like protein	-0.351	0.787	0.844	0.054
RBXJA2T_13244	gi|332111311	Thiol:disulfide interchange protein	-0.572	0.045	*-0.339*	*0.054*
RBXJA2T_10459	gi|332110112	Tetratricopeptide repeat family protein	-0.871	0.187	-0.770	0.195
RBXJA2T_10284	gi|332110077	Putative extracellular solute-binding protein	-0.869	0.121	*-0.637*	*0.157*
RBXJA2T_01195	gi|332107684	Transglutaminase domain-containing protein	0.972	0.203	0.986	0.293
RBXJA2T_17801	gi|332112224	Putative outer membrane signal peptide protein	1.227	0.296	2.170	0.323
RBXJA2T_01365	gi|332107718	Dual specificity protein phosphatase	1.546	0.049	*1.172*	*0.135*
RBXJA2T_12602	gi|332111135	Cysteine desulfurase	*-0.283*	*0.142*	-0.489	0.202
RBXJA2T_18428	gi|332112532	Putative lipoprotein	*0.345*	*0.146*	0.685	0.230
RBXJA2T_03026	gi|332108045	Dinb family protein	*0.048*	*0.112*	0.609	0.035
RBXJA2T_18613	gi|332112569	Aldehyde dehydrogenase	*-0.391*	*0.003*	*-0.158*	*0.460*
RBXJA2T_10084	gi|332110037	Aminotransferase class V	*0.075*	*0.122*	*-0.382*	*0.112*
RBXJA2T_11902	gi|332110850	Peroxiredoxin protein	*0.253*	*0.163*	*-0.424*	*0.155*
RBXJA2T_11698	gi|332110810	Signal recognition particle-docking protein FtsY	*0.364*	*0.042*	*0.351*	*0.177*
RBXJA2T_16932	gi|332112051	LemA protein	*-0.382*	*0.083*	*0.129*	*0.282*
RBXJA2T_06305	gi|332108694	Putative lipase / esterase protein	*-0.725*	*0.220*	*0.429*	*0.263*
RBXJA2T_07768	gi|332109286	SAF domain-containing protein	*-0.141*	*0.046*	*-0.487*	*0.215*
RBXJA2T_18523	gi|332112551	Diguanylate cyclase	*0.524*	*0.061*	*-0.543*	*0.184*
RBXJA2T_07358	gi|332109204	Pullanase-associated protein	*0.205*	*0.420*	*-1.100*	*0.398*

RBXJA2T_15418	gi|332111745	Acyl-CoA-binding protein	*0.489*	*0.024*	*-0.174*	*0.618*
RBXJA2T_16722	gi|332112008	UDP-N-Acetylenolpyruvoylglucosamine reductase	*-0.053*	*0.234*	*0.578*	*0.129*
RBXJA2T_18313	gi|332112509	Sec-c motif domain protein	*-0.468*	*0.069*	-0.638	0.174
RBXJA2T_18693	gi|332112585	AAA type ATPase	*0.020*	*0.187*	0.592	0.093
RBXJA2T_16107	gi|332111884	Rhodanese domain-containing protein	*-0.227*	*0.257*	*-1.106*	*0.551*
RBXJA2T_13434	gi|332111349	SWIB/MDM2 domain-containing protein	*-0.348*	*0.025*	-1.451	0.687
RBXJA2T_04513	gi|332108340	D-(-)-3-Hydroxybutyrate oligomer hydrolase	*1.021*	*0.285*	2.245	0.409
Hypothetical proteins						
RBXJA2T_08635	gi|332109456	Hypothetical protein RBXJA2T_08635	0.655	0.192	1.021	0.201
RBXJA2T_14391	gi|332111542	Hypothetical protein RBXJA2T_14391	-0.763	0.046	-0.482	0.137
RBXJA2T_17951	gi|332112437	Hypothetical protein RBXJA2T_17951	0.479	0.119	*0.450*	*0.111*
RBXJA2T_08990	gi|332109527	Hypothetical protein RBXJA2T_08990	0.829	0.344	1.085	0.280
RBXJA2T_12317	gi|332111078	Hypothetical protein RBXJA2T_12317	-0.688	0.056	*0.560*	*0.061*
RBXJA2T_16832	gi|332112030	Hypothetical protein RBXJA2T_16832	0.499	0.184	*-0.067*	*0.231*
RBXJA2T_00015	gi|332107452	Hypothetical protein RBXJA2T_00015	0.902	0.259	1.616	0.039
RBXJA2T_17187	gi|332112102	Hypothetical protein RBXJA2T_17187	-0.572	0.140	*-0.331*	*0.125*
RBXJA2T_05398	gi|332108517	Hypothetical protein RBXJA2T_05398	0.564	0.099	0.927	0.196
RBXJA2T_18423	gi|332112531	Hypothetical protein RBXJA2T_18423	1.543	0.058	1.593	0.120
RBXJA2T_06300	gi|332108693	Hypothetical protein RBXJA2T_06300	0.501	0.132	0.857	0.216
RBXJA2T_17926	gi|332112432	Hypothetical protein RBXJA2T_17926	-0.875	0.132	*-0.670*	*0.191*
RBXJA2T_13569	gi|332111376	Hypothetical protein RBXJA2T_13569	-0.797	0.254	-0.999	0.410
RBXJA2T_16222	gi|332111907	Hypothetical protein RBXJA2T_16222	-0.886	0.132	-0.755	0.314
RBXJA2T_05208	gi|332108479	Hypothetical protein RBXJA2T_05208	-0.687	0.001	*-0.259*	*0.131*
RBXJA2T_14176	gi|332111498	Hypothetical protein RBXJA2T_14176	0.478	0.110	*0.380*	*0.097*
RBXJA2T_13559	gi|332111374	Hypothetical protein RBXJA2T_13559	-0.752	0.282	*-0.457*	*0.115*
RBXJA2T_15922	gi|332111847	Hypothetical protein RBXJA2T_15922	0.379	0.070	*0.755*	*0.272*
RBXJA2T_09522	gi|332109927	Hypothetical protein RBXJA2T_09522	-1.097	0.168	*-0.797*	*0.263*

RBXJA2T_05278	gi|332108493	Hypothetical protein RBXJA2T_05278	0.531	0.229	0.540	0.211
RBXJA2T_12312	gi|332111077	Hypothetical protein RBXJA2T_12312	0.574	0.084	1.062	0.171
RBXJA2T_16917	gi|332112048	Hypothetical protein RBXJA2T_16917	0.064	0.518	*-0.322*	*0.254*
RBXJA2T_09802	gi|332109981	Hypothetical protein RBXJA2T_09802	0.860	0.213	1.786	0.144
RBXJA2T_15178	gi|332111697	Hypothetical protein RBXJA2T_15178	0.473	0.128	*0.382*	*0.176*
RBXJA2T_05995	gi|332108634	Hypothetical protein RBXJA2T_05995	1.079	0.045	*1.115*	*0.010*
RBXJA2T_15867	gi|332111836	Hypothetical protein RBXJA2T_15867	0.584	0.164	*0.844*	*0.257*
RBXJA2T_06670	gi|332108767	Hypothetical protein RBXJA2T_06670	-0.497	0.062	*-0.843*	*0.323*
RBXJA2T_07418	gi|332109216	Hypothetical protein RBXJA2T_07418	*-0.018*	*0.104*	0.885	0.225
RBXJA2T_17731	gi|332112210	Hypothetical protein RBXJA2T_17731	*0.319*	*0.040*	0.502	0.069
RBXJA2T_10926	gi|332110510	Hypothetical protein RBXJA2T_10926	*0.247*	*0.185*	-0.795	0.144
RBXJA2T_16717	gi|332112007	Hypothetical protein RBXJA2T_16717	*0.501*	*0.149*	0.627	0.125
RBXJA2T_05353	gi|332108508	Hypothetical protein RBXJA2T_05353	*0.313*	*0.061*	1.195	0.106
RBXJA2T_00914	gi|332107629	Hypothetical protein RBXJA2T_00914	*-0.035*	*0.273*	0.786	0.071
RBXJA2T_05548	gi|332108547	Hypothetical protein RBXJA2T_05548	*-0.872*	*0.232*	-2.021	0.269
RBXJA2T_10329	gi|332110086	Hypothetical protein RBXJA2T_10329	*-0.613*	*0.222*	-0.801	0.258
RBXJA2T_01190	gi|332107683	Hypothetical protein RBXJA2T_01190	*0.296*	*0.487*	0.166	0.735
RBXJA2T_00005	gi|332107450	Hypothetical protein RBXJA2T_00005	*0.013*	*0.332*	*0.737*	*0.194*
RBXJA2T_15563	gi|332111774	Hypothetical protein RBXJA2T_15563	*-0.077*	*0.419*	*-0.167*	*0.547*
RBXJA2T_07848	gi|332109302	Hypothetical protein RBXJA2T_07848	*0.590*	*0.162*	0.591	0.296
RBXJA2T_11388	gi|332110748	Hypothetical protein RBXJA2T_11388	*-1.233*	*0.293*	-1.232	0.238
RBXJA2T_06570	gi|332108747	Hypothetical protein RBXJA2T_06570	*-0.028*	*0.200*	*0.617*	*0.158*

Proteome from early (G9) and late (G18) stationary phase cells was compared with that of exponential phase (G3) grown cells (average (with SD) of their log_2 transformed fold change ratios are presented in the table). Proteins listed were sorted out by considering the following parameters from the raw result file generated by Protein Pilot 5.0:

Unused prot score >2.0 with minimum of two unique peptides for each protein and *p*- value < 0.05 in atleast two of four fold change expression values (Italicised values are not *p*-value significant at that time point but are at other time point).

[#]Protein fold change (FC) ratios (stationary phase/exponential phase) of identified proteins were log_2 transformed, and the values represented are average of log_2FC ratios generated from two experiments

(as described in the materials and methods). Proteins with unused prot score >2, $|\log_2 FC| \geq 0.26$, *p*-value ≤ 0.05 were considered as dysregulated and are presented in the table.

[#]FC value shaded in red represents down-regulated proteins and the ones shaded green represent up-regulated proteins. Intensity of colour is proportional to the fold change value.

G3, proteome at 3rd day of growth; G9, proteome at 9th day of growth; G18, proteome at 18th day of growth.

Table S 3: Nucleotide variations observed in the coding sequences (CDS) of both the genomes.

Contig	Position	Genome	Function	Score	Substitution type	Ref_nt	Var_nt	Ref_nt position change	Ref_aa position change	SNP effect type	SNP impact
NZ_AEWG01000002	37370	Both	Signal transduction histidine kinase CheA	134.0	Nonsyn	ctg	cAg	386T>A	Leu129Gln	Missense variant	Moderate
NZ_AEWG01000004	13606	Both	Hypothetical protein	119.0	Nonsyn	ctg	cAg	356T>A	Leu119Gln	Missense variant	Moderate
NZ_AEWG01000007	3627	Glc-genome	Geranylgeranyl reductase	154.5	Insertion	ggggcc	GGGGGCc	669_670insG	Glu223_Gly224fs	Frameshift variant	High
NZ_AEWG01000008	9312	Glc-genome	Hypothetical protein	141.5	Insertion	gccccc gcc	GCCCCCCgcc	460_461insC	Ala154_Arg155fs	Frameshift variant	High
NZ_AEWG01000013	174	Both	Pyruvate formate-lyase (EC 2.3.1.54)	131.0	Synon	gag	gaA	66G>A	Glu22Glu	Synonymous variant	Low
NZ_AEWG01000019	6134	Glc-genome	Hypothetical protein	94.5	Insertion	gcccccc cgcac	gCCCCCCCCCGcac	424_425insC	Ala142_Pro143fs	Frameshift variant	High
NZ_AEWG01000022	12956	Both	RND multidrug efflux transporter	129.0	Nonsyn	tcg	tAg	461C>A	Ser154*	Stop gained	High
NZ_AEWG01000033	5247	Both	Transcriptional regulator, LysR family	111.0	Nonsyn	gtg	gAg	668T>A	Val223Glu	Missense variant	Moderate
NZ_AEWG01000034	26319	Glc-genome	GGDEF domain protein	132.5	Insertion	ctccccc gt	ctCCCCCCGt	20_21insC	Leu7_Pro8fs	Frameshift variant	High
NZ_AEWG01000040	6085	Both	Hypothetical protein	121.0	Nonsyn	ggc	gCc	5426G>C	Gly1809Ala	Missense variant	Moderate
NZ_AEWG01000040	6086	Both	Hypothetical protein	123.0	Synon	ggc	ggG	5427C>G	Gly1809Gly	Synonymous variant	Low
NZ_AEWG01000040	6087	Both	Hypothetical protein	121.0	Nonsyn	gag	Cag	5428G>C	Glu1810Gln	Missense variant	Moderate
NZ_AEWG01000040	63812	Both	Two-component system sensor histidine kinase	136.0	Nonsyn	gcc	gTc	2558C>T	Ala853Val	Missense variant	Moderate

NZ_AEWG01000047	52201	Both	Hypothetical protein	104.5	Insertion	gccttttttgc	gcCTTTTTTTTgc	119_120insT	Cys40_Ser41fs	Frameshift variant	High
NZ_AEWG01000052	2214	Glc-genome	Esterase/lipase/thioesterase family active site	107.5	Deletion	tctggggg	tcTGGGGG	27delG	Gly9fs	Frameshift variant	High
NZ_AEWG01000056	1515	Glc-genome	Hypothetical protein	85.5	Deletion	gggggtcg	GGGGGTcg	124delG	Gly42fs	Frameshift variant	High
NZ_AEWG01000057	9972	Glc-genome	Hypothetical protein	104.5	Insertion	acaaaaaaaggcacgtccaag	aCAAAAAAAAA, CAAAAAAAAAAggcacgtccaag	115_116insA	Gly39_Thr40fs	Frameshift variant	High
NZ_AEWG01000059	22715	Both	N5-carboxyaminoimidazole ribonucleotide synthase (EC 6.3.4.18)	111.0	Nonsyn	ccg	cAg	287C>A	Pro96Gln	Missense variant	Moderate
NZ_AEWG01000068	1946	Glc-genome	Inner membrane protein translocase and chaperone YidC, long form	214.5	Insertion	gaccagaacgtggtcctgctggaccgtgtcgccgcgcgc	gACCAGAACGTGGTCCTGCTCCAGAACGTGGTCCTGCTgaccgtgtcgccgcgcgc	360_361insCCAGAACGTGGTCCTGCT	Leu120_Asp121insLeuGlnAsnValValLeuLeu	Disruptive inframe insertion	Moderate
NZ_AEWG01000070	24600	Glc-genome	Para-aminobenzoate synthase, aminase component (EC 2.6.1.85) / aminodeoxychorismate lyase (EC 4.1.3.38)	125.5	Deletion	ctgggg	cTGGG	1308delG	Gly436fs	Frameshift variant	High
NZ_AEWG01000073	7020	Glc-genome	Outer membrane component of tam transport system	119.5	Deletion	tggggggca	TGGGGGca	1753delG	Ala585fs	Frameshift variant	High

NZ_AEWG01000074	153409	Both	ATP-dependent RNA helicase RhlE (EC 3.6.4.13)	124.5	Insertion	gggggcgcggtggtgcgt	GGGGGGGC,GGGGGCgcggtggtgcgt	1302_1303insG	Ala434_Gly435fs	Frameshift variant	High
NZ_AEWG01000076	103003	Both	5'-nucleotidase SurE (EC 3.1.3.5)	131.0	Nonsyn	tgc	tgG	69C>G	Cys23Trp	Missense variant	Moderate
NZ_AEWG01000076	133060	Glc-genome	Hypothetical protein	214.5	Insertion	gagacc	gAGGacc	1303_1304insG	Thr435_Arg436fs	Frameshift variant	High
NZ_AEWG01000077	1459	Glc-genome	Lead, cadmium, zinc and mercury transporting ATPase (EC 3.6.3.3) (EC 3.6.3.5)	126.5	Insertion	ccgccccccg	ccGCCCCCCg	249_250insC	Pro83_Ala84fs	Frameshift variant	High
NZ_AEWG01000079	14994	Both	Malate dehydrogenase (EC 1.1.1.37)	107.0	Nonsyn	cag	cTg	149A>T	Gln50Leu	Missense variant	Moderate
NZ_AEWG01000084	19755	Both	ABC transporter, permease protein (cluster 12, methionine/phosphonates)	126.0	Synon	gtc	gtA	204C>A	Val68Val	Synonymous variant	Low
NZ_AEWG01000090	20	Both	ATP-dependent helicase HrpA	97.5	Deletion	cacccccag	cACCCCCag	25delC	Gln9fs	Frameshift variant	High
NZ_AEWG01000101	26265	Glc-genome	Hypothetical protein	160.5	Insertion	gcccgg	gCCCCGg	91_92insC	Ala31_Arg32fs	Frameshift variant	High
NZ_AEWG01000101	26289	Both	Hypothetical protein	119.5	Insertion	gtggtt	gtGGGTt	68_69insG	Val23_Val24fs	Frameshift variant	High
NZ_AEWG01000105	37553	Both	Hypothetical protein	87.5	Deletion	gccccccgt	gCCCCCGt	134delC	Ala45fs	Frameshift variant	High
NZ_AEWG01000106	13465	Both	Geranyl-CoA carboxylase biotin-containing subunit (EC 6.4.1.5)	67.5	Insertion	ccgccccccgctgcggccagccg	ccGCCCCCCCC,GCCCCCCCCCgctgcggccagccg	1562_1563insC	Arg521_Cys522fs	Frameshift variant	High
NZ_AEWG01000113	53096	Both	Dolichol-p-glucose synthetase, (glycosyltransferase)	96.0	Synon	atc	atA	135C>A	Ile45Ile	Synonymous variant	Low

NZ_AEWG01000113	62484	Both	Hypothetical protein	125.0	Nonsyn	gtg	gAg	2T>A	Val1Glu	Missense variant	Moderate
NZ_AEWG01000122	1338	Both	Hypothetical protein	198.5	Deletion	tgggca	tGGCa	74delG	Trp25fs	Frameshift variant	High
NZ_AEWG01000128	7701	Both	Putative iron-regulated membrane protein	115.5	Deletion	gccgggggc	gcCGGGGc	1502delG	Gly501fs	Frameshift variant	High
NZ_AEWG01000141	60983	Both	Long chain acyl-CoA dehydrogenase [fadn-fada-fade operon] (EC 1.3.8.8)	133.0	Nonsyn	tgc	Cgc	754T>C	Cys252Arg	Missense variant	Moderate
NZ_AEWG01000141	66601	Glc-genome	3-ketoacyl-CoA thiolase [fadn-fada-fade operon] (EC 2.3.1.16)	96.5	Deletion	atggggga	aTGGGGca	1168delG	Ala390fs	Frameshift variant	High
NZ_AEWG01000141	66673	Glc-genome	3-ketoacyl-CoA thiolase [fadn-fada-fade operon] (EC 2.3.1.16)	120.5	Insertion	ggccccaa	gGCCCCCCaa	1241_1242insC	Gln414_Pro415fs	Frameshift variant	High
NZ_AEWG01000157	7770	Both	Flagellar biosynthesis protein FlhF	88.0	Nonsyn	acc	Gcc	58A>G	Thr20Ala	Missense variant	Moderate
NZ_AEWG01000158	30172	Both	Transcriptional regulator, AcrR family	88.0	Nonsyn	aag	Gag	52A>G	Lys18Glu	Missense variant	Moderate
NZ_AEWG01000159	30352	Both	Porin, Gram-negative type	106.0	Nonsyn	cgc	Agc	283C>A	Arg95Ser	Missense variant	Moderate
NZ_AEWG01000159	54093	Both	Fumarylacetoacetate hydrolase family protein	149.0	Nonsyn	cac	cGc	698A>G	His233Arg	Missense variant	Moderate

Both, variation observed in both the genomes; Glc-genome, variation observed only in the glc-genome; Synon, synonymous substitution; Nonsyn, nonsynonymous substitution; Ref_nt, nucleotide of the reference genome; Var_nt, nucleotide of the aligned genome; Ref_aa, amino acid of the reference genome.

References

References

Adams, M. D., Celniker, S. E., Holt, R. A., Evans, C. A., Gocayne, J. D., Amanatides, P. G., Scherer, S. E., Li, P. W., Hoskins, R. A., Galle, R. F., George, R. A., Lewis, S. E., Richards, S., Ashburner, M., Henderson, S. N., Sutton, G. G., Wortman, J. R., Yandell, M. D., Zhang, Q., Craig Venter, J. (2000). The genome sequence of *Drosophila melanogaster*. *Science*, *287*(5461), 2185–2195.

Adnan, F., Weber, L., and Klug, G. (2015). The sRNA SorY confers resistance during photooxidative stress by affecting a metabolite transporter in *Rhodobacter sphaeroides*. *RNA Biology*, *12*(5), 569–577.

Agalidis, I., Rivas, E., and Reiss-Husson, F. (1990). Reaction center light harvesting B875 complexes from *Rhodocyclus gelatinosus*: characterization and identification of quinones. *Photosynthesis Research*, *23*(3), 249–255.

Aidelberg, G., Towbin, B. D., Rothschild, D., Dekel, E., Bren, A., and Alon, U. (2014). Hierarchy of non-glucose sugars in *Escherichia coli*. *BMC Systems Biology*, *8*(1), 133.

Allen, J., Davey, H. M., Broadhurst, D., Heald, J. K., Rowland, J. J., Oliver, S. G., and Kell, D. B. (2003). High-throughput classification of yeast mutants for functional genomics using metabolic footprinting. *Nature Biotechnology*, *21*(6), 692–696.

Argos, P., Kamer, G., Nicklin, M. J. H., and Wimmer, E. (1984). Similarity in gene organization and homology between proteins of animal picomaviruses and a plant comovirus suggest common ancestry of these virus families. In *Nucleic Acids Research* (Vol. 12, Issue 18, pp. 7251–7267).

Aziz R.K., Bartels D., Best A.A., DeJongh M., Disz T., Edwards R.A., Formsma K., Gerdes S., Glass E.M., Kubal M., Meyer F., Olsen G.J., Olson R., Osterman A.L., Overbeek R.A., McNeil L.K., Paarmann D., Paczian T., Parrello B., Pusch G.D., Reich C., Stevens R., Vassieva O., Vonstein V., Wilke A. and Zagnitko O. 2008. The RAST server: rapid annotations using subsystems technology. *BMC Genomics* **9**, 75-89.

Badenoch-Jones, J., Summons, R. E., and Djordjevic, M. A. (1982). Mass spectrometric quantification of indole-3-acetic acid in *Rhizobium* culture supernatants: Relation to root hair curling and nodule initiation. *Applied and Environmental Microbiology*, *44*(2), 275–280.

Bakan, E., Yildirim, A., Kurtul, N., Polat, M. F., Dursun, H., and Cayir, K. (2006). Effects of type 2 diabetes mellitus on plasma fatty acid composition and cholesterol content of erythrocyte and leukocyte membranes. *Acta Diabetologica*, *43*(4), 109–113.

Barros e Silva, A. E., and Guerra, M. (2010). The meaning of DAPI bands observed after C-banding and FISH procedures. *Biotechnic & Histochemistry : Official Publication of the Biological Stain Commission*, *85*(2), 115–125.

Batzoglou, S., Pachter, L., Mesirov, J. P., Berger, B., and Lander, E. S. (2000). Human and mouse gene structure: Comparative analysis and application to exon prediction. *Genome Research*, *10*(7), 950–958.

Bergkessel, M., Basta, D. W., and Newman, D. K. (2016). The physiology of growth arrest: uniting molecular and environmental microbiology. *Nature Reviews Microbiology*, *14*(9), 549–562.

Bester, E., Kroukamp, O., Hausner, M., Edwards, E. A., and Wolfaardt, G. M. (2011). Biofilm form and function: Carbon availability affects biofilm architecture, metabolic activity and planktonic cell yield. *Journal of Applied Microbiology*, *110*(2), 387–398.

Bhattacharyya A., et al., 2002. Draft sequencing and comparative genomics of *Xylella fastidiosa* strains reveal novel biological insights. Genome Res. 12; 1556-563.

Blankenship R.E., 2002. Molecular mechanism of Photosynthesis Oxford: Blackwell Science Ltd.

Boller, T., and Felix, G. (2009). A Renaissance of Elicitors: Perception of Microbe-Associated Molecular Patterns and Danger Signals by Pattern-Recognition Receptors. *Annual Review of Plant Biology*, *60*(1), 379–406.

Bobrovskyy, M., and Vanderpool, C. K. (2013). Regulation of Bacterial Metabolism by Small RNAs Using Diverse Mechanisms. *Annual Review of Genetics*, *47*(1), 209–232.

Boutte, C. C., and Crosson, S. (2013). Bacterial lifestyle shapes stringent response activation. *Trends in Microbiology*, *21*(4), 174–180.

Braatsch, S., Gomelsky, M., Kuphal, S., and Klug, G. (2002). A single flavoprotein, AppA, integrates both redox and light signals in *Rhodobacter sphaeroides*. *Molecular Microbiology*, *45*(3), 827–836.

Bren, A., Park, J. O., Towbin, B. D., Dekel, E., Rabinowitz, J. D., and Alon, U. (2016). Glucose becomes one of the worst carbon sources for *E.coli* on poor nitrogen sources due to suboptimal levels of cAMP. *Scientific Reports*, *6*(December 2015), 2–11.

Buddhi, S., G., S., Gupta, D., Ch., S., and Ch. V., R. (2020). *Afifella aestuarii* sp. nov., a phototrophic bacterium. *International Journal of Systematic and Evolutionary Microbiology*, *70*(1), 327–333.

Carbonero, F., Oakley, B. B., and Purdy, K. J. (2014). Metabolic flexibility as a major predictor of spatial distribution in microbial communities. *PLoS ONE*, *9*(1).

Carja, O., Liberman, U., and Feldman, M. W. (2014). The evolution of phenotypic switching in subdivided populations. *Genetics*, *196*(4), 1185–1197.

Carneiro, S., Villas-Bôas, S., Ferreira, E. C., and Rocha, I. (2016). A Comparative Proteome Analysis of *Escherichia coli* ΔrelA Mutant Cells. *Frontiers in Bioengineering and*

Biotechnology, *4*(October), 1–12.

Chantranupong, L., Wolfson, R. L., and Sabatini, D. M. (2015). Nutrient-sensing mechanisms across evolution. *Cell*, *161*(1), 67–83.

Chen, X., Schreiber, K., Appel, J., Makowka, A., Fähnrich, B., Roettger, M., Hajirezaei, M. R., Sönnichsen, F. D., Schönheit, P., Martin, W. F., and Gutekunst, K. (2016). The Entner–Doudoroff pathway is an overlooked glycolytic route in cyanobacteria and plants. *Proceedings of the National Academy of Sciences*, *113*(19), 5441–5446.

Choi, M. Y., Wang, Y., Wong, L. L. Y., Lu, B. tai, Chen, W. yang, Huang, J. D., Tanner, J. A., and Watt, R. M. (2012). The two PPX-GppA homologues from *Mycobacterium tuberculosis* have distinct biochemical activities. *PLoS ONE*, *7*(8).

Consortium, C. elegans S. (1998). Genome Sequence of the Nematode *C. elegans:* A Platform for Investigating Biology. *Science*, *282*(5396), 2012–2018.

Das, G., and Varshney, U. (2006). Peptidyl-tRNA hydrolase and its critical role in protein biosynthesis. *Microbiology*, *152*(8), 2191–2195.

De Maayer, P., Anderson, D., Cary, C., and Cowan, D. A. (2014). Some like it cold: Understanding the survival strategies of psychrophiles. *EMBO Reports*, *15*(5), 508–517.

Denich, T. J., Beaudette, L. A., Lee, H., and Trevors, J. T. (2003). Effect of selected environmental and physico-chemical factors on bacterial cytoplasmic membranes. In *Journal of Microbiological Methods* (Vol. 52, Issue 2).

Deutscher, M. P. (2003). Degradation of Stable RNA in Bacteria. *Journal of Biological Chemistry*, *278*(46), 45041–45044.

Dunlop, M.J. (2011) Engineering microbes for tolerance to next-generation biofuels. Biotechnol Biofuels 4: 32.

Eckstein, A., Zieba, P., and Gabryś, H. (2012). Sugar and Light Effects on the Condition of the Photosynthetic Apparatus of *Arabidopsis thaliana* Cultured in vitro. *Journal of Plant Growth Regulation*, *31*(1), 90–101.

Errington, J. (2003). Regulation of endospore formation in *Bacillus subtilis*. *Nature Reviews Microbiology*, *1*(2), 117–126.

Fakhruddin, S., Alanazi, W., and Jackson, K. E. (2017). Diabetes-Induced Reactive Oxygen Species: Mechanism of Their Generation and Role in Renal Injury. *Journal of Diabetes Research*, *2017*.

Flamholz, A., Noor, E., Bar-Even, A., Liebermeister, W., and Milo, R. (2013). Glycolytic strategy as a tradeoff between energy yield and protein cost. *Proceedings of the National Academy of Sciences*, *110*(24), 10039–10044.

Fleischmann, R. D., Adams, M. D., White, O., Clayton, R. A., Kirkness, E. F., Kerlavage, A.

R., Bult, C. J., Tomb, J. F., Dougherty, B. A., Merrick, J. M., McKenney, K., Sutton, G., FitzHugh, W., Fields, C., Gocayne, J. D., Scott, J., Shirley, R., Liu, L. I., Glodek, A., Venter, J. C. (1995). Whole-genome random sequencing and assembly of *Haemophilus influenzae* Rd. *Science*, *269*(5223), 496–512.

Fu, Z., Verderame, T. D., Leighton, J. M., Sampey, B. P., Appelbaum, E. R., Patel, P. S., and Aon, J. C. (2014). Exometabolome analysis reveals hypoxia at the up-scaling of a *Saccharomyces cerevisiae* high-cell density fed-batch biopharmaceutical process. *Microbial Cell Factories*, *13*(1), 1–22.

Fraser, C. M., Gocayne, J. D., White, O., Adams, M. D., Clayton, R. A., Fleischmann, R. D., Bult, C. J., Kerlavage, A. R., Sutton, G., Kelley, J. M., Fritchman, J. L., Weidman, J. F., Small, K. V., Sandusky, M., Fuhrmann, J., Nguyen, D., Utterback, T. R., Saudek, D. M., Phillips, C. A., Venter, J. C. (1995). The minimal gene complement of *Mycoplasma genitalium*. *Science*, *270*(5235), 397–403.

Gaca, A. O., Colomer-Winter, C., and Lemos, J. A. (2015). Many means to a common end: The intricacies of (p)ppGpp metabolism and its control of bacterial homeostasis. In *Journal of Bacteriology* (Vol. 197, Issue 7, pp. 1146–1156).

Galan, B., Dinjaski, N., Maestro, B., de Eugenio, L.I., Escapa, I.F., Sanz, J.M. et al. (2012) Nucleoid-associated PhaF phasin drives intracellular location and segregation of polyhydroxyalkanoate granules in *Pseudomonas putida* KT2442. Mol Microbiol 79: 402- 418.

Gengenbacher, M., and Kaufmann, S. H. E. (2012). *Mycobacterium tuberculosis*: Success through dormancy. In *FEMS Microbiology Reviews* (Vol. 36, Issue 3, pp. 514–532).

Gennis, R. B., Barquera B., Hacker B., Doren S. R. V., Arnaud S., Crofts A. R., Davidson E., Gray K. A. and Daldal F., 1993. The bc1 complexes of *Rhodobacter sphaeroides* and *Rhodobacter capsulatus*. *Journal of Bioenergetics and biomembranes*. Vol. 25; 195-209.

GEST, H., and KAMEN, M. D. (1949). Studies on the metabolism of photosynthetic bacteria; photochemical. *Journal of Bacteriology*, *58*(2), 239–245.

Glaeser, J., and Klug, G. (2005). Photo-oxidative stress in *Rhodobacter sphaeroides*: Protective role of carotenoids and expression of selected genes. *Microbiology*, *151*(6), 1927–1938.

Goffeau, A., Barrell, B. G., Bussey, H., Davis, R. W., Dujon, B., Feldmann, H., Galibert, F., Hoheisel, J. D., Jacq, C., Johnston, M., Louis, E. J., Mewes, H. W., Murakami, Y., Philippsen, P., Tettelin, H., and Oliver, S. G. (1996). Life with 6000 Genes. *Science*, *274*(October), 546–567.

Goo Y. A., Roach J., Glusman G., Baliga N. S., Deutsch K., Pan M., Kennedy S., Das Sharma S., Wallap V. and Hood L., 2004. Low-pass sequencing for microbial comparative genomics, *BMC Genomcis* 5; 3.

Gorenflo, V., Steinbuchel, A., Marose, S., Rieseberg, M., and Scheper, T. (1999) Quantification of bacterial polyhydroxyalkanoic acids by Nile red staining. Appl Microbiol Biotechnol 51: 765-772.

Görke, B., and Stülke, J. (2008). Carbon catabolite repression in bacteria: Many ways to make the most out of nutrients. *Nature Reviews Microbiology*, *6*(8), 613–624.

Graverholt, O. S., and Eriksen, N. T. (2007). Heterotrophic high-cell-density fed-batch and continuous-flow cultures of *Galdieria sulphuraria* and production of phycocyanin. *Applied Microbiology and Biotechnology*, *77*(1), 69–75.

Grabowicz, M., and Silhavy, T. J. (2017). Envelope Stress Responses: An Interconnected Safety Net. *Trends in Biochemical Sciences*, *42*(3), 232–242.

Graverholt, O. S., and Eriksen, N. T. (2007). Heterotrophic high-cell-density fed-batch and continuous-flow cultures of *Galdieria sulphuraria* and production of phycocyanin. *Applied Microbiology and Biotechnology*, *77*(1), 69–75.

Gupta, D., Mohammed, M., Mekala, L. P., Chintalapati, S., and Chintalapati, V. R. (2019). iTRAQ-based quantitative proteomics reveals insights into metabolic and molecular responses of glucose-grown cells of *Rubrivivax benzoatilyticus* JA2. *Journal of Proteomics*, *194*, 49–59.

Hardison, R. C. (2003). Comparative genomics. *PLoS Biology*, *1*(2), 156–160.

Hassani, B. K., Steunou, A. S., Liotenberg, S., Reiss-Husson, F., Astier, C., and Ouchane, S. (2010). Adaptation to oxygen: Role of terminal oxidases in photosynthesis initiation in the purple photosynthetic bacterium, *Rubrivivax gelatinosus*. *Journal of Biological Chemistry*, *285*(26), 19891–19899.

Hdider, C., and Desjardins, Y. (1994). Effects of sucrose on photosynthesis and phosphoenolpyruvate carboxylase activity of in vitro cultured strawberry plantlets. *Plant Cell, Tissue and Organ Culture*, *36*(1), 27–33.

Hecker, M., and Völker, U. (1990). General stress proteins in *Bacillus subtilis*. *FEMS Microbiology Ecology*, *7*(2–3), 197–213.

Hiraishi, A., Shi, J. L., and Kitamura, H. (1989). Effects of Organic Nutrient Strength on the Purple Nonsulfur Bacterial Content and Metabolic Activity of Photosynthetic Sludge for Wastewater Treatment. *Journal of Fermentation and Bioengineering*, *68*(4), 269–276.

Hu, B., Xie, G., Lo, C. C., Starkenburg, S. R., and Chain, P. S. G. (2011). Pathogen comparative genomics in the next-generation sequencing era: Genome alignments, pangenomics and metagenomics. *Briefings in Functional Genomics*, *10*(6), 322–333.

Hülsen, T., Barry, E. M., Lu, Y., Puyol, D., Keller, J., and Batstone, D. J. (2016). Domestic wastewater treatment with purple phototrophic bacteria using a novel continuous photo anaerobic membrane bioreactor. *Water Research*, *100*, 486–495.

Huylenbroeck, J. M., and Debergh, P. C. (1996). Impact of sugar concentration in vitro on photosynthesis and carbon metabolism during ex vitro acclimatization of *Spathiphyllum* plantlets. *Physiologia Plantarum*, *96*(2), 298–304.

Imhoff, J. F. (2001). True marine and halophilic anoxygenic phototrophic bacteria. *Arch Microbiol*, *176*, 243–254.

Jang, J.-C., and Sheen ', J. (1994). Sugar Sensing in Higher Plants. *The Plant Cell*, *6*(Box 1), 1665–1679.

Kaberdin, V. R., Montánchez, I., Parada, C., Orruño, M., Arana, I., and Barcina, I. (2015). Unveiling the metabolic pathways associated with the adaptive reduction of cell size during *Vibrio harveyi* persistence in seawater microcosms. *Microbial Ecology*, *70*(3), 689–700.

Kashmiri, Z. N., and Mankar, S. A. (2014). Free radicals and oxidative stress in bacteria. *Int.J.Curr.Microbiol.App.Sci*, *3*(9), 34–40.

Kell, D. B., Brown, M., Davey, H. M., Dunn, W. B., Spasic, I., and Oliver, S. G. (2005). Metabolic footprinting and systems biology: The medium is the message. *Nature Reviews Microbiology*, *3*(7), 557–565.

Kiley, P. J., and Kaplan, S. (1988). Molecular genetics of photosynthetic membrane biosynthesis in *Rhodobacter sphaeroides*. *Microbiological Reviews*, *52*(1), 50–69.

Kim, S. A., and Copeland, L. (1997). Acetyl coenzyme A acetyltransferase of *Rhizobium* sp. (Cicer) strain CC 1192. *Applied and Environmental Microbiology*, *63*(9), 3432–3437.

Kobayashi, M., and Kobayashi, M. (1995). Waste Remediation and Treatment Using Anoxygenic Phototrophic Bacteria. In *Anoxygenic Photosynthetic Bacteria* (pp. 1269–1282). Kluwer Academic Publishers.

Koch, A. L. (1997). Microbial physiology and ecology of slow growth. *Microbiology and Molecular Biology Reviews : MMBR*, *61*(3), 305–318.

Koch, K. E. (1996). Carbohydrate-Modulated Gene Expression in Plants. *Annual Review of Plant Physiology and Plant Molecular Biology*, *47*(1), 509–540.

Koonin, E. V., and Deutscher, M. P. (1993). Rnase T shares conserved sequence motifs with DNA proofreading exonucleases. *Nucleic Acids Research*, *21*(10), 2521–2522.

Kotte, O., Volkmer, B., Radzikowski, J. L., and Heinemann, M. (2014). Phenotypic bistability in *Escherichia coli*'s central carbon metabolism. *Molecular Systems Biology*, *10*(7), 736–736.

Kotte, Oliver, Zaugg, J. B., and Heinemann, M. (2010). Bacterial adaptation through distributed sensing of metabolic fluxes. *Molecular Systems Biology*, *6*(355), 1–9.

Koziel, A., Woyda-Ploszczyca, A., Kicinska, A., and Jarmuszkiewicz, W. (2012). The

influence of high glucose on the aerobic metabolism of endothelial EA.hy926 cells. *Pflugers Archiv European Journal of Physiology*, *464*(6), 657–669.

Krebs, S. J., and Taylor, R. K. (2011). Nutrient-dependent, rapid transition of *Vibrio cholerae* to coccoid morphology and expression of the toxin co-regulated pilus in this form. *Microbiology*, *157*(10), 2942–2953.

Kwak, J.M., Nguyen, V., and Schroeder, J.I. (2006) The role of reactive oxygen species in hormonal responses. *Plant Physiol* 141: 323-329.

Larimer, F. W., Chain, P., Hauser, L., Lamerdin, J., Malfatti, S., Do, L., Land, M. L., Pelletier, D. A., Beatty, J. T., Lang, A. S., Tabita, F. R., Gibson, J. L., Hanson, T. E., Bobst, C., Torres Y Torres, J. L., Peres, C., Harrison, F. H., Gibson, J., and Harwood, C. S. (2004). Complete genome sequence of the metabolically versatile photosynthetic bacterium *Rhodopseudomonas palustris*. *Nature Biotechnology*, *22*(1), 55–61.

Lebedeva, N. V., Boichenko, V. A., Semenova, L. R., Pronina, N. A., and Stadnichuk, I. N. (2005). Effects of glucose during photoheterotrophic growth of the cyanobacterium *Calothrix* sp. PCC 7601 capable for chromatic adaptation. *Russian Journal of Plant Physiology*, *52*(2), 235–241.

Lee, K., Xia, L., Goldberg, H., Whiteside, C., and Fantus, G. (2012). High Glucose Induces ROS Production by NADPH Oxidases via a SRC-dependent Mechanism. *Canadian Journal of Diabetes*, *36*(5), S50–S51.

Lin, Y., Bogdanov, M., Tong, S., Guan, Z., and Zheng, L. (2016). Substrate selectivity of lysophospholipid transporter LplT involved in membrane phospholipid remodeling in Escherichia coli. *Journal of Biological Chemistry*, *291*(5), 2136–2149.

Lindahl, T. (1993). Instability and decay of the primary structure of DNA. *Nature*, *362*, 709–715.

Lo, R. L., and Pe, R. (2004). Differential regulation of soluble and membrane-bound inorganic pyrophosphatases in the photosynthetic bacterium *Rhodospirillum rubrum* provides insights into pyrophosphate-based stress bioenergetics. *Journal of Bacteriology*, *186*(16), 5418–5426.

Liotenberg S., Steunou A. S., Picaud M., Reiss-Husson F., Astier G., et al., 2008. Organisation and expression of photosynthesis genes and operons in anoxygenic photosynthetic proteobactria. *Environ. Microbiol*. 10; 2267-2276.

Louie, K. B., Bowen, B. P., Cheng, X., Berleman, J. E., Chakraborty, R., Deutschbauer, A., Arkin, A., and Northen, T. R. (2013). "Replica-Extraction-Transfer" nanostructure-initiator mass spectrometry imaging of acoustically printed bacteria. *Analytical Chemistry*, *85*(22), 10856–10862.

Lu, Y., Goodson, C., Blankenship, R. E., and Gross, M. L. (2018). Primary and higher order structure of the reaction center from the purple phototrophic bacterium *Blastochloris*

viridis: A test for native mass spectrometry. *Journal of Proteome Research*, *17*(4), 1615–1623.

Luo, J., Xiang, Y., Xu, X., Fang, D., Li, D., Ni, F., Zhu, X., Chen, B., and Zhou, M. (2018). High glucose-induced ROS production stimulates proliferation of pancreatic cancer via inactivating the JNK pathway. *Oxidative Medicine and Cellular Longevity*, *2018*.

Madigan, M. T. (2003). Anoxygenic phototrophic bacteria from extreme environments. *Photosynthesis Research*, *76*, 157–171.

Mackie, G. A. (2013). RNase E : at the interface of bacterial RNA processing and decay. *Nature Reviews Microbiology*, *11*(1), 45–57.

Madigan, M. T., and Jung, D. O. (2009). An overview of purple bacteria: systematics, physiology, and habitats. In *The Purple Phototrophic Bacteria* (eds. Hunter C. N., Daldal F., Thurnauer M. C. and Beatty J. T.) (pp. 1–15).

Madukasi, E. I., Dai, X., He, C., and Zhou, J. (2010). Potentials of phototrophic bacteria in treating pharmaceutical wastewater. *International Journal of Environmental Science and Technology*, *7*(1), 165–174.

Mahidhara, G., Gupta, D., Sasikala, C., and Ramana, C. V. (2020). Insights into discrepancy in power generation among glucose and malate grown *Rubrivivax benzoatilyticus* JA2 microbial fuel cells. *International Journal of Hydrogen Energy*, *46*(4), 3090–3104.

Maness, P. C., Smolinski, S., Dillon, A. C., Heben, M. J., and Weaver, P. F. (2002). Characterization of the oxygen tolerance of a hydrogenase linked to a carbon monoxide oxidation pathway in *Rubrivivax gelatinosus*. *Applied and Environmental Microbiology*, *68*(6), 2633–2636.

Mapelli, V., Olsson, L., and Nielsen, J. (2008). Metabolic footprinting in microbiology: methods and applications in functional genomics and biotechnology. *Trends in Biotechnology*, *26*(9), 490–497.

Mcgeoch, D. J., and Davison, A. J. (1986). DNA sequence of the herpes simplex virus type 1 gene encoding glycoprotein gH, and identification of homologues in the genomes of varicella-zoster virus and Epstein-Barr virus. In *Nucleic Acids Research* (Vol. 14, Issue 10, pp. 4281–4292).

Mekala, L. P., Mohammed, M., Chintalapati, S., and Chintalapati, V. R. (2018). Stable Isotope-Assisted Metabolic Profiling Reveals Growth Mode Dependent Differential Metabolism and Multiple Catabolic Pathways of l -Phenylalanine in *Rubrivivax benzoatilyticus* JA2. *Journal of Proteome Research*, *17*(1), 189–202.

Mekala, L. P., Mohammed, M., Chintalapati, S., and Chintalapati, V. R. (2019). Precursor-feeding and altered-growth conditions reveal novel blue pigment production by *Rubrivivax benzoatilyticus* JA2. *Biotechnology Letters*, *41*(6–7), 813–822.

Mohammed, M., Isukapatla, A., Mekala, L. P., Venkata, R. P. E. V., Chintalapati, S., and Chintalapati, V. R. (2011). Genome sequence of the phototrophic betaproteobacterium *Rubrivivax benzoatilyticus* strain JA2T. *Journal of Bacteriology*, *193*(11), 2898–2899.

Molière, N., and Turgay, K. (2009). Chaperone-protease systems in regulation and protein quality control in *Bacillus subtilis*. *Research in Microbiology*, *160*(9), 637–644.

Morishige, Y., Tanda, M., Fujimori, K., Mino, Y., and Amano, F. (2014). Induction of Viable but Non-culturable (VBNC) State in *Salmonella* cultured in m9 minimal medium containing high glucose. *Biological and Pharmaceutical Bulletin*, *37*(10), 1617–1625.

Mujahid, M., Prasuna, M. L., Sasikala, C., and Ramana, C. V. (2015). Integrated metabolomic and proteomic analysis reveals systemic responses of *Rubrivivax benzoatilyticus* JA2 to aniline stress. *Journal of Proteome Research*, *14*(2), 711–727.

Mujahid, M., Sasikala, C., and Ramana, C. V. (2013). Carbon catabolite repression-independent and ph-dependent production of indoles by *Rubrivivax benzoatilyticus* JA2. *Current Microbiology*, *67*(4), 399–405.

Nagashima, K. V. P., Hiraishi, A., Shimada, K., and Matsuura, K. (1997). Horizontal transfer of genes coding for the photosynthetic reaction centers of purple bacteria. *J Mol. Evol.*, *45*, 131–136.

Naylor G. W., Addlesee H. A., Gibson L. C. D. and Hunter C. N., 1999. The photosynthetic gene cluster of *Rhodobacter sphaeroides*, *Photosynthesis Research*, 62; 121-39.

Njoroge, J. W., Nguyen, Y., Curtis, M. M., Moreira, C. G., and Sperandio, V. (2012). Virulence meets metabolism: Cra and KdpE gene regulation in enterohemorrhagic Escherichia coli. *MBio*, *3*(5), 1–12.

Nyström, T., and Gustavsson, N. (1998). Maintenance energy requirement: what is required for stasis survival of *Escherichia coli*? *Biochimica et Biophysica Acta (BBA) - Bioenergetics*, *1365*(1–2), 225–231.

Oesterhelt, C., Schmälzlin, E., Schmitt, J. M., and Lokstein, H. (2007). Regulation of photosynthesis in the unicellular acidophilic red alga *Galdieria sulphuraria*. *Plant Journal*, *51*(3), 500–511.

Pasupulati, A. K., Dunna, N. R., and Talluri, S. (2019). Metabolic Adaptations in Diabetes Mellitus and Cancer. In G. P. Nagaraju and A. BM Reddy (Eds.), *Exploring Pancreatic Metabolism and Malignancy* (pp. 53–69). Springer Singapore.

Pfennig, N. (1969). *Rhodospirillum acidophila* sp. n., a new species of the budding purple nonsulfur bacteria. *Journal of Bacteriology*, *99*(2), 597–602.

Pfennig, N. (1974). *Rhodopseudomonas globiformis*, sp. n., a new species of the Rhodospirillaceae. *Arch. Microbiol.*, *206*, 197–206.

Pfennig, N. (1977). Phototrophic green and purple bacteria : A comparative, systematic

survey. *Ann. Rev. Microbiol.*, 275–290.

Pinto, D., Santos, M. A., and Chambel, L. (2013). Thirty years of viable but nonculturable state research: Unsolved molecular mechanisms. *Critical Reviews in Microbiology*, *41*(1), 61–76.

Pinu, F. R., Granucci, N., Daniell, J., Han, T. L., Carneiro, S., Rocha, I., Nielsen, J., and Villas-Boas, S. G. (2018). Metabolite secretion in microorganisms: the theory of metabolic overflow put to the test. *Metabolomics*, *14*(4), 1–16.

Poulsen, R. C., Knowles, H. J., Carr, A. J., and Hulley, P. A. (2014). Cell differentiation versus cell death: Extracellular glucose is a key determinant of cell fate following oxidative stress exposure. *Cell Death and Disease*, *5*(2), 1–12.

Quillaguaman, J., Guzman, H., Van-Thuoc, D., and Hatti-Kaul, R. (2010) Synthesis and production of polyhydroxyalkanoates by halophiles: current potential and future prospects. Appl Microbiol Biotechnol 85: 1687-1696.

Ramana, C. V., Sasikala, C., Arunasri, K., Anil Kumar, P., Srinivas, T. N. R., Shivaji, S., Gupta, P., Süling, J., and Imhoff, J. F. (2006). *Rubrivivax benzoatilyticus* sp. nov., an aromatic hydrocarbon-degrading purple betaproteobacterium. *International Journal of Systematic and Evolutionary Microbiology*, *56*(9), 2157–2164.

Ramaprasad, E. V. V., Sasikala, C., and Ramana, C. V. (2013). Neurosporene is the major carotenoid accumulated by *Rhodobacter viridis* JA737. *Biotechnology Letters*, *35*(7), 1093–1097.

Raymond J., Zhaxybayeva O., Gogarten J. P. and Blankenship R. E.., 2003. Evolution of photosynthetic prokaryotes: A maximum likelihood mapping approach. *Phil Tran Roy Soc Lond B Biol Sci.* 358; 223-30.

Roh, J. H., Smith, W. E., and Kaplan, S. (2004). Effects of oxygen and light intensity on transcriptome expression in *Rhodobacter sphaeroides* 2.4.1: Redox active gene expression profile. *Journal of Biological Chemistry*, *279*(10), 9146–9155.

Rubin, G. M., Rubin, G. M., Yandell, M. D., Wortman, J. R., Miklos, G. L. G., Nelson, C. R., Hariharan, I. K., Fortini, M. E., Li, P. W., Apweiler, R., Fleischmann, W., Cherry, J. M., Henikoff, S., Skupski, M. P., Misra, S., Ashburner, M., Birney, E., Boguski, M. S., Vosshall, L. B., … Gibbs, R. (2000). Comparative Genomics of the Eukaryotes. *Science*, *287*(5461), 2204–2215.

Ruiz, B., Chávez, A., Forero, A., García-Huante, Y., Romero, A., Snchez, M., Rocha, D., Snchez, B., Rodríguez-Sanoja, R., Sánchez, S., and Langley, E. (2010). Production of microbial secondary metabolites: Regulation by the carbon source. *Critical Reviews in Microbiology*, *36*(2), 146–167.

Rybczyński, J. J., Borkowska, B., Fiuk, A., Gawrońska, H., Śliwińska, E., and Mikuła, A. (2007). Effect of sucrose concentration on photosynthetic activity of in vitro cultures

Gentiana kurroo (Royle) germlings. *Acta Physiologiae Plantarum*, *29*(5), 445–453.

Salma, M., Rousseaux, S., Sequeira-Le Grand, A., Divol, B., and Alexandre, H. (2013). Characterization of the Viable but Nonculturable (VBNC) State in *Saccharomyces cerevisiae*. *PLoS ONE*, *8*(10), e77600.

Sasikala, C., and Ramana, C. V. (1996). Biodegradable Polyesters. In *Adv Appl Microbiol.* (Vol. 42, pp. 97–218).

Sasikala, C., and Ramana, C. V. (1995a). Biotechnological Potentials of Anoxygenic Phototrophic Bacteria. I. Production of Single-Cell Protein, Vitamins, Ubiquinones, Hormones, and Enzymes and Use in Waste Treatment. In *Advances in Applied Microbiology* (Vol. 41, Issue C, pp. 173–226).

Sasikala, C., and Ramana, C. V. (1995b). Biotechnological Potentials of Anoxygenic Phototrophic Bacteria. II. Biopolyesters, Biopesticide, Biofuel, and Biofertilizer. *Advances in Applied Microbiology*, *41*(C), 227–278.

Sasikala, K., Ramana, V., and Raghuveer, P. (1993). Anoxygenic Phototrophic Bacteria : Physiology and Advances in Hydrogen Production Technology. *ADVANCES IN APPLIED MICROBIOLOGY*, *38*, 211–295.

Schurr, A. (2017). Lactate, Not Pyruvate, Is the End Product of Glucose Metabolism via Glycolysis. In *Carbohydrate*. InTech.

Siefert, E., Irgens, R. L., and Pfennig, N. (1978). Phototrophic purple and green bacteria in a sewage treatment plant. *Applied and Environmental Microbiology*, *35*(1), 38–44.

Ssewanyana, D., Abubakar, A., van Baar, A., Mwangala, P. N., and Newton, C. R. (2018). Perspectives on Underlying Factors for Unhealthy Diet and Sedentary Lifestyle of Adolescents at a Kenyan Coastal Setting. *Frontiers in Public Health*, *6*(February).

Stadnichuk, I. N., Rakhimberdieva, M. G., Bolychevtseva, Y. V., Yurina, N. P., Karapetyan, N. V., and Selyakh, I. O. (1998). Inhibition by glucose of chlorophyll *a* and phycocyanobilin biosynthesis in the unicellular red alga *Galdieria partita* at the stage of coproporphyrinogen III formation. *Plant Science*, *136*(1), 11–23.

Stanley, N. R., and Lazazzera, B. A. (2004). Environmental signals and regulatory pathways that influence biofilm formation. *Molecular Microbiology*, *52*(4), 917–924.

Steunou, A. S., Astier, C., and Ouchane, S. (2004). Regulation of Photosynthesis Genes in *Rubrivivax gelatinosus*: Transcription Factor PpsR Is Involved in both Negative and Positive Control. *Journal of Bacteriology*, *186*(10), 3133–3142.

Suresh, G., Lodha, T. D., Indu, B., Sasikala, C., and Ramana, C. V. (2019). Taxogenomics Resolves Conflict in the Genus *Rhodobacter*: A Two and Half Decades Pending Thought to Reclassify the Genus *Rhodobacter*. *Frontiers in Microbiology*, *10*(OCT), 1–16.

Swingley W. D., Blankenship R. E. and Raymond J., 2009. Evolutionary relationships among purple photosynthetic bacteria and the origin of proteobacterial photosynthetic systems. In: In: Hunter C. N., Daldal F., Thurnauer M. C. and Beatty J. T. (eds) The Purple Photosynthetic Bacteria; 17-29. Springer Science.

Tadros, M. H., Garcia, F., Drews, G., Gad, N., and Skatchkov, M. P. (2000). Isolation and characterization of a light harvesting complex II lacking the 7-polypeptide from *Rhodobacter capsulatus*. *Biochimica et Biophysica Acta*, *1019*(1990), 245–249.

Tambiev, A. H., Shelyastina, N. N., and Kirikova, N. N. (1989). Exometabolites of Lipid Nature from Two Species of Marine Microalgae. *Functional Ecology*, *3*(2), 245–247.

Tang, J. (2011) Microbial metabolomics. Curr Genomics 12: 391-403.

Thomas, V. C., Sadykov, M. R., Chaudhari, S. S., Jones, J., Endres, J. L., Widhelm, T. J., Ahn, J. S., Jawa, R. S., Zimmerman, M. C., and Bayles, K. W. (2014). A central role for carbon-overflow pathways in the modulation of bacterial cell death. *PLoS Pathogens*, *10*(6).

Torres, M.A., Jones, J.D., and Dangl, J.L. (2006) Reactive oxygen species signaling in response to pathogens. Plant Physiol 141: 373-378.

Tremaroli, V., Workentine, M.L., Weljie, A.M., Vogel, H.J., Ceri, H., Viti, C. et al. (2009) Metabolomic investigation of the bacterial response to a metal challenge. Appl Environ Microbiol 75: 719-728.

Vavilova, N. A., Ustinova, M. V., Voinova, T. M., Stepanichenko, N. N., Ten, L. N., Mukhamedzhanov, S. Z., and Dzhavakhiya, V. G. (1988). Polyketide exometabolites of the causative agent of rice blast and their role in pathogenesis. *Chemistry of Natural Compounds*, *24*(4), 487–491.

Volpicella, M., Costanza, A., Palumbo, O., Italiano, F., Claudia, L., Placido, A., Picardi, E., Carella, M., Trotta, M., and Ceci, L. R. (2014). *Rhodobacter sphaeroides* adaptation to high concentrations of cobalt ions requires energetic metabolism changes. *FEMS Microbiology Ecology*, *88*(2), 345–357.

Wang, W., Vinocur, B., Shoseyov, O., and Altman, A. (2004) Role of plant heat-shock proteins and molecular chaperones in the abiotic stress response. In Trends Plant Sci. , 9: 244-252.

Wang, J., Mei, H., Qian, H., Tang, Q., Liu, X., Yu, Z., and He, J. (2013). Expression Profile and Regulation of Spore and Parasporal Crystal Formation-Associated Genes in *Bacillus thuringiensis*. *Journal of Proteome Research*, *12*(12), 5487–5501.

Wang, X., and Tang, C. (2017). Optimal Growth Of Microbes On Mixed Carbon Sources. *BioRxiv*, 120667.

Wasai, S., Kanno, N., Matsuura, K., and Haruta, S. (2018). Increase of Salt Tolerance in

Carbon-Starved Cells of *Rhodopseudomonas palustris* Depending on Photosynthesis or Respiration. *Microorganisms*, *6*(1), 4.

Waschina, S., D'Souza, G., Kost, C., and Kaleta, C. (2016). Metabolic network architecture and carbon source determine metabolite production costs. *FEBS Journal*, *283*(11), 2149–2163.

Westfall, C. S., and Levin, P. A. (2018). Comprehensive analysis of central carbon metabolism illuminates connections between nutrient availability, growth rate, and cell morphology in *Escherichia coli*. *PLoS Genetics*, *14*(2), 1–25.

Wolfe, A. J. (2005). The Acetate Switch. *Microbiology and Molecular Biology Reviews*, *69*(1), 12–50.

Yatsunami, R., Ando, A., Yang, Y., Takaichi, S., Kohno, M., Matsumura, Y. et al. (2014) Identification of carotenoids from the extremely halophilic archaeon *Haloarcula japonica*. *Front Microbiol* 5: 100.

York, G.M., Junker, B.H., Stubbe, J.A., and Sinskey, A.J. (2001) Accumulation of the PhaP phasin of *Ralstonia eutropha* is dependent on production of polyhydroxybutyrate in cells. *J Bacteriol* 183: 4217-4226.

Youvan D. C. and Ismail S., 1985. Light-harvesting II (B800-B850 complexes) structural genes from *Rhodopseudomonas capsulate*. *Proc. Natl Acad Sci* USA 82: pp. 58-62.

Zeng, Y. H., Chen, X. H., and Jiao, N. Z. (2007). Genetic diversity assessment of anoxygenic photosynthetic bacteria by distance-based grouping analysis of pufM sequences. *Letters in Applied Microbiology*, *45*, 639–645.

Zhang, Y., Zhou, J., Wang, T., and Cai, L. (2007). High level glucose increases mutagenesis in human lymphoblastoid cells. *International Journal of Biological Sciences*, *3*(6), 375–379.

Zhao, C., Zhang, Y., Chan, Z., Chen, S., and Yang, S. (2015). Insights into arsenic multi-operons expression and resistance mechanisms in *Rhodopseudomonas palustris* CGA009. *Frontiers in Microbiology*, *6*(SEP), 1–8.

Zhang J., Chiodini R., Badr A. and Zhang G., 2010. Impact of next-generation sequencing on genomics J. of Gen. and Genom. 38: pp. 95-109.

Zhang, Y., Zhou, J., Wang, T., and Cai, L. (2007). High level glucose increases mutagenesis in human lymphoblastoid cells. *International Journal of Biological Sciences*, *3*(6), 375–379.

Zhang, Y., Zhou, J., Wang, T., and Cai, L. (2007). High level glucose increases mutagenesis in human lymphoblastoid cells. *International Journal of Biological Sciences*, *3*(6), 375–379.

Publications

Publications

Research articles

1. Ganesh M.[†], **Deepshikha G**[†]., Sasikala, Ch. and Ramana, Ch.V. (2021) Insights in to discrepancy in power generation among glucose and malate grown *Rubrivivax* microbial fuel cells. *Int. J. Hydrog. Energy* ([†]contributed equally) *46*(4), 3090–3104 (Impact factor: 4.93).
2. Dhanesh Kumar., Kumar, G., Jagadeeshwari, U., **Deepshikha G**, Sasikala, Ch. and Ramana, Ch.V. (2020). *Roseimaritima sediminicola* sp. nov., a new member of *Planctomycetaceae* isolated from Chilika lagoon. *Int J Syst Evol Microbiol* 70, 2616-2623 (Impact factor: 2.53).
3. Anusha Rai., Smita, N., Suresh, G., Shabbir, A., **Deepshikha G**, Sasikala, Ch. and Ramana, Ch.V. (2020). *Paracoccus aeridis* sp. nov., an indole producing bacterium isolated from the rhizosphere of an orchid, Aerides maculosa. *Int J Syst Evol Microbiol* 70, 1720-1728 (Impact factor: 2.53).
4. Sailaja Buddhi., Suresh, G, **Deepshikha G**, Sasikala, Ch. and Ramana, Ch.V. (2020). Description of a phototrophic bacterium, *Afifella aestuarii* sp. nov. *Int J Syst Evol Microbiol*. 70, 327-333 (Impact factor: 2.53).
5. **Deepshikha Gupta**, Mujahid Mohammed, Lakshmi Prasuna Mekala, Sasikala Chintalapati and Venkata Ramana Chintalapati (2019). iTRAQ-Based quantitative proteomics revealed insights into metabolic and molecular responses of glucose-grown cells of *Rubrivivax benzoatilyticus* JA2. *J. Proteomics* 194, 49-59 (Impact factor: 3.5).

Book chapter

6. Anusha Rai, Indu, Smita N, **Deepshikha G**, Gaurav K, Dhanesh K, Suresh G, Sasikala Ch and Ramana Ch.V. (2019). Emerging concepts in bacterial taxonomy. In Microbial Diversity in Ecosystem Sustainability and Biotechnological Applications - Volume 1. Microbial Diversity in Normal and Extreme Environments (Eds. T. Satyanarayana, S.K. Das and B.N. Johri), Springer Nature Singapore (Invited introductory chapter).

Symposia and conference presentation

7. **Deepshikha G**, Sasikala, Ch. and Ramana, Ch.V. Diabetic bacteria? 59th Annual Conference of Association of Microbiologists of India and International Symposium on Host Pathogen Interaction. December 09-12, 2018.
8. **Deepshikha G** and Ramana, Ch.V. Glucose induces photosynthetic damage leading to viable but non-culturable (VBNC) state in *Rubrivivax benzoatilyticus* JA2 8th International Conference Photosynthesis and Hydrogen Energy Research for Sustainability. October 30 – November 4, 2017.

Available online at www.sciencedirect.com

ScienceDirect

journal homepage: www.elsevier.com/locate/he

Insights into discrepancy in power generation among glucose and malate grown *Rubrivivax benzoatilyticus* JA2 microbial fuel cells

Ganesh Mahidhara [a,1], *Deepshikha Gupta* [a,1], *Ch. Sasikala* [b], *Ch. V. Ramana* [a,*]

[a] *Department of Plant Sciences, School of Life Sciences, University of Hyderabad, P.O Central University, Hyderabad, 500 046, India*

[b] *Bacterial Discovery Laboratory, Centre for Environment, Institute of Science and Technology,J.N.T. University Hyderabad, Kukatpally, Hyderabad, 500 085, India*

HIGHLIGHTS

- Strain JA2 grown in 2 chambered MFC in varied carbon & electrogenicity is measured.
- Carbon source is malate/glucose & JA2 has dissimilar electrogenic response.
- Malate grown resting JA2 in the bio- anode produced high power compared to glucose.
- When connected together malate JA2 acted as anode, glucose JA2 as cathode.
- Dense colonization & different metabolome of the malate JA2 caused such discrepancy.

GRAPHICAL ABSTRACT

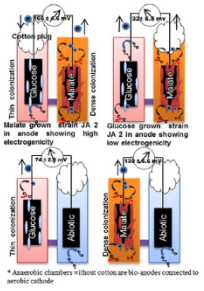

ARTICLE INFO

Article history:
Received 3 September 2019
Received in revised form
24 July 2020
Accepted 25 July 2020
Available online 15 August 2020

Keywords:
Rubrivivax benzoatilyticus JA2

ABSTRACT

In this study, *Rubrivivax benzoatilyticus* JA2^T (=ATCC BAA-35^T = JCM 13220^T = MTCC 7087^T), an anoxygenic photosynthetic bacterium, was subjected to altered conditions and observed for changes in power outcome in the two chambered microbial fuel cells (MFCs), the basis of which was established using metabolomic studies. This is an extension to our previous studies, which showed that, under photo heterotrophic conditions, glucose in the form of a solitary carbon resource in minimal media, caused the strain JA2 to exhibit altered growth rates, progressive loss of pigmentation and reduced cell size (3–4 μm), compared to malate grown cells (6–7 μm). When *R. benzoatilyticus* JA2 cells were grown in malate bio-anodes, they presented higher potentials (289.22 ± 4.6 mV or 436.22 OCV per mg

* *Corresponding author.*
E-mail addresses: cvramana449@gmail.com, chvrsl@uohyd.ernet.in (Ch.V. Ramana).
[1] Both the authors contributed equally to this work.
https://doi.org/10.1016/j.ijhydene.2020.07.227

INTERNATIONAL JOURNAL OF SYSTEMATIC AND EVOLUTIONARY MICROBIOLOGY

TAXONOMIC DESCRIPTION

Kumar *et al.*, *Int. J. Syst. Evol. Microbiol.* 2020;70:2616–2623

DOI 10.1099/ijsem.0.004076

MICROBIOLOGY SOCIETY

Roseimaritima sediminicola sp. nov., a new member of *Planctomycetaceae* isolated from Chilika lagoon

Dhanesh Kumar[1]†, Kumar Gaurav[1]†, Jagadeeshwari U[2], Deepshikha G[1], Sasikala Ch.[2,*] and Ramana Ch.V.[1,*]

Abstract

Strain JC651^T was isolated from a sediment sample collected from Chilika lagoon, which is one of the world's most important brackish water lakes with estuarine characteristics. Colonies of this strain are light pink and cells are Gram-stain negative, spherical to pear shaped and form rosettes. Strain JC651^T grows well up to pH 9.0 and tolerates up to 5% NaCl (w/v). The respiratory quinone is MK6. The detected major fatty acids are $C_{18:1}$ $\omega 9c$ and $C_{16:0}$. Its polar lipids are diphosphatidylglycerol, an unidentified phospholipid, phosphatidylglycerol and phosphatidylcholine. Strain JC651^T shows highest 16S rRNA gene sequence similarity (97.8%) to the type species of the genus *Roseimaritima*, *Roseimaritima ulvae* UC8^T. The genome size of strain JC651^T is 6.2 Mb with a G+C content of 62.4 mol%. For the resolution of the phylogenetic congruence of the novel strain, the phylogeny was also reconstructed with the sequences of 92 core genes. Based on the phylogenetic analyses, low digital DNA–DNA hybridization values (19.5%), low (74.9%) genome average nucleotide identity results, chemotaxonomic characteristics and differential physiological properties, strain JC651^T is recognized as a new species of the genus *Roseimaritima* for which we propose the name *Roseimaritima sediminicola* sp. nov. The type strain is JC651^T (=KCTC 72178^T=NBRC 113926^T).

The genus *Roseimaritima* of the phylum *Planctomycetes* was described by Bondoso and co-workers [1] to accommodate a planctomycetes of the family *Planctomycetaceae* isolated from the biofilm of marine macroalga *Ulva* sp., collected from the Northern coast of Portugal. *Roseimaritima ulvae* is the only species of this genus. It is a chemoheterotrophic, strictly aerobic and mesophilic marine bacterium with spherical to oval-shaped cells forming rosettes. $C_{18:1}$ ω9*c* and $C_{16:0}$ are the major fatty acids with MK6 as the respiratory quinone. The predominant polar lipids are phosphatidylcholine, phosphatidylglycerol and diphosphatidylglycerol.

Chilika lagoon is the largest brackish water lagoon of India and is situated in the Eastern part of the country. With an area of about 1100 km^2, it is connected to sea on one side and fed by rivers on other, making a salinity gradient of about 0–3%. The lagoon is an ecological hotspot with great diversity of flora and fauna and declared as Ramsar site in 1981. During our survey for planctomycetes of this lagoon, we have isolated a few members of this phylum; however, most of these became non-cultivable on passaging. Here we describe strain JC651^T isolated from a sediment sample of Chilika lagoon and propose it as a representative of a new species of the genus *Roseimaritima* using the polyphasic approach together with genomic information. This is apparently the first report of planctomycetes from India.

HOME, HABITAT AND ISOLATION

Strain JC651^T was isolated from a sediment sample collected from the Satapada region (19° 40′ 12.0″ N 85° 25′ 48.0″ E) of the Chilika lagoon from a depth of 1.5 meters. The pH and temperature of the sample site were 7.5 and 24 °C, respectively. The Satapada region is near to the sea mouth of the lagoon with about 3% (w/v) salinity. Modified M30 medium [2] containing 1.0 g l^{-1} $MgCl_2 \cdot 6H_2O$, 2.0 g l^{-1} *N*-acetylglucosamine, 0.1 g l^{-1} $Na_2HPO_4 \cdot 2H_2O$, 10 ml l^{-1} vitamin solution, 50 ml l^{-1} 0.1 M Tris–HCl (pH 8) and 20 ml l^{-1} Hutner's basal salts

Author affiliations: [1]Department of Plant Sciences, School of Life Sciences, University of Hyderabad, P.O. Central University, Hyderabad 500046, India; [2]Bacterial Discovery Laboratory, Centre for Environment, Institute of Science and Technology, J. N. T. University Hyderabad, Kukatpally, Hyderabad-500085, India.

***Correspondence:** Ramana Ch.V., cvr449@gmail.com; Sasikala Ch., sasi449@yahoo.ie

Keywords: Planctomycetaceae, Roseimaritima, sp. nov., Chilika lagoon.

Abbreviations: AAI, average amino acid identity; ANI, average nucleotide indentity; ASW, artificial sea water; dDDH, digital DNA–DNA hybridization; LCB, local collinear block; ME, minimum-evolution; ML, maximum-likelihood; NJ, neighbour-joining.

The GenBank/EMBL/DDBJ accession number for the 16S rRNA gene sequence of strains JC651^T is LR133893. The GenBank/EMBL/DDBJ accession for the whole genome shotgun sequence is WIAD01000000.

†These authors contributed equally to this work

Four supplementary figures and one supplementary table are avaliable with the online version of this article.

INTERNATIONAL JOURNAL OF SYSTEMATIC AND EVOLUTIONARY MICROBIOLOGY

TAXONOMIC DESCRIPTION
Rai *et al.*, *Int. J. Syst. Evol. Microbiol.* 2020;70:1720–1728
DOI 10.1099/ijsem.0.003962

MICROBIOLOGY SOCIETY

Paracoccus aeridis sp. nov., an indole-producing bacterium isolated from the rhizosphere of an orchid, *Aerides maculosa*

Anusha Rai[1], Smita N[1], Suresh G[1], Shabbir A[1], Deepshikha G[1], Sasikala Ch[2,*] and Ramana Ch.V[1,*]

Abstract

A Gram-stain-negative, non-motile, coccoid-shaped, catalase- and oxidase-positive, non-denitrifying, neutrophilic bacterium designated as strain JC501^T was isolated from an epiphytic rhizosphere of an orchid, *Aerides maculosa*, growing in the Western Ghats of India. Phylogenetic analyses based on the 16S rRNA gene sequence indicated that strain JC501^T belonged to the genus *Paracoccus* and had the highest levels of sequence identity with *Paracoccus marinus* KKL-A5^T (98.9 %), *Paracoccus contaminans* WPAn02^T (97.3%) and other members of the genus *Paracoccus* (<97.3 %). Strain JC501^T produced indole-3 acetic acid and other indole derivatives from tryptophan. The dominant respiratory quinone was Q-10 and the major fatty acid was $C_{18:1}\omega7c/C_{18:1}\omega6c$, with significant quantities of $C_{18:1}\omega9c$, $C_{17:0}$ and $C_{16:0}$. The polar lipids of strain JC501^T comprised phosphatidylglycerol, phosphatidylcholine, diphosphatidylglycerol, an unidentified glycolipid, two unidentified aminolipids, two unidentified lipids and four unidentified phospholipids. The genome of strain JC501^T was 3.3 Mbp with G+C content of 69.4 mol%. For the resolution of the phylogenetic congruence of the novel strain, the phylogeny was also reconstructed with the sequences of eight housekeeping genes. Based on the results of phylogenetic analyses, low (<85.9%) average nucleotide identity, digital DNA–DNA hybridization (<29.8%), chemotaxonomic analysis and physiological properties, strain JC501^T could not be classified into any of the recognized species of the genus *Paracoccus*. Strain JC501^T represents a novel species, for which the name *Paracoccus aeridis* sp. nov. is proposed. The type strain is JC501^T (=LMG 30532^T=NBRC 113644^T).

Bacteria residing in the rhizosphere of the plants play a vital role in the holistic development of the plant system [1–3]. Epiphytic orchid-associated bacteria have functional and ecological roles in the development of their host plant [4]. Epiphytes do not interact directly with the soil or its microbiota and thus constitute a unique system of ecology. Therefore, epiphytes have their own distinctive structural system for their sustenance, wherein they take up the nutrients and moisture from the atmosphere on the surface of the host plant aided by the microbial association [5, 6]. While investigating this unique diversity and its subsequent role in the development of the orchids, we have isolated strain JC501^T from the rhizosphere of an epiphytic orchid (*Aerides maculosa*). This strain belongs to the genus *Paracoccus* based on 16S rRNA gene sequence analysis. The genus *Paracoccus* was first described by Davis and his co-workers in 1969 [7] and belongs to the family '*Rhodobacteraceae*' of the class *Alphaproteobacteria* in the phylum *Proteobacteria*. There are more than 50 species of *Paracoccus* with validly published names (www.bacterio.net). Members have been isolated from environmental samples such as soil [8, 9], sediment [10, 11], water [12, 13], sludges [14, 15], foodstuffs [16], clinical specimens [17] and insects [18]. *Paracoccus halotolerans* [19], *Paracoccus salipaludis* [20], *Paracoccus fontiphilus* [13], *Paracoccus alimentarius* [16], *Paracoccus endophyticus* [21], *Paracoccus haematequi* [22] and *Paracoccus nototheniae* [23] are the valid names published during the year 2018–2019, while *Paracoccus jeotgali* [24] and *Paracoccus indicus* [25] are effective publications. Members of this genus are Gram-stain-negative, mostly non-motile and chemoorganotrophs [26]. Their major fatty acid is $C_{18:1}\omega7c$ and they are metabolically versatile [27]. The members of the genus *Paracoccus* have a genome size ranging from 2.9 to 5.6

Author affiliations: [1]Department of Plant Sciences, School of Life Sciences, University of Hyderabad P.O. Central University, Hyderabad 500046, India; [2]Bacterial Discovery Laboratory, Centre for Environment, Institute of Science and Technology, J. N. T. University Hyderabad, Kukatpally, Hyderabad 500085, India.
***Correspondence:** Sasikala Ch, sasi449@yahoo.ie; Ramana Ch.V, cvr449@gmail.com
Keywords: *Paracoccus*; epiphytic orchid; Proteobacteria; indole.
Abbreviations: AIC, Akaike information criterion; ANI, average nucleotide identity; dDDH, digital DNA–DNA hybridization; IAA, indole-3-acetic acid; IAM, indole-3-acetamide; LCB, local collinear block; ML, maximum-likelihood; MLSA, multilocus sequence analysis; NA, nutrient agar.
The GenBank/EMBL/DDBJ accession number for the 16S rRNA gene sequence of strain JC501^T is LT799401. The Whole Genome Shotgun project is SELD00000000. The genome sequence of *P. marinus* NBRC 100637^T is VJYZ00000000.
Five supplementary tables and ten supplementary figures are available with the online version of this article.

INTERNATIONAL JOURNAL OF SYSTEMATIC AND EVOLUTIONARY MICROBIOLOGY

TAXONOMIC DESCRIPTION

Buddhi *et al.*, *Int. J. Syst. Evol. Microbiol.* 2020;70:327–333

DOI 10.1099/ijsem.0.003756

MICROBIOLOGY SOCIETY

Afifella aestuarii sp. nov., a phototrophic bacterium

Sailaja Buddhi[1], Suresh G.[2], Deepshikha Gupta[2], Sasikala Ch.[1,*] and Ramana Ch. V.[2,*]

Abstract

An oval- to rod-shaped, motile, Gram-stain-negative, oxidase-positive, catalase-negative, pink-coloured phototrophic bacterium (designated as strain JA968^T) was isolated from an estuary near Pata, Gujarat, India. Cells had an intracytoplasmic membrane architecture as lamellae and divided by budding. Strain JA968^T had bacteriochlorophyll-*a* and spirilloxanthin series carotenoids as photosynthetic pigments. The strain exhibited photolithoautotrophic, photoorganoheterotrophic and chemoorganoheterotrophic growth modes and required thiamine as a growth factor. Strain JA968^T had $C_{18:1}\omega7c/C_{18:1}\omega6c$ as the predominant fatty acid with ubiquinone-10 (Q-10) and menaquinone-10 (MK-10) forming the quinone composition. The genomic DNA G+C content of the strain was 63.5 mol%. Pairwise comparison of 16S rRNA gene sequences showed that strain JA968^T was highly similar to *Afifella marina* DSM 2698^T (99.9 %) and *Afifella pfennigii* DSM 17143^T (98.4 %). The average nucleotide identity values were 92% between strain JA968^T and *A. marina* DSM 2698^T, and 78% between strain JA968^T and *A. pfennigii* DSM 17143^T. The digital DNA–DNA hybridization values between strain JA968^T and *A. marina* and *A. pfennigii* were 49 and 19%, respectively. The genomic distinction was also supported by differences in phenotypic and chemotaxonomic characteristics. We propose that strain JA968^T represents a new species of the genus *Afifella* with the name *Afifella aestuarii* sp. nov. The type strain is JA968^T (=KCTC 15634^T=NBRC 113338^T).

The genus *Afifella* of the family *Rhodobiaceae* proposed by Urdiain *et al.* [1] accommodates two species with validly published names (*Afifella marina* and *Afifella pfennigii*) of purple non-sulfur anoxygenic phototrophic bacteria. These members are phototrophic, commonly isolated from marine habitats, require NaCl for optimum growth and multiply by budding [2–4]. Through this study, we propose strain JA968^T as representing a new species of this genus. It was isolated from an estuarine sample collected from Pata, Gujarat, India (21° 218′ N; 69° 931′ E). The sample had a pH of 7.0 and salinity of 0.5%.

The sample was kept for enrichment in a media described previously [5] with pyruvate (22 mM) as the carbon source/electron donor in fully filled (45 ml) screw-capped glass bottles and incubated at 2400 lux (light), 28 °C for 5 days. Strain JA968^T was purified by repeated streaking on agar slants. Purified cultures were maintained on agar slants or as lyophilized cultures preserved at 4 °C. Further characterization of strain JA968^T was carried out in the medium described previously [5].

Genomic DNA was extracted using the nucleopore gDNA bacterial/fungal mini kit as per the manufacturer's instructions. The same DNA was used for 16S rRNA gene amplification and whole-genome sequencing. A nearly full-length (1463) 16S rRNA gene sequence of strain was achieved using the protocol of Divyasree *et al.* [6]. Whole-genome sequencing was outsourced to Agrigenome labs Pvt. Ltd, Kochi, India. Whole-genome DNA sequencing was carried out using the Illumina Hiseq-4000 platform. The sequenced data was assembled using VELVET 1.2.10 *de novo* assembly software.

The results of 16S rRNA gene sequence BLAST search analysis on the EzBioCloud database [7] indicated that the strain shared highest similarity with the type strains of the genus *Afifella*. Therefore, the 16S rRNA gene sequences of strain JA968^T, *A. marina* DSM 2698^T and *A. pfennigii* DSM 17143^T were derived from whole-genome sequencing and used for phylogenetic analysis. Genome sequences of *A. marina* and *A. pfennigii* were obtained from NCBI (www.ncbi.nlm.nih.gov/

Author affiliations: [1]Bacterial Discovery Laboratory, Centre for Environment, Institute of Science and Technology, J.N.T. University Hyderabad, Kukatpally, Hyderabad-500085, India; [2]Department of Plant Sciences, School of Life Sciences, University of Hyderabad, P.O. Central University, Hyderabad 500046, India.

***Correspondence:** Sasikala Ch., sasikala.ch@gmail.com; sasi449@yahoo.ie; Ramana Ch. V., cvr449@gmail.com

Keywords: *Afifella*; photosynthetic; alphaproteobacteria.

Abbreviations: ANI, average nucleotide identity; dDDH, digital DNA–DNA hybridization.

The GenBank/EMBL/DDBJ accession number for the 16S rRNA gene sequence of strain JA968^T is LT622289. The accession number for the draft genome sequence of strain JA968^T is SAUF00000000.

One supplementary table and nine supplementary figures are available with the online version of this article.

Emerging Concepts in Bacterial Taxonomy

1

Anusha Rai, Indu, N. Smita, G. Deepshikha, K. Gaurav, K. Dhanesh, G. Suresh, Ch. Sasikala, and Ch. V. Ramana

Abstract

Bacterial taxonomy has progressed over the years by virtue of the brisk and competent scientific developments. Ground-breaking molecular techniques have added an edge in the phylogenetic studies, resulting in the quality description of the taxa under studies. New avenues are rapidly developing whose validation has always been embraced and included, which will assist in resolution. It began with the simple application of objective procedures for classification, and now we have arrived at the genome-based taxonomy. This pedantic step has led to the meticulous examination and served to reconcile certain conflicts of the status of the taxa. This field is dynamic and is exploring more options like proteomics and metabolomics in gaining more insights into the lineal heritage. Even though there has been a significant change and addition, there is an ever-growing need for a comprehensive study, which would thread all the attributes together into one functional unit of classification. In this review, we examine the paradigm shift from traditional taxonomy to integrated taxonomy useful in the characterisation of bacteria which in addition aids in the identity of biotechnological targets.

Keywords

Bacterial taxonomy · Polyphasic · Phylogenomics · Integrated taxonomy · Average nucleotide sequence index (ANI)

A. Rai · Indu · N. Smita · G. Deepshikha · K. Gaurav · K. Dhanesh · G. Suresh · C. V. Ramana (✉)
Department of Plant Sciences, School of Life Sciences, University of Hyderabad, Hyderabad, Telangana, India

C. Sasikala (✉)
Centre for Environment, Institute of Science & Technology, JNT University Hyderabad, Hyderabad, Telangana, India

T. Satyanarayana et al. (eds.), *Microbial Diversity in Ecosystem Sustainability and Biotechnological Applications*, https://doi.org/10.1007/978-981-13-8315-1_1

Journal of Proteomics 194 (2019) 49–59

Contents lists available at ScienceDirect

Journal of Proteomics

journal homepage: www.elsevier.com/locate/jprot

iTRAQ-based quantitative proteomics reveals insights into metabolic and molecular responses of glucose-grown cells of *Rubrivivax benzoatilyticus* JA2

Deepshikha Gupta[a], Mujahid Mohammed[a], Lakshmi Prasuna Mekala[a], Sasikala Chintalapati[b], Venkata Ramana Chintalapati[a,*]

[a] Department of Plant Sciences, P.O. Central University, University of Hyderabad, Hyderabad 500046, India
[b] Bacterial Discovery Laboratory, Centre for Environment, IST, JNT University Hyderabad, Kukatpally, Hyderabad 500085, India

ARTICLE INFO

Keywords:
Rubrivivax benzoatilyticus JA2
Anoxygenic photosynthetic bacteria (APB)
Glucose
Metabolic remodelling
Loss of pigmentation
Membrane adaptation
iTRAQ
Fatty acid

ABSTRACT

Anoxygenic photosynthetic bacteria thrive under diverse habitats utilising an extended range of inorganic/organic compounds under different growth modes. Although they display incredible metabolic flexibility, their responses and adaptations to changing carbon regimes is largely unexplored. In the present study, we employed iTRAQ-based global proteomic profiling and physiological studies to uncover the adaptive strategies of a phototrophic bacterium, *Rubrivivax benzoatilyticus* JA2 to glucose. Strain JA2 displayed altered growth rates, reduced cell size and progressive loss of pigmentation when grown on glucose compared to malate under photoheterotrophic condition. A ten-fold increase in the saturated to unsaturated fatty acid ratio of glucose-grown cells indicates a possible membrane adaptation. Proteomic profiling revealed extensive metabolic remodelling in the glucose-grown cells wherein signal-transduction, selective-transcription, DNA-repair, transport and protein quality control processes were up-regulated to cope with the changing milieu. Proteins involved in DNA replication, translation, electron-transport, photosynthetic machinery were down-regulated possibly to conserve the energy. Glycolysis/gluconeogenesis, TCA cycle and pigment biosynthesis were also down-regulated. The cell has activated alternative energy metabolic pathways viz., fatty acid β-oxidation, glyoxylate, acetate-switch and Entner-Doudoroff pathways. Overall, the present study deciphered the molecular/metabolic events associated with glucose-grown cells of strain JA2 and also unraveled how a carbon source modulates the metabolic phenotypes.

Significance: Anoxygenic photosynthetic bacteria (APB) exhibit incredible metabolic flexibility leading to diverse phenotypes. They thrive under diverse habitat using an array of inorganic/organic compounds as carbon sources, yet their metabolic adaptation to varying carbon regime is mostly unexplored. Present study uncovered the proteomic insights of the cellular responses of strain JA2 to changing carbon sources viz. malate and glucose under photoheterotrophic conditions. Our study suggests that carbon source can also determine the metabolic fate of the cells and reshape the energy dynamics of APB. Here, for the first time study highlighted the plausible carbon source (glucose) mediated regulation of photosynthesis in APB. The study sheds light on the plausible cellular events and adaptive metabolic strategies employed by strain JA2 in presence of non-preferred carbon source. It also revealed new insights into the metabolic plasticity of APB to the changing milieu.

1. Introduction

Microorganisms are continuously exposed to the ever-changing environmental conditions and they perceive a myriad of stimuli. The successful colonization of niche and survival depends on sensing and orchestrating the gene expression which is under the control of the sophisticated complex regulatory system. Diverse environmental factors such as pH, temperature, salinity, light, nutrients, oxygen modulates

Abbreviations: ACN, Acetonitrile; Aldh, Aldehyde dehydrogenase; APB, Anoxygenic photosynthetic bacteria; DEP, Differentially expressed proteins; DIC, Differential interference contrast; ED, Entner Doudoroff pathway; EMP, Embden-Meyerhof-Parnas pathway; ETC, Electron transport chain; FAME, Fatty acid methyl esters; FC, Fold change; GO, Gene ontology; GRAVY, Grand average hydropathy index; HPLC, High performance liquid chromatography; iTRAQ, Isobaric tag for relative and absolute quantitation; KEGG, Kyoto encyclopedia of genes and genomes; LHC, Light harvesting complex; MK-8, Menaquinone-8; OD, Optical density; PBS, Phosphate buffered saline; PMF, Proton motive force; PPP, Pentose phosphate pathway; Q8, Ubiquinone-8; RC, Reaction center; TCA cycle, Tricarboxylic acid cycle

* Corresponding author.
E-mail address: chvrsl@uohyd.ernet.in (V.R. Chintalapati).

https://doi.org/10.1016/j.jprot.2018.12.027
Received 3 November 2018; Received in revised form 19 December 2018; Accepted 26 December 2018
Available online 28 December 2018
1874-3919/

Insights into the glucose photometabolism by Rubrivivax benzoatilyticus JA2

by Deepshikha Gupta

Submission date: 25-Jan-2021 03:22PM (UTC+0530)
Submission ID: 1493934425
File name: DeepshikaThesis_16LPPH03.docx (284.93K)
Word count: 25384
Character count: 150553

Insights into the glucose photometabolism by Rubrivivax benzoatilyticus JA2

ORIGINALITY REPORT

29%	9%	27%	3%
SIMILARITY INDEX	INTERNET SOURCES	PUBLICATIONS	STUDENT PAPERS

PRIMARY SOURCES

1	Deepshikha Gupta, Mujahid Mohammed, Lakshmi Prasuna Mekala, Sasikala Chintalapati, Venkata Ramana Chintalapati. "iTRAQ-based quantitative proteomics reveals insights into metabolic and molecular responses of glucose-grown cells of Rubrivivax benzoatilyticus JA2", Journal of Proteomics, 2019 Publication	20
2	baadalsg.inflibnet.ac.in Internet Source	2
3	pubmed.ncbi.nlm.nih.gov Internet Source	<1
4	Tao Yu, Geng Li, Shuting Dong, Peng Liu, Jiwang Zhang, Bin Zhao. "Proteomic analysis of maize grain development using iTRAQ reveals temporal programs of diverse metabolic processes", BMC Plant Biology, 2016 Publication	<1
5	www.nature.com	

This paper is published by student herself.
29/1/2021

Prof. Ch. Venkata Ramana Ph.D
Department of Plant Sciences School of Life Sciences
University of Hyderabad P.O. Central University,
Hyderabad-500 046

	Internet Source	<1%
6	Denich, T.. "Effect of selected environmental and physico-chemical factors on bacterial cytoplasmic membranes", Journal of Microbiological Methods, 200302 Publication	<1%
7	Advances in Photosynthesis and Respiration, 2009. Publication	<1%
8	link.springer.com Internet Source	<1%
9	Mujahid, Md, M Lakshmi Prasuna, Ch Sasikala, and Ch Venkata Ramana. "Integrated metabolomic and proteomic analysis reveals systemic responses of Rubrivivax benzoatilyticus JA2 to aniline stress", Journal of Proteome Research, 2014. Publication	<1%
10	www.annualreviews.org Internet Source	<1%
11	en.wikipedia.org Internet Source	<1%
12	brcdownloads.vbi.vt.edu Internet Source	<1%

13	Elodie Barbau-Piednoir, Jacques Mahillon, Julie Pillyser, Wim Coucke, Nancy H. Roosens, Nadine Botteldoorn. "Evaluation of viability-qPCR detection system on viable and dead Salmonella serovar Enteritidis", Journal of Microbiological Methods, 2014 Publication	<1%
14	Anil Kumar Pasupulati, Nageswara Rao Dunna, Srikanth Talluri. "Chapter 4 Metabolic Adaptations in Diabetes Mellitus and Cancer", Springer Science and Business Media LLC, 2019 Publication	<1%
15	Submitted to Jawaharlal Nehru Technological University Student Paper	<1%
16	www.dojindo.com Internet Source	<1%
17	Submitted to North West University Student Paper	<1%
18	Megan Bergkessel, David W. Basta, Dianne K. Newman. "The physiology of growth arrest: uniting molecular and environmental microbiology", Nature Reviews Microbiology, 2016 Publication	<1%

19	Submitted to University of Hyderabad, Hyderabad Student Paper	<1%
20	www-u.life.uiuc.edu Internet Source	<1%
21	crdd.osdd.net Internet Source	<1%
22	T.J Denich, L.A Beaudette, H Lee, J.T Trevors. "Effect of selected environmental and physico-chemical factors on bacterial cytoplasmic membranes", Journal of Microbiological Methods, 2003 Publication	<1%
23	tel.archives-ouvertes.fr Internet Source	<1%
24	Farhana R. Pinu, Ninna Granucci, James Daniell, Ting-Li Han, Sonia Carneiro, Isabel Rocha, Jens Nielsen, Silas G. Villas-Boas. "Metabolite secretion in microorganisms: the theory of metabolic overflow put to the test", Metabolomics, 2018 Publication	<1%
25	krishikosh.egranth.ac.in Internet Source	<1%
26	www.coursehero.com Internet Source	<1%

27	Alessandra A. Vireque, Alessandra Tata, Katia Roberta A. Belaz, João Gabriel V. Grázia et al. " MALDI mass spectrometry reveals that cumulus cells modulate the lipid profile of matured bovine oocytes ", Systems Biology in Reproductive Medicine, 2017 Publication	<1%
28	K. V. N. S. Lakshmi. "Phaeospirillum oryzae sp. nov., a spheroplast forming phototrophic alphaproteobacterium from a paddy soil", INTERNATIONAL JOURNAL OF SYSTEMATIC AND EVOLUTIONARY MICROBIOLOGY, 08/13/2010 Publication	<1%
29	livrepository.liverpool.ac.uk Internet Source	<1%
30	Dhanesh Kumar, Nandardhane Smita, Gaurav Kumar, Gandham Suresh et al. "Arenibacter lacus sp. nov., Isolated from Chilika Lagoon, India", Current Microbiology, 2020 Publication	<1%
31	Dhanesh Kumar, Gaurav Kumar, Jagadeeshwari Uppada, Shabbir Ahmed, Chintalapati Sasikala, Chintalapati Venkata Ramana. "Descriptions of Roseiconus nitratireducens gen. nov. sp. nov. and Roseiconus lacunae sp. nov.", Archives of	<1%

Microbiology, 2020
Publication

32	pubmed.cn Internet Source	<1%
33	Md Mujahid, M Lakshmi Prasuna, Ch Sasikala, Ch Venkata Ramana. " Integrated Metabolomic and Proteomic Analysis Reveals Systemic Responses of JA2 to Aniline Stress ", Journal of Proteome Research, 2014 Publication	<1%
34	www.labome.org Internet Source	<1%
35	www.researchsquare.com Internet Source	<1%
36	Moriscot, C.. "MnTMPyP, a metalloporphyrin-based superoxide dismutase/catalase mimetic, protects INS-1 cells and human pancreatic islets from an in vitro oxidative challenge", Diabetes and Metabolism, 200702 Publication	<1%
37	Rishabh Kaushik, Meesha Sharma, Kumar Gaurav, U. Jagadeeshwari, A. Shabbir, Ch. Sasikala, Ch. V. Ramana, Maharaj K. Pandit. "Paludisphaera soli sp. nov., a new member of the family Isosphaeraceae isolated from high altitude soil in the Western Himalaya", Antonie	<1%

	van Leeuwenhoek, 2020 Publication	
38	Submitted to Mansoura University Student Paper	<1%
39	dspace.umh.es Internet Source	<1%
40	theses.gla.ac.uk Internet Source	<1%
41	Submitted to Fort Valley State Univeristy Student Paper	<1%
42	patents.justia.com Internet Source	<1%
43	worldwidescience.org Internet Source	<1%
44	Ch. V. Ramana. "Rubrivivax benzoatilyticus sp. nov., an aromatic, hydrocarbon-degrading purple betaproteobacterium", INTERNATIONAL JOURNAL OF SYSTEMATIC AND EVOLUTIONARY MICROBIOLOGY, 09/01/2006 Publication	<1%
45	Submitted to University of Abertay Dundee Student Paper	<1%
46	www.frontiersin.org Internet Source	<1%

47	shodhganga.inflibnet.ac.in Internet Source	<1%
48	hdl.handle.net Internet Source	<1%
49	Ganesh Mahidhara, Deepshikha Gupta, Ch. Sasikala, Ch. V. Ramana. "Insights into discrepancy in power generation among glucose and malate grown Rubrivivax benzoatilyticus JA2 microbial fuel cells", International Journal of Hydrogen Energy, 2020 Publication	<1%
50	Submitted to King's College Student Paper	<1%
51	Submitted to University of Durham Student Paper	<1%
52	www.theseed.org Internet Source	<1%
53	Submitted to University of Birmingham Student Paper	<1%
54	Submitted to University of Seoul Student Paper	<1%
55	"Bergey's Manual® of Systematic Bacteriology", Springer Science and Business Media LLC, 2005 Publication	<1%

Exclude quotes	On	Exclude matches	< 14 words
Exclude bibliography	On		